UNIVERSITY OF SOUTHAMPTON
FACULTY OF PHYSICAL SCIENCES AND ENGINEERING
SCHOOL OF ELECTRONICS AND COMPUTER SCIENCE

Co-Located and Distributed Multicarrier Space-Time Shift Keying for Wideband Channels

by

Mohammad Ismat Kadir

A thesis submitted in the partial fulfilment of the requirements for the award of Doctor of Philosophy at the University of Southampton

January 2014

SUPERVISORS:
Professor Lajos Hanzo and Professor Sheng Chen

University of Southampton
Southampton SO17 1BJ
United Kingdom

Dedicated to my family

UNIVERSITY OF SOUTHAMPTON

ABSTRACT

FACULTY OF PHYSICAL SCIENCES AND ENGINEERING
SCHOOL OF ELECTRONICS AND COMPUTER SCIENCE

Doctor of Philosophy

CO-LOCATED AND DISTRIBUTED MULTICARRIER SPACE-TIME SHIFT KEYING FOR WIDEBAND CHANNELS

by Mohammad Ismat Kadir

Multicarrier (MC) transmissions are proposed for the space-time shift keying (STSK) concept. Specifically, OFDM, MC-CDMA and OFDMA/SC-FDMA-aided STSK are proposed for transmissions over dispersive wireless channels. Additionally, a successive relaying (SR) aided cooperative MC STSK scheme is conceived for gleaning cooperative space-time diversity and for mitigating the half-duplex throughput loss of conventional relaying. Furthermore, a multiple-symbol differential sphere decoding (MSDSD) aided multicarrier STSK arrangement is proposed to dispense with channel estimation (CE).

We design a novel modality of realizing STSK amalgamated with OFDM for facilitating high-rate data-transmissions through a number of low-rate parallel subchannels, thus overcoming the dispersion induced by broadband channels. A MC-CDMA aided STSK system is also proposed for mitigating the channel-induced dispersion, while providing additional frequency-domain (FD) diversity and supporting multiuser transmissions. As a further advance, we design OFDMA and SC-FDMA-aided STSK systems, which are capable of communicating in dispersive multiuser scenarios, whilst maintaining a low peak-to-average power ratio (PAPR) in the SC-FDMA-aided STSK uplink. Additionally, complexity reduction techniques are proposed for OFDMA/SC-FDMA-aided STSK.

We also conceive the concept of SR aided cooperative multicarrier STSK for frequency-selective channels for mitigating the typical 50% throughput loss of conventional half-duplex relaying in the context of MC-CDMA and for reducing the SR-induced interferences. We additionally propose a differentially encoded cooperative MC-CDMA STSK scheme for facilitating communications over hostile dispersive channels without requiring CE.

Finally, the noncoherent multicarrier STSK arrangement is further developed by using MSDSD. The conventional differential detection suffers from a typical 3-dB performance loss, which is further aggravated in the presence of high Doppler frequencies. Hence, for the sake of mitigating this performance loss in the face of high-Doppler scenarios, while maintaining a modest decoding complexity, both a hard-decision-based as well as an iterative soft-decision multiple-symbol differential sphere decoding aided multicarrier STSK arrangement is developed.

Declaration of Authorship

I, **Mohammad Ismat Kadir**, declare that the thesis entitled

Co-Located and Distributed Multicarrier Space-Time Shift Keying for Wideband Channels

and the work presented in it are my own and has been generated by me as the result of my own original research. I confirm that:

1. This work was done wholly or mainly while in candidature for a research degree at this University;
2. Where any part of this thesis has previously been submitted for a degree or any other qualification at this University or any other institution, this has been clearly stated;
3. Where I have consulted the published work of others, this is always clearly attributed;
4. Where I have quoted from the work of others, the source is always given. With the exception of such quotations, this thesis is entirely my own work;
5. I have acknowledged all main sources of help;
6. Where the thesis is based on work done by myself jointly with others, I have made clear exactly what was done by others and what I have contributed myself;
7. Parts of this work have been published, as seen in the list of publications.

Signed: Mohammad Ismat Kadir
Date: 23 January 2014

Acknowledgements

I would like to express my heartfelt gratitude to Professor Lajos Hanzo for his outstanding supervision, guidance and support throughout the entire process. His advice, inspiration and encouragement have greatly benefited me not only in work but also in life. He has not only impressed me by his attitude to work, but also has managed to cultivate in me the desire to be a good researcher through his enthusiasm and perseverance in research. Most importantly, I would like to thank him for his invaluable friendship, not only during the times of work but also in social gatherings.

I also express my gratitude to my second supervisor Professor Sheng Chen for his continued guidance and inspiration during my research work. His thoughtful supervision and careful observations helped me to proceed with the work in a proper way.

Many thanks also to my colleagues and the staff of the Communications, Signal Processing and Control (CSPC) Research Group of University of Southampton for their support, help and discussions throughout my research. Special thanks go to Prof Lie-lang Yang, Dr. Soon Xin Ng, Dr. Rob Maunder, Dr. Rong Zhang and Dr. Mohammed El-Hajjar for their technical support and collaborative work. Special thanks are also due to Shinya Sugiura, who introduced the space-time shift keying (STSK) concept and co-authored two papers with me.

The financial support of the Commonwealth Scholarship Commission in the United Kingdom is also gratefully acknowledged.

I would also like to express my gratitude to my parents who taught me how to be a good man and who form the persistent inspiration for my journey in this life. Finally, I am grateful to my wife and to my siblings for their great support and encouragement.

List of Publications

Journal papers:

1. **M. I. Kadir**, L. Li, S. Chen and L. Hanzo, "Successive-relaying-aided decode-and-forward coherent versus non-coherent cooperative multicarrier space-time shift keying," *IEEE Transactions on Vehicular Technology*, vol. 62, no. 6, pp 2544-2557, July 2013.

2. **M. I. Kadir**, S. Sugiura, J. Zhang, S. Chen and L. Hanzo, "OFDMA/SC-FDMA-aided space-time shift keying for dispersive multiuser scenarios," *IEEE Transactions on Vehicular Technology*, vol. 62, no. 1, pp 408-414, January 2013.

3. **M. I. Kadir**, S. Chen, K. V. S. Hari, K. Giridhar and L. Hanzo, "Iterative soft- multiple-symbol differential sphere decoding for multicarrier space-time shift keying," *IEEE Transactions on Vehicular Technology*, (under review).

4. **M. I. Kadir**, S. Chen and L. Hanzo, "A survey and tutorial on unified MIMO-multicarrier designs based on space-time shift keying," *IEEE Communications Surveys and Tutorials*, (to be submitted).

Conference papers:

1. **M. I. Kadir**, S. Chen and L. Hanzo, "A reduced-complexity detector for OFDMA/SC-FDMA-aided multicarrier space-time shift keying," in *Proceedings of the 78th IEEE Vehicular Technology Conference (VTC) Fall,* Las Vegas, USA, September 2013, pp. 1-5.

2. **M. I. Kadir**, S. Sugiura, S. Chen and L. Hanzo, "MC-CDMA aided multiuser space-time shift keying in wideband channels," in *Proceedings of the IEEE Wireless Communications and Networking Conference (WCNC)*, Shanghai, China, April 2013, pp. 2643-2648.

3. M. Driusso, **M. I. Kadir**, F. Babich and L. Hanzo, "OFDM-aided space-time shift keying for dispersive downlink channels," in *Proceedings of the 76th IEEE Vehicular Technology Conference (VTC) Fall*, Quebec City, Canada, September 2012, pp. 1-5.

4. **M. I. Kadir**, S. Chen and L. Hanzo, "Decode-and-forward relaying aided noncoherent cooperative multicarrier space-time shift keying using soft- multiple-symbol differential sphere decoding," *IEEE Vehicular Technology Conference (VTC) Fall*, 2014, (to be submitted).

Contents

List of Symbols

General Conventions

Mathematical Operators and Functions

$\boldsymbol{A}^T$	The transpose of the matrix $\boldsymbol{A}$
$\boldsymbol{A}^H$	The Hermitian transpose of the matrix $\boldsymbol{A}$
$\mathrm{tr}(\boldsymbol{A})$	The trace of the matrix $\boldsymbol{A}$
$\mathbf{det}\,[\boldsymbol{A}]$	The determinant of the matrix $\boldsymbol{A}$
$\parallel \boldsymbol{A} \parallel$	The Euclidean norm of $\boldsymbol{A}$
$\mid a \mid$	The complex norm of the complex number a
$\mathcal{E}\{\cdot\}$	The expected value of '$\cdot$'
$(\cdot)^*$	The complex conjugate of '$\cdot$'
$P(\cdot)$	The probability of '$\cdot$'
$\ln(\cdot)$	The natural logarithm
$\mathrm{vec}(\bullet)$	The vectorial stacking operation on the matrix '$\bullet$'
$\log_2(\cdot)$	The logarithm to base 2
$\exp[\cdot]$	The exponential function
$\mathrm{jac}[\cdot]$	The Jacobian logarithm
$[\cdot]_N$	The modulo-N operator
$\mathrm{DFT}_{N_c}\{\cdot\}$	The N_c- point discrete Fourier transform

$\text{IDFT}_{N_c}\{\cdot\}$	The N_c- point inverse discrete Fourier transform
$\text{comp}[\cdot]$	The complexity associated with the computation of '$\cdot$'
$\circledast_{N_c}$	The length-N_c circular convolution operator
$\star$	The linear convolution operator
$\arg\max_{x\in\mathcal{A}}\{f(x)\}$	The argument $x_0 \in \mathcal{A}$ yielding the maximum of $f(x)$
$\arg\min_{x\in\mathcal{A}}\{f(x)\}$	The argument $x_0 \in \mathcal{A}$ yielding the minimum of $f(x)$
$\max_i[x_i]$	The maximum value of x_i
$\mathcal{CN}(\mu,\sigma^2)$	Circularly symmetric complex Gaussian distribution with mean μ and variance σ^2
$\delta(\cdot)$	Dirac delta function (Continuous-time)
$\delta[\cdot]$	Dirac delta function (Discrete-time)
$J_0(\cdot)$	The zeroth-order Bessel function of the first kind

Constants and Sets

π	The number pi
e	Euler's number
$\mathbb{C}$	Set of complex numbers
$\mathbb{Z}$	Set of integer numbers
$\mathbb{R}$	Set of real numbers

Mathematical Symbols

$\mathfrak{R}(\cdot)$	The real part of a complex number
$\mathfrak{I}(\cdot)$	The imaginary part of a complex number
$\boldsymbol{\mathcal{F}}_{N_c}$	The N_c-point DFT matrix
$\boldsymbol{\mathcal{F}}_{N_c}^H$	The N_c-point IDFT matrix
$\triangleq$	Defining a quantity
$\otimes$	The Kronecker product

$\in$	The element of a set
$\mathbf{0}_{M\times N}$	The $(M \times N)$ zero matrix
$\boldsymbol{I}_T$	$(T \times T)$ identity matrix
$O\left(f(x)\right)$, $o\left(f(x)\right)$	Landau symbols
$\texttt{diag}\left\{\boldsymbol{X}_1, \ldots, \boldsymbol{X}_N\right\}$	Block-diagonal matrix with $\boldsymbol{X}_1, \ldots, \boldsymbol{X}_N$ on its main diagonal
$\texttt{diag}\left\{x_1, \ldots, x_N\right\}$	Diagonal matrix with $x_1, \ldots, x_N$ on its main diagonal
$\texttt{toeplitz}\left\{x_1, \ldots, x_N\right\}$	A symmetric $(N \times N)$ Toeplitz matrix

Specific Variables

Conventions

$\boldsymbol{X}$	Boldface letter, matrix or column vector
$\hat{x}$	Estimate of x
$\hat{\boldsymbol{X}}$	Codeword estimate
$\tilde{\boldsymbol{X}}$	Candidate codewords
$(\boldsymbol{X})_t$	The $t-$th column of the matrix $\boldsymbol{X}$
$\tilde{h}, \tilde{\boldsymbol{H}}$	Frequency-domain channel transfer function or matrix
$\bar{\boldsymbol{X}}, \bar{\boldsymbol{Y}}, \bar{\boldsymbol{H}}$	Equivalent parameters by the linearized system model
$\boldsymbol{X}^w, \boldsymbol{Y}^w, \boldsymbol{H}^w$	Parameters of an MSDSD processing block (*window*)
$\mathcal{S}_u$	The set of sub-carriers allocated to user u
$\boldsymbol{\mathcal{S}}$	The set of STSK codewords
$\boldsymbol{\mathcal{S}}$	The set of STSK codewords
$\mathcal{C}_{\mathcal{L}}$	The set of $\mathcal{L}-$PSK/QAM symbols

List of Variables

M	The number of transmit antenna elements (AEs)
N	The number of receive antenna elements (AEs)

T	The number of symbol intervals spanned by the space-time codewords
Q	The number of dispersion matrices considered for constructing the STSK codewords
$\boldsymbol{A}_q$	The q-th ($q = 1, 2, ..., Q$) linear dispersion matrix
$\mathcal{L}$	Modulation order of the STSK symbols
$\mathcal{L}'$	Modulation order of the SN symbols in the distributed MC STSK
R	Throughput
$\boldsymbol{\chi}$	Dispersion character matrix (DCM)
N_c	The number of sub-carriers
N_d	DFT length of the DFT precoding stage of SC-FDMA transmission
E_b	Bit energy
E_s	Symbol energy
n_c	Subcarrier index, $n_c = 1, 2, ..., N_c$
n	The index of the receive antenna element, $n = 1, 2, ..., N$
m	The index of the transmit antenna element, $m = 1, 2, ..., M$
s_f	Spreading factor index, $s_f = 1, 2, ..., S_f$
γ	Signal-to-noise ratio (SNR)
$\sigma^2_{\mathbf{n}},\ N_0$	The noise variance
$L_e(\cdot)$	The extrinsic log-likelihood ratio (LLR) of '$\cdot$'
$L_a(\cdot)$	The *a priori* log-likelihood ratio (LLR) of '$\cdot$'
$L_p(\cdot)$	The *a posteriori* log-likelihood ratio (LLR) of '$\cdot$'
$\boldsymbol{K}_{q,l_c}$	The equivalent transmit signal vector of the STSK scheme
$\mathcal{T}$	Symbol duration
u	The generalized user
v	The desired user
L	The number of channel multipath components

l	The index of a channel multipath component
l_c, l_c^u	The index of the constellation symbol (superscript u refers to user u)
q, q^u	The index of the dispersion matrix activated (superscript u refers to user u)
l_c'	The index of the constellation symbol that lies in the first quadrant only
$\mathcal{L}^1$	Total number of the constellation symbols that lies in the first quadrant only
$L_{\mathbf{cp}}$	The cyclic prefix length
$\boldsymbol{D}$	The diagonal matrix containing the Fourier transform of the channel transfer functions along its main diagonal
$\breve{\boldsymbol{H}}$	The $(N_c \times N_c)-$element channel circulant matrix
$\boldsymbol{Q}$	The $(N \times N)-$element unitary matrix obtained by the singular value decomposition of the $(N \times M)-$element channel matrix $\boldsymbol{H}$
$\breve{\boldsymbol{Q}}$	The $(M \times M)-$element unitary matrix obtained by the singular value decomposition of the $(N \times M)-$element channel matrix $\boldsymbol{H}$
$\boldsymbol{\Xi}$	The $(N \times M)-$element diagonal matrix of the ordered singular values of the $(N \times M)-$element channel matrix
σ_i	The ordered singular values of the channel matrix $\boldsymbol{H}$
λ_i	The eigenvalues of $\boldsymbol{H}\boldsymbol{H}^H$
g, g_r	The generator polynomial of the forward and the feedback path of convolutional code
r	The rank of the space-time codeword matrix
r_H	The rank of the channel matrix $\boldsymbol{H}$
$\boldsymbol{\Lambda}$	The matrix representing the fading-plus-noise statistics of the channel in terms of the autocorrelation functions
$\boldsymbol{\Lambda}_Y$	The conditional covariance matrix
$\boldsymbol{U}$	The upper triangular matrix obtained by applying the Cholesky factorization of $\boldsymbol{\Lambda}^{-1} = \boldsymbol{U}^{\mathrm{H}}\boldsymbol{U}$

$h_{n,m}(t)$	The channel impulse response (CIR) of the channel between m-th transmit and n-th receive AE
$\boldsymbol{H}$	The $(N \times M)$-element CIR matrix
$\tilde{\boldsymbol{H}}$	The $(N \times M)$-element FD channel transfer function matrix
$\boldsymbol{C}_{add}(\bullet)$	A matrix which adds a time-domain cyclic prefix to the vector '$\bullet$'
$\boldsymbol{P}^u$	The sub-carrier allocation matrix for user u
$\tilde{\boldsymbol{P}}^u$	The sub-carrier de-allocation matrix for user u
$\boldsymbol{W}^u$	The weight matrix of the MIMO ZF or MMSE FDE of user u
α	The path-loss exponent
τ	Channel coherence block interval
$D_{aa'}$	The distance between the nodes a and a'
$G_{aa'}$	The path-loss gain of the path between the nodes a and a'
b	The number of symbols in any transmit block of the source node in the cooperative scheme
B	The number of channel-encoded bits
L_f	The frame length defined the number of signalling blocks in a frame
$\boldsymbol{C}_B^u$	The spreading code of user u, $(u = 1, 2, ..., U)$ during the transmission of frame-B
$\boldsymbol{C}_A^u$	The spreading code of user u, $(u = 1, 2, ..., U)$ during the transmission of frame-A
S_f	The spreading factor
f_m	Maximum Doppler frequency
f_d	Normalized Doppler spread
σ_τ	Delay spread
B_c	Coherence bandwidth
$b, \bar{b}$	Bits, complemented bits
α_m	The activation/deactivation parameter of relay node m

$\boldsymbol{v}$,$\boldsymbol{V}$	AWGN added to the transmitted signal
N_0	Single-sided power spectral density of white noise
$\boldsymbol{S}$, $\boldsymbol{X}$	The STSK space-time codeword
$\boldsymbol{\mathcal{S}}$	The set of STSK codewords
P_b	Bit error probability
P_m	The probability of mutation in GA
x_k	The transmitted symbol at instance k
$x_{v,I}$, $x_{v,Q}$	Real and imaginary parts of the unit vectors having the same phase angles as those of the first-quadrant constellation points
G	The number of generations of GA
gen	The index to the number of generations of GA
σ_S^2	The complex signal's variance
Π	Interleaver
Π^{-1}	Deinterleaver

Chapter 1

Introduction

Multiple-input multiple-output (MIMO) wireless communication systems have attracted substantial research interests over the last two decades as a benefit of mainly their capability to provide reliable high-throughput communications without extending the bandwidth of a single-antenna system. Against the background of the explosive expansion of the Internet and of the continued dramatically increased demand for high-speed multimedia wireless systems, a flexible and spectrally efficient transceiver technology is essential. In this context, MIMO systems, which employ multiple antennas at both the transmitter and the receiver ends, are very much important, because they provide a very high capacity without increasing the bandwidth requirement of the system. The throughput of a MIMO system may be increased linearly with the number of antennas [1]. Apart from this multiplexing gain, MIMOs are also capable of benefitting from a spatial diversity gain that is attained by the spatially separated antennas in a dense multipath scattering environment, provided that the antenna-elements are sufficiently far apart for the sake of experiencing independent fading. Thus MIMO systems have the potential of improving both the spectral efficiency and the link reliability of future wireless communications systems.

A particularly promising candidate for the next generation fixed and mobile wireless systems is the combination of MIMO technology with the family of multicarrier communications systems. Realistic wireless channels are dispersive by nature. Dispersive MIMO channels potentially exhibit frequency diversity due to the channel's delay-spread, where the subcarriers of a multicarrier system may fade independently. Alternatively, this phenomenon may also be viewed as the independent fading of the channel impulse response (CIR) taps. A multicarrier system effectively converts the wideband channels into a number of low-rate parallel narrowband frequency-flat subchannels. The subcarriers are required to maintain a minimum frequency separation in order to maintain orthogonality, but the signal spectra corresponding to the different subcarriers may overlap in frequency-domain. Hence, the available frequency

spectrum can be efficiently utilized. Furthermore, multicarrier systems are capable of significantly reducing the receiver complexity in broadband channels with the aid of using single-tap frequency-domain (FD) equalization. Field tests of wideband MIMO multicarrier systems have revealed that while increased capacity and reliability can be achieved by employing MIMO techniques [2], multicarrier transmissions make equalization more efficient [3, 4]. Thus MIMO systems combined with multicarrier communications appear to be a promising solution for broadband wireless communications systems, which motivates the investigations of this thesis.

1.1 Classification of MIMO Systems

In this section, we would like to commence with a brief classification of MIMO systems according to the applications they are employed in. Again, MIMO systems may be employed for achieving high-rate transmissions with the aid of spatial multiplexing as well as for attaining spatial diversity for the sake of combatting the deliterious effects of the hostile fading channels. In general, MIMO schemes employing M transmit as well as N receive antenna elements may be described by the block-based MIMO model:

$$\boldsymbol{Y}[i] = \boldsymbol{H}[i]\,\boldsymbol{S}[i] + \boldsymbol{V}[i], \tag{1.1}$$

where $\boldsymbol{Y}[i]$ is a $(N \times T)$-element matrix corresponding to block i, whose n^{th} row represents the signal received by the n^{th} antenna over T consecutive symbol periods. Furthermore, $\boldsymbol{H}[i]$ is a $(N \times M)$-element matrix, whose elements represent the fading between a transmit-receive antenna pair, $\boldsymbol{S}[i]$ is the $(N \times T)$-element MIMO signal block and i is the block index. The fading is assumed to be constant over a MIMO-symbol interval, and changes independently from block to block in an uncorrelated manner. Finally, $\boldsymbol{V}[i]$ is a $(N \times T)$-element matrix, whose n^{th} row represents the additive white Gaussian noise (AWGN) at the n^{th} receive antenna over the MIMO symbol period T, which is modelled as an i.i.d AWGN process with zero mean and a variance of $N_0/2$ per dimension.

To be more specific, MIMO systems may be classified into four categories [5], namely the diversity architecture, the multiplexing architecture, the multiple access architecture and the beamforming architecture. These four categories of MIMOs are briefly summarized below.

1.1.1 Spatial Diversity

Spatial diversity is used in wireless communications systems for combatting small scale fading and thereby for improving the link's reliability. The basic principle is that several replicas of the same information sequence are independently transmitted and received by employing multiple antennas and thereby increasing the probability that at least some of the links will not be

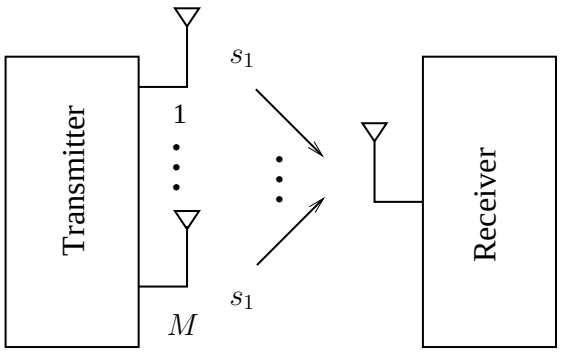

Figure 1.1: Simplified spatial transmit diversity scheme, where M transmit AEs transmit the same signal s_1 through a number of M independent transmission path.

subjected to deep fading. For the sake of experiencing independent fading, the antennas have to be spaced as far apart as possible. More specifically, the signals transmitted from or received at the antennas that are spaced more than say five times the wavelength may be expected to be independent.

Spatial diversity schemes fall into two main categories: receive diversity and transmit diversity arrangements. Receive diversity is the classic diversity technique [6], where multiple antennas are employed at the receiver for combining the independently fading signals. Given the requirement of a sufficiently high spacing, they are more suitable for the uplink. Receive diversity techniques include equal gain combining (EGC), selection combining (SC) and maximal ratio combining (MRC). The upper bound on the capacity of receive diversity schemes employing different diversity-combining techniques were derived in [7]. Although receive diversity was shown to provide an achievable diversity order which is equal to the number of receive antennas employed, it is not practical to employ multiple antennas in the handset. In order to facilitate diversity-aided transmissions, a simple but witty transmit diversity was proposed in [8], which inspired a spate of transmit diversity ideas, as proposed in [9–12]. Furthermore, another transmit diversity concept namely space-time spreading (STS) was also proposed [13] for the downlink of wideband code division multiple access (WCDMA), which is capable of achieving a beneficial transmit diversity gain. Attaining a transmit diversity gain is more practical than achieving a receive diversity gain for the downlink, since the user terminals are typically small in size and have a severe power consumption constraint. The maximum diversity order achievable by a multiple-antenna architecture is equal to $(M \cdot N)$, where M and N are the number of transmit and receive antennas respectively and each of the channel links between a transmit and a receive antenna pair is assumed to be independently faded. A simple spatial transmit diversity oriented MIMO scheme is illustrated in Figure 1.1, where M transmit AEs transmit the same replica of the signal s_1.

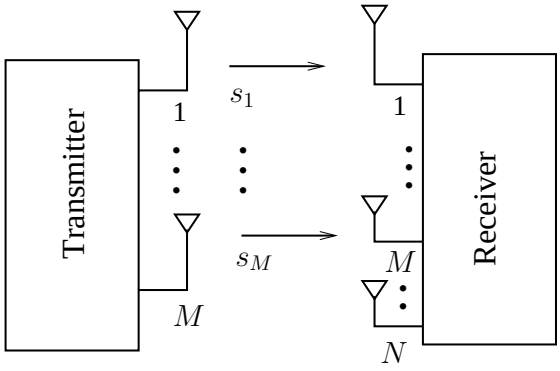

Figure 1.2: Spatial division multiplexing (SDM) having M transmit and N receive AEs. It is assumed that $N > M$, hence the achievable multiplexing or degrees-of-freedom gain is $N_S = \min(M, N) = M$, and a maximum of M data stream may be transmitted.

1.1.2 Spatial Division Multiplexing

MIMO systems may be designed for attaining an improved bandwidth efficiency by transmitting different signal streams indepently over each of the transmit antennas. Again, the pioneering studies by Paulraj and Kailath [14], Foschini [15] and Telatar [16] reveal that MIMO systems have the potential of high-rate transmission without the requirement of additional bandwidth. For example, the vertical Bell Laboratories layered space-time (V-BLAST) [17] code has the capability of attaining a high spatial division multiplexing (SDM) gain at the cost of a substantially increased decoding complexity. The achievable capacity was shown to be proportional to the number of antennas used [1].

The spatial division multiplexing MIMO systems are illustrated by Figure 1.2. Spatial multiplexing arises from the fact that the MIMO channel can be decomposed into a number of independent parallel channels. Multiplexing independent data streams onto these independent channels results in a commensurately increased throughput. The increased throughput normalized by the throughput of a single-antenna system is termed as the multiplexing gain. If the MIMO system is equipped with M transmit and N receive AEs, then the maximum achievable multiplexing gain is given by $N_S = \min(M, N)$.

Considering the MIMO channel model formulated in (1.1) and dropping the block index i for the sake of simplicity, the channel matrix $\boldsymbol{H}$ may be equivalently expressed by its singular value decomposition (SVD) as follows:

$$\boldsymbol{H} = \boldsymbol{Q}\boldsymbol{\Xi}\breve{\boldsymbol{Q}}^H, \tag{1.2}$$

where $\boldsymbol{Q} \in \mathbb{C}^{N\times N}$ and $\breve{\boldsymbol{Q}} \in \mathbb{C}^{M\times M}$ are unitary matrices, $\boldsymbol{\Xi} \in \mathbb{C}^{N\times M}$ is a diagonal matrix of the ordered singular values σ_i of $\boldsymbol{H}$ ($\sigma_1 \geq \sigma_2 \geq \cdots \geq \sigma_{r_H}$ and $\lambda_i = \sigma_i^2$ are the eigenvalues λ_i of $\boldsymbol{H}\boldsymbol{H}^H$. Note that there are r_H singular values, where r_H is the rank of the matrix $\boldsymbol{H}$. If $\boldsymbol{H}$ has a full rank, as characterized by a rich scattering environment, then we have

$r_H = \min(M, N)$. Otherwise, under a rank-deficient scenario characterized by a high correlation among the individual channel gains of the MIMO channel, we have $r_H < \min(M, N)$.

The parallel decomposition of the channel may be achieved by defining two transformations [18, 19]:

$$\boldsymbol{S} := \breve{\boldsymbol{Q}}\tilde{\boldsymbol{S}} \tag{1.3}$$

$$\tilde{\boldsymbol{Y}} := \boldsymbol{Q}^H\boldsymbol{Y} \tag{1.4}$$

Note that the transformations (1.3) and (1.4) have been chosen for converting $\boldsymbol{S}$ to $\tilde{\boldsymbol{S}}$ and $\boldsymbol{Y}$ to $\tilde{\boldsymbol{Y}}$, respectively using $\breve{\boldsymbol{Q}}$ and $\boldsymbol{Q}$, respectively which are obtained by the SVD of the channel matrix $\boldsymbol{H}$ given by (1.2). Hence, (1.3) and (1.4) may br termed as the *transmit precoding* and *receiver shaping*, respectively.

Upon applying the above two transformations to (1.1) and making use of (1.2) where both $\boldsymbol{Q}$ and $\breve{\boldsymbol{Q}}$ are unitary matrices, we arrive at:

$$\begin{aligned}
\tilde{\boldsymbol{Y}} &= \boldsymbol{Q}^H\boldsymbol{Y} \\
&= \boldsymbol{Q}^H(\boldsymbol{H}\boldsymbol{S} + \boldsymbol{V}) \\
&= \boldsymbol{Q}^H\left(\boldsymbol{Q}\boldsymbol{\Xi}\breve{\boldsymbol{Q}}^H\boldsymbol{S} + \boldsymbol{V}\right) \\
&= \boldsymbol{Q}^H\boldsymbol{Q}\boldsymbol{\Xi}\breve{\boldsymbol{Q}}^H\breve{\boldsymbol{Q}}\tilde{\boldsymbol{S}} + \breve{\boldsymbol{Q}}^H\boldsymbol{V} \\
&= \boldsymbol{\Xi}\tilde{\boldsymbol{S}} + \tilde{\boldsymbol{V}},
\end{aligned} \tag{1.5}$$

where $\tilde{\boldsymbol{V}} = \boldsymbol{Q}^H\boldsymbol{V} \sim \mathcal{CN}(0, N_0\boldsymbol{I}_M)$ has the same distribution as $\boldsymbol{V}$. We see in (1.5) that the MIMO channel is now decomposed into r_H independent parallel channels, which may be modelled as shown in Figure 1.3.

1.1.3 Spatial Division Multiple Access

Space-division multiple access (SDMA) employs multiple antennas for the sake of supporting multiple users [20, 21]. In this scheme, the transmitted signals of a number of simultaneous uplink mobile users (where each user is equipped with a single transmit antenna) are received by different receive antennas of the base station (BS). More explicitly, SDMA systems rely on the unique, user-specifc spatial signatures constituted by their channel impulse responses (CIRs) for separating the different users' signal [5]. Similarly to SDM, SDMA allows us to increase the capacity of a mobile cellular system by exploiting the users' spatial separation, which leads to unique CIRs. Both the SDM and the SDMA schemes benefit from a capacity gain achieved by decomposing the multiplexed MIMO channels into parallel channels. However, SDMA differs from the VBLAST-like spatial division multiplexing schemes in that SDMA utilizes its multiplexing gain for supporting an increased number of users, whereas spatial division multiplexing exploits it in order to increase the throughput of a single-user link.

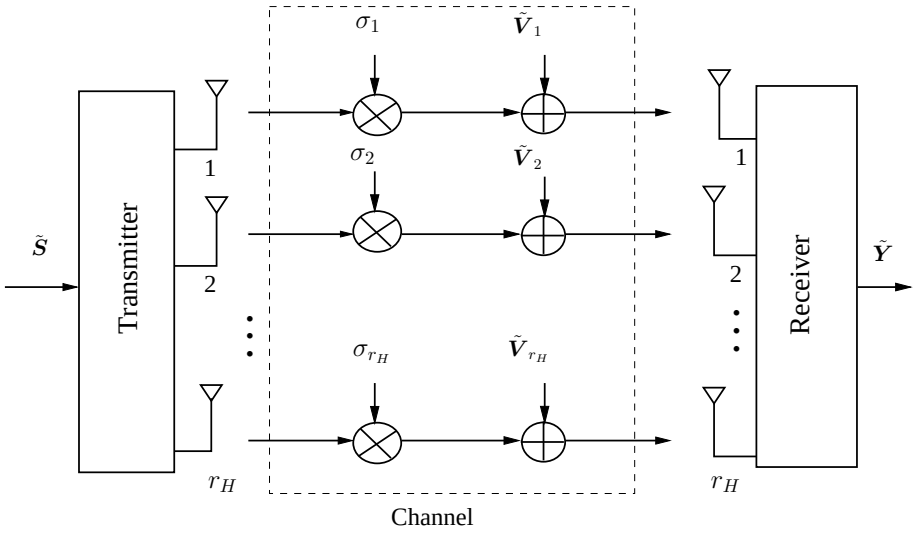

Figure 1.3: Spatial division multiplexing MIMO channel decomposed into $r_H = \min(M, N)$ number of independent channels employing the transformations (1.3) and (1.4), where $\tilde{\boldsymbol{S}}$ and $\tilde{\boldsymbol{Y}}$ have been transformed from the input and output signals $\boldsymbol{S}$ and $\boldsymbol{Y}$ respectively using $\breve{\boldsymbol{Q}}$ and $\boldsymbol{Q}$, respectively obtained by the SVD of the channel matrix $\boldsymbol{H}$ given by (1.2).

1.1.4 Beamforming

Beamforming architectures are specifically designed for reducing the interference levels with the aid of creating angularly selective beams [22–25]. Typically, half-wavelength spaced antenna elements are used for creating a spatially selective transmitter/receiver beam. Again, beamforming assists in mitigating the effects of co-channel interference (CCI), provided that the interference components arrive from sufficiently different directions. Hence they are capable of supporting multiple users by angularly separating them. This type of angular separation becomes possible, when the different users are distinguished by their different direction-of-departure (DOD) and/or direction-of-arrival (DOA).

1.2 MIMO Systems: Historical Perspective and Major Contributions

MIMO sytems have been investigated for decades. Diversity combining schemes, such as equal gain combining (EGC), selection combining (SC) and maximum ratio combining (MRC) can be traced back to the 1950s with reference to Brennan's excellent paper [6], while Kaye and George [26] introduced the idea of multiplexed pulse-amplitude-modulated (PAM) transmission employing diversity and multichannel operation. The early forms of MIMO systems including phased arrays used for beamforming were studied in [27–30]. In 1993, Wittneben [31] proposed a modulation scheme for multiple transmit antennas. On the other hand, MIMO systems were

first conceived by Paulraj and Kailath [14] for providing a beneficial multiplexing gain. Specifically, they observed that co-channel wireless signals emerging from closely spaced transmit antennas were potentially separable by an adaptive receiver antenna array in the presence of scattering. Paulraj and Kailath in [14] patented the "Distributed Transmit - Directional Receive (DTDR)" concept originally conceived for broadcast applications. Later, Foschini [15] introduced the spatial multiplexing concept in 1996 under the terminology of Bell Laboratories space-time (BLAST) codes, which later evolved to a modified architecture proposed by Wolniansky termed as the vertical BLAST or V-BLAST arrangement in 1998 [17]. The characterization of the maximum throughput supported at a given channel outage percentage corroborated the proposal of [14], namely that for a fixed radiated power and bandwidth, the capacity increases linearly with the number of transmit-receive antenna pairs, which was further supported by Telatar [16]. The concept of achieving transmit diversity rather than the conventional receive diversity of [6] was proposed by Alamouti [8], which was later extended to space-time block codes [9] by Tarokh *et al.* In order to strike a flexible trade-off between the achievable diversity and mutiplexing gain, Hochwald and Hassibi [11] proposed linear dispersion codes (LDCs), which were extended by Heath and Paulraj [32] based on frame theory. The state-of-the-art contributions on spatial diversity and spatial multiplexing schemes are summarized in Table 1.1, while those on beamforming, SDMA and multifunctional MIMO systems are summarized in Table 1.2.

In contrast to these classic MIMOs, Chau and Yu [46] conceived the space modulation philosophy, which allocates source bits to antenna elements (AEs) and simultaneously activates multiple AEs. Again, Mesleh *et al.* introduced the concept of spatial modulation (SM) for activating only one of the transmit antennas at a time, where the antenna index itself carries additional information, thus attaining an increased throughput [47]. This developement was followed by Jeganathan *et al.* [48], who simply used the presence or absence of energy to transmit information without using any signal constellations, which led to the concept of space-shift keying (SSK). By intrinsically amalgamating the concept of LDCs and the recently developed concept of spatial modulation (SM) [47] as well as space-shift keying (SSK) [48], Sugiura *et al.* proposed the design philosophy of space-time shift keying (STSK) [49].

Although the STSK scheme exhibits an excellent performance in narrowband channels, its performance in wideband channels is eroded. Hence, in order to mitigate the performance degradation experienced in dispersive channels, we conceive a suite of multicarrier systems, such as orthogonal frequency division multiplexing (OFDM), multicarrier code division multiple access (MC-CDMA), orthogonal frequency division multiple access (OFDMA) and/or single carrier frequency division multiple access (SC-FDMA) combined both with coherently and differentially detected STSK. We also propose a range of coherent and noncoherent cooperative MC-CDMA STSK schemes employing successive relaying (SR) for recovering the half-duplex

Table 1.1: Major contributions conceived for different MIMO applications: Part 1

Category	Year	Author(s)	Contribution
Diversity	1959	Brennan [6]	Introduced and analyzed EGC, SC and MRC.
	1993	Wittneben [31]	A modulation scheme was proposed for multiple transmit antennas.
	1994	Seshadri and Winters [33]	A transmit diversity scheme was inspired by Wittneben's delay diversity design.
	1998	Alamouti [8]	Proposed a transmit diversity scheme relying on two antennas.
		Tarokh *et al.* [9]	Conceived space-time block codes based on orthogonal designs.
		Tarokh *et al.* [10]	Provided design criteria for achieving the maximum attainable diversity and coding gain.
	2000	Hughes [34]	Introduced a new DSTBC design based on group codes.
		Jafarkhani *et al.* [35]	Proposed a differential detection scheme for transmit diversity arrangements.
	2004	B. L. Yeap and L. Hanzo [36]	Conceived reduced-complexity turbo detection for STTC.
	2006	T.-H. Liew and L. Hanzo [37]	Studied STBC and space-time trellis code (STTC) versus adaptive Modulation and coding aided OFDM in wideband channels.
Multiplexing	1994	Paulraj and Kailath [14]	Patented the first spatial multiplexing scheme conceived for broadcast applications.
	1996	Foschini [15]	Conceived the encoding and decoding of the diagonal BLAST structure.
	1998	Wolniansky *et al.* [17]	The V-BLAST architecture was introduced for reducing complexity in implementing Foscini's approach [15].
	1999	Telatar [16]	Quantified the MIMO channel capacity.
		Golden *et al.* [38]	Provided the detection strategy and initial real-time demonstration of BLAST.
	2005	Huang *et al.* [39]	Bayesian method of detection for BLAST was proposed.

Table 1.2: Major contributions categorized on different MIMO applications: Part 2

Category	Year	Author(s)	Contribution
Beamforming	1976	S. Applebaum [27]	Adaptive antenna arrays were studied for adaptively optimizing the signal-to-noise ratio of an antenna array.
	1984	Winters [28]	Optimal diversity combiner for antenna arrays was proposed.
	1994	Winters and Salz [29]	The impact of diversity of directional transmission on the capacity was studied.
	1996	H. Krim and M. Viberg [30]	Two decades of array signal processing research were reviewed.
	1997	L.C. Godara [23]	Antenna arrays were proposed for mobile communications and their performance was studied.
SDMA	1996	M. Cooper and M. Goldburg [21]	Introduced spatial division multiple access.
	2000	Vandenameele *et al.* [40]	Amalgamated OFDM with SDMA.
	2005	M. Munster and L. Hanzo [41]	Parallel interference cancellation aided SDMA-OFDM systems were conceived.
Multifunctional	1999	Tarokh *et al.* [42]	Combined beamforming and space-time coding was advocated.
	2001	Hochwald *et al.* [13]	The concept of space-time spreading was proposed for CDMA.
	2002	Hassibi and Hochwald [11]	LDCs were introduced for achieving a flexible diversity-multiplexing tradeoff.
		R.W.J. Heath & A. Paulraj [32]	Improved LDC designs based on frame theoretic matrix linearization were advocated.
	2003	J. Liu and E. Gunawan [43]	Combined beamforming with Alamouti's transmit diversity scheme.
	2004	H. Kim and J. Chun [44]	Proposed a MIMO structure, which combines spatial multiplexing and beamforming.
		M. Tao and R. S. Cheng [45]	Proposed a generalized layered space-time code for high-rate communications.
	2009	Hanzo *et al.* [5]	Elaborated LDC design based on CCMC capacity and DCMC capacity criterion.

throughput loss of conventional relaying schemes.

The major contributions related to spatial modulation (SM), space-shift keying(SSK) and space-time shift keying (STSK) are summarized in Table 1.3.

1.3 Multicarrier Systems

Multicarrier modulation-aided wireless communications systems were first conceived and implemented with the aid of analog oscillators in the 1960s. But it was not until the 1990s, when they were included in numerous standards conceived for diverse applications, because their all-digital implementations became feasible with the aid of the discrete Fourier transform (DFT). Hence, they sparked widespread interest in various single-user and multiuser applications. The rudimentary idea is to divide the transmit bitstream into many low-rate bitstreams, which are transmitted in parallel over different-frequency subchannels. The transmission rate of each subchannel is thus considerably reduced and the corresponding subchannel bandwidth becomes much lower than the overall system's bandwidth. If the number of subchannels is chosen so that each subchannel bandwidth becomes lower than the channel's coherence bandwidth, then each of the individual subchannel signals experiences frequency-flat fading. Additionally, the inter-symbol interference (ISI) imposed by dispersive channels can be mitigated by introducing a sufficiently long cyclic prefix (CP).

1.3.1 Orthogonal Frequency Division Multiplexing

Again, orthogonal frequency division multiplexing (OFDM) was ratified by numerous standardization bodies, such as the European Digital Audio Broadcasting (DAB) [58] and the Digital Video Broadcasting (DVB) [59] standards. OFDM was also proposed for Digital Cable Television Systems [60] and Local Area Mobile Wireless Networks such as the IEEE 802.11a [61] and HIPERLAN/2 [62]. OFDM transmissions are motivated mainly by two of its most attractive features: it is bandwidth-efficient and the equalization of dispersive slow fading channels requires low-complexity single-tap multiplications. Furthermore, the digital implementation of OFDM employing DFT is convenient.

To elaborate on the concept of parallel data transmissions, it was introduced by Doelz *et al.* [63] in 1957 and the first OFDM scheme was proposed by Chang [64] in 1966 for dispersive channels. Weinstein *et al.* [66] demonstrated that the OFDM modulation/demodulation can be efficiently performed using the DFT, which was a driving force behind the development of the OFDM scheme. In 1985, Cimini [68] proposed OFDM for mobile communications, whereas its application for digital broadcasting was proposed by Alard and Lassale [69] in 1985 and 1987 respectively. Van Nee and Prasad advocated OFDM for multimedia communications [71]. The

Table 1.3: Major contributions on SM/SSK/STSK

Year	Author(s)	Contribution
2001	Chau and Yu [46]	Conceived the space modulation philosophy, which allocates source bits to antenna elements (AEs) and simultaneously activates multiple AEs.
2006	Mesleh *et al.* [50]	Proposed spatial modulation (SM) for low-complexity spectral efficiency enhancement.
2008	Mesleh *et al.* [47]	Presented an analytical investigation of SM.
	Mesleh *et al.* [51]	Analyzed the symbol-error-ratio (SER) of SM.
2009	Jeganathan *et al.* [48]	Conceived space shift keying (SSK).
	Jeganathan *et al.* [52]	Studied SM as well as SSK and proposed a single-stream optimal ML detection algorithm.
2010	S. Sugiura *et al.* [53]	Proposed a unified MIMO scheme subsuming SSK, OSTBC, BLAST and LDC.
	S. Sugiura *et al.* [49]	Introduced both coherent and differential STSK based on LDCs.
	S. Sugiura *et al.* [54]	Proposed both coherent and noncoherent cooperative STSK.
	S. Sugiura *et al.* [55]	Conceived reduced-complexity detectors for QAM-aided STSK schemes.
2011	S. Sugiura *et al.* [56]	Introduced a generalized space-time shift keying arrangement.
2012	S. Sugiura *et al.* [57]	Provided a survey of STSK as a universal MIMO space-time architecture.

Table 1.4: Major contributions on OFDM

Year	Author(s)	Contribution
1957	Doelz [63]	The concept of parrallel data transmission was introduced.
1966	Chang [64]	The concept of OFDM was proposed for dispersive channels.
1970	Chang [65]	U.S. Patent 3,488,445 on OFDM was issued.
1971	Weinstein and Ebert [66]	DFT was first applied for OFDM modulation.
1981	Hirosaki [67]	Suggested a refined DFT-based implementation of OFDM.
1985	Cimini [68]	The feasibility of OFDM in mobile communications was studied.
1987	Alard and Lasalle [69]	Proposed OFDM for digital broadcasting.
1991	Cioffi [70]	Introduced the ANSI ADSL standard.
1999		IEEE 802.11a standard
2000	V. Nee and Prasad [71]	First book on OFDM.
	C. Lee, T. Keller and L. Hanzo [72]	Designed enhanced turbo-coded OFDM receivers for DVB-T.
2003	L. Hanzo *et al.* [73]	Design-recipes and analytical insights were detailed in the context of broadband multiuser communications, WLANs and broadcasting.
2005	Williams *et al.* [74]	A pre-FFT synchronisation method was designed for OFDM.
2009	Chen *et al.* [75]	Spectrum sensing of pilot tone based OFDM systems was studied.

major contributions on OFDM can be summarized in Table 1.4.

OFDM constitutes a block-based transmission technique. The simplified architecture of an OFDM-aided transceiver is shown in Figure 1.4. Let the N_c frequency-domain (FD) data symbols of the $k-$th OFDM block to be transmitted over N_c subchannels be represented by

$$\boldsymbol{X}_k = [X_k[1] \quad X_k[2] \quad \dots \quad X_k[N_c]]^T. \tag{1.6}$$

Furthermore, let the N_c-point DFT and inverse DFT (IDFT) matrices be represented by $\boldsymbol{\mathcal{F}}_{N_c}$ and $\boldsymbol{\mathcal{F}}_{N_c}^H$ respectively, so that we have $\boldsymbol{\mathcal{F}}_{N_c}\boldsymbol{\mathcal{F}}_{N_c}^H = \boldsymbol{\mathcal{F}}_{N_c}^H\boldsymbol{\mathcal{F}}_{N_c} = \boldsymbol{I}_{N_c}$, where $\boldsymbol{I}_{N_c}$ is the $(N_c \times N_c)-$element identity matrix. Then we can represent the time-domain (TD) signal $\boldsymbol{x}_k = [x_k[1] \quad x_k[2] \quad \dots \quad x_k[N_c]]^T$ as

$$\boldsymbol{x}_k = \boldsymbol{\mathcal{F}}_{N_c}^H \boldsymbol{X}_k. \tag{1.7}$$

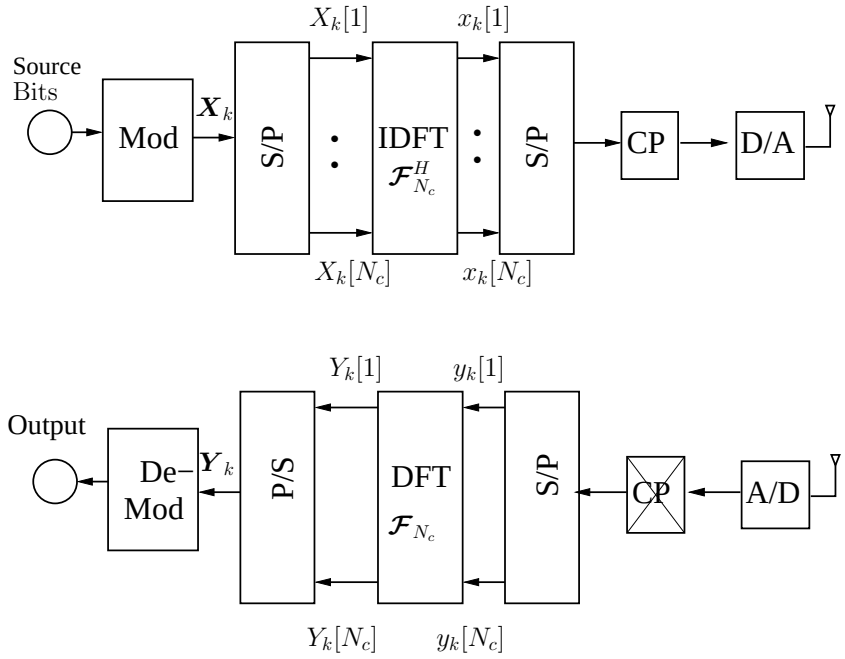

Figure 1.4: Simplified OFDM transceiver architecture.

When the OFDM signal of (1.7) is transmitted over a frequency-selective channel having a CIR-length L given by $\boldsymbol{h} = [h[1] \quad h[2] \quad \dots \quad h[L]]^T$, the noiseless channel output $\boldsymbol{y}_k = [y_k[1] \quad y_k[2] \quad \dots \quad y_k[N_c]]^T$ may be represented by

$$y_k[i] = x_k[i] \star h[i] = \sum_{l=1}^{L} h[l]\, x_k[i-l], \qquad i = 1, 2, \dots, N_c \tag{1.8}$$

When a cyclic prefix (CP) having a minimum length of $L_{\text{cp}} = (L-1)$ is appended to the TD transmit signal $\boldsymbol{x}_k$, the resultant signal is denoted by $\tilde{\boldsymbol{x}}_k$. Then the linear convolution of (1.8) is converted to the N_c-point circular convolution of

$$y_k[i] = \tilde{x}_k[i] \star h[i] = x_k[i] \circledast h[i] = \sum_{l=1}^{L_{\text{cp}}+1} h[l]\, x_k[i-l]_{N_c}, \qquad i = 1, 2, \dots, N_c \tag{1.9}$$

where $[i-l]_{N_c}$ denotes $[i-l]$ modulo N_c. The incorporation of a CP thus benefits from the specific circular convolution property that the TD circular convolution leads to multiplication in the FD, yielding

$$Y_k[n_c] = \text{DFT}_{N_c}\{y_k[i] = x_k[i] \circledast h[i]\} = X_k[n_c]\, H_k[n_c], \qquad n_c = 1, 2, \dots, N_c. \tag{1.10}$$

In order to provide a compact matrix-based representation of the system, both the channel's output sequence $y_i = y_k[i]$ relying on the input $x_i = x_k[i]$ and the channel transfer function

$h_i = h[i]$ as well as the additive noise $v_i = v_k[i]$ may be expressed in matrix form as [18]

$$\begin{bmatrix} y_1 \\ y_2 \\ \vdots \\ y_{N_c} \end{bmatrix} = \begin{bmatrix} h_{L_{\text{cp}}+1} & h_{L_{\text{cp}}} & \cdots & h_1 & 0 & \cdots & 0 \\ 0 & h_{L_{\text{cp}}+1} & \cdots & h_2 & h_1 & \cdots & 0 \\ \vdots & \vdots & \ddots & \ddots & \ddots & \ddots & \vdots \\ 0 & \cdots & 0 & h_{L_{\text{cp}}+1} & \cdots & h_2 & h_1 \end{bmatrix} \begin{bmatrix} x_{-L_{\text{cp}}+1} \\ \vdots \\ x_0 \\ x_1 \\ \vdots \\ x_{N_c} \end{bmatrix} + \begin{bmatrix} v_1 \\ v_2 \\ \vdots \\ v_{N_c} \end{bmatrix} \tag{1.11}$$

which may be written more compactly as

$$\boldsymbol{y} = \boldsymbol{H}\boldsymbol{x} + \boldsymbol{v}. \tag{1.12}$$

The symbols $x_0 = x_k[N_c], \ldots, x_{-L_{\text{cp}}+1} = x_k[N_c - L_{\text{cp}} + 1]$ correspond to the CP. Furthermore, the received symbols $y_0, \ldots, y_{-L_{\text{cp}}+1}$ are affected by the intersymbol interference (ISI) imposed by the previous TD OFDM block, albeit this has not been shown in (1.11).

Equation (1.11) may be further reduced to

$$\begin{bmatrix} y_1 \\ y_2 \\ \vdots \\ y_{N_c} \end{bmatrix} = \begin{bmatrix} h_1 & 0 & \cdots & h_{L_{\text{cp}}} & \cdots & h_3 & h_2 \\ h_2 & h_1 & \cdots & h_{L_{\text{cp}}+1} & \cdots & h_3 & h_3 \\ \vdots & \vdots & \ddots & \ddots & \ddots & \ddots & \vdots \\ h_{L_{\text{cp}}+1} & h_{L_{\text{cp}}} & \cdots & h_1 & \ddots & 0 & 0 \\ \vdots & \vdots & \ddots & \ddots & \ddots & \ddots & \vdots \\ 0 & 0 & \cdots & h_{L_{\text{cp}}} & \ldots & h_1 & 0 \\ 0 & 0 & \cdots & h_{L_{\text{cp}}+1} & \cdots & h_2 & h_1 \end{bmatrix} \begin{bmatrix} x_1 \\ x_2 \\ \vdots \\ \vdots \\ x_{(N_c-1)} \\ x_{N_c} \end{bmatrix} + \begin{bmatrix} v_1 \\ v_2 \\ \vdots \\ v_{N_c} \end{bmatrix}, \tag{1.13}$$

which may be expressed more compactly as

$$\boldsymbol{y} = \breve{\boldsymbol{H}}\boldsymbol{x} + \boldsymbol{v}, \tag{1.14}$$

where the channel has been modelled by the *circulant* matrix, $\breve{\boldsymbol{H}} \in \mathbb{C}^{N_c \times N_c}$.

The employment of the circulant matrix [76] in this context is advantageous, because the eigen-value decomposition (EVD) of the circulant matrix $\breve{\boldsymbol{H}}$ results in a diagonal matrix $\boldsymbol{D} \in \mathbb{C}^{N_c \times N_c}$, containing the eigenvalues of $\breve{\boldsymbol{H}}$ along its main diagonal. To be more specific, $\breve{\boldsymbol{H}}$ may be decomposed into:

$$\breve{\boldsymbol{H}} = \boldsymbol{\mathcal{F}}_{N_c}^H \boldsymbol{D} \boldsymbol{\mathcal{F}}_{N_c}, \tag{1.15}$$

where we have

$$\boldsymbol{D} = \text{diag}\left\{ \boldsymbol{\mathcal{F}}_{N_c} \begin{bmatrix} h_1 & \cdots & h_{L_{\text{cp}}+1} & 0 & \cdots & 0 \end{bmatrix}^T \right\} \in \mathbb{C}^{N_c \times N_c}. \tag{1.16}$$

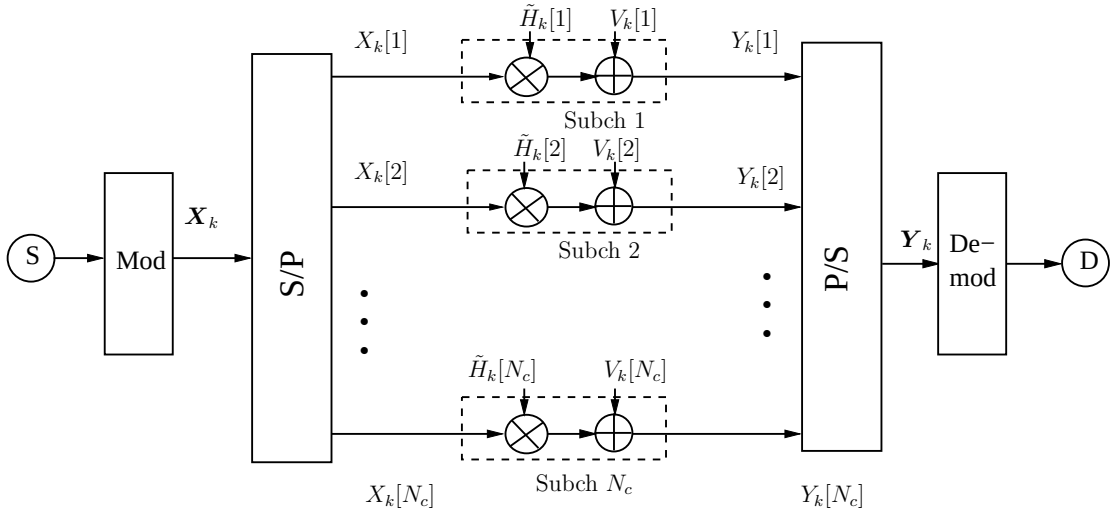

Figure 1.5: Simplified OFDM model portraying transmission over a number of non-dispersive channels.

The diagonal matrix $\boldsymbol{D}$ contains the Fourier transform of the channel transfer functions along its main diagonal defined as the channel's frequency response, where we define the channel's frequency response matrix $\tilde{\boldsymbol{H}}$ as

$$\tilde{\boldsymbol{H}} \triangleq \boldsymbol{D} \in \mathbb{C}^{N_c \times N_c}. \tag{1.17}$$

Substituting (1.15) and (1.16) in (1.10), we arrive at:

$$\begin{aligned} \boldsymbol{Y} &= \boldsymbol{\mathcal{F}}_{N_c} \boldsymbol{\mathcal{F}}_{N_c}^H \boldsymbol{D} \boldsymbol{\mathcal{F}}_{N_c} \boldsymbol{x} + \boldsymbol{\mathcal{F}}_{N_c} \boldsymbol{v} \\ &= \boldsymbol{\mathcal{F}}_{N_c} \boldsymbol{\mathcal{F}}_{N_c}^H \tilde{\boldsymbol{H}} \boldsymbol{\mathcal{F}}_{N_c} \boldsymbol{\mathcal{F}}_{N_c}^H \boldsymbol{X} + \boldsymbol{\mathcal{F}}_{N_c} \boldsymbol{v} \\ &= \tilde{\boldsymbol{H}} \boldsymbol{X} + \boldsymbol{V}. \end{aligned} \tag{1.18}$$

Since $\tilde{\boldsymbol{H}}$ is a diagonal matrix in the form $\tilde{\boldsymbol{H}} = \text{diag}\left\{\tilde{H}\left[1\right], \tilde{H}\left[2\right], \ldots, \tilde{H}\left[N_c\right]\right\}$, it is plausible that the channel's output $Y_k\left[n_c\right]$ corresponding to subcarrier n_c can be expressed by the input and channel parameters of the corresponding subcarrier by

$$Y_k\left[n_c\right] = \tilde{H}_k\left[n_c\right] X_k\left[n_c\right] + V_k\left[n_c\right], \qquad n_c = 1, 2, \ldots, N_c \tag{1.19}$$

which implies that the individual subcarriers experience frequency-flat fading.

Figure 1.5 illustrates the transmission of the OFDM signal over a dispersive channel, which is decomposed into a number of non-dispersive frequency-flat subchannels. Although OFDM is highly beneficial for transmission over frequency-selective channels, it suffers from two disadvantages - the peak-to-average power ratio (PAPR) of the multicarrier signal is high, hence it requires a high-linearity amplifier and the synchronization at the receiver becomes complex.

It is worth noting at this point that the decomposition of the OFDM system's dispersive channel into narrowband parallel subchannels is reminiscent of that of the spatial division

multiplexing MIMO channel into independent parallel 'subchannels', as mentioned in Subsection 1.1.2. The difference, however, is that the DFT and IDFT matrices $\boldsymbol{\mathcal{F}}_{N_c}$ and $\boldsymbol{\mathcal{F}}_{N_c}^H$ obtained by the eigen-value decomposition (EVD) of the circulant matrix $\breve{\boldsymbol{H}}$ in (1.15) are not dependent on the specific realization of the dispersive channel, whereas the unitary matrices $\boldsymbol{Q}$ and $\breve{\boldsymbol{Q}}$ obtained by the singular-value decomposition (SVD) of $\boldsymbol{H}$ do depend on the MIMO channel [19].

The combination of OFDM with MIMO systems has attracted substantial interests due to OFDM's capability of converting realistic wideband channels into a number of narrowband subchannels. As mentioned in Subsection 1.1.2, MIMO systems are capable of increasing the capacity of the system, where the matrix algebra of MIMO systems is based on narrowband assumptions. Furthermore, OFDM facilitates the employment of single-tap linear equalizers at the receiver, which is highly beneficial in the context of MIMO systems. In 2001, Blum *et al.* [77] proposed an improved space-time coding arrangement for MIMO-OFDM. As a further advance, Piechocki *et al.* [78] characterized the performance of ML decoding in the context of V-BLAST based spatial multiplexing OFDM systems. Several MIMO-OFDM schemes were proposed in 2002 for enhancing the capacity and for mitigating the detrimental effects of both the inter-symbol interference (ISI) and of the co-channel interference (CCI) [3, 79, 80]. In 2007, Jiang and Hanzo [20] advocated multiuser MIMO-OFDM for employment in next generation wireless. In [81], the authors summarized the physical layer research challenges of MIMO-OFDM systems for broadband applications. Furthermore, Hanzo and Choi [82] studied High-Speed Downlink Packet Access (HSDPA)-style adaptive modulation assisted OFDM and MC-CDMA transceivers, while Chen *et al.* [75] introduced spectrum sensing in the context of pilot tone based OFDM systems in 2009. During the recent decade, MIMO-OFDM has been developed explosively, hence the major contributions on MIMO-OFDM are summarized in Table 1.5.

The simplified family-tree of multicarrier systems is shown in Figure 1.6. The most widespread family is constituted by OFDM, which dispenses with spreading and hence it is vulnerable to both time-domain (TD) and frequency-domain (FD) fading. This is why it was combined with TD, FD or multidimensional spreading, which led to the multicarrier direct sequence code division multiple access (MC DS-CDMA), FD-spread MC-CDMA or simply MC-CDMA and multidimensional MC-CDMA families, as shown in Figure 1.6. To elaborate a little further, the benefit of DS spreading is that even if a few chips of the DS spreading sequence are corrupted by TD fading, this only affects a fraction of the entire DS-spreading code. Hence the chances are that the corresponding data symbol might still be recovered [89]. Similarly, if a fraction of the FD-spreading code's chips are corrupted, this only partially affects some of the chips of the superimposed codes, hence still potentially allowing the spread subcarrier symbols to be recovered [73]. Finally, multidimensional MC-CDMA is capable of combining the benefits of TD and FD MC-CDMA. Let us now focus our attention on FD MC-CDMA, noting that the different types of MC-based CDMA systems will be compared in Chapter 3.

Table 1.5: Major contributions on MIMO-OFDM

Year	Author(s)	Contribution
2001	Blum *et al.* [77]	Improved space-time coding was proposed for MIMO-OFDM .
	Piechocki *et al.* [78]	Studied the performance of ML decoding-aided V-BLAST OFDM.
2002	Bolcskei, Gesbert and Paulraj [3]	Both the ergodic capacity and the outage capacity of spatial multiplexing aided MIMO OFDM were determined.
	Li *et al.* [79]	Space-time coding based MIMO OFDM was proposed for mitigating the ISI and for enhancing the system's capacity.
	Stamoulis *et al.* [83]	Studied STBC based MIMO OFDM for transmission over time-varying channels.
	Giangaspero *et al.* [80]	Two schemes were proposed for co-channel interference cancellation in MIMO OFDM systems.
2003	El-Gamal *et al.* [84]	Employed OFDM for frequency-selective MIMO channels to construct space-frequency codes (SFC) for exploiting the FD diversity.
	Moon *et al.* [85]	Proposed a peak-to-average power ratio (PAPR) control scheme for MIMO-OFDM.
2004	Stuber *et al.* [81]	Summarized the physical layer research challenges of MIMO-OFDM wireless systems.
	Huang and Letaief [86]	A coded OFDM-aided MIMO symbol-based space diversity scheme was conceived.
2005	Su *et al.* [87]	Proposed a full-rate, full-diversity OFDM-aided space-frequency code for MIMO assisted wireless systems.
	Borgmann and Bolcskei [88]	Non-coherent space-frequency coded OFDM was proposed for dispersive MIMO channels.
2006	Liew and Hanzo [37]	Investigated space-time block and space-time trellis codes versus adaptive modulation and coding (AMC) aided OFDM.
2007	Jiang and Hanzo [20]	Reduced-complexity genetic algorithm assisted multiuser MIMO-OFDM was investigated.

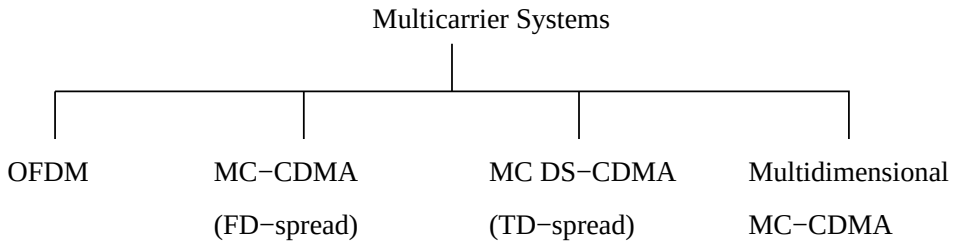

Figure 1.6: Simplified family-tree of multicarrier systems.

1.3.2 Multicarrier Code Division Multiple Access

Multicarrier code division multiple access (MC-CDMA) is a multiple access scheme, where the symbols of different users are first spread across the FD using unique, user-specific spreading sequences, which are then mapped to multiple parallel subcarriers.

The majority of breakthroughs associated with combining the multicarrier concepts with the code division multiple access (CDMA) philosophy were made in 1993. The underlying objective was to overcome the detrimental effects of dispersion in high-rate wireless systems, which were particularly vulnerable owing to their extremely short symbol duration. Historically speaking, Yee, Linnartz and Fettweis developed the MC-CDMA scheme of [90], which was later combined with convolutional codes by Fazel and Papke [91]. Chouly *et al.* [92] as well as DaSilva and Sousa developed the MC DS-CDMA scheme of [93], whereas the so-called multitone (MT)-CDMA scheme was developed by Vandendorpe [94], all in the same year. In 1997, Hara and Prasad [95] provided a well-cited overview of multicarrier based CDMA systems, while Hanzo *et al.* [73] contributed further detailed insights both on OFDM and MC-CDMA based systems in the context of wideband multiuser applications, including wireless local area networks (WLANs) and broadcasting.

1.3.3 Single-Carrier Frequency Division Multiple Access

In order to benefit from the above-mentioned multicarrier transmissions in overcoming the potential performance degradations typically experienced in dispersive channels, while reducing the peak-to-average power ratio (PAPR), the single-carrier frequency division multiple access (SC-FDMA) scheme has been proposed for supporting multiuser communications [96, 97]. Its employment is particularly beneficial in the uplink, because it assists in improving the mobile handset's power-efficiency and battery recharge time. Basically, SC-FDMA may be viewed as a DFT-precoded orthogonal frequency domain multiple access (OFDMA) scheme, which constitutes a multiuser version of OFDM. Since a block of TD symbols is transformed to the FD by employing the above-mentioned DFT-precoding, the FD fading only partially affects the TD symbols when communicationg over a frequency-selective channel. Hence, similarly to

the FD-spread MC-CDMA, it provides additional diversity benefits. As a further advantage, SC-FDMA relies on low-complexity single-tap frequency domain equalization (SC-FDE). In a SC-FDMA scheme, the available subcarriers may be allocated to the users in a contiguous manner, which was hence termed as the localized frequency domain multiple access (LFDMA) scheme [96]. Another design alternative is known as the interleaved frequency domain multiple access (IFDMA) arrangement. The IFDMA scheme is capable of further enhancing the achievable diversity gain by placing those carriers far apart in the FD, which otherwise would fade together. Apart from its low PAPR, SC-FDMA has the additional benefit that in a perfect synchronization scenario the orthogonality of the subcarriers is retained, hence the scheme is free from multiuser interference (MUI), albeit the FD equalization may impose self-interference (SI) [98].

The concept of FDE was first studied in [99]. However, the full benefit of SC-FDE was gradually realized after Sari *et al.* [100] proposed it as a low-complexity solution to digital terrestrial TV broadcasting, which was later reviewed by Falconer *et al.* [101,102]. The concept of SC-FDMA as a DFT-precoded OFDMA arrangement was proposed as a multiple-access scheme for the LTE system by Myung *et al.* [96] as well as by the Pan-European Wireless INitiative NEw Radio (WINNER) project [103] in the context of the uplink of wide area cellular systems. A comprehensive review of nonlinear FDE in the context of single-carrier modulation was provided in [104]. A range of recent advances in multicarrier systems was also elaborated on in [98], while SC-FDMA-based multiple antenna systems were modelled and analyzed by Wilzeck *et al.* in [105]. The major contributions on MC-CDMA, SC-FDMA and MIMO SC-FDMA are summarized in Table 1.6.

1.4 Cooperative Communications

Although space-time block codes [9], space-time trellis codes [10] and linear dispersion codes [11, 32] are capable of attaining a beneficial diversity gain, their tightly-packed co-located antennas may experience correlated fading. Hence, MIMO systems relying on co-located elements may suffer from a reduced spatial diversity gain. This diversity gain erosion is typically aggravated by shadow fading. Therefore cooperative communication techniques [110, 111] have been proposed as a remedy for mitigating the effects of spatially correlated fading. The first attempt towards cooperative communication was perhaps made by Van der Meulen, who introduced the three-terminal relay channel model of [112]. Cover and El Gamal [110] studied both discrete memoryless and additive white Gaussian noise (AWGN) relay channels and determined their capacity. The philosophy mentioned in [111] was referred to as *user cooperation*. Communication from the source to the destination without the aid of any other communicating terminal is usually termed as direct or point-to-point communication. By contrast, if there is at least

Table 1.6: Major contributions on MC-CDMA and SC-FDMA

Year	Author(s)	Contribution
1973	Walzman and Schwartz [99]	Introduced frequency domain equalization (FDE).
1993	Yee *et al.* [90]	The concept of FD MC-CDMA combining FD-spreading and OFDM was introduced.
	Fazel and Papke [91]	The performance of convolutional coded MC-CDMA was investigated.
	Chouly *et al.* [92]	Combined multicarrier techniques to DS-CDMA.
	DaSilva & Sousa [93]	Developed MC DS-CDMA.
	Vandendorpe [94]	Introduced the concept of multitone DS-CDMA.
1995	Sari *et al.* [100]	Proposed SC-FDE for digital terrestrial TV broadcasting.
1997	Hara and Prasad [95]	Provided an overview of MC-CDMA systems.
1998	Sorger *et al.* [106]	Introduced IFDMA applicable for both the uplink and the downlink of a mobile radio communications system.
2002	Falconer *et al.* [101]	SC-FDE was reviewed and compared to OFDM.
	Benvenuto and Tomasin [97]	Proposed a new FD decision feedback equalizer (DFE) for SC-FDE.
2003	Hanzo *et al.* [73]	The state-of-the-art in OFDM and MC-CDMA aided broadband multiuser communications, WLANs and broadcasting was reviewed.
2006	Myung *et al.* [96]	Introduced the concept of SC-FDMA for the wireless uplink.
2007	Wilzeck *et al.* [105]	Conceived a MIMO-SC-FDMA system model and analyzed the effect of carrier frequency offsets.
	Hanzo and Choi [82]	HSDPA-style OFDM and MC-CDMA transceivers were investigated.
2008	Berardinelli *et al.* [107]	A comparative performance study of OFDMA and SC-FDMA was carried out.
2010	Ciochina & Sari [108]	Another comparative study of OFDMA versus SC-FDMA was offered.
	Benvenuto *et al.* [104]	Provided a comprehensive review of nonlinear FDE in the context of single-carrier modulation.
2012	Dalakas *et al.* [109]	OFDMA and SC-FDMA were compared for satellite uplink.

one additional node willing to assist in their communication, then this arrangement may be referred to as user cooperation. In [111], the authors proposed user cooperation as a form of diversity. In [113], Laneman *et al.* studied the performance of important relaying protocols designed for fading channels.

In cooperative communications relay nodes are invoked for forwarding the signal from the source. The resource allocation scheme has to appoint relays, which are sufficiently far apart and hence do not experience correlated fading. A relay is said to be half-duplex when it cannot simultaneously transmit and receive. By contrast, the design of full-duplex relays, which are capable of simultaneously transmit and receive remains as open challenge at the time of writing. Hence, although the early literature focused on the information theoretic analysis of full-duplex relaying, the practical relay protocols are of half-duplex [113] nature. The cooperative diversity protocols studied in [113] employ different types of processing at the relay nodes as well as different combining schemes at the destination. There are two basic processing techniques at the relay nodes. Specifically, the amplify-and-forward (AF) protocol allows the relays to amplify their received signal before re-transmitting it. By contrast, the decode-and-forward (DF) relays decode the received message, re-encode it and re-transmits it.

Recently, the concept of cooperative STSK [54] was proposed for frequency-flat Rayleigh fading channels in order to benefit from cooperation. The introduction of successive relaying (SR) [114] is potentially capable of recovering the half-duplex multiplexing loss and hence it was successfully used in [115] for conceiving a near-capacity space-time coding architecture. Against this background, in Chapter 5, we will propose both coherent and noncoherent detection aided decode-and forward relaying assisted MC-CDMA cooperative STSK schemes.

1.5 Thesis Outline and Novel Contributions

1.5.1 Organization of the Thesis

Having briefly reviewed the literature related to the subject covered in this thesis, let us now highlight its outline, which is explicitly shown in Figure 1.7.

- Chapter 2: OFDM Aided Multicarrier Space-Time Shift Keying
  In Chapter 2, we propose the novel OFDM-aided space-time shift keying concept for facilitating STSK transmissions over dispersive channels without any performance degradation compared to the narrowband scenarios investigated in the literature. We provide the basic guidelines for amalgamating the multicarrier concept with the STSK scheme and elaborate on the different strategies that may be invoked for mapping the STSK codewords to the orthogonal subcarriers. Section 2.2 provides a brief review of the family of MIMO

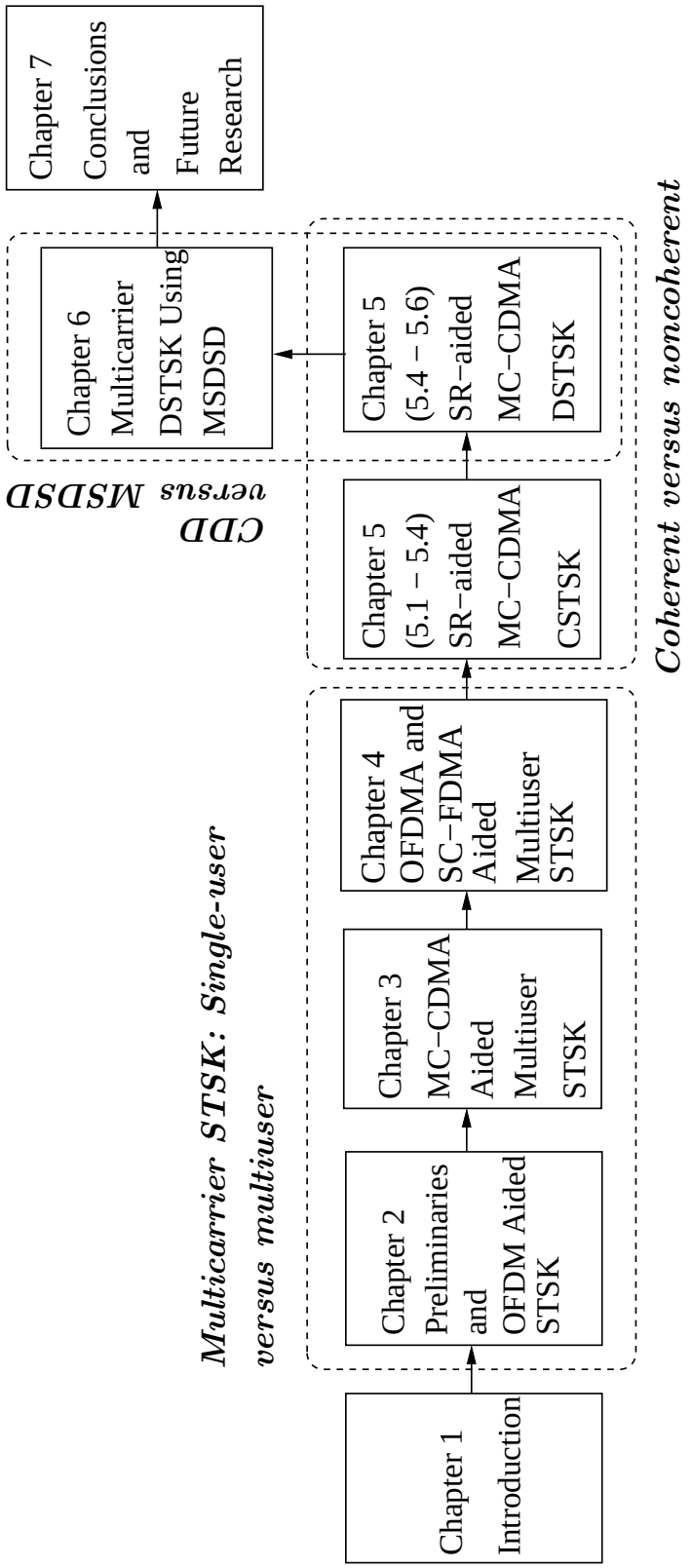

Figure 1.7: Outline of the thesis.

systems and outlines their chronological development, paving the way for the development of the STSK concept. The optimization of the DMs utilized in the STSK system will be reviewed in Section 2.3. The wideband channel model, the OFDM-aided STSK concept and the specific mapping of STSK codewords to OFDM subcarriers are illustrated in Section 2.4. We propose our channel-coded OFDM-aided STSK scheme in Section 2.5. Finally, Section 2.6 characterizes the achievable performance of our OFDM-aided STSK system.

- Chapter 3: MC-CDMA Aided Multiuser Space-Time Shift Keying
  In this chapter, we introduce the concept of MC-CDMA-aided multiuser STSK. Apart from mitigating the dispersion-induced performance degradation, this allows us to facilitate multiuser transmissions as well as to exploit the benefits accruing from FD spreading. We also conceive a near-capacity channel-coded MC-CDMA aided STSK arrangement in this chapter. Section 3.3 presents our channel model and our transceiver architecture proposed for both uplink and downlink scenarios, whereas the channel-coded design is elaborated on in Section 3.4. Section 3.5 characterizes the performance of both the uncoded and of our channel-coded MC-CDMA-aided STSK both in single-user and in multiuser scenarios.

- Chapter 4: OFDMA/SC-FDMA Aided STSK for Dispersive Multi-User Scenarios
  An OFDMA-aided multiuser STSK downlink and SC-FDMA-aided multiuser STSK uplink architecture is proposed for dispersive channels in this chapter. Furthermore, a novel reduced-complexity detector is conceived. Section 4.3 illustrates the associated transmission and decoding principles. The proposed reduced-complexity detector is detailed and characterized in terms of its complexity in Section 4.4, while an improved three-stage serially concatenated convolutional coded OFDMA/SC-FDMA-aided STSK arrangement is proposed in Section 4.5. Finally, the performance of the proposed scheme relying both on the localized and interleaved sub-carrier allocation regimes [96] is characterized in Section 4.6. The associated performance versus complexity trade-off and the PAPR of the SC-FDMA-aided STSK uplink are also detailed in Section 4.6.

- Chapter 5: Cooperative Multicarrier STSK Employing Successive Relaying
  In this chapter, we present a new successive relaying (SR)-aided coherent versus non-coherent selective decode-and forward relaying assisted cooperative multicarrier STSK scheme. We invoke SR for recovering the typical 50% throughput loss associated with the conventional half-duplex relaying and employ MC-CDMA for alleviating the performance degradation imposed by a single-carrier based STSK system as well as for mitigating both the SR-induced inter-relay interference (IRI) and the co-channel interference (CCI). A near-capacity channel-coded cooperative STSK arrangement is also proposed in this

chapter. Section 5.3 elaborates on the transmission protocol of the proposed cooperative multicarrier STSK scheme. Furthermore, a detection regime is conceived in Section 5.4 for combining the signals received from the direct source node (SN)-destination node (DN) link as well as from the relay nodes (RNs). We additionally design a noncoherent cooperative multicarrier STSK arrangement in Section 5.5 and its channel-coded soft-decision based cooperative multicarrier STSK counterpart in Section 5.6. Finally, the achievable performance of the decode-and- forward cooperative multicarrier system is investigated in Section 5.7.

- Chapter 6: MSDSD Aided Multicarrier Space-Time Shift Keying
  Chapter 6 proposes multiple-symbol differential sphere decoding (MSDSD)-aided differential STSK (DSTSK) for attaining an improved performance even in high-mobility dispersive channels by employing multiple-symbol detection, while imposing a reduced complexity by employing sphere decoding. The transmission model of both the hard-decision based MC DSTSK scheme, the associated channel model and the ML-MSDSD are described in Section 6.3. Section 6.4 elaborates on the iterative soft-decision based MC DSTSK scheme, on the maximum *a posteriori* MSDSD (MAP-MSDSD) philosophy advocated and on the generation of the soft information along with the overall soft-MSDSD-aided DSTSK architecture. The design criteria for the DMs employed and the complexity metrics employed for characterizing the proposed scheme are described in Section 6.5. Section 6.6 investigates the achievable performance of the proposed soft-MSDSD-aided DSTSK and its associated complexity.

- Chapter 7: Conclusions and Future Research
  In this chapter, we conclude with a summary of the results and provide future research directions. We conclude with a range of future research ideas.

1.5.2 Novel Contributions

The thesis is based on the published papers [116], [117], [118]− [119] and on the submitted paper [120]. The novel contributions of this thesis rely mainly on the amalgamation of multicarrier concepts with STSK-based MIMO systems. I propose OFDM, MC-CDMA and OFDMA/SC-FDMA aided STSK in this thesis. In order to further benefit from the distributed nature of cooperating nodes while avoiding the half-duplex throughput loss of conventional cooperative schemes, I propose both successive relaying aided coherent as well as noncoherent cooperative multi-carrier STSK systems. The novel contributions of this thesis may be summarized as follows:

- A novel OFDM aided STSK scheme for broadband channels is proposed [119]. More specifically, the SD, TD and FD spreading is amalgamated, since each sub-carrier carries one symbol of the STSK codewords.

- In order to mitigate the performance degradation imposed by dispersive channels, I also spread STSK space-time blocks to different sub-carriers of an MC-CDMA system, thus yielding an MC-CDMA STSK scheme [121]. Our simulations demonstrate that the EXIT trajectory of the proposed MC-CDMA aided STSK system reaches the point of perfect decoding convergence at $(I_A, I_E) = (1.0, 1.0)$, thus resulting in an infinitesimally low BER after a few iterations. It is worth mentioning here that I_A and I_E denote the *a priori* mutual information and the extrinsic mutual information, respectively, of the inner decoder of the concatenated coding arrangement used. The number of iterations required for achieving decoding convergence becomes lower upon increasing the value of the spreading factor.

- To mitigate the performance degradation imposed by dispersive channels, I also intrinsically amalgamate the OFDMA and SC-FDMA concept with the STSK system [117]. OFDMA/SC-FDMA aided STSK systems are capable of striking an attractive diversity-multiplexing tradeoff even in a multipath environment, whilst additionally supporting multiuser transmissions and maintaining a low PAPR in uplink SC-FDMA/STSK scenarios. A salient feature of our OFDMA/SC-FDMA STSK is that the OFDMA/SC-FDMA STSK signal can be detected at a low complexity, because the detection process does not rely on either the FD channel transfer function or the TD channel impulse response, while still benefitting from the inherent single-stream detection procedure of STSK. I quantify the relative merits of OFDMA and SC-FDMA, when combined with STSK and advocate the specific SC-FDMA based STSK scheme relying on the interleaved subcarrier allocation in the uplink scenario, as a benefit of its low PAPR.

- A reduced-complexity detector is proposed in [118] for OFDMA/SC-FDMA-aided STSK. I propose a new reduced-complexity detector for the OFDMA-aided STSK DL and the SC-FDMA-aided STSK UL. The complexity of the detector is quantified in terms of the number of real-valued multiplications (RMOs) per bit of information and is compared to that of other detectors. The proposed detector is seen to impose a significantly reduced complexity and can be employed in OFDMA/SC-FDMA-aided STSK transmissions over frequency-selective channels.

- SR aided cooperative multicarrier STSK is proposed for frequency-selective channels [116] for the sake of mitigating the typical 50% throughput loss of conventional half-duplex relaying schemes,which is combined with MC-CDMA for circumventing the dispersive effects of wireless channels and for reducing the SR-induced interferences. We also propose

a differentially encoded cooperative MC-CDMA STSK arrangement for facilitating communications over hostile dispersive channels without requiring channel estimation (CE). Dispensing with CE is important, since the relays cannot be expected to altruistically estimate the SN-to-RN links for simply supporting the source. We also propose a new modality of the joint detection of the FD-despread signals gleaned from two successively arriving frames at the DN, namely via the SN-to-DN and via the VAA-to-DN links, which is carried out by a single-stream based ML detector.

- In order to mitigate the typical 3-dB performance degradation of the classic differentially detected scheme, while dispensing with channel estimation, I propose multiple-symbol differential detection for the multicarrier differential STSK scheme [120]. Sphere decoding is utilized for reducing the computational complexity of jointly detecting multiple symbols. Furthermore, for facilitating soft-decision aided decoding, I design an iterative detection aided concatenated channel coded scheme.

Chapter 2

OFDM Aided Multicarrier Space-Time Shift Keying

2.1 Introduction

MULTIPLE-input multiple-output (MIMO) systems are capable of improving the throughput [15, 17, 122] and/or the bit-error-ratio (BER) [8–10] within the same bandwith as a single-input single-output (SISO) system. Motivated by the flexible diversity versus multiplexing gain tradeoff as offered by linear dispersion codes (LDCs) [11, 32] and by the low-complexity designs of spatial modulation (SM) [47] and space-shift keying (SSK) [48], Sugiura *et al.* proposed the space-time shift keying (STSK) framework of [49], which is capable of striking the same diversity-multiplexing tradeoff (DMT) as LDCs, whilst exhibiting a range of further advantages. The STSK framework is based on the idea of spreading a $\mathcal{L}$-PSK/QAM symbol across T symbol intervals and M antennas, while activating only one out of Q space-time dispersion matrices $\boldsymbol{A}_q$ at a time. Depending on the specific values of the parameters M, T and Q, this approach is capable of providing both multiplexing and transmit diversity gains in a narrowband scenario. However, STSK exhibits a residual BER for transmission over dispersive wideband channels.

Hence, in this chapter, we amalgamate orthogonal frequency division multiplexing (OFDM) with STSK transmissions for the sake of mitigating the performance degradation of STSK in realistic wideband channels. The remainder of this chapter is organized as follows. In Section 2.2, we outline the chronological development of the family of MIMO systems, which paved the way for the STSK concept. More specifically, in this section, a brief overview of the conventional MIMO arrangements, including the vertical Bell laboratories layered space-time (V-BLAST) schemes [17], space-time block codes (STBCs) [9], space-time trellis codes (STTCs) [10], linear

dispersion codes [11, 32] as well as of the recent concepts of SM/SSK [47, 48] and STSK [49, 57] is provided. Section 2.3 outlines the optimization procedure of the dispersion matrices (DMs) used in constructing our multicarrier STSK. The proposed OFDM aided multicarrier STSK arrangement is detailed in Section 2.4 in the context of wideband channels, while its performance is investigated in Section 2.6. Finally, this chapter is concluded in Section 2.7.

2.2 Recent Developments in MIMO Techniques

In this section, the traditional MIMO arrangements outlining the STBC, the BLAST/V-BLAST and the LDC arrangements are reviewed, followed by the rationale as well as the design of the STSK architecture.

2.2.1 Spatial Division Multiplexing

Spatial Division Multiplexing (SDM) constitutes a specific MIMO transmission technique, where independent encoded data streams are transmitted from each of the multiple transmit antenna elements (AEs). BLAST and V-BLAST constitute the seminal SDM-type MIMO systems [15, 17, 122]. The employment of multiple AEs at the transmitter and receiver allows us to create multiple data streams within the same bandwidth, which provides an additional multiplexing gain at the cost of no additional bandwidth and/or power consumption.

The performance of SDM MIMO depends largely on the detection algorithm and decomposition of MIMO channels imposes a potentially high complexity. Optimal maximum-likelihood (ML) detection may be applied for the sake of achieving the best attainable performance, albeit at the expense of a prohibitively high complexity which increases exponentially with the number of transmit antennas. To be specific, a $(M \times N)-$element SDM MIMO system transmits $M \cdot \log_2 \mathcal{L}$ bits during each symbol interval and each ML search involves $(4MN + 2N)$ real multiplication operations, whereas the ML detector has to carry out $\mathcal{L}^M$ searches, where $\mathcal{L}$ denotes the modulation order. Hence, the computational complexity imposed by the ML detector may be evaluated in terms of the number of real-valued multiplcation operations (RMOs) for decoding each bit of information, which may be expressed as:

$$\text{RMOs per bit} = \frac{(4MN + 2N)\mathcal{L}^M}{M \cdot \log_2 \mathcal{L}}. \tag{2.1}$$

The ML detector's complexity may, however, be mitigated by the family of linear detectors, such as the zero forcing (ZF) or the minimum mean square error (MMSE) detectors, albeit at the cost of a reduced performance. The employment of suboptimal detectors, for example of sphere decoders [123] or of ant-colony optimization-aided (ACO) detectors [124] is capable of attaining a near-ML performance at a moderate complexity. The transmission rate of a full-rank

SDM MIMO employing an $\mathcal{L}$-PSK/QAM constellation is given by $R_{\text{SDM}} = \min(M, N) \cdot \log_2 \mathcal{L}$ bits/symbol.

2.2.2 Spatial Diversity Schemes

Spatial diversity refers to the technique of enhancing the signal's reliability by transmitting multiple signal replicas over independently faded transmission links. The antenna elements of a MIMO system are required to be spaced as far as possible for the sake of facilitating the link's independent fading.

Spatial diversity may be of two types: receive diversity and transmit diversity. In [8], Alamouti proposed a witty low-complexity transmit diversity scheme utilizing two antennas, which is usually termed as Alamout's $\mathcal{G}_2-$ STBC. Provided that the two transmit time-slots are not smeared into each other by channel-induced dispersion, a low-complexity single-stream detection may be employed for avoiding the complex joint detection of multiple symbols. In [9], Alamouti's two-antenna based space-time block code (STBC) was extended to a higher number of antennas and introduced the so-called $\mathcal{G}_3-$ and $\mathcal{G}_4-$ STBC based on the *theory of orthogonal designs.*

Space-time block codes (STBC) [9] were proposed for combatting the hostile phenomenon of fading with the aid of spatial diversity. The simple philosophy of STBCs is that when one of the antennas is in a deep fade, another one might not be in the same condition. The independently fading replicas are combined at the receiver, so that the links become more reliable by making use of suitable diversity combining schemes. To be specific, the $\mathcal{G}_2-$ STBC achieves the maximum attainable diversity gain and simplifies the receiver's structure, since the joint detection problem is decomposed into a pair of low-complexity detection problems. Space-time trellis codes (STTC) [10], on the other hand, constitute extensions of trellis codes [125] to the multiple transmit as well as receive antenna scenarios. STTCs generally offer an improved performance and provide not only a diversity gain but also a coding gain, albeit at the cost of an increased decoding complexity. It is to be noted here that STBCs and/or STTCs cannot provide a multiplexing gain and hence their transmission rate is limited to $\log_2 \mathcal{L}$ bits/symbol, where $\mathcal{L}$ is the modulation order.

2.2.3 Diversity-Multiplexing Tradeoff

Whereas the SDM schmes are capable of attaining a high throughput gain, the family of STBCs and STTCs are designed for achieving the maximum possible diversity gain. It is, however, rarely desirable to employ multiple AEs either purely for achieving multiplexing gain or for achieving a diversity gain. More explicitly, a multiple-antenna architecture is typically required

to provide both some multiplexing gain and some diversity benefits. The pioneering work of Zheng and Tse [126] demonstrated that there is an upper limit on the achievable diversity versus multiplexing tradeoff (DMT) in the context of employing MIMO systems. To expound a little further, a scheme supporting a data rate $R(\gamma)$ at SNR γ is capable of achieving a multiplexing gain formulated as:

$$r = \lim_{\gamma \to \infty} \frac{R(\gamma)}{\log_2 R(\gamma)}, \tag{2.2}$$

while the diversity gain d may be defined in terms of the average error probability as:

$$d = -\lim_{\gamma \to \infty} \frac{\log_2 P_e(\gamma)}{\gamma}. \tag{2.3}$$

For example, if the rate $R(\gamma)$ of a particular multiple-antenna scheme scales like $3\log_2\gamma$ and the average error probability $P_e(\gamma)$ decays like $1/\gamma^4$, then the scheme is said to have a spatial multiplexing gain of 3 and a diversity advantage of 4.

It was shown in [126] that for a MIMO system with M transmit and N receive AE communicating over T symbol durations in any transmission block, optimal tradeoff is attained when $T \geq M + N - 1$, and the corresponding maximum diversity order and the maximum multiplexing gain are obtained as

$$d_{\max} = MN \qquad r_{\max} = \min(M, N),$$

respectively.

Motivated by these ideas, there had been endeavours to achieve both the multiplexing gain as well as the diversity gain employing a single scheme. To this end, linear dispersion codes (LDCs) were developed in [11] subsuming both the V-BLAST and the STBCs as special cases and generally outperforming both.

2.2.4 Linear Dispersion Codes

The concept of linear dispersion codes (LDC) [11, 32] was introduced as a general framework for designing space-time codes that are capable of striking any arbitrary trade-off between the achievable multiplexing and diversity gain offered by the MIMO system, albeit this is achieved at the cost of a potentially high en/decoding complexity. As a further benefit, they can be designed for any arbitrary antenna configurations, whilst satisfying specific spatial diversity order requirements, as well as for any throughput requirements. Hence LDCs subsume both the family of STBCs [9] as well as V-BLAST [17] schemes, and are capable of outperforming both, but again, they impose a higher decoding complexity.

Detailed discussions on the design and performance of LDCs have been provided in [5]. Specifically, a MIMO system consisting of M transmit and N receive AEs employs the Q-

element transmit symbol vector $\boldsymbol{K} = [s_1, s_2, \cdots, s_Q]^T$ and generates the space-time transmission matrix $\boldsymbol{S} \in \mathbb{C}^{M \times T}$ using the relationship:

$$\boldsymbol{S} = \sum_{q=1}^{Q} \boldsymbol{A}_q s_q, \tag{2.4}$$

where $\boldsymbol{A}_q \in \mathbb{C}^{M \times T}$ $(q = 1, 2, ..., Q)$ [32] represents the pre-assigned dispersion matrices (DMs), which are generated by optimizing an objective function (OF) under the power constraint of

$$\mathrm{tr}(\boldsymbol{\chi}\boldsymbol{\chi}^H) = T, \tag{2.5}$$

or more strictly

$$\mathrm{tr}(\boldsymbol{A}_q \boldsymbol{A}_q^H) = \frac{T}{Q}, \qquad \forall q \tag{2.6}$$

where $\boldsymbol{\chi}$ is the dispersion character matrix (DCM) given by:

$$\boldsymbol{\chi} = [\mathrm{vec}(\boldsymbol{A}_1), \cdots, \mathrm{vec}(\boldsymbol{A}_Q)] \in \mathbb{C}^{MT \times Q}. \tag{2.7}$$

Specifically, $\boldsymbol{S}$ may be represented in the form:

$$\boldsymbol{S} = \begin{bmatrix} \boldsymbol{S}_{1,1} & \boldsymbol{S}_{1,2} & \cdots & \boldsymbol{S}_{1,T} \\ \boldsymbol{S}_{2,1} & \boldsymbol{S}_{2,2} & \cdots & \boldsymbol{S}_{2,T} \\ \vdots & \vdots & \ddots & \vdots \\ \boldsymbol{S}_{M,1} & \boldsymbol{S}_{M,2} & \cdots & \boldsymbol{S}_{M,T} \end{bmatrix}. \tag{2.8}$$

The LDC system is uniquely specified by the LDC (M, N, T, Q) parameters in conjunction with the $\mathcal{L}-$ary phase shift keying (PSK) or $\mathcal{L}-$ary quadrature amplitude modulation (QAM) modulation. The achievable transmission rate of the system is given by

$$R_{\mathrm{LDC}} = \frac{Q}{T} \cdot \log_2 \mathcal{L} \quad \text{bits/symbol}. \tag{2.9}$$

The design of the LDCs depends mainly on the dispersion matrix (DM) optimization procedure and on the related objective function (OF) involved. The DMs may be designed by maximizing their continuous input continuous output memoryless channel (CCMC) capacity [5] or maximizing the discrete input continuous output memoryless channel (DCMC) capacity [127] or even by minimizing the error-probability, as detailed in [5, 11]. More specifically, the CCMC capacity of the MIMO system relying on M transmit and N receive antennas as well as T symbol intervals at SNR γ can be expressed as [16, 128]:

$$C_{\mathrm{LDC}}^{\mathrm{CCMC}} = \mathcal{E}\left\{\log_2\left(\det\left[\boldsymbol{I}_N + \frac{\gamma}{M}\boldsymbol{H}\boldsymbol{H}^H\right]\right)\right\}. \tag{2.10}$$

Instead of the CCMC capacity based design, Ng and Hanzo [127] proposed the DCMC capacity-based optimal design for LDC codes. It was argued that directly maximising the MIMO system's capacity is a beneficial design objective, because it leads both to a diversity

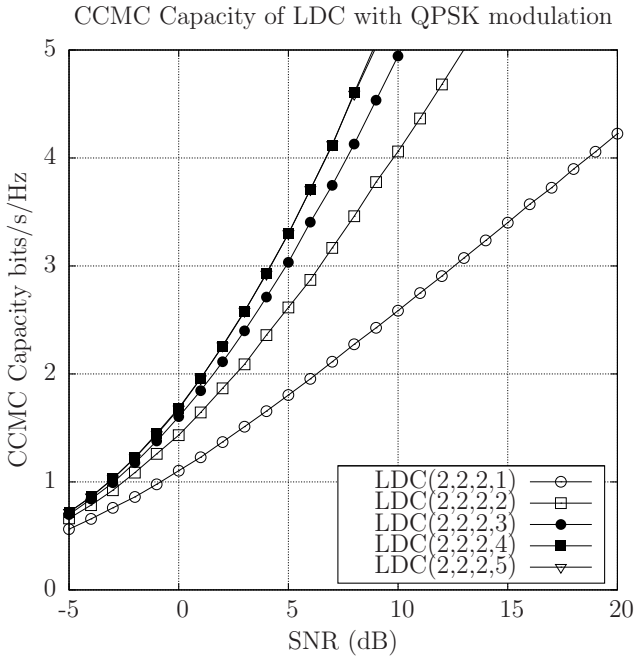

Figure 2.1: CCMC capacity evaluated from (2.10) for different (M, N, T, Q) parameters of the LDC scheme mentioned in the legend for QPSK modulation.

gain as well as to a coding gain [5]. The DCMC capacity of the equivalent MIMO channel formulated for the transmit signal vector $\boldsymbol{K}_f$, $f \in (1, 2, \ldots, F)$ is given by [127]:

$$C_{\text{LDC}}^{\text{DCMC}} = \frac{1}{T}\left[\log_2(F) - \frac{1}{F}\sum_{f=1}^{F}\mathcal{E}\left\{\log_2\left(\sum_{g=1}^{F}\exp\left[\Psi_{f,g}\right] \mid \boldsymbol{K}_f\right)\right\}\right], \tag{2.11}$$

where $\Psi_{f,g}$ within $\exp[\cdot]$ is given by:

$$\Psi_{f,g} = \frac{-\parallel \bar{\boldsymbol{H}}\boldsymbol{\chi}(\boldsymbol{K}_f - \boldsymbol{K}_g) + \bar{\boldsymbol{V}} \parallel^2 + \parallel \bar{\boldsymbol{V}} \parallel^2}{N_0}. \tag{2.12}$$

2.2.4.1 CCMC and DCMC Capacity Curves of LDCs

The CCMC capacity of LDC associated with different LDC parameters is shown in Figure 2.1. It is worth mentioning here that LDCs associated with $Q \geq MT$ achieve the maximum attainable CCMC capacity. By contrast, when we have $Q < MT$, the CCMC capacity increases linearly with the ratio $\frac{Q}{T}$.

The DCMC capacity of LDCs evaluated from (2.11) and associated with different parameters as a function of Q is shown in Figure 2.2. It can be seen that LDCs have an ever increasing DCMC capacity upon increasing Q for $Q > MT$.

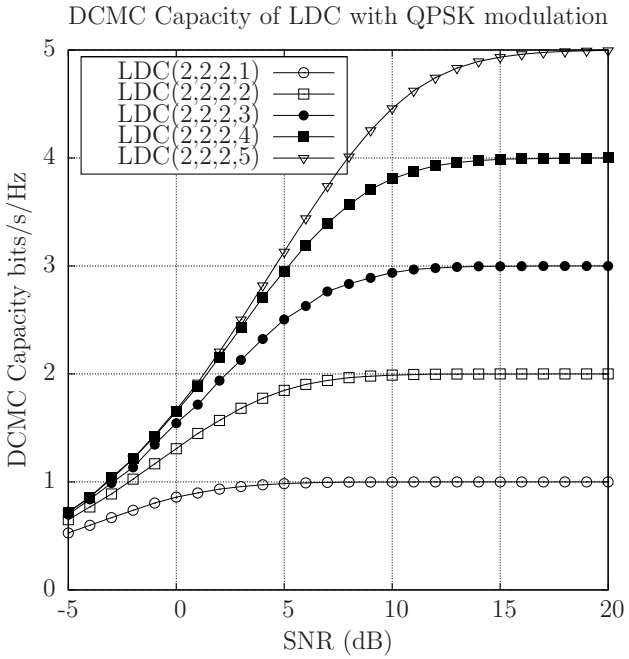

Figure 2.2: DCMC capacity evaluated from (2.11) for different (M, N, T, Q) parameters of the LDC scheme mentioned in the legend for QPSK modulation.

2.2.5 Differential Linear Dispersion Codes

Before differential encoding, the incoming bits are uniquely mapped to the space-time matrices $\tilde{\boldsymbol{X}}_i$, $i = 1, 2, \ldots$, where the differential linear dispersion codes (DLDC) first disperse the i^{th} transmitted symbol block, for example, $\boldsymbol{K}_i = [s_i^1, \cdots, s_i^Q]$ to M spatial and T temporal dimensions by invoking the following dispersion operation [5]:

$$\tilde{\boldsymbol{X}}_i = \sum_{q=1}^{Q} \boldsymbol{A}_q s_i^q, \tag{2.13}$$

where $\boldsymbol{A}_q \in \mathbb{C}^{M \times T} (q = 1, 2, ..., Q)$ [32] are the linear dispersion matrices. The universal differential encoding of space-time matrices requires the matrix to be unitary [5]. Although $\tilde{\boldsymbol{X}}_i$ might not be expected to be automatically unitary, the Cayley transform can be used for converting the Hermitian matrix $\tilde{\boldsymbol{X}}_i$ to the unitary matrix $\boldsymbol{X}_i$. The Cayley transform employed for converting the Hermitian matrix $\tilde{\boldsymbol{X}}_i$ to the unitary matrix $\boldsymbol{X}_i$ may be expressed as [5, 129]:

$$\boldsymbol{X}_i = (\boldsymbol{I}_M + j\tilde{\boldsymbol{X}}_i)^{-1}(\boldsymbol{I}_M - j\tilde{\boldsymbol{X}}_i). \tag{2.14}$$

Similarly, the inverse of the Cayley tranform may be invoked for converting the unitary matrix $\boldsymbol{X}_i$ to the Hermitian matrix $\tilde{\boldsymbol{X}}_i$, which may be expressed as:

$$\tilde{\boldsymbol{X}}_i = -j(\boldsymbol{I}_M - \boldsymbol{X}_i)(\boldsymbol{I}_M + \boldsymbol{X}_i)^{-1}. \tag{2.15}$$

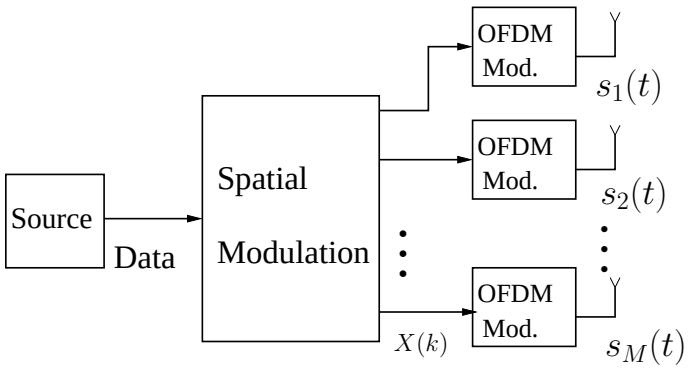

Figure 2.3: Spatial modulation transmitter architecture [47] using OFDM modulation in all the M transmit antennas

The differential encoding is now performed on the unitary space-time matrix $\boldsymbol{X}_i$ in order to yield $\boldsymbol{S}_i$, $i = 0, 1, 2, \ldots$ according to

$$\boldsymbol{S}_i = \begin{cases} \boldsymbol{X}_i \boldsymbol{S}_{i-1}, & \text{if } i \geq 1 \\ \boldsymbol{I}_T, & i = 0, \end{cases} \tag{2.16}$$

where $\boldsymbol{I}_T$ represents the $(T \times T)$-element identity matrix.

2.2.6 Spatial Modulation and Space Shift Keying

Spatial modulation (SM) is a recently developed multiple antenna aided transmission technique, which was conceived by Chau and Yu [46] and then it was refined by Mesleh *et al.* [47,50]. Recall that the MIMO schemes discussed above invoke the spreading of the conventional phase shift keying (PSK)/quadrature amplitude modulation (QAM) symbols across the spatial- and time-domain. By contrast, SM maps the symbols to the activated transmit antenna index, as an implicit means of conveying extra information. Hence it maps a block of information bits to two information carrying units: to a classic symbol chosen from the constellation and to the unique index of the activated transmit antenna.

The exploitation of the transmit antenna index as an information-bearing unit improves the overall spectral efficiency by $\log_2 M$ bits, where M denotes the number of transmit antennas. The transmitter architecture of a SM-OFDM scheme is shown in Figure 2.3, where the input bits are mapped partly to the antenna index and partly to the transmit symbol according to the SM mapping table of Figure 2.4.

In Figure 2.4, a transmit block of 3 source bits has been shown to be mapped by the SM scheme to the constellation symbol as well as to the activated transmit antenna index. The mapping here shows 1 bit to be mapped to the constellation symbol, whereas 2 bits are mapped to the antenna index. Naturally, $M = 4$ transmit antennas will be required at the transmitter

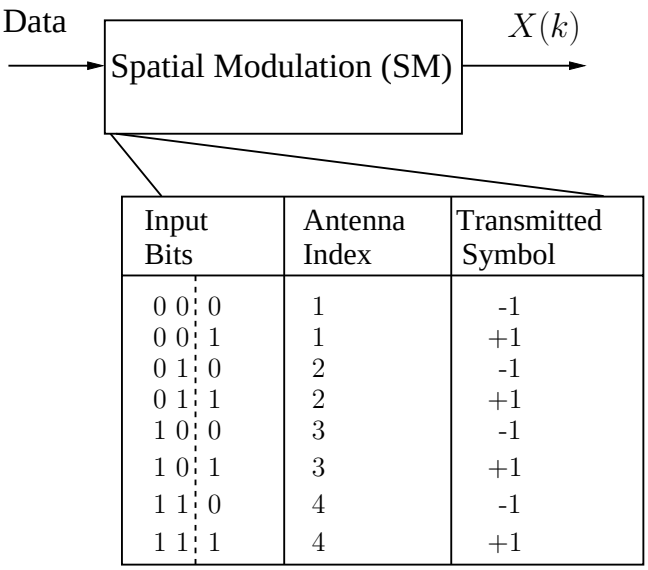

Input Bits	Antenna Index	Transmitted Symbol
0 0 0	1	-1
0 0 1	1	+1
0 1 0	2	-1
0 1 1	2	+1
1 0 0	3	-1
1 0 1	3	+1
1 1 0	4	-1
1 1 1	4	+1

Figure 2.4: Spatial modulation based mapping [47] of the source bits to the antenna index as well as to the BPSK symbol.

and BPSK modulation will be used. The bits are separated by 'dotted' lines to distinguish the bits mapped to the antenna index from those mapped to the BPSK symbol in Figure 2.4. Alternatively, 2 transmit antennas and QPSK/4−QAM symbols may also be employed, where only one bit will be mapped to the antenna index and the remaining 2 bits will be mapped to the QPSK symbol. The bit mapping of the SM scheme employing 3 bits per transmit block using $M = 2$ and $\mathcal{L} = 4$ is illustrated in Table 2.1. However, the scheme has the design flexibility to adaptively select the number of bits transmitted per block, depending on the number of transmit AEs as well as on the modulation order employed.

The number of bits transmitted using an $\mathcal{L}-$ary constellation equals to $\log_2\mathcal{L}$, whereas that using the activated antenna index will be $\log_2 M$. Hence, the SM-OFDM scheme shown in Figure 2.3 is capable of transmitting R bits on each OFDM subchannel, where R is given by

$$R = \log_2(M \cdot \mathcal{L}), \tag{2.17}$$

The most attractive feature of the SM scheme is that it imposes a substantially reduced decoding complexity in comparison to its SDM counterpart. As it becomes evident from (2.1), the decoding complexity of SDM schemes increases exponentially with the modulation order $\mathcal{L}$. By contrast, the decoding complexity imposed by the SM scheme increases linearly with $\mathcal{L}$. More specifically, the decoding complexity of the SM scheme per bit expressed in terms of the number of RMOs is given by [57, 130]:

$$\text{RMOs per bit} = \frac{6MN\mathcal{L}}{\log_2(M \cdot \mathcal{L})}. \tag{2.18}$$

Since the SM scheme activates a single AE at any signalling interval, only a single radio-frequency (RF) chain is necessitated. Furthermore, the SM scheme is capable of operating using

Table 2.1: Bit mapping of the SM scheme using $M = 2$ and $\mathcal{L} = 4$ for 3 bits per transmit block.

Input bits	$M = 2, \mathcal{L} = 4$	
	Antenna index	Transmit symbol
0 00	1	1
0 01	1	$e^{j\frac{\pi}{2}}$
0 10	1	$e^{j\frac{2\pi}{2}}$
0 11	1	$e^{j\frac{3\pi}{2}}$
1 00	2	1
1 01	2	$e^{j\frac{\pi}{2}}$
1 10	2	$e^{j\frac{2\pi}{2}}$
1 11	2	$e^{j\frac{3\pi}{2}}$

only loose synchronization among the AEs, i.e. it is robust to inter-antenna synchronization (IAS) errors.

In case of space shift keying (SSK) aided transmission, the classic PSK/QAM constellation signalling is deactivated and only the presence or absence of energy is detected at the receiver antenna [48], which facilitates an extremely low-complexity decoding.

2.2.7 Space-Time Shift Keying: A Universal MIMO Architecture

As already mentioned, Chau and Yu [46] as well as Mesleh *et al.* [47] introduced the concept of spatial modulation (SM) for the sake of increasing the spectral efficiency, which can be effectively used as a MIMO encoding principle and which is fundamentally different from spatial division multiplexing (SDM). Although the SM/SSK scheme has the capability of outperforming other MIMO arrangements, it has the limitation of relying purely on receive diversity, whilst it has no transmit diversity provision. Hence, motivated by the appealingly low SM/SSK complexity, Sugiura *et al.* proposed the more sophisticated space-time shift keying (STSK) concept [49, 57].

To elaborate further, the STSK transmitter activates one out of Q dispersion matrices $\boldsymbol{A}_q \in C^{M\times T}(q = 1, 2, ..., Q)$, which are pre-assigned before transmission. A total of $B = \log_2(Q \cdot \mathcal{L})$ source bits are mapped to each space-time block $\boldsymbol{X}[i] \in C^{M\times T}$ by the STSK scheme according to

$$\boldsymbol{X}[i] = s[i]\,\boldsymbol{A}_q[i], \tag{2.19}$$

where the $\mathcal{L}$-PSK/QAM symbol $s[i]$ is represented by $B_1 = \log_2\mathcal{L}$ number of input bits, whereas the specific dispersion matrix $\boldsymbol{A}_q[i]$ is selected from the set of Q dispersion matrices, $\boldsymbol{A}_q(q =$

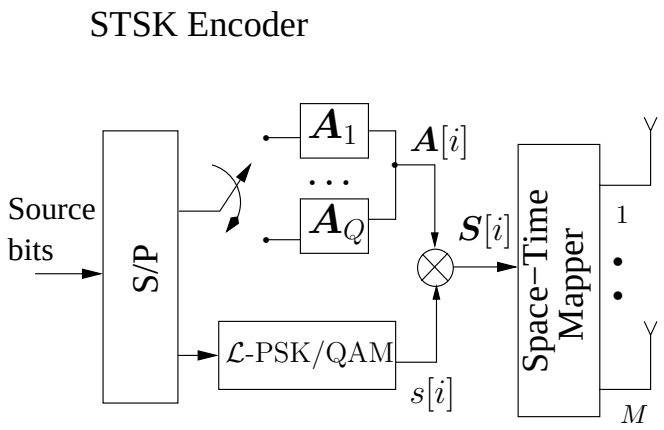

Figure 2.5: Transmitter architecture of the STSK scheme, where at any symbol instant i, the $\mathcal{L}$-PSK/QAM symbol $s[i]$ together with the activated DM $\boldsymbol{A}_q[i]$ forms the space-time codeword $\boldsymbol{X}[i]$, according to (2.19), which is transmitted at T time-slots over M transmit AEs.

$1, 2, ..., Q$) by the $B_2 = \log_2 Q$ number of input bits. Additionally, in order to maintain a unity average transmission power within each STSK symbol duration, each of the dispersion matrices has to obey the power constraint of [49, 57]:

$$\mathrm{tr}(\boldsymbol{A}_q \boldsymbol{A}_q^H) = T, \tag{2.20}$$

where $\mathrm{tr}(\bullet)$ indicates the trace of the matrix '$\bullet$'. Furthermore, the STSK system is uniquely specified by the STSK (M, N, T, Q) parameters in conjunction with the $\mathcal{L}-$PSK/QAM constellation.

The transmitter architecture of the STSK system is shown in Figure 2.5 and the correponding mapping of the source bits of a 3−bit transmit block to the dispersion matrix (DM) activated as well as to the $\mathcal{L}$-PSK/QAM symbols can be better understood from Table 2.2. The bits mapped to the index of the DM activated and those mapped to the constellation symbol have been separated by a dashed line in Table 2.2. Note that the dashed line is in front of the bits in the first column of Table 2.2, indicating that all the bits are mapped to the constellation symbols under this configuration. By contrast, the dashed lines follow the bits in the last column of Table 2.2, which represents the bits will be mapped only to the index of the DM activated. Furthermore, similarly to the SM scheme, the STSK scheme is capable of adaptively selecting the size of the transmit blocks, depending on the number of DMs as well as on the constellation size $\mathcal{L}$.

Finally, the benefits of the STSK schme may be summarized as follows [57]:

- The STSK scheme is capable of striking the same DMT as the LDC, but at a substantially reduced complexity. On the other hand, STSK is capable of achieving both transmit as

Table 2.2: Illustration of STSK bit-mapping [49, 57] for 3−bits per block, employing Q dispersion matrices and $\mathcal{L}$-PSK symbols

Input bits	$Q=1$, $\mathcal{L}=8$		Input bits	$Q=2$, $\mathcal{L}=4$		Input bits	$Q=4$, $\mathcal{L}=2$		Input bits	$Q=8$, $\mathcal{L}=1$	
	$A[i]$	$s[i]$		$A[i]$	$s[i]$		$A[i]$	$s[i]$		$A[i]$	$s[i]$
000	A_1	1	0 00	A_1	1	00 0	A_1	1	000	A_1	1
001	A_1	$e^{j\frac{\pi}{4}}$	0 01	A_1	$e^{j\frac{\pi}{2}}$	00 1	A_1	$e^{j\pi}$	001	A_2	1
010	A_1	$e^{j\frac{\pi}{2}}$	0 10	A_1	$e^{j\frac{2\pi}{2}}$	01 0	A_2	1	010	A_3	1
011	A_1	$e^{j\frac{3\pi}{4}}$	0 11	A_1	$e^{j\frac{3\pi}{2}}$	01 1	A_2	$e^{j\pi}$	011	A_4	1
100	A_1	$e^{j\frac{4\pi}{4}}$	1 00	A_2	1	10 0	A_3	1	100	A_5	1
101	A_1	$e^{j\frac{5\pi}{4}}$	1 01	A_2	$e^{j\frac{\pi}{2}}$	10 1	A_3	$e^{j\pi}$	101	A_6	1
110	A_1	$e^{j\frac{3\pi}{2}}$	1 10	A_2	$e^{j\frac{2\pi}{2}}$	11 0	A_4	1	110	A_7	1
111	A_1	$e^{j\frac{7\pi}{4}}$	1 11	A_2	$e^{j\frac{3\pi}{2}}$	11 1	A_4	$e^{j\pi}$	111	A_8	1

well as receive diversity gains, while the SM and SSK schemes attain only receive diversity gain.

- Since only a single one of the Q dispersion matrices is activated at any symbol instant, the STSK scheme imposes no inter-stream interference and - as a further benefit - a single-stream based maximum likelihood (ML) detection can be employed [49].
- The STSK scheme is capable of dispensing with IAS, similarly to the SM/SSK scheme.
- STSK is capable of adaptively supporting an arbitrary number of transmit as well as receive AEs.

The normalized throughput per symbol duration of the STSK scheme may be expressed as

$$R = \frac{\log_2(\mathcal{L}\cdot Q)}{T} \quad \left[\frac{\text{bits}}{\text{symbol duration}}\right], \tag{2.21}$$

whereas the computational complexity per bit imposed by the optimal single-stream ML detector quatified in terms of the number of RMOs for both fast block-fading and slow fading scenarios are given, respectively, by [49]

$$\text{Complexity}= \begin{cases} \dfrac{NTQ\left(4MT+6\mathcal{L}\right)}{\log_2(Q\cdot\mathcal{L})}, & \text{(fast fading)} \\ \dfrac{NTQ\left[\left(4M+4\mathcal{L}\right)/\tau+2\mathcal{L}\right]}{\log_2(Q\cdot\mathcal{L})}, & \text{(slow fading)} \end{cases}$$

where τ denotes the coherence interval of a slow fading channel. The STSK system is uniquely and unambiguously specified by the parameters (M, N, T, Q) in conjunction with the classic $\mathcal{L}$-PSK or $\mathcal{L}$-QAM modulation. Unless stated otherwise, by 'STSK' we refer to the perfect

channel state information (CSI) based coherent STSK (CSTSK) in this thesis. By contrast, its differentially encoded and noncoherently detected counterpart will be specifically referred to as differential STSK (DSTSK).

2.3 Optimization of the Dispersion Matrices

The performance of the STSK system substantially depends on the choice of the DMs. More specifically, it depends firstly on the specific objective function (OF) utilized and secondly on the DM optimization procedure. The optimization of the DMs set is thus of utmost importance for the performance of the STSK scheme.

In the STSK encoder described by (2.19), Q linear dispersion matrices, $A_q(q = 1, ..., Q)$ are pre-assigned to the trasmitter in advance of transmission, which may be generated by searching exhaustively through a large set of randomly generated matrices and selecting the best ones using some optimization criterion as mentioned in [32] and detailed further in [5]. More specifically, the search process consists of generating a set of for example 10^6 DMs, which have entries distributed according to the complex Gaussian distribution $\mathcal{CN}(0, 1)$ and which are normalized in order to satisfy the power-constraint criterion of (2.20) and then picking the best Q matrices, $\boldsymbol{A}_q(q = 1, ..., Q)$. More explicitly, the 'quality' of the set generated is evaluated in terms of an OF, such as for example, the corresponding CCMC capacity and the DCMC capacity, the pairwise serror probability (PEP) etc. The OFs that may be utilized for the optimization of DMs are briefly described below. Further insights on the optimization of the DMs may be found in [131, 132].

2.3.1 Objective Functions for DM Optimization

As already mentioned, the DMs may be optimized using the CCMC capacity, the DCMC capacity and/or the PSEP as the OFs. Below we provide a brief definition of these OFs in the context of the STSK system.

2.3.1.1 CCMC Capacity

The CCMC capacity of the STSK system associated with M transmit and N receive antenna elements and T symbol intervals at SNR γ may be formulated, similarly to the LDCs, as (2.10) of Subsection 2.2.4.

2.3.1.2 DCMC Capacity

The DCMC capacity of the STSK scheme may be formulated using (2.11) for the LDCs, but it requires appropriately re-defining the transmit symbol vector $\boldsymbol{K}_f$ for the STSK system. Hence the DCMC capacity of the STSK system may be expressed as [49, 57]:

$$C_{\text{STSK}}^{\text{DCMC}} = \frac{1}{T}\left[\log_2(Q\cdot\mathcal{L}) - \frac{1}{Q\cdot\mathcal{L}}\times\sum_{l_c,\,q}\mathcal{E}\left\{\log_2\left(\sum_{l_c',\,q'}\exp\left[\Psi_{l_c,\,q}^{l_c',\,q'}\right]\mid \boldsymbol{K}_{l_c',q'}\right)\right\}\right], \tag{2.22}$$

where we have

$$\Psi_{l_c,\,q}^{l_c',\,q'} = \frac{-\|\bar{\boldsymbol{H}}_{\text{eq}}\boldsymbol{\chi}(\boldsymbol{K}_{l_c,q}-\boldsymbol{K}_{l_c',q'})+\bar{\boldsymbol{V}}\|^2+\|\bar{\boldsymbol{V}}\|^2}{N_0}. \tag{2.23}$$

2.3.1.3 The Rank and Determinant Criterion

The rank and the determinant criteria were first proposed in [10] and were detailed for a generalized space-time architecture in [5]. To be specific, the PEP $P(\boldsymbol{X}\rightarrow\boldsymbol{X}')$ that a ML detector wrongly decodes a space-time transmission matrix $\boldsymbol{X}$ defined in (2.19) for another matrix $\boldsymbol{X}'$ is upper-bounded by [32]

$$P(\boldsymbol{X}\rightarrow\boldsymbol{X}') \leq \frac{1}{\det\left[\boldsymbol{I}_{NM}+\frac{\gamma}{4M}\boldsymbol{X}_\Delta\otimes\boldsymbol{I}_N\right]}. \tag{2.24}$$

Equation (2.24) may also be rewritten as [10]:

$$P(\boldsymbol{X}\rightarrow\boldsymbol{X}') \leq \left(\prod_{i=1}^{r}\lambda_i\right)^{-N}\left(\frac{\gamma}{4M}\right)^{-rN}, \tag{2.25}$$

where γ denotes the average signal-to-noise ratio (SNR) at each receive antenna, $\boldsymbol{X}_\Delta = (\boldsymbol{X}-\boldsymbol{X}')(\boldsymbol{X}-\boldsymbol{X}')^H$, while r and λ_i indicate the rank and the non-zero eigenvalues of $\boldsymbol{X}_\Delta$, respectively.

The Rank Criterion Equation (2.25) shows that the term $\left(\frac{\gamma}{4M}\right)^{-rN}$ determines how rapidly the PSEP decays with the SNR, where the diversity order is determined by rN. To be more specific, the diversity order [10] is determined by the minimum rank $r_{\min}$ of the matrix $\boldsymbol{X}_\Delta$:

$$r_{\min} = \min\{r\,(\boldsymbol{X}_\Delta)\}. \tag{2.26}$$

Hence to achieve the full diversity order, the matrix $\boldsymbol{X}_\Delta$ has to be full rank for any codeword pair $(\boldsymbol{X},\boldsymbol{X}')$.

The Determinant Criterion The determinant criterion [10] states that the minimum of $(\prod_{i=1}^{r} \lambda_i)$ in (2.24) evaluated over all possible $(\boldsymbol{X}, \boldsymbol{X}')$ pairs determines the achievable coding gain and has to be maximized.

After evaluating the OF for quantifying the 'quality' of the DMs generated, the process is repeated for example 10^6 times and the best set of Q matrices in accordance with one of the above-mentioned 'quality' metrics is selected.

The DMs generated so far for the STSK scheme mainly relied on randomly generating a large set of DMs and then picking the best Q DMs based on the OF. However, this requires a potentially excessive computation time when relying on an exhaustive search and might get trapped in local maxima or minima. Genetic algorithms (GA) are capable of reducing the computation time by searching through only a fraction of the DMs, yet finding the best ones with a high probability. A GA was used successfully in [133] for generating optimal space-time block codes (STBCs) [8,9]. As a further advance, GA aided unitary DM design and optimization was invoked for LDC-based MIMO systems in [134] using the determinant criterion. Finally, structured DMs were designed in [131, 132]

In the following, we outline the GA aided optimization procedure of the DMs to be used in our multi-carrier STSK scheme and evaluate its performance. We will demonstrate that GA assists us in the optimization of the OF using less OF evaluations than the exhaustive search technique. Viewing their relationship from a different perspective, the GA aided scheme performs better than the scheme using the same number of OF evaluations picking the DMs on a random basis.

2.3.2 Genetic Algorithm Aided DM Optimization

Genetic algorithms (GAs) [135, 136] constitute adaptive heuristic search algorithms, where a population of *individuals* follows the evolutionary concepts of natural *selection* and genetic operators of *crossover* and *mutation* to optimize the OF or *fitness function*. The particular definition of individuals of the population of legitimate solutions, and of the OFs are specific to the individual applications. In our DM optimization problem, we define an individual to be a set of DMs, which will be used for constructing our STSK scheme using the *power constraint* of (2.20) and the individuals to be the columns of the DMs. The OF of our optimization problem is taken as any of the OFs mentioned in Subsection 2.3.1, for example, the DCMC capacity [5, 127] or the rank and determinant criterion as detailed in [5, 10].

Again, the initial population of DMs is randomly selected from a complex-valued Gaussian distribution of zero mean and unity variance. Thereafter the algorithm proceeds recursively. Each recursive iteration stage is termed as a generation and after the fitness function or OF evaluation, the parents about to create new, potentially increased-fitness individuals are selected

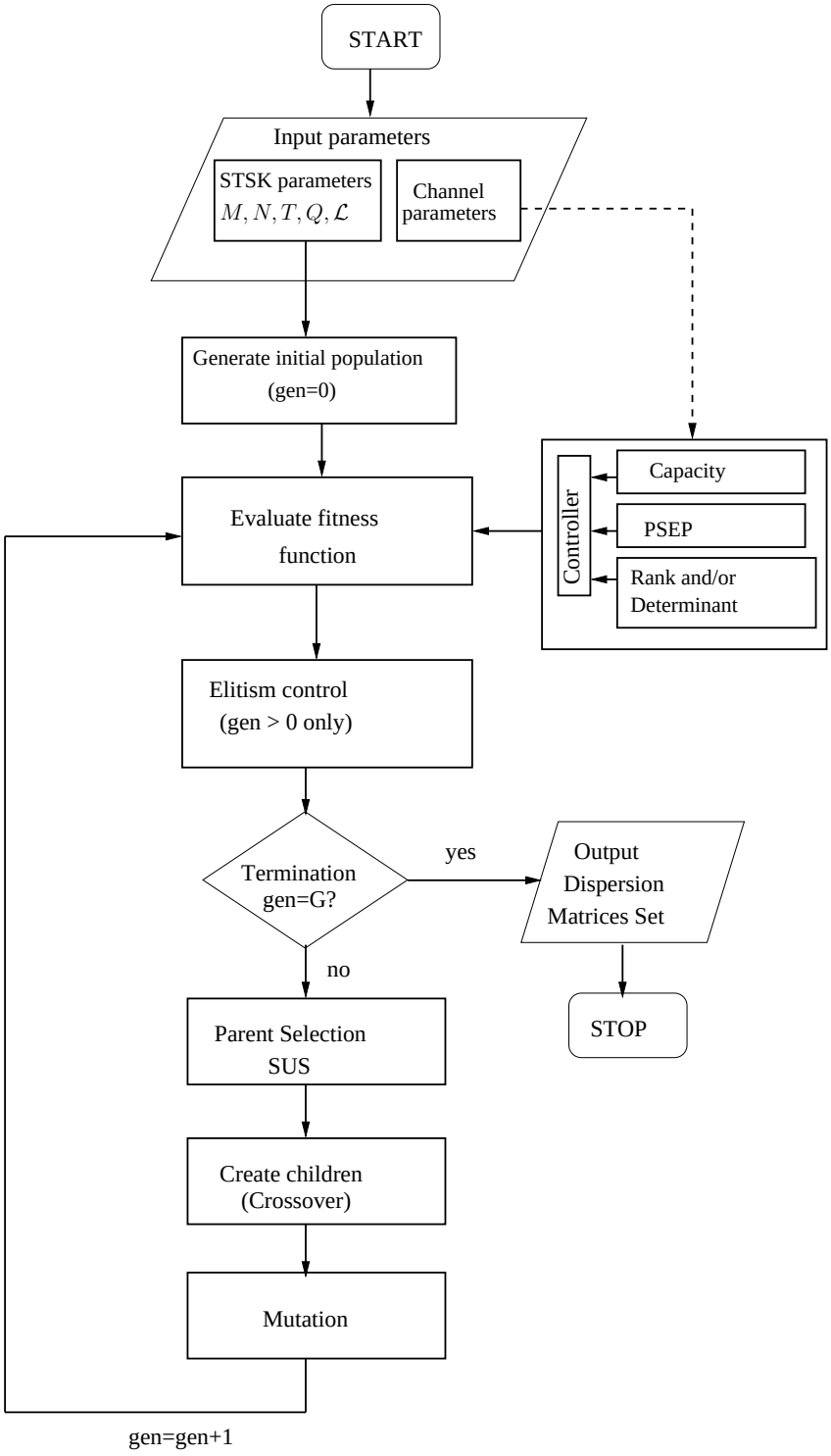

Figure 2.6: Generation of the GA-optimized dispersion matrix set to be used in STSK.

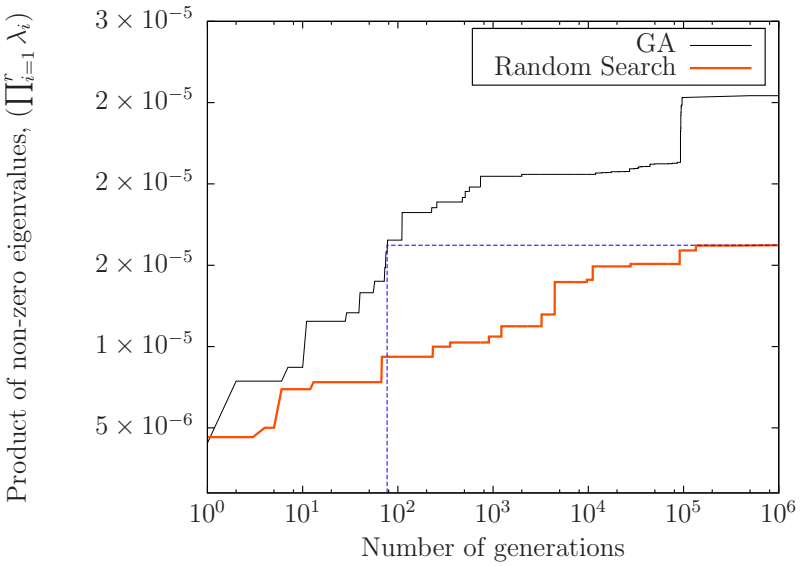

Figure 2.7: Fitness function versus the number of generations in both GA optimization and in random search.

using a particular selection method such as the stochastic universal sampling (SUS) of [137] based on the fitness function just evaluated. Given a pair of appropriately selected individuals or parents, a binary crossover mask may be generated randomly, where the specific components of each parent may be picked with a *crossover probability* p_c. Next, the resultant children might mutate by exchanging some of their components subject to a specific mutation probability. The goal of mutation is to prevent 'premature' convergence without exploring the entire search-space sufficiently thoroughly. If the best individual of the previous generation is better than the worst one of the new generation even after mutation, the so-called *elitism* control is invoked for retaining the high-fitness individuals [135]. The whole process is continued upto a pre-specified number of generations, G. The flowchart of the elitism-based GA process is portrayed in Figure 2.6.

2.3.3 Performance of GA Aided Optimization

The performance of the GA-based DM optimization can be visualized in Figure 2.7. Observe that for the fitness function as defined by the determinant criterion, we approach the same fitness value at about 80 generations which were only approached by the random search after 10^6 iterations. This clearly demonstrates the efficacy of the GA based optimization of DMs.

2.3.4 Wideband Channel Model

Wideband channels are generally modelled by tapped delay lines. If we partition the time-delay axis into equal-delay segments referred to as delay bins, then there will be, in general,

a number of received signals in each bin corresponding to the different paths, namely to those whose time of arrival is within the bin duration. These signals, when vectorially combined, can be represented by a delta function occurring in the bin center having a Rayleigh distributed magnitude [138]. As the transmission bandwidth is increased, the effects of frequency-selective fading become prominent. Thus the channel has a filtering effect, which linearly distorts the transmitted waveform.

The impulse response of the flat Rayleigh fading channel consists of a single Dirac delta function whose weight obeys a Rayleigh probability distribution function (pdf). This occurs because all the multipath components are assumed to arrive simultaneously and their combined effect gives rise to Rayleigh fading. Provided that the transmission frequency is less than the channel's coherence bandwidth, the different components encounter identical propagation delays and non-dispersive reception is facilitated.

On the other hand, dispersive multipath propagation has the effect of spreading the received symbols. If the delay spread is longer than the symbol duration, it gives rise to intersymbol interference (ISI). Under these circumstances, several echoes of the transmitted modulated symbols are received over a number of symbol periods and each symbol is spread into adjacent symbols [138].

A time-invariant broadband channel has an impulse response that can be modelled as [139, 140]:

$$h(t,\tau) = \sum_{l=1}^{L} a_l g_l(t)\delta\left(\tau - \tau_l\right), \tag{2.27}$$

where L is the number of multipath components in the channel, a_l, τ_l and $g_l(t)$ are the channel's envelope, delay and Rayleigh-distributed magnitude fading process exhibiting a particular normalized Doppler frequency f_d respectively, associated with the l-th path, while $\delta(.)$ is the Dirac Delta function.

In fact, the wideband propagation channel is constituted by the superposition of a number of dispersive fading paths, suffering from various attenuations and delays, aggravated by the Doppler shift as a result of the mobile station (MS)'s movement. Again, in serially modulated systems, this results in the adverse phenomenon of ISI. By contrast, as long as the channel's delay spread is lower than the cyclic prefix (CP) incorporated in the OFDM scheme, the spreading of each symbol over the consecutive symbol is absorbed by CP and hence the detrimental effects of ISI are eliminated.

Delay Spread and Coherence Bandwidth: The maximum delay spread is quantified by the CIR duration, over which a non-negligible amount of energy is dispersed, while coherence bandwidth, B_c of the channel is specified by the range of frequencies over which the signal experiences correlated fading.

The coherence bandwidth exhibits an inverse relatioship with the rms delay spread. Specifically, we have:

$$B_c \approx \frac{1}{\alpha\sigma_\tau}, \tag{2.28}$$

where σ_τ denotes the rms delay spread, and α is a constant.

We have characterized the performance of the schemes proposed in this thesis using the COST 207-RA, COST 207-RA6 and COST 207-TU12 channel models. The detailed power delay profile of the different taps which determine the coherence bandwidth and/or delay spread of this channel model may be found in [139] and [141].

2.3.5 Performance of the STSK Scheme under Different Channel Scenarios

We characterize the single-carrier STSK both in narrowband and wideband environments. The basic simulation parameters are listed in Table 2.3.

It is demonstrated in Figure 2.8 that the single-carrier STSK ($M = 2, N = 2, T = 2, Q = 2$) scheme operating in conjunction with BPSK modulation works well in narrowband scenarios, but it exhibits a severe error floor in dispersive channels, when the COST207-RA [141] channel model is considered. In the more dispersive typical urban (TU) scenario [139, 141], the STSK scheme suffers from a substantial further performance degradation. The simulation results characterizing STSK for different channel situations are shown in Figure 2.8. Observe that the STSK scheme's performance is better for transmission over the COST207-RA6 channel model than that over the COST207-RA model, although the number of channel taps is higher in the COST207-RA6 model. This is because although the COST207-RA model has less taps, it has a higher total delay spread than the COST207-RA6 channel model.

The eroded performance of the single-carrier STSK scheme motivated us to conceive a multicarrier based STSK system relying on the OFDM system philosophy to be developed in Section 2.4.

2.4 OFDM Aided Space-Time Shift Keying

The STSK system proposed in [49, 57] and discussed in Subsection 2.2.7 exhibits an excellent multiple-antenna performance in narrowband channels. However, in a wideband environment the STSK system suffers from the inter-symbol interference (ISI) imposed by the channel and consequently the performance degrades. In [5], the authors proposed space-time-frequency shift keying (STFSK) as a technique capable of overcoming the effects of dispersive channels, whilst striking the required diversity-multiplexing trade-offs, similarly to the STSK scheme. STFSK is capable of exploiting both time-, space- and frequency diversity, hence attaining a good

Table 2.3: Main system parameters for STSK

Simulation parameter	*Value*
Fast fading model	Correlated Rayleigh fading
Doppler frequency	0.01
Channel specification	Narrowband channel
No. of OFDM subcarriers	64
Length of cyclic prefix	32
No. of Tx AE, M	2
No. of Rx AE, N	2
No. of Tx time slots, T	2
No. of dispersion matrices	$Q = 2, 4$
STSK specification	$(M = 2, N = 2, T = 2, Q = 2, 4)$
Modulation Order	$\mathcal{L}$ =2, 4

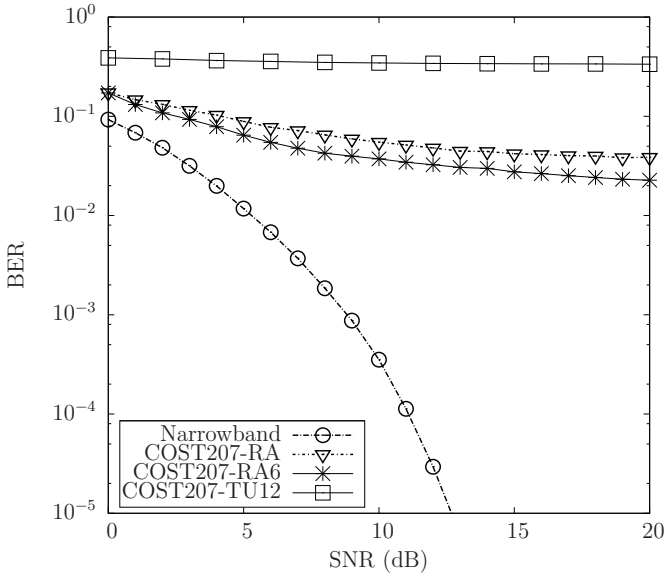

Figure 2.8: BER performance of STSK $(M = 2, N = 2, T = 2, Q = 2)$, BPSK scheme of Figure 2.5 using the optimal ML detector of [49] under different channel conditions. Although STSK performs well in non-dispersive channels, its performance in multipath channels becomes poor. The system parameters are listed in Table 2.3.

performance even in dispersive channels. The frequency dimension is exploited using frequency shift keying (FSK) modulation at the transmitter and a square-law detector at the receiver. Nevertheless, this realization of the STFSK scheme suffers from the typical drawbacks of non-coherent FSK demodulation. These impediments of STFSK may be eliminated by reduced-rate OFDM-style parallel transmissions over numerous non-dispersive sub-carriers.

In this section, we propose a novel modality of realizing space-time coding designed for broadband channels using orthogonal frequency division multiplexing (OFDM) combined with the STSK scheme. More particularly, the OFDM modem transforms the time-domain (TD) spreading operation of the STSK scheme to frequency domain (FD) spreading. This allows us to overcome the typical broadband channel's impairments.

2.4.1 OFDM-Aided STSK: System Overview

The basic idea of the proposed STSK-OFDM system is to use the OFDM technique in order to create a number of parallel FD sub-channels, where the sub-channel bitrate is sufficiently low for the sub-channel symbols to avoid dispersion.

The resultant system employs an OFDM modulator having N_c sub-carriers, where $\mathcal{T}$ is the symbol sampling interval and each STSK block consists of T symbol durations.

2.4.1.1 Transmitter

The model of [73, 142] has been adopted for realizing a STSK-based MIMO-OFDM system obeying the system's architecture of Figure 2.9. The first block of the transmission scheme is a STSK encoder [49] followed by OFDM transmissions. The OFDM-aided STSK encoding process relying on M transmit antenna elements (AEs) and T symbol durations is described as follows:

1. The encoder is fed with a block of $B = \log_2(\mathcal{L} \cdot Q)$ bits, which are spread over T time slots of an STSK symbol; the $\log_2 Q$ bits select one of the Q space-time matrices taken from the set $\{\boldsymbol{A}_q\}_{q=1}^{Q}$, where we have $\boldsymbol{A}_q \in \mathbb{C}^{M \times T}$ $\forall q$; $\log_2(\mathcal{L})$ bits correspond to a specific symbol in a $\mathcal{L}$-PSK/QAM constellation $\mathcal{C}_\mathcal{L}$;

2. The resultant STSK codeword is then $\boldsymbol{X} = \boldsymbol{A}_q s_l$, where we have $s_l \in \mathcal{C}_\mathcal{L}$ and $\boldsymbol{A}_q \in \{\boldsymbol{A}_q\}_{q=1}^{Q}$; $\mathcal{C}_\mathcal{L}$ has to be a unity-energy constellation, where the space-time dispersion matrices have to satisfy the power constraint of:

$$\mathrm{tr}(\boldsymbol{A}_q^{\mathrm{H}} \boldsymbol{A}_q) = T \quad \forall q, \tag{2.29}$$

in order to have unity energy for each sub-carrier.

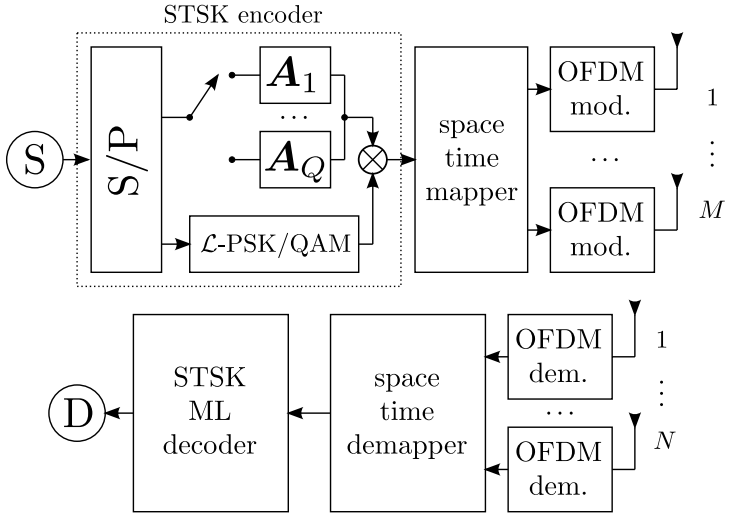

Figure 2.9: The transceiver architecture of the proposed STSK-OFDM system.

We will refer to this system as an OFDM-aided STSK(M, N, T, Q) scheme in conjunction with the $\mathcal{L}-$ary modulation, where M is the number of transmit antennas and N is the number of receive antennas.

2.4.1.2 Mapping of STSK Codewords to Subcarriers

Having generated the STSK blocks, the blocks of symbols are then mapped to N_c subcarriers. We have considered two mapping strategies, which are discussed in the context of Figure 2.10 and Figure 2.11, respectively. These two mapping strategies were proposed in the context of our collaborative work on OFDM aided STSK [119]. We describe the STSK symbol-to-subcarrier mapping illustrated in Figure 2.10 here, while that illustrated in Figure 2.11 in Section 2.4.1.3. Both mapping schemes have their respective merits and disadvantages, as discussed in Section 2.4.1.4. As shown in Figure 2.10, N_c space-time blocks are collected for constructing an STSK-OFDM frame, where N_c is the number of OFDM subcarriers. At any of the M AEs and in any of the T time slots, N_c STSK blocks are mapped to the N_c subcarriers and thus constitute an OFDM symbol.

Hence the TD STSK-OFDM signal transmitted from the mth transmit AE at the T_i time slot ($T_i = 1, 2, \ldots, T$) may be formulated as [73] [98]:

$$x_{m,T_i}(t) = \frac{1}{\sqrt{N_c}} \sum_{n_c=1}^{N_c} X_{m,T_i}[n_c] e^{j2\pi f_{n_c} t}, \qquad \mathcal{T} \leq t \leq (N_c + 1)\,\mathcal{T} \tag{2.30}$$

where $X_{m,T_i}[n_c]$ is the n_c-th data symbol, while $N_c\mathcal{T}$ is the length of the OFDM symbol. In order to maintain the orthogonality of the subcarriers, the subcarrier frequencies have to be equally spaced by:

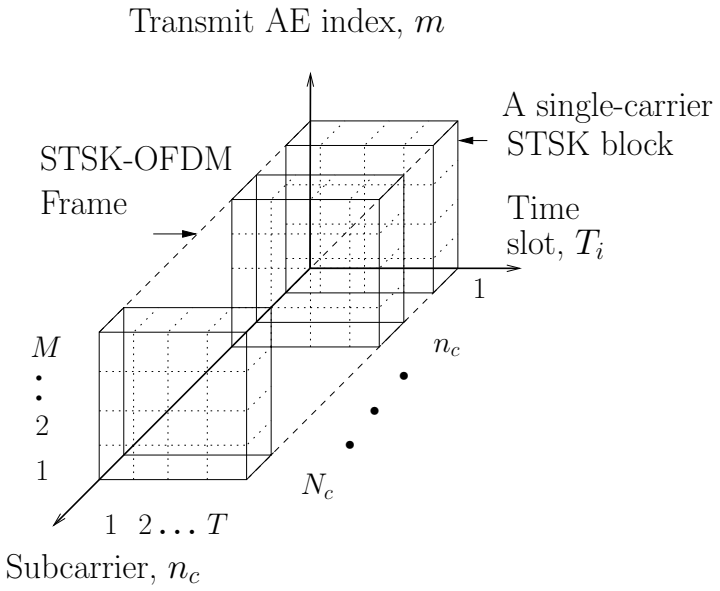

Figure 2.10: Formation of an STSK-OFDM frame consisting of N_c parallel STSK blocks to be transmitted over N_c parallel subcarriers.

$$f_{n_c} = \frac{n_c}{N_c \mathcal{T}}. \tag{2.31}$$

The TD sampling of the OFDM symbol can be formulated as:

$$x_{m,T_i}(n_s \mathcal{T}) = \frac{1}{\sqrt{N_c}} \sum_{n_c=1}^{N_c} X_{m,T_i}[n_c] e^{j2\pi \frac{n_s n_c}{N_c}}, \quad 1 \leq n_s \leq N_c \tag{2.32}$$

which is expressed in terms of the inverse discrete Fourier transform (IDFT) of the symbol stream $\boldsymbol{X}_{m,T_i} = \left\{ X_{m,T_i}[n_c] \right\}_{n_c=1}^{N_c}$ as:

$$\boldsymbol{x}_{m,T_i} = \mathrm{IDFT}_{N_c} \left\{ \boldsymbol{X}_{m,T_i} \right\}. \qquad m = 1, \ldots, M \quad T_i = 1, ..., T. \tag{2.33}$$

As usual, a cyclic prefix (CP), which has to be longer than the channel's delay spread, has to be appended to each of the TD OFDM symbols in order to eliminate the effects of ISI. After appending the cyclic prefix of length $L_{\mathrm{cp}} = (L-1)$, the resultant sequence, $\boldsymbol{x}_{m,T_i,\mathrm{cp}} = \left\{ x_{m,T_i,\mathrm{cp}}[n_c] \right\}_{n_c=-L_{\mathrm{cp}}+1}^{N_c}$ can be expressed as:

$$\left\{ x_{m,T_i}[N_c - L_{\mathrm{cp}} + 1] \ldots x_{m,T_i}[N_c] \; x_{m,T_i}[1] \; x_{m,T_i}[2] \ldots x_{m,T_i}[N_c] \right\}, \tag{2.34}$$

for every transmit antenna $m = 1, 2, \ldots, M$, with L being the length of the finite impulse response (FIR) filter that models the frequency-selective channel.

2.4.1.3 Alternative Mapping of STSK Codewords to Subcarriers

In contrast to the mapping of Section 2.4.1.2, it is also possible to carry out the mapping of bits to non-dispersive subcarriers as follows.

The space-time mapper collects J space-time codewords, where $J = N_c/T$ and the J STSK symbols constitute the frame $\mathcal{F}_T$, defined as the matrix:

$$\mathcal{F}_T = \Big[\boldsymbol{X}\,[1]\ \boldsymbol{X}\,[2]\ \ldots\ \boldsymbol{X}\,\Big[J\Big]\Big] \in \mathbb{C}^{M\times N_c}, \tag{2.35}$$

where $\boldsymbol{X}[j]$ is the j^{th} space-time codeword in the frame. Clearly, in this mapping N_c has to be a multiple of T. The frame $\mathcal{F}_T$ can also be written as:

$$\mathcal{F}_T = \Big[\tilde{\mathbf{S}}[0]\,\tilde{\mathbf{S}}[1]\ \ldots\ \tilde{\mathbf{S}}[N_c]\Big] \in \mathbb{C}^{M\times N_c}, \tag{2.36}$$

where $\tilde{\mathbf{S}}[n_c] \in \mathbb{C}^{M\times 1}$ for every $n_c = 0,\ldots,N_c$ represents the columns of $\mathcal{F}_T$. The OFDM modulation is applied along the rows of the frame $\mathcal{F}_T$. Hence the vector $\tilde{\mathbf{S}}[n_c]$ is defined as:

$$\tilde{\mathbf{S}}[n_c] = \Big(\boldsymbol{X}(\lceil n_c/T\rceil)\Big)_{[n_c]_T+1} \quad n_c = 1,\ldots,N_c, \tag{2.37}$$

implying that the $([n_c]_T+1)^{\text{th}}$ column of the $\lceil n_c/T\rceil^{\text{th}}$ space-time codeword in the frame $\mathcal{F}_T$ is transmitted via the ${n_c}^{\text{th}}$ sub-carrier of the OFDM system, where the $(\cdot)_t$ operator selects the t^{th} column of a matrix, $[\cdot]_N$ represents the modulo-N operator and $\lceil\cdot\rceil$ is the ceiling operator.

Let the m^{th} component of the vector $\tilde{\mathbf{S}}[n_c]$ be denoted by $\tilde{S}_m[n_c]$, hence we have

$$\tilde{\mathbf{S}}[n_c] = \Big[\tilde{S}_1[n_c]\tilde{S}_2[n_c]\ldots\tilde{S}_M[n_c]\Big]^T, \tag{2.38}$$

where $(\cdot)^T$ is the transpose operator. The N_c symbols $\big\{\tilde{S}_m[n_c]\big\}_{n_c=1}^{N_c}$ represent a length-N_c sequence that is denoted by $\tilde{\boldsymbol{S}}_m$. As explained in Figure 2.11, the sequence $\big\{\tilde{\boldsymbol{S}}_m\big\}$ is OFDM-modulated using the IDFT-based OFDM modulator, resulting in the sequence:

$$\tilde{\boldsymbol{s}}_m = \text{IDFT}_{N_c}\Big\{\tilde{\boldsymbol{S}}_m\Big\}, \tag{2.39}$$

for each transmit antenna $m = 1,\ldots,M$. The sequences $\big\{\tilde{s}_m[n_c]\big\}_{n_c=1}^{N_c}\ \forall m$ may be grouped in the sequence of vectors $\big\{\tilde{\mathbf{s}}[n_c]\big\}_{n_c=1}^{N_c} \in \mathbb{C}^{M\times 1}$, where:

$$\tilde{\mathbf{s}}[n_c] = \Big[\tilde{s}_1[n_c]\tilde{s}_2[n_c]\ldots\tilde{s}_M[n_c]\Big]^T\ n_c = 1,\ldots,N_c. \tag{2.40}$$

Equation (2.40) represents the N_c TD samples of each of the M OFDM symbols transmitted by the M transmit antennas.

Again, the usual CP is attached to each TD OFDM symbol of $\big\{\tilde{\mathbf{s}}[n_c]\big\}_{n_c=1}^{N_c}$, leading to the signal vector $\big\{\tilde{\mathbf{s}}_{\text{cp}}[n_c]\big\}_{n_c=1}^{N_c}$, which is transmitted through the frequency-selective MIMO channel. Each component of the signal vector $\big\{\tilde{\mathbf{s}}_{\text{cp}}[n_c]\big\}_{n_c=1}^{N_c}$ is given by Eq. (2.34) for every transmit antenna $m = 1,\ldots,M$. The parameter $L_{\text{cp}} = L_{\text{ch}} - 1$ in (2.34) is the length of the CP and L_{ch} is the length of the FIR filter that models the frequency selective channel.

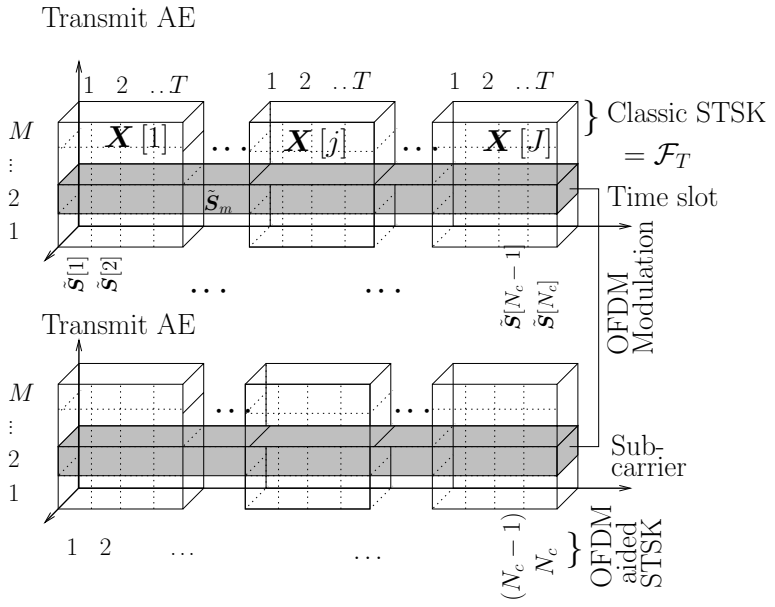

Figure 2.11: Illustration of the alternative mapping of STSK space-time blocks to the subcarriers. In the classic STSK framework the t^{th} column of the j^{th} space-time codeword is transmitted during the $[T \cdot (j-1)+t]^{\text{th}}$ time interval. In our OFDM-aided STSK system J space-time codewords are transmitted at the same time in a single OFDM frame, by spreading the codewords in the frequency domain.

2.4.1.4 Comparison of the Two Mapping Strategies

Figure 2.10 and Figure 2.11 illustrate the strategies of mapping the STSK codewords to the N_c orthogonal subcarriers of the OFDM scheme. The mapping method illustrated in Figure 2.10 takes N_c consecutively generated STSK codewords and transmits the codewords in parallel. To be more specific, the codewords are arranged in parallel as seen in Figure 2.10 and then all the N_c symbols corresponding to a particular AE in a particular time slot (TS) jointly form a N_c-symbol pipe having a square-shaped cross-section and spanning N_c subcarriers, as shown in Figure 2.12.(a). Then OFDM modulation is performed over every block of such N_c symbols.

By contrast, N_c/T STSK codewords are arranged serially in the alternative mapping scheme of Figure 2.11. Now, since each STSK codeword row consists of T symbols, the total number of symbols in any row of the serially concatenated arrangement will be N_c. OFDM modulation is performed over these N_c symbols and the resultant signal is transmitted over the specific transmit AE corresponding to the row.

For example, consider a OFDM-STSK scheme specified by the parameters $(M, N, T, Q) = (4, 4, 4, 4)$ in conjunction with QPSK modulation and employing 16 OFDM subcarriers. The first mapping considers the 16 STSK codewords to be placed in parallel, as shown in Figure 2.12.(a), each of which is represented by an $(M \times T) = (4 \times 4)$-element matrix. OFDM modulation is then carried out over the shaded symbol-pipe for mapping an AE- and TS-specific

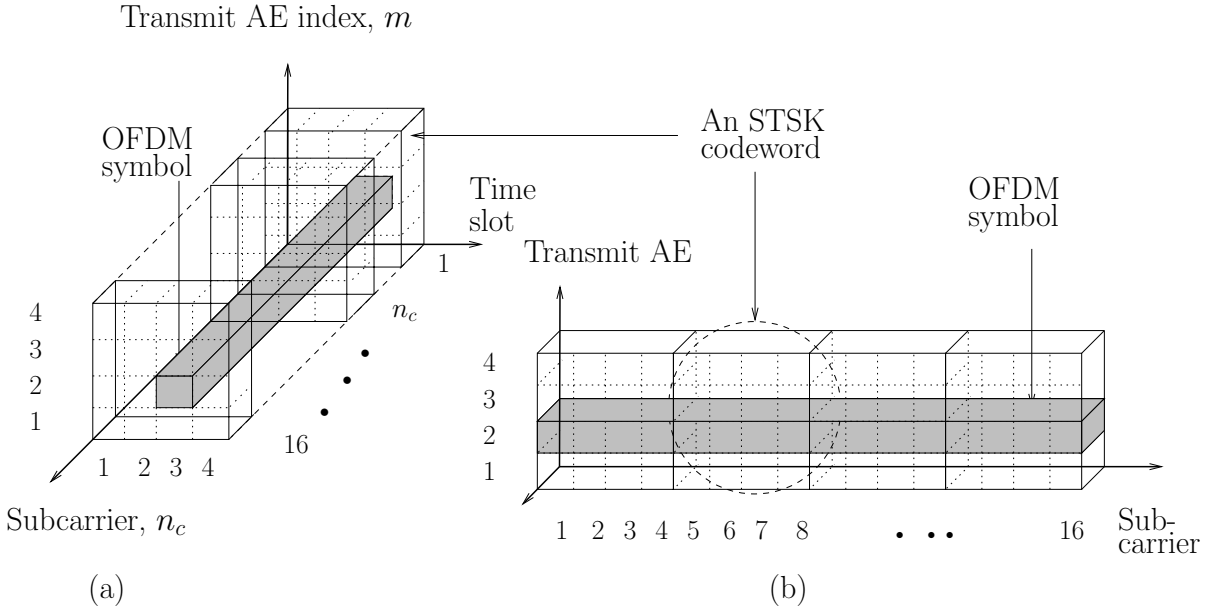

Figure 2.12: Comparison of the two strategies shown in Figure 2.10 and Figure 2.11 for mapping the STSK codewords to OFDM subcarriers. OFDM modulation over N_c symbols as well as the construction of the OFDM symbol is shown as a symbol-pipe having a square-shaped cross-section, which is formed from N_c STSK blocks at a particular (m, T_i).

QPSK symbols to one of the 16 subcarriers. By contrast, the alternative mapping is shown in Figure 2.12.(b), where a total of 16 QPSK symbols of AE=2, which belong to $N_c/T = 4$ consecutive STSK codewords, are mapped to a total of 16 subcarriers. OFDM is invoked over the 16 shaded QPSK symbols and a total of four such two-dimensional frames are requiredto for transmitting 16 STSK codewords.

Note furthermore that owing to the parallel mapping depicted in Figure 2.10, the scheme benefits both from the space-time diversity gain provided by the STSK scheme and from the reduced-rate parallel transmissions achieved by parallel mapping of the transmitted signal and is particularly helpful for for the sake of avoiding the detrimental effects of inter-symbol interferences (ISI) imposed by dispersive broadband channels. By contrast, the mapping illustrated by Figure 2.11 transmits the T TD symbols of an STSK codeword on T consecutive subcarriers, which might experience correlated fading.

The mapping of Figure 2.11 imposes some additional restrictions on the system's design. Firstly, since N_c/T STSK codewords are arranged serially, N_c always has to be a multiple of T. Secondly, owing to the inverse fast Fourier transform (IFFT) invoked for facilitating OFDM modulation, N_c has to be a power of 2. Hence the STSK parameter T in the alternative mapping of Figure 2.11 has to be an even number.

Due to the above-mentioned design restrictions, we advocate the mapping shown in Figure 2.10 in the forthcoming chapters.

2.4.1.5 Achievable Throughput

The proposed scheme transmits an OFDM symbol every (N_c+L_{cp}) symbols (the duration of an OFDM symbol including the CP). Every OFDM symbol carries N_c STSK symbols and every STSK symbol carries $\log_2(\mathcal{L}\cdot Q)$ bits. Hence the system's throughput is:

$$R_{\text{cp}} = \frac{N_c \log_2(\mathcal{L}\cdot Q)}{T(N_c + L_{\text{cp}})} = \frac{\log_2(\mathcal{L}\cdot Q)}{T\left(1+\dfrac{L_{\text{cp}}}{N_c}\right)} \quad \left[\frac{\text{bits}}{\text{symbol duration}}\right] \tag{2.41}$$

When using a high number of subcarriers, however, the effect of the CP on the throughput gradually becomes negligible, hence we have:

$$R = \frac{\log_2(\mathcal{L}\cdot Q)}{T} \quad \left[\frac{\text{bits}}{\text{symbol duration}}\right]. \tag{2.42}$$

2.4.1.6 Receiver

In this section, we consider the OFDM-aided STSK receiver based on the mapping of Figure 2.10. Let us consider a frequency-selective channel, where the discrete-time CIR matrix may be modelled as:

$$\boldsymbol{H}[n_c] = \sum_{l=1}^{L} \boldsymbol{H}[l]\delta[n_c - l] \ \in \mathbb{C}^{N\times M}, \tag{2.43}$$

where the matrix $\boldsymbol{H}[l] \in \mathbb{C}^{N\times M}$ has complex-valued normally distributed entries according to $\mathcal{CN}(\mu_l, \sigma_l^2)$ for every $l = 1, \ldots, L$ and $\delta[\cdot]$ is the discrete-time Dirac delta function. The parameters L_{ch}, μ_l and σ_l^2 depend on the specific channel model adopted. Assuming perfect synchronization at the receiver of Figure 2.9, the discrete-time signal received after CP removal at the receive AE n at time slot T_i may be written as [73]:

$$\boldsymbol{y}_{n,T_i} = \sum_{m=1}^{M} \boldsymbol{h}_{n,m} \circledast_{N_c} \boldsymbol{x}_{m,T_i} + \boldsymbol{v}_{n,T_i}, \qquad n = 1, \ldots, N, \tag{2.44}$$

where $\circledast_{N_c}$ represents the length-N_c circular convolution operator.

After applying the N_c-point discrete Fourier transform (DFT) operation at each receive AE, the FD channel-output matrix $\boldsymbol{Y}$ at the receiver may be expressed in terms of its components as: $\boldsymbol{Y}_{n,T_i} = \text{DFT}_{N_c}\left\{\boldsymbol{y}_{n,T_i}\right\}$. Upon using (2.44) , $\boldsymbol{Y}_{n,T_i}$ reduces to [73]:

$$\boldsymbol{Y}_{n,T_i} = \sum_{m=1}^{M} \tilde{\boldsymbol{H}}_{n,m}\boldsymbol{X}_{m,T_i} + \boldsymbol{V}_{n,T_i}, \qquad n = 1, \ldots, N, \tag{2.45}$$

where $\tilde{\boldsymbol{H}}_{n,m} = \text{diag}\{\tilde{h}_{n,m}[1], \tilde{h}_{n,m}[2], ..., \tilde{h}_{n,m}[N_c]\} \in \mathbb{C}^{N_c\times N_c}$ is a diagonal matrix whose diagonal elements are $\tilde{\boldsymbol{h}}_{n,m} = \text{DFT}_{N_c}\left\{\boldsymbol{h}_{n,m}\right\}$, representing the FD channel transfer gains [18, 73]. More

particularly, $\tilde{\boldsymbol{H}}[n_c]$ may be viewed as the MIMO channel's FD transfer matrix, since it represents the $(N \times M)$-element MIMO channels' response for each subcarrier n_c. Still referring to (2.45), we have $\boldsymbol{V}_{n,T_i} = \text{DFT}_{N_c}\{\boldsymbol{v}_{n,T_i}\}$, which represents the FD additive white Gaussian noise (AWGN) vector. Equation (2.45) can be re-written in a matrix form as:

$$\boldsymbol{Y}[n_c] = \tilde{\boldsymbol{H}}[n_c]\boldsymbol{X}[n_c] + \boldsymbol{V}[n_c] \qquad n_c = 1, \ldots, N_c \tag{2.46}$$

where $\boldsymbol{Y}[n_c] \in \mathbb{C}^{N\times T}$, $\tilde{\boldsymbol{H}}[n_c] \in \mathbb{C}^{N\times M}$, $\boldsymbol{X}[n_c] \in \mathbb{C}^{M\times T}$ and $\boldsymbol{V}[n_c] \in \mathbb{C}^{N\times T}$.

Thus we see from (2.46) that our STSK-based scheme OFDM modulates the symbols to be transmitted from a particular AE and in a particular time slot, which are then mapped to N_c adjacent parallel orthogonal sub-carriers having different channel gains.

Following the OFDM demodulation at the space-time demapper, the received symbols $\boldsymbol{Y}[n_c] \in \mathbb{C}^{N\times T}$ are then passed through the single-stream ML decoder [49]. The resultant system may then be expressed in terms of the linearized system model of [32] as:

$$\bar{\boldsymbol{Y}} = \bar{\tilde{\boldsymbol{H}}}\boldsymbol{\chi}\boldsymbol{K}_{l_c,q} + \bar{\boldsymbol{V}} \tag{2.47}$$

where

$$\bar{\boldsymbol{Y}} = vec(\boldsymbol{Y}) \in \mathbb{C}^{NT\times 1}, \tag{2.48}$$

$$\bar{\tilde{\boldsymbol{H}}} = \boldsymbol{I}\otimes\tilde{\boldsymbol{H}} \in \mathbb{C}^{NT\times MT}, \tag{2.49}$$

$$\boldsymbol{\chi} = [vec(\boldsymbol{A}_1), \cdots, vec(\boldsymbol{A}_Q)] \in \mathbb{C}^{MT\times Q}, \tag{2.50}$$

$$\boldsymbol{K}_{l_c,q} = [\underbrace{0, \cdots, 0}_{q-1}, s_{l_c}, \underbrace{0, \cdots, 0}_{Q-q}]^T \in \mathbb{C}^{Q\times 1}, \tag{2.51}$$

and

$$\bar{\boldsymbol{V}} = vec(\boldsymbol{V}) \in \mathbb{C}^{NT\times 1}, \tag{2.52}$$

where l_c stands for the index of the $\mathcal{L}$-point constellation symbol s_{l_c}, which is placed in the q-th position of the equivalent transmit symbol vector $\boldsymbol{K}_{l_c,q}$. Now, the single-stream based ML estimates $(\hat{l_c}, \hat{q})$ of the n_c-th STSK-OFDM symbol and its constituent transmitted bits are obtained from [48, 49] as:

$$\left(\hat{l_c}, \hat{q}\right) = \arg\min_{l_c,q}\left\{\left\|\bar{\boldsymbol{Y}} - \bar{\tilde{\boldsymbol{H}}}\boldsymbol{\chi}\boldsymbol{K}_{l_c,q}\right\|^2\right\}. \tag{2.53}$$

2.4.1.7 Receiver Corresponding to Mapping of Figure 2.11

The received signal associated with the mapping of Figure 2.11 is detected in a manner similar to that described in Section 2.4.1.6, but bearing in mind that the OFDM-STSK frame under this mapping consists of N_c columns of the STSK codewords, rather than of N_c parallel codewords.

The receiver operation corresponding to this mapping is summarized in Figure 2.13. The signal received by AE n may be expressed as:

$$\boldsymbol{r}_n = \sum_{m=1}^{M} \boldsymbol{h}_{n,m} \circledast_{N_c} \tilde{\boldsymbol{s}}_m + \boldsymbol{v}_n. \qquad n = 1, \ldots, N. \tag{2.54}$$

After DFT-based OFDM demodulation of each receive antenna's signal according to $\boldsymbol{R}_n = \mathrm{DFT}_{N_c}\{\boldsymbol{r}_n\}$, the FD output may be written as:

$$\boldsymbol{R}_n[n_c] = \sum_{m=1}^{M} \tilde{\boldsymbol{H}}_{n,m}[n_c]\tilde{\boldsymbol{S}}_m[n_c] + \boldsymbol{V}_n[n_c], \tag{2.55}$$

for $n = 1, 2, \ldots, N$ and for $n_c = 1, 2, \ldots, N_c$. In (2.55) we have $\boldsymbol{V}_n = \mathrm{DFT}_{N_c}\{\boldsymbol{v}_n\}$ and $\tilde{\boldsymbol{H}}_{n,m} = \mathrm{diag}\{\tilde{h}_{n,m}[1], \tilde{h}_{n,m}[2], ..., \tilde{h}_{n,m}[N_c]\} \in \mathbb{C}^{N_c \times N_c}$ is the diagonal matrix whose diagonal elements are the FD channel tranfer gains [18, 73]. Equation (2.55) may be expressed in a matrix form as:

$$\boldsymbol{R}[n_c] = \tilde{\boldsymbol{H}}[n_c]\tilde{\mathbf{S}}[n_c] + \boldsymbol{V}[n_c] \quad n_c = 1, \ldots, N_c, \tag{2.56}$$

where we have $\boldsymbol{R}[n_c] = [R_1[n_c], R_2[n_c], \ldots, R_N[n_c]]^T$ and $\boldsymbol{V}[n_c] = [V_1[n_c], V_2[n_c], \ldots, V_N[n_c]]^T$. Finally, using Eq. (2.37), (2.56) may be written as:

$$\boldsymbol{R}[n_c] = \tilde{\boldsymbol{H}}[n_c]\Big(\boldsymbol{X}(\lceil n_c/T \rceil)\Big)_{[n_c]_T+1} + \boldsymbol{V}[n_c]. \tag{2.57}$$

As seen from (2.57), each space-time codeword grouped in the frame $\mathcal{F}_T$ is transmitted through a set of adjacent sub-carriers with different channel gains $\tilde{\boldsymbol{H}}[n_c]$. Furthermore, we may conclude that the OFDM regime transforms the TD spreading of the STSK codewords to FD spreading, since the $\mathcal{L}$-ary symbol is spread across the sub-carriers. More particularly, as detailed in Figure 2.13, each column of a space-time codeword is transmitted over a specific sub-carrier and hence through a non-dispersive subchannel.

Following OFDM demodulation, the space-time demapper decomposes every received frame $\mathcal{F}_{\mathrm{R}}$ into J constituent space-time codewords. More particularly, the received frame becomes:

$$\mathcal{F}_{\mathrm{R}} = \Big[(\boldsymbol{Y}[1])_1 \ \ldots \ (\boldsymbol{Y}[1])_T \ \ldots \qquad \ldots \ (\boldsymbol{Y}[J])_1 \ \ldots \ (\boldsymbol{Y}[J])_T\Big] \in \mathbb{C}^{N \times N_c}, \tag{2.58}$$

where $\boldsymbol{Y}[j] \in \mathbb{C}^{N \times T}$ is the j^{th} received space-time codeword in the frame $\mathcal{F}_{\mathrm{R}}$, the operator $(\cdot)_t$ selects the t^{th} column of a matrix (hence we have $(\mathbf{Y}[j])_t \in \mathbb{C}^{N \times 1}\ \forall j, t$) and:

$$(\boldsymbol{Y}[j])_t = \tilde{\boldsymbol{H}}_t^j (\boldsymbol{X}[j])_t + \boldsymbol{V}[T \cdot (j-1) + t - 1] \qquad t = 1, \ldots, T. \tag{2.59}$$

In (2.59) the matrices $\tilde{\boldsymbol{H}}_t^j$ are defined as:

$$\tilde{\boldsymbol{H}}_t^j = \tilde{\boldsymbol{H}}[T \cdot (j-1) + t - 1] \tag{2.60}$$

for every $t = 1, \ldots, T$ and every $j = 1, \ldots, J$.

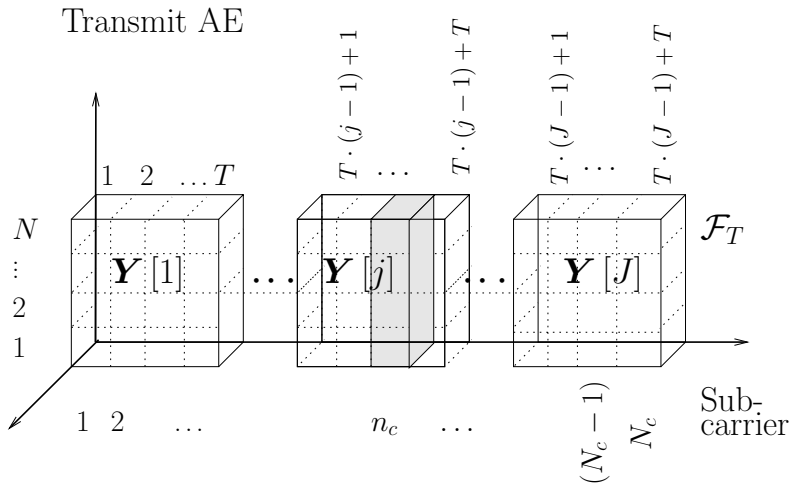

Figure 2.13: The received column vectors $\boldsymbol{R}[n_c] \quad n_c = 1, 2, \ldots, N_c$ are demapped to J matrices $\boldsymbol{Y}[j] \quad j = 0, 1, \ldots, J$ at the receiver. Note that the t^{th} column of the j^{th} space-time codeword $\boldsymbol{X}[j] \in \mathbb{C}^{M \times T}$ is transmitted through the $n_c^{\text{th}} = [T \cdot (j-1) + t - 1]^{\text{th}}$ sub-carrier, i.e. through a flat-fading sub-channel with channel gain $\tilde{\boldsymbol{H}}_t^j = \tilde{\boldsymbol{H}}[T \cdot (j-1) + t - 1]$.

Finally, the STSK decoder invokes the optimal single-antenna-based maximum likelihood (ML) decision rule of [49] for decoding the space-time codewords with the aid of a ML detector. Specifically, the estimate $\left(\hat{l}_c[j], \hat{q}[j]\right)$ for the j^{th} space-time codeword is given by minimizing the following metric:

$$\left(\hat{l}_c[j], \hat{q}[j]\right]) = \arg\min_{l_c,q} \left\{ \left\| \overline{\boldsymbol{Y}}[j] - \overline{\tilde{\boldsymbol{H}}}^j \boldsymbol{\chi} \boldsymbol{K}_{l_c,q} \right\|^2 \right\}, \tag{2.61}$$

where we have:

$$\overline{\boldsymbol{Y}}[j] = \text{vec}(\boldsymbol{Y}[j]) \in \mathbb{C}^{NT \times 1}, \tag{2.62}$$

$$\boldsymbol{\chi} = [\text{vec}(\boldsymbol{A}_1) \cdots \text{vec}(\boldsymbol{A}_Q)] \in \mathbb{C}^{MT \times Q}, \tag{2.63}$$

$$\boldsymbol{K}_{l_c,q} = [\underbrace{0 \cdots 0}_{q-1}, s_l, \underbrace{0 \cdots 0}_{Q-q}]^T \in \mathbb{C}^{Q \times 1} \tag{2.64}$$

and $\overline{\boldsymbol{H}}_{\text{eq}}^j \in \mathbb{C}^{NT \times MT}$ is:

$$\overline{\tilde{\boldsymbol{H}}}^j = \begin{bmatrix} \tilde{\boldsymbol{H}}_1^j & \boldsymbol{0} & \cdots & \boldsymbol{0} \\ \boldsymbol{0} & \tilde{\boldsymbol{H}}_2^j & \cdots & \boldsymbol{0} \\ \vdots & \vdots & \ddots & \vdots \\ \boldsymbol{0} & \boldsymbol{0} & \cdots & \tilde{\boldsymbol{H}}_T^j \end{bmatrix}, \tag{2.65}$$

where $\boldsymbol{0} \in \mathbb{C}^{N \times M}$ is an $(N \times M)$-element zero matrix.

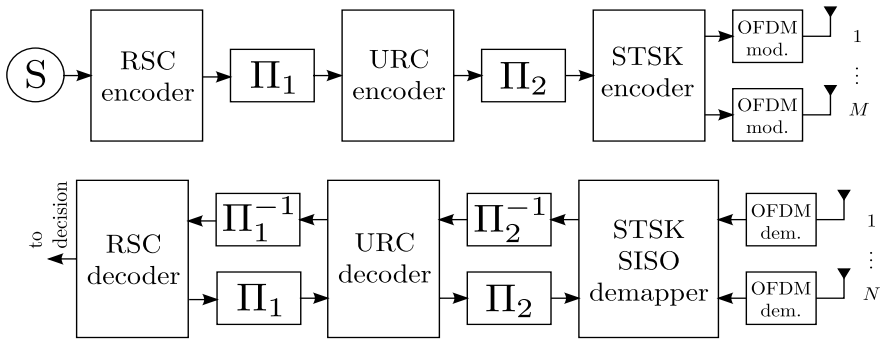

Figure 2.14: Three stage RSC-URC coded OFDM-aided STSK scheme.

2.5 Channel-Coded OFDM-aided STSK

In a serially concatenated turbo-coded scenario a recursive systematic convolutional (RSC) encoder and a unity rate convolutional (URC) encoder are introduced before the STSK encoder, as detailed in [5], with the aim of attaining a near-capacity performance. The explicit benefit of using the URC encoder of Figure 2.14 is that it has an infinite impulse response and hence spreads the extrinsic information efficiently without increasing the interleaver delay. As a benefit, it results in a near-capacity performance. According to Figure 2.14, the source bits are convolutionally encoded and then interleaved by a random bit interleaver π_1. A (2,1,2) RSC code is employed and following channel interleaving, the symbols are precoded by a URC encoder, which has an infinite impulse response. Then the precoded bits are further interleaved by a second interleaver π_2 and the inteleaved bits are passsed through the STSK-OFDM scheme to be transmitted through an M-element MIMO transmitter in the TD.

The received complex-valued symbols of Figure 2.14 are passed through the FFT unit in order to OFDM-demodulate the symbols and the resultant FD symbols are then fed to the STSK demapper. We note that if the equivalent FD received signal $\overline{\mathbf{Y}}$ carries B channel-coded binary bits $b = [b_1, b_2, ..., b_B]$, then the extrinsic log-likelihood ratio (LLR) of the bits, $b_k,\ k = 1, ..., B$ gleaned from the demapper can be expressed as [5, 143]:

$$L_e(b_k) = \ln \frac{\sum_{\boldsymbol{K}_{lc,q} \in K:\{b=1\}} e^{-\|\bar{\boldsymbol{Y}} - \bar{\boldsymbol{H}}_{\text{eq}} \boldsymbol{\chi} \boldsymbol{K}_{lc,q}\|^2 / N_0 + \sum_{j \neq k} b_j L_a(b_j)}}{\sum_{\boldsymbol{K}_{lc,q} \in K:\{b=0\}} e^{-\|\bar{\boldsymbol{Y}} - \bar{\boldsymbol{H}}_{\text{eq}} \boldsymbol{\chi} \boldsymbol{K}_{lc,q}\|^2 / N_0 + \sum_{j \neq k} b_j L_a(b_j)}}, \tag{2.66}$$

where $\boldsymbol{K}$ **:** b_k represents the set of equivalent transmit vectors as in Eq.(2.51) mapped from the B bits, $\{b_k\}_{k=1}^{B}$, while $L_a(b_j)$ is the *a priori* LLR corresponding to bits b_j. As a further

advance, we can use the max-log-MAP algorithm to simplify (2.66), yielding:

$$L_e(b_k) = \max_{\boldsymbol{K}_{l_c,q} \in K:\{b=1\}} \left[-\| \bar{\boldsymbol{Y}} - \bar{\boldsymbol{H}}_{\text{eq}} \boldsymbol{\chi} \boldsymbol{K}_{l_c,q} \|^2 / N_0 + \sum_{j \neq k} b_j L_a(b_j) \right] - \max_{\boldsymbol{K}_{l_c,q} \in K:\{b=0\}} \left[-\| \bar{\boldsymbol{Y}} - \bar{\boldsymbol{H}}_{\text{eq}} \boldsymbol{\chi} \boldsymbol{K}_{l_c,q} \|^2 / N_0 + \sum_{j \neq k} b_j L_a(b_j) \right]. \quad (2.67)$$

The Max-Log-MAP can be further modified by using the Jacobian logarithm [144,145] to reduce (2.67) to:

$$L_e(b_k) = \text{jac}_{\boldsymbol{K}_{l_c,q} \in K:\{b=1\}} \left[-\| \bar{\boldsymbol{Y}} - \bar{\boldsymbol{H}}_{\text{eq}} \boldsymbol{\chi} \boldsymbol{K}_{l_c,q} \|^2 / N_0 + \sum_{j \neq k} b_j L_a(b_j) \right] - \text{jac}_{\boldsymbol{K}_{l_c,q} \in K:\{b=0\}} \left[-\| \bar{\boldsymbol{Y}} - \bar{\boldsymbol{H}}_{\text{eq}} \boldsymbol{\chi} \boldsymbol{K}_{l_c,q} \|^2 / N_0 + \sum_{j \neq k} b_j L_a(b_j) \right], \quad (2.68)$$

where $\text{jac}_{\boldsymbol{K}_{l_c,q} \in K:\{b=1\}}[\bullet]$ and $\text{jac}_{\boldsymbol{K}_{l_c,q} \in K:\{b=0\}}[\bullet]$ represents the Jacobian logarithm of '$\bullet$', when the equivalent transmit symbol vector is a subset corresponding to k-th bits of 1 and 0, respectively and are usually implemented by look-up table.

The URC decoder processes the extrinsic information gleaned from the STSK demapper, in conjunction with its *a priori* information and generates extrinsic information for both the RSC decoder and the demapper. The RSC channel decoder exchanges extrinsic information with the URC decoder and after a number of iterations, outputs the estimated bits. It is noteworthy here that for each of the outer iterations between the RSC decoder and URC, there are a number of specified inner iterations between the URC and the STSK demapper.

2.6 Performance Results

Against the background of the performance degradation of the STSK system in wideband channels as elaborated in Subsection 2.3.5, we have investigated the performance of our OFDM-aided STSK system of Figure 2.9 and that of our channel-coded OFDM-STSK system of Figure 2.14 in dispersive channels using the parameters listed in Table 2.4. We have adopted the parallel mapping of STSK codewords to subcarriers as illustrated in Figure 2.10.

The performance of our STSK-OFDM scheme recorded for different channels is presented in Figure 2.15. Observe from Figure 2.15 that the STSK-OFDM performance in wideband channels essentially remains unaffected by the channel's dispersion. We see from Figure 2.15 that if the channel is nondispersive, there is virtually no difference in the performance of STSK, regardless whether OFDM has been incorporated into the system or not. In such channel conditions, both the STSK and the STSK-OFDM are capable of attaining excellent diversity

Table 2.4: Main system parameters for OFDM STSK

Simulation parameter	*Values*
Fast fading model	Correlated Rayleigh fading
Normalized Doppler frequency	0.01
Channel specification	COST207-RA, 4-tap channel
	COST207-RA6, 6-tap channel
	COST207-TU12, 12-tap channel
No. of OFDM subcarriers	64
Length of cyclic prefix	32
No. of Tx AE, M	2
No. of Rx AE, N	2
No. of Tx Time slots, T	2
No. of dispersion matrices	$Q = 2, 4$
STSK specification	$(M = 2, N = 2, T = 2, Q = 2, 4)$
Modulation order	$\mathcal{L}$ =2, 4
Outer decoder	RSC $(2, 1, 2)$
Generator polynomials	$(g_r, g) = (3, 2)_8$
Size of interleavers	240, 000 bits
Outer decoding iterations, I_{outer}	8
Inner decoder	URC
Inner decoding iterations, I_{inner}	2

versus multiplexing gain tradeoffs. By contrast, under dispersive channel conditions, STSK-OFDM is capable of maintaining its superiority not only in the rural scenario of the COST207-RA channel model, but also in the typical urban scenario modelled by the COST207-TU12 channel model. In fact, the STSK-OFDM performance recorded in different channel situations remains more or less similar to that of the narrowband benchmarker.

The BER performance of the coherent STSK $(M = 2, N = 2, T = 2, Q = 2)$ scheme employing BPSK modulation for transmission over a narrowband channel and that of our OFDM STSK $(M = 2, N = 2, T = 2, Q = 2)$ scheme employing BPSK modulation for transmission over COST207-RA6 channel, whilst relying both on genetically optimized DMs and on random choices for minimizing the PEP over 10^6 searches are compared in Figure 2.16. We observe that our scheme relying on the GA-optimized dispersion matrices exhibits a better performance than that of the random search based DMs.

We also investigated the achievable performance of our three stage concatenated RSC- and URC-coded STSK-OFDM $(M = 2, N = 2, T = 2, Q = 4)$ scheme of Figure 2.14 employing QPSK modulation for transmission over wideband channel using the parameters in Table 2.4.

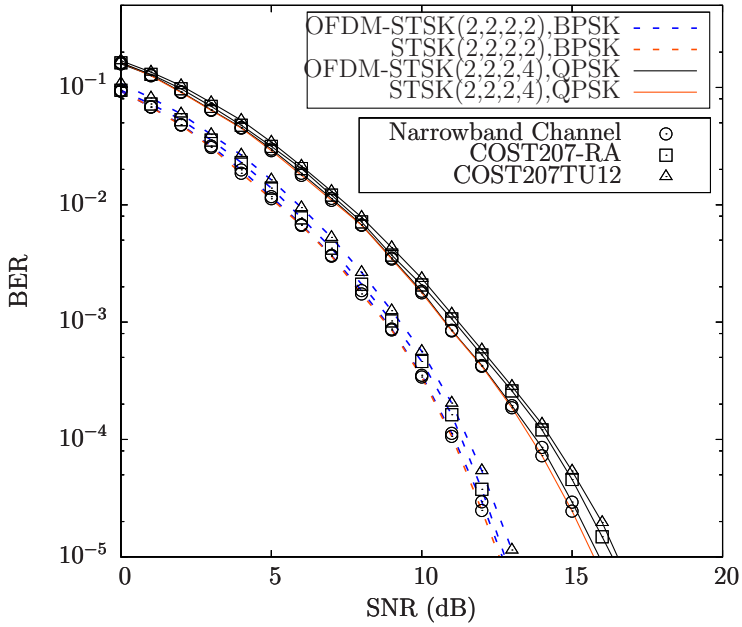

Figure 2.15: Performance of our OFDM-aided STSK system of Figure 2.9 in dispersive channels. The simulation parameters and the STSK specification used are shown in Table 2.4 and in the figure legend. No channel-coding was used and the optimal ML detector of [49] was employed. OFDM-aided STSK exhibits a performance in dispersive channels, which is similar to that in nondispersive environments.

We have employed a half-rate RSC code having a constraint length $k = 2$ and octrally represented generator polynomials of $(g_r, g) = (3, 2)_8$ as well as two random interleavers having a memory of $240,000$ bits. The number of inner and outer decoder iterations was set to $I_{\text{inner}} = 2$ and $I_{\text{outer}} = 8$ respectively. The BER performance of our coded arrangement applied in dispersive wideband COST207-TU12 scenarios is depicted in Figure 2.17. As observed in Figure 2.17, our channel-coded STSK-OFDM scheme of Figure 2.14 exhibits a near-capacity performance even in dispersive channel scenario. Upon increasing the number of iterations, the BER of our system is substantially reduced. The performance of the proposed scheme is also compared against the maximum achievable rate benchmarker for the scheme. To be specific, as discussed in [49, 146], the area under the inner decoder's EXIT characteristic gives the maximum achievable rate for the specific scheme. The signal-to-noise ratio (SNR) which provides maximum achievable rate for the scheme are computed and are shown in Figure 2.17. Our system exhibits an infinitesimally-low BER at SNR= 0 dB, which is observed to be -2.0 dB away from the maximum achievable rate benchmarker.

The EXIT charts of our STSK-OFDM system at 1.0 dB for four different coherent STSK (CSTSK) arrangements ($M = 2, N = 2, T = 2, Q = 2$) with QPSK, ($M = 2, N = 2, T = 2, Q = 4$) with BPSK, ($M = 2, N = 2, T = 2, Q = 4$) with QPSK and ($M = 2, N = 2, T = 2, Q = 8$) with BPSK modulation along with the EXIT chart of the outer RSC decoder in dispersive

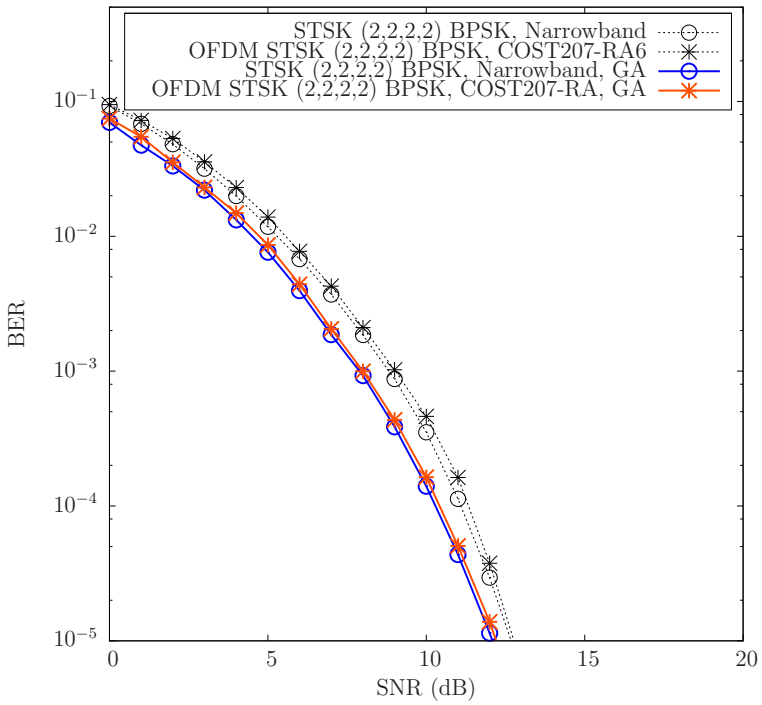

Figure 2.16: BER performance of STSK ($M = 2, N = 2, T = 2, Q = 2$) scheme of Figure 2.5 in conjunction with BPSK modulation communicating over nondispersive channel and that of the OFDM-STSK ($M = 2, N = 2, T = 2, Q = 2$), BPSK scheme of Figure 2.9 communicating over dispersive COST207-RA6 channel. DMs were optimized using both the GA-based and randomly searched optimization procedure. We employ the system parameters listed in Table 2.4 and no channel-coding is employed.

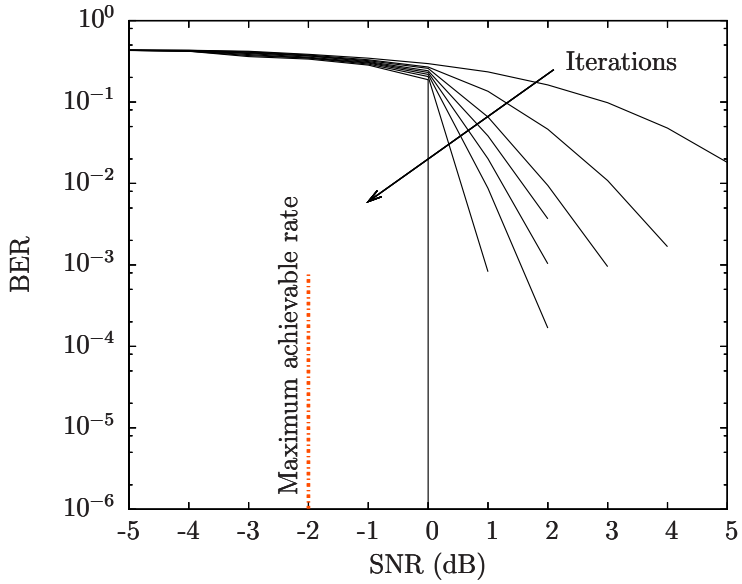

Figure 2.17: BER performance of our channel coded OFDM STSK ($M = 2, N = 2, T = 2, Q = 4$) system of Figure 2.14 in conjunction with QPSK modulation in COST207-TU12 dispersive channel using the system parameters of Table 2.4. With iterations, OFDM STSK converges very fast to low BER at low SNR.

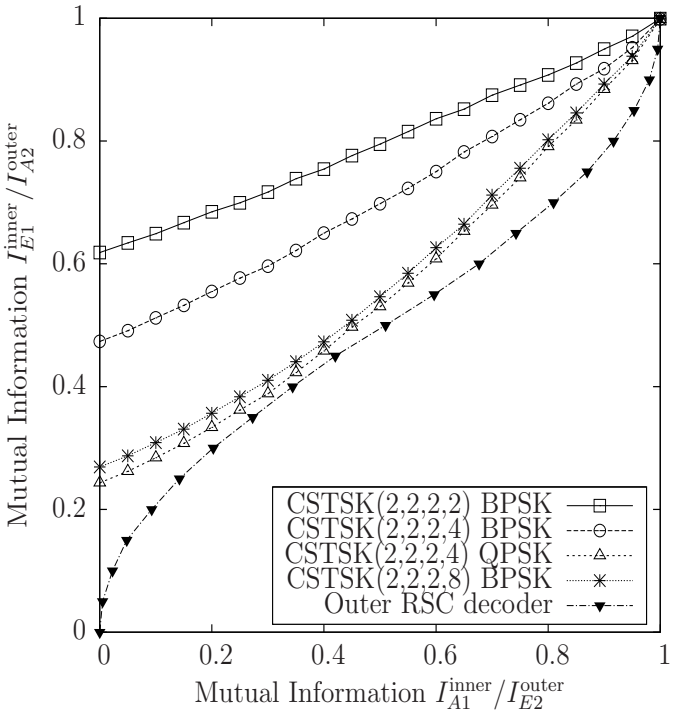

Figure 2.18: EXIT charts of the three-stage turbo detected STSK-OFDM scheme of Figure 2.14 under COST207-RA6 scenarios at SNR = 1.0 dB using different parameters shown in the legend. CSTSK ($M = 2, N = 2, T = 2, Q = 2$) based design with BPSK shows the widest 'EXIT' tunnel. The remaining simulation parameters are listed in Table 2.4.

COST207-RA6 channel model are shown in Figure 2.18. Observe in Figure 2.18 that all the inner EXIT curves reach the $(1, 1)$ point indicating perfect convergence as a benefit of URC precoding. As expected, the shape of the EXIT curve was different for different (M, N, T, Q) parameters in conjunction with the $\mathcal{L}-$ary modulation. Note that the STSK-OFDM ($M = 2, N = 2, T = 2, Q = 2$), BPSK scheme exhibits the widest EXIT tunnel among the scenarios considered in Figure 2.18.

Figure 2.19 portrays the EXIT chart of the OFDM aided STSK ($M = 2, N = 2, T = 2, Q = 4$), QPSK system, where the SNR was varied from -4 dB to 4 dB in steps of 0.5 dB. It can be seen in Figure 2.19 that all the inner decoder EXIT curves associated with our proposed scheme reached the point of perfect decoding convergence at $(1.0, 1.0)$, which is the explicit benefit of employing URC precoding [5]. We also observe that an open EXIT tunnel was 'just' formed at SNR $= -0.5$ dB, and the EXIT curve at SNR = 0 dB was also confirmed by the corresponding Monte-Carlo simulation based staircase-shaped decoding trajectory [147]. Therefore, it may be predicted that an infinitesimally low BER is achieved at SNR = 0 dB using $I_{\text{outer}} = 8$ outer iterations.

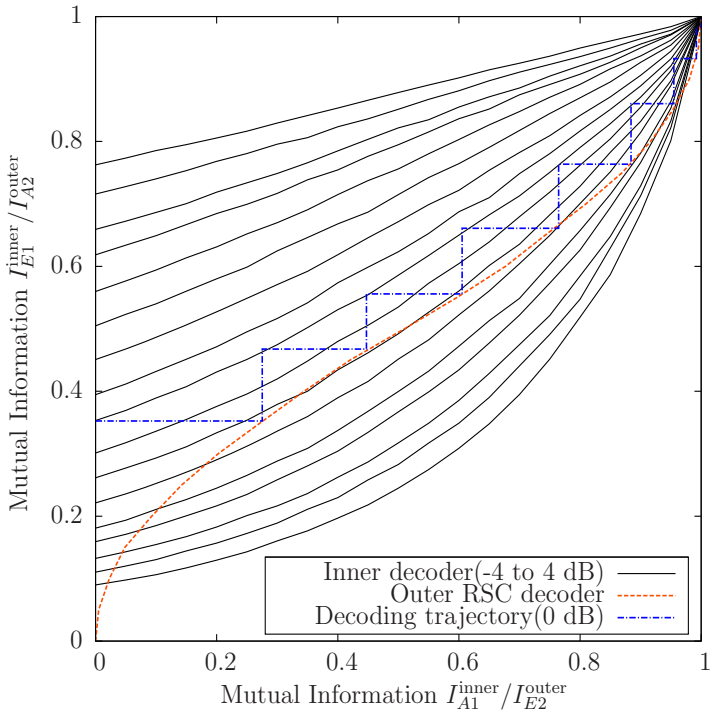

Figure 2.19: EXIT trajectory recorded at 0 dB of our three-stage turbo detected OFDM STSK ($M = 2, N = 2, T = 2, Q = 4$) system of Figure 2.14 employing QPSK communicating over the COST207-TU12 channel ($f_d = 0.01$). The inner decoder EXIT curves from -4 dB to 4 dB in steps of 0.5 dB and the outer RSC decoder's EXIT function are also shown. The remaining simulation parameters are listed in Table 2.4.

2.7 Chapter Summary and Conclusions

We commenced our discourse in this chapter with a review of the chronological development of the STSK system, starting with a brief introduction to V-BLAST, STBC, LDC, SM/SSK in Section 2.2. The STSK system was proposed with a view to striking the same DMT achievable by LDCs at a significantly reduced complexity, which was motivated by the low-complexity design architecture of SM/SSK. In Section 2.3, we have detailed the DM optimization procedure and the related OFs. Specifically, the DMs to be used were found by searching through a large, randomly generated DM set, either exhaustively or using a reduced-complexity GA-aided optimization. We have presented both the CCMC and DCMC capacity based optimal design as well as the PEP-optimal design of the DMs in Section 2.3. Motivated by the eroded performance of the serial-modulation-based STSK scheme in dispersive channels, a novel OFDM aided STSK scheme has been proposed for wideband channels in Section 2.4. We proposed two different techniques for the mapping of the STSK codewords to the OFDM subcarriers and compared their designs and benefits. A near-capacity coded OFDM STSK scheme was proposed in Section 2.5. Finally, the performance of both the OFDM-aided STSK scheme and that of the channel-coded OFDM-aided STSK arrangement was investigated in different

Table 2.5: Summary of the achievable BER performance of the OFDM-aided STSK scheme

Scheme	*Schematic diagram*	*Figure number*	*SNR, dB at BER*		*SNR gain/difference, dB at BER (benchmark scheme)*	
			10^{-3}	10^{-4}	10^{-3}	10^{-4}
OFDM-aided STSK $(2,2,2,2)$, *BPSK COST207-TU12*	Figure 2.9	Figure 2.15	9.4	11.0	0.2 (Narrowband channel)	0.2 (Narrowband channel)
OFDM-aided STSK $(2,2,2,2)$, *BPSK COST207-RA*	Figure 2.9	Figure 2.15	9.25	10.9	0.05 (Narrowband channel)	0.02 (Narrowband channel)
OFDM-aided STSK $(2,2,2,4)$, *QPSK COST207-TU12*	Figure 2.9	Figure 2.15	12.0	14.0	0.4 (Narrowband channel)	0.5 (Narrowband channel)
OFDM-aided STSK $(2,2,2,4)$, *QPSK COST207-RA*	Figure 2.9	Figure 2.15	11.8	13.8	0.2 (Narrowband channel)	0.3 (Narrowband channel)
OFDM-aided STSK $(2,2,2,2)$, *BPSK, COST207-RA, GA-optimized DMs*	Figure 2.9	Figure 2.16	8.5	10.0	0.75 (randomly searched DMs)	0.09 (randomly searched DMs)
Channel-coded OFDM-STSK $(2,2,2,4)$ *QPSK COST207-TU12*	Figure 2.14	Figure 2.17	0.0	0.0	2.0 (maximum achievable rate at BER ≈ 0)	

propagation scenarios in Section 2.6. Specifically, we demonstrated that in wideband channel scenarios, where STSK fails to perform well, our OFDM aided STSK arrangement is capable of combatting the channel impairments, whilst striking a flexible diversity versus multiplexing gain trade-off. The performance of the OFDM-aided STSK scheme of Figure 2.9 and of the channel-coded OFDM-aided STSK arrangement of Figure 2.14 is summarized in Table 2.7.

Our results seen in Table 2.5 confirm that the proposed OFDM-aided STSK scheme exhibits a similar performance to that of the single-carrier STSK scheme, when the latter operates in a narrowband channel while the former in a dispersive wideband channel, provided that the system parameters are appropriately chosen. Finally, the OFDM-aided STSK system has been incorporated in a three-stage serially concatenated turbo coded scheme, leading to near capacity performance in a dispersive broadband scenario.

The proposed OFDM-aided STSK system may be used as the basis of an OFDM-aided space-time-frequency shift keying (STFSK) system, where three-dimensional space-time-frequency dispersion matrices will spread a symbol taken from a $\mathcal{L}-$PSK/QAM constellation in the space, time and frequency domains. Finally, instead of using an exhaustive search method for designing the dispersion matrix sets, a GA assisted optimization may be applied, which improves the attainable performance of the proposed scheme.

Having proposed the OFDM-aided STSK scheme, we now conceive a range of MC-CDMA-aided and OFDMA/SC-FDMA-aided STSK schemes in Chapter 3 and Chapter 4, respectively in order to facilitate multiuser transmissions.

Chapter 3

MC-CDMA Aided Multiuser Space-Time Shift Keying

3.1 Introduction

Multi-carrier code division multiple access (MC-CDMA)-aided STSK is proposed in this chapter for mitigating the performance erosion of the classic STSK scheme in dispersive channels, while supporting multiple users. The codewords generated by the STSK scheme are appropriately spread across the frequency-domain (FD) and transmitted over a number of parallel frequency-flat subchannels. In this chapter, we also propose a new receiver architecture amalgamating the single-stream maximum-likelihood (ML) detector of the STSK system and the multiuser detector (MUD) of the MC-CDMA system.

STSK [49, 57] extends the concept of pure spatial-domain antenna activation of SM/SSK schemes of [47, 48] to both the spatial- and temporal dimensions. As detailed in Section 2.2.7, the idea is to rely on beneficial dispersion matrix (DM) activation, rather than on the simple antenna activation process of SM/SSK in addition to the conventional modulation based signalling. The STSK system can thus provide substantial diversity- as well as multiplexing gains.

The majority of STSK studies were, however, focused on narrowband scenarios [49, 56, 57], rather than on realistic wideband scenarios. Although the mitigation of the impairments due to channel dispersion was studied in [119, 148], the spreading of user information of the STSK scheme across the FD or across the time-domain (TD) remained an open problem. Against this background, in this chapter we propose an FD-spread MC-CDMA-aided STSK scheme in order to benefit from additional frequency diversity.

The idea of combining multicarrier concepts with classic code division multiple access (CDMA)

was introduced in 1993 [90]. The concepts of multicarrier code division multiple access (MC-CDMA), multicarrier direct sequence code division multiple access (MC DS-CDMA) and multitone code division multiple access (MT-CDMA) were conceived for overcoming the channel-induced dispersion imposed by high-rate wireless systems. The main difference between MC-CDMA and MC DS-CDMA or MT-CDMA is that while the former relies on FD spreading, the latter relies on TD spreading. A brief overview of the TD-spread and FD-spread multicarrier systems will be provided in Section 3.2.

The main contributions of this chapter may be listed as follows:

1. We propose FD-spread MC-CDMA-aided STSK systems, which are capable of attaining a beneficial diversity versus multiplexing gain tradeoff even in multi-path environments, while supporting multi-user transmissions. The space-time codewords generated by STSK are appropriately mapped to the MC-CDMA subcarriers. As a result, the STSK signal generated for each subcarrier of the parallel modem experiences frequency-flat fading. FD spreading provides additional diversity benefits.

2. We propose a novel multiuser detector (MUD) amalgamated with the low-complexity single-stream ML detector of [49, 57] in order to estimate the user information, which is spread over different subcarriers. We consider both multiuser downlink (DL) and uplink (UL) scenarios and evaluate their performance against both single-user and narrowband benchmarkers.

3. Furthermore, we design a near-capacity coding assisted MC-CDMA STSK arrangement and evaluate its performance.

The rest of the chapter is organized as follows. Section 3.2 provides a brief overview of multicarrier-based CDMA systems and outlines the main differences between FD-spread and TD-spread multicarrier systems. Section 3.3 details the transceiver model of our MC-CDMA aided STSK system. The channel-coded MC-CDMA aided STSK philosophy is discussed in Section 3.4. In Section 3.5, the system performance is characterized for both uncoded and channel-coded scenarios. Finally, we conclude in Section 3.6.

3.2 Classification of Multicarrier-based CDMA

The classification of multicarrier-aided CDMA schemes are illustrated in Figure 3.1. As seen in Figure 3.1, multicarrier based CDMA schemes are of two types: FD-spread MC CDMA and TD-spread MC CDMA. TD-spread MC CDMA schemes are further classified into multicarrier direct sequence code division multiple access (MC DS-CDMA) and multitone code division multiple access (MT-CDMA) schemes.

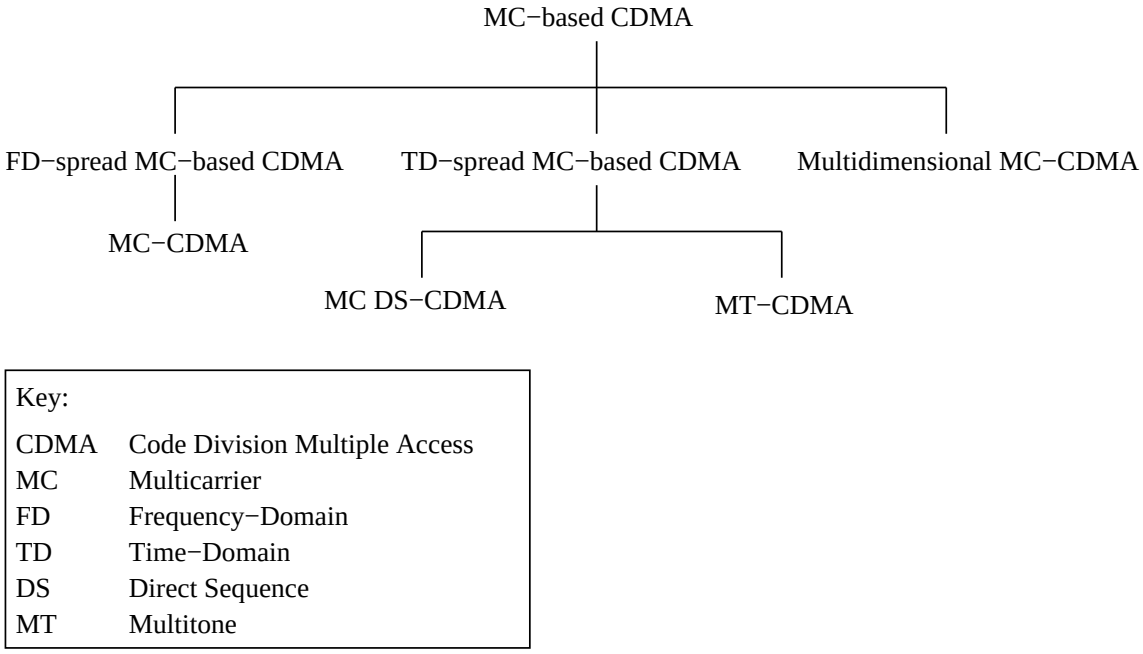

Figure 3.1: Classification of the multicarrier-based CDMA schemes.

The different types of multicarrier-based CDMA schemes along with the classic single-carrier DS-CDMA using the Rake receivers have been studied in [95]. In the following, we provide a concise overview of the FD-spread and the TD-spread MC-CDMA schemes.

3.2.1 FD-spread MC-CDMA

The combination of FD spreading and multicarrier modulation results in the FD-spread MC-CDMA or, in short, MC-CDMA scheme. The MC-CDMA transmitter spreads the original data stream across the FD using user-specific spreading sequences. As shown in Figure 3.2, in a FD-spread MC-CDMA scheme, N_c/S_f data symbols are serial-to-parallel (S/P) converted, where N_c and S_f represent the number of subcarriers and the spreading factor, respectively. For the sake of simplicity, we have assumed $N_c = S_f$ in Figure 3.2, although N_c may be some other multiple of S_f. Each of the S/P converted symbols is copied S_f times so that the total number of symbol copies available to modulate the subcarriers is equal to N_c. Each of the symbol copies is then multipled by one chip of the user-specific spreading sequence of length S_f, before being mapped to the orthogonal subcarriers usually implemented by the inverse discrete Fourier transform (IDFT) operation.

In the MC-CDMA receiver of Figure 3.2, the received signal is combined in the FD so that the receiver can combine all the received signal energy spread across the FD [95]. However, the frequency selective channel destroys the orthogonality among users. As shown in Figure 3.2, after the discrete Fourier transform (DFT) operation, the n_c-th subcarrier is multiplied by the gain $q_{n_c}^u$ of user u for combining the signal energy spread across the FD, where the gain $q_{n_c}^u$

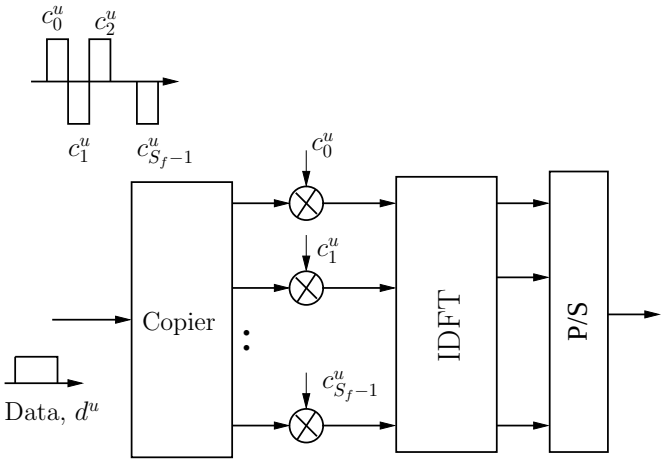

(a) Transmitter

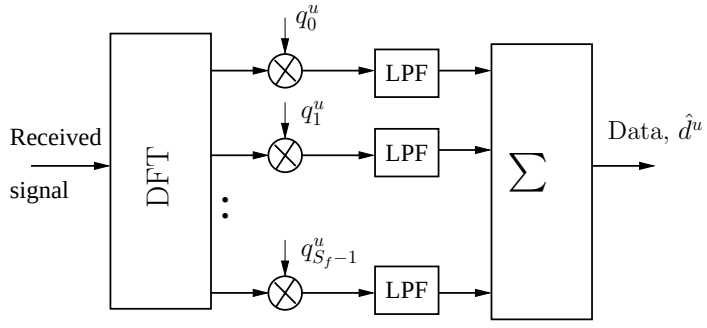

(b) Receiver

Figure 3.2: Simplified transceiver architecture of the FD-spread multicarrier-CDMA scheme: (a) transmitter (b) receiver.

is computed in accordance with the specific diversity combining strategy employed. The most popular combining strategies are orthogonality restoring combining (ORC) [95], maximum ratio combining (MRC) [6,95], controlled equalization [95], equal gain combining (EGC) [90,95] and minimum mean squared error combining (MMSEC) [90,95]. Rather than employing the single-user detection (SUD) strategy mentioned, a MUD may be applied at the receiver for jointly estimating the information of different users, as detailed in [73,89].

3.2.2 TD-spread MC DS-CDMA

As seen in Figure 3.1, there are two fundamental categories of multicarrier schemes combined with TD-spread DS-CDMA, namely the MC DS-CDMA and the MT-CDMA schemes. In the MC DS-CDMA scheme portrayed in Figure 3.3, the data stream is first divided into a number of parallel substreams. Each substream is then spread across the TD with the aid of the spreading sequences and then transmitted over one of the subcarriers [95,149]. MC DS-CDMA may thus

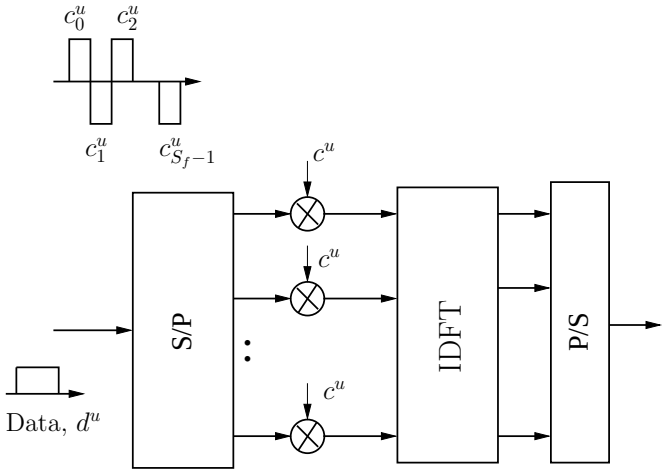

(a) Transmitter

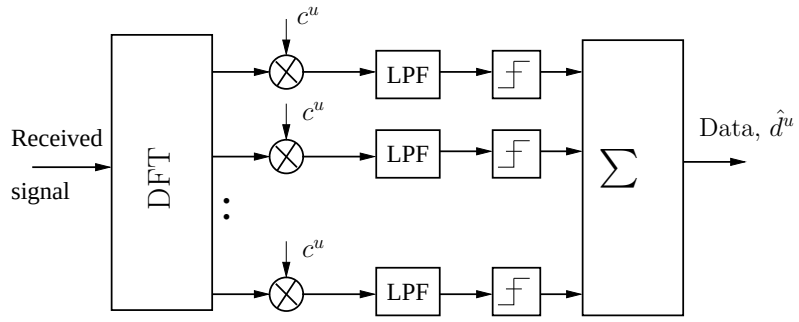

(b) Receiver

Figure 3.3: The transmitter and receiver architecture of the multicarrier DS-CDMA scheme.

be viewed as a natural extension of OFDM, which makes use of CDMA as a multiple access scheme.

The MT-CDMA scheme, originally proposed in [94] and depicted in Figure 3.4, relies on similar operations to those of MC DS-CDMA, except that the subcarriers are orthogonal before spreading, but the spectrum of subcarriers no longer exhibits orthogonality after TD-spreading. MT-CDMA typically employs longer spreading sequences than MC DS-CDMA, hence the spreading factor of MT-CDMA is typically N_c times that of the MC DS-CDMA scheme. Therefore the MT-CDMA system is capable of accommodating more users than the MC DS-CDMA and the MC-CDMA schemes. Figure 3.4 depicts the transmitter as well as the receiver of the MT-CDMA system, where the MT-CDMA receiver is composed of N_c Rake combiners. The receiver is optimum for transmission over AWGN channels, but suboptimum in frequency-selective channels [94]. The longer spreading codes utilized in the system efficiently mitigates the self-interference (SI) as well as the multiuser interference (MUI). However, as a price to pay, MT-CDMA suffers from more substantial inter-subcarrier interference than its MC-CDMA counterpart [94].

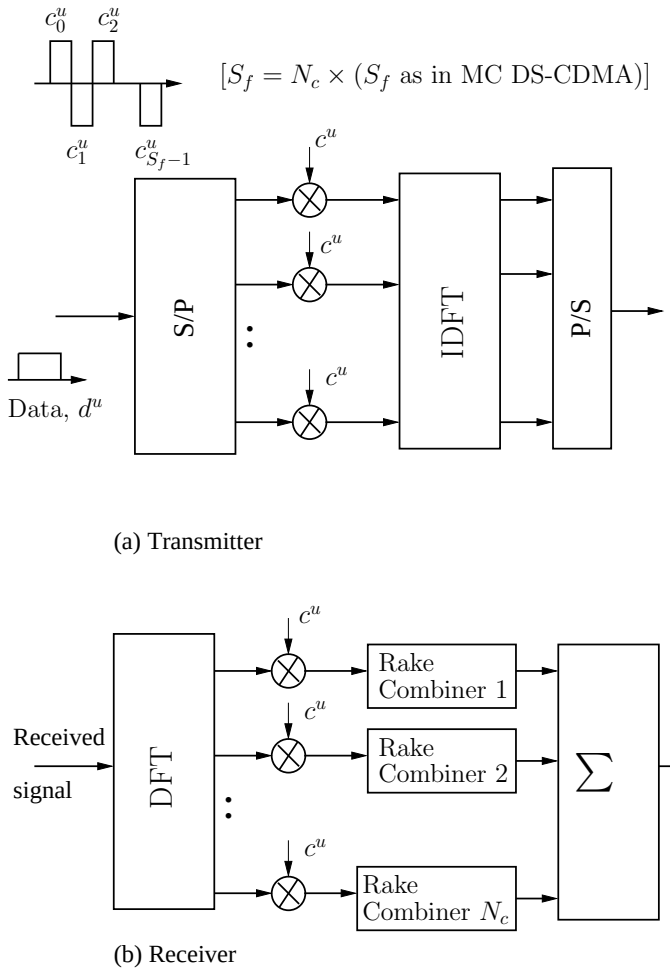

Figure 3.4: The transceiver configuration of the MT-CDMA scheme.

It is worth mentioning at this point that while each of the parallel substreams is spread using a 'single' chip of the spreading sequence in FD-spread MC-CDMA, it is spread by using the entire spreading sequence in a TD-spread MC DS-CDMA or MT-CDMA arrangement.

3.2.3 Multidimensional MC-CDMA

There have also been substantial developements in the context of multidimensional spreading assisted MC-based CDMA schemes [73, 89]. This family of multicarrier-based CDMA systems spreads the user information across both the spatial- as well as time- domains or even over the spatial domain (SD) [150, 151]. For example, a MC DS-CDMA scheme using both time- and frequency-domain spreading was proposed in [150] and a multiuser detector for the scheme was proposed in [151]. Specifically, this scheme utilizes two spreading sequences, one for the TD and another for FD spreading. The data stream is first spread across the TD and then S/P-converted for facilitating FD spreading, before being mapped to the subcarriers. The authors of [152] proposed a MC DS-CDMA scheme using space-time and frequency domain spreading

in the context of broadband communications over dispersive channels. The results of [152] suggest that multiuser detector assisted multidimensional spreading is capable of supporting a substantially increased number of users, while maintaining a similar performance to that of the TD-spread MC DS-CDMA scheme. A hybrid of MC-CDMA and MC DS-CDMA was proposed for wideband scenarios in [153], which also benefits from both the spatial- and time-domain spreading, and it is capable of attaining a high spectrum efficiency as well as a high flexibility in terms of selecting the system parameters. Two-dimensional (2D) orthogonal variable spreading factor (OVSF) codes were proposed for MC DS-CDMA in [154], where the orthogonality of these codes were explored for improving the bandwidth efficiency and interference rejection capability of the conventional DS-CDMA systems. In short, multidimensional spreading aided MC-based CDMA systems are capable of attaining diverse design objectives, while potentially providing a diversity gain in the TD, FD and SD.

Having provided a brief overview of the multicarrier-based CDMA systems, let us now embark on our FD-spread MC-CDMA aided STSK scheme in Section 3.3.

3.3 MC-CDMA-aided STSK: System Model

Consider an MC-CDMA aided STSK system having M transmit and N receive AEs and communicating over frequency-selective Rayleigh fading channels. Furthermore, N_c subcarriers are employed by our MC-CDMA modem for transmitting N_p STSK codewords. In general, N_c is related to N_p by: $N_c = (N_p \times S_f)$. However, it is possible to spread each of the codewords across all the subcarriers, where $S_f = N_c$ [73, 89].

3.3.1 The Transmitter and the Channel

Figure 3.5 depicts the transmitter model of our MC-CDMA aided STSK scheme. The STSK transmitter generates space-time codewords from the users' source information. These codewords are further spread across the FD and are then mapped to a number of subcarriers, before being transmitted using M transmit AEs over T time slots. More specifically, each STSK signalling block $\boldsymbol{X}^u[n_p]$, $n_p = 1, 2, ..., N_p$ is created from $\log_2(\mathcal{L} \cdot Q)$ source bits of user u, $u = 1, 2, \ldots, U$, in accordance with [49, 57]

$$\boldsymbol{X}^u[n_p] = x^u[n_p]\boldsymbol{A}^u[n_p], \tag{3.1}$$

where $x^u[n_p]$ is an $\mathcal{L}$-ary modulation symbol mapped by $\log_2 \mathcal{L}$ bits of u-th user's source information and $\boldsymbol{A}^u[n_p]$ is the DM activated from among Q DMs $(\boldsymbol{A}_1, \boldsymbol{A}_2, \ldots, \boldsymbol{A}_Q)$, determined by the remaining $\log_2 Q$ bits. The DMs are appropriately optimized employing a certain objective function under the power constraint: $\mathrm{tr}(\boldsymbol{A}_q^H \boldsymbol{A}_q) = T \quad \forall q$, as detailed in [5, 49, 57]. The STSK

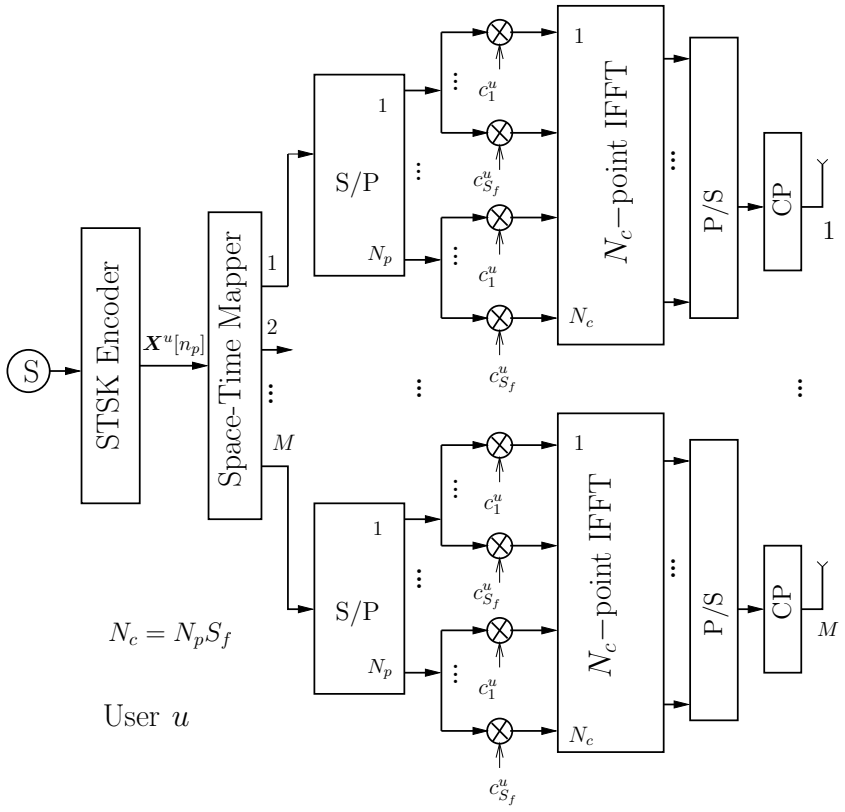

Figure 3.5: Transmission model of the proposed MC-CDMA aided multiuser STSK scheme of user u.

scheme may be unambiguously described by the (M, N, T, Q) parameters in conjunction with the $\mathcal{L}-$ ary modulation employed.

The mapping of the STSK codewords to the N_c subcarriers is illustrated in Figure 3.6. A number of N_p space-time codewords generated by the STSK encoder are spread across all the N_c subcarriers by the user-specific spreading sequence, $\boldsymbol{C}^u = [c_1^u, c_2^u, \ldots, c_{S_f}^u]$, where S_f represents the spreading factor and u is the user index. To be more specific, assuming the relationship $N_c = (N_p \times S_f)$, FD spreading of the N_p codeword symbols results in a number of N_c FD symbols.

The complex baseband representation of the MC-CDMA STSK time-domain (TD) signal of user u transmitted in a particular signalling interval may thus be expressed as [73, 95]:

$$\boldsymbol{s}_{m,T_i}^u(t) = \frac{1}{\sqrt{N_c}} \sum_{n_p=1}^{N_p} \sum_{s_f=1}^{S_f} c_{s_f}^u \boldsymbol{X}_{m,T_i}^u[n_p] e^{j2\pi f_{n_c} t}, \quad T_i = 1, 2, \ldots, T \quad 1 \leq t \leq (N_c + 1)\,\mathcal{T}, \quad (3.2)$$

where $(\bullet)_{m,T_i}^u$ denotes the (m, T_i) element of the matrix $(\bullet)^u$, $\mathcal{T}$ represents the TD sampling interval, while $N_c\mathcal{T}$ is the TD frame interval. Furthermore, f_{n_c} is the frequency of the n_c-th subcarrier and $n_c = (n_p S_f + s_f)$. In order to maintain orthogonality, the subcarrier frequencies have to be equally spaced with

$$f_{n_c} = \frac{n_c}{N_c \mathcal{T}}. \quad (3.3)$$

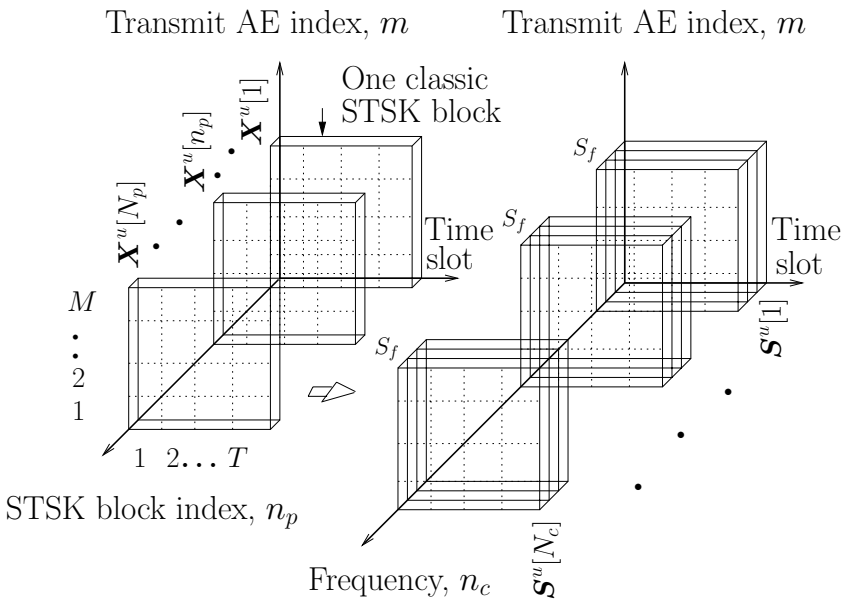

Figure 3.6: Illustration of the mapping of N_p STSK codewords to N_c orthogonal sub-carriers. The STSK codewords are spread in FD by the user-specific S_f-chip spreading sequence and are then mapped to the sub-carriers.

Defining the FD-spread symbol stream of user u by $\boldsymbol{S}^u_{m,T_i} = c^u_{s_f}\boldsymbol{X}^u_{m,T_i}, \quad s_f = 1, 2, \ldots, S_f$, the transmit frame before and after FD spreading are

$$[\boldsymbol{X}^u[1], \boldsymbol{X}^u[2], \ldots, \boldsymbol{X}^u[n_p], \ldots, \boldsymbol{X}^u[N_p]]$$

and

$$[\boldsymbol{S}^u[1], \boldsymbol{S}^u[2], \ldots, \boldsymbol{S}^u[n_c], \ldots, \boldsymbol{S}^u[N_c]]\,,$$

respectively.

The MC-CDMA TD samples may thus be expressed by

$$\boldsymbol{s}^u_{m,T_i}[n_s] = \frac{1}{\sqrt{N_c}}\sum_{n_c=1}^{N_c}\boldsymbol{S}^u_{m,T_i}[n_c]e^{j2\pi\frac{n_s n_c}{N_c}}, \quad 1 \le n_s \le N_c, \tag{3.4}$$

which is given by the N_c-point IDFT of $\boldsymbol{S}^u_{m,T_i}$:

$$\boldsymbol{s}^u_{m,T_i} = \mathrm{IDFT}_{N_c}\left\{\boldsymbol{S}^u_{m,T_i}\right\}. \tag{3.5}$$

After the IDFT operation, cyclic prefices (CP) of appropriate length are incorporated for eliminating the effects of inter-symbol interference (ISI).

Example 3.1: FD spreading and symbol mapping to subcarriers: $N_c = 16,\ S_f = 4$

For the sake of exemplifying the FD spreading operation and the subsequent mapping of the spread codeword symbols to the orthogonal subcarriers, consider an MC-CDMA aided

STSK scheme employing $N_c = 16$ subcarriers and a FD-spreading factor $S_f = 4$. We will then take $N_p = N_c/S_f = 16/4 = 4$ STSK codewords of a particular user u and place them in parallel, as shown in Figure 3.7. Let the 4 codewords be denoted by:

$$[\boldsymbol{X}^u[1], \boldsymbol{X}^u[2], \boldsymbol{X}^u[2], \boldsymbol{X}^u[4]] .$$

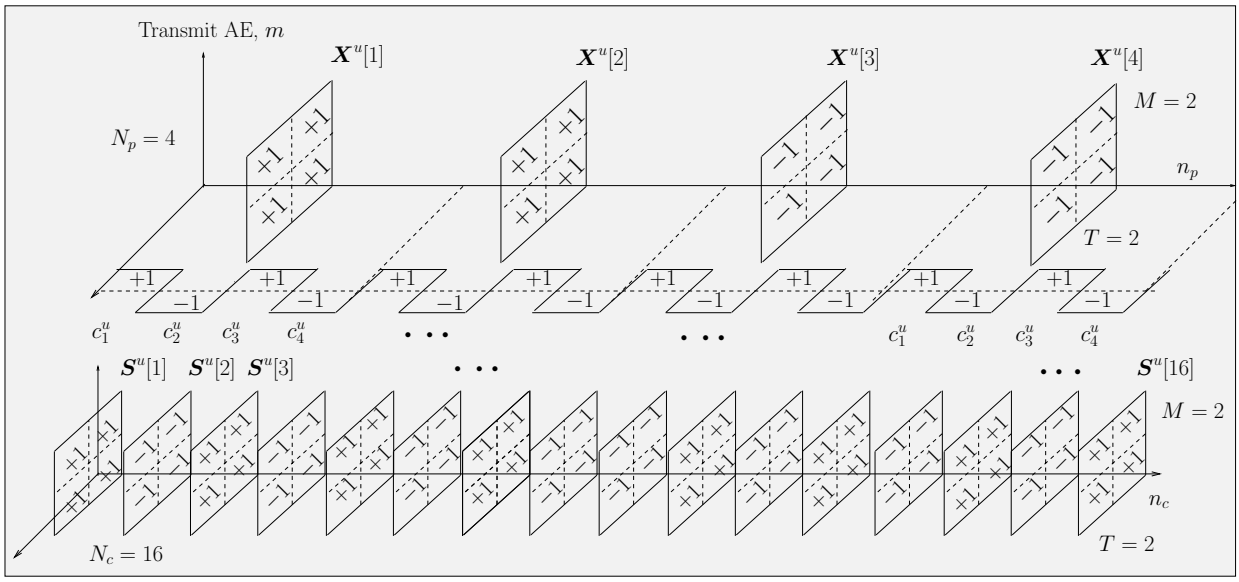

Figure 3.7: FD spreading example of the STSK codewords. 4 STSK codewords $\boldsymbol{X}^u[1]$, $\boldsymbol{X}^u[2]$, $\boldsymbol{X}^u[3]$ and $\boldsymbol{X}^u[4]$ are considered, which are spread in FD by the user-specific spreading sequence $\boldsymbol{C}^u = [+1, -1, +1, -1]$, resulting in 16 spread space-time matrices, which are denoted by $\boldsymbol{S}^u[1]$, $\boldsymbol{S}^u[2]$, ..., $\boldsymbol{S}^u[16]$, respectively

Let us further assume for example that the spreading sequence corresponding to user u is:

$\boldsymbol{C}^u = [+1, -1, +1, -1]$.

Each of the codewords $\boldsymbol{X}^u$ will now be multipled by each single chip of the spreading sequence $\boldsymbol{C}^u$, resulting in $4 \times 4 = 16$ spread codewords. More explicitly, $\boldsymbol{X}^u[1]$ multiplied by the chips will produce 4 spread codewords denoted by:

$$\begin{aligned}
\boldsymbol{S}^u[1] &= c_1^u \boldsymbol{X}^u[1] = +1 \times \boldsymbol{X}^u[1], \\
\boldsymbol{S}^u[2] &= c_2^u \boldsymbol{X}^u[1] = -1 \times \boldsymbol{X}^u[1], \\
\boldsymbol{S}^u[3] &= c_3^u \boldsymbol{X}^u[1] = +1 \times \boldsymbol{X}^u[1], \\
\text{and } \boldsymbol{S}^u[4] &= c_4^u \boldsymbol{X}^u[1] = -1 \times \boldsymbol{X}^u[1].
\end{aligned}$$

Thus the 4 codewords $[\boldsymbol{X}^u[1], \boldsymbol{X}^u[2], \boldsymbol{X}^u[3], \boldsymbol{X}^u[4]]$ will produce a total of 16 spread codewords denoted by:

$$[\boldsymbol{S}^u[1], \boldsymbol{S}^u[2], \ldots, \boldsymbol{S}^u[16]] .$$

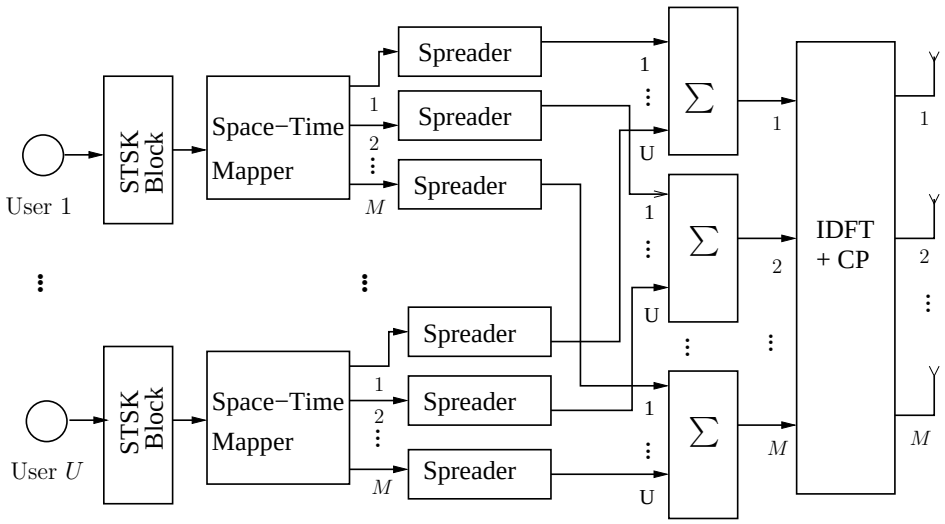

Figure 3.8: Multiuser DL transmitter model of MC-CDMA aided STSK.

In Figure 3.7, we assume all the STSK codewords to be $(2 \times 2)-$element matrices, i.e. we assume $M = 2,\ T = 2$. We also consider, for the sake of simplicity, all the elements of the STSK codewords $\boldsymbol{X}^u[1]$ and $\boldsymbol{X}^u[2]$ to be $+1$, while those of $\boldsymbol{X}^u[3]$ and $\boldsymbol{X}^u[4]$ to be -1. As a result, all the elements of the spread codewords $\boldsymbol{S}^u[1]$, $\boldsymbol{S}^u[2]$, $\boldsymbol{S}^u[3]$ and $\boldsymbol{S}^u[4]$ are $+1$, -1, $+1$ and -1, respectively. By contrast, all the elements of for example $\boldsymbol{S}^u[9]$, $\boldsymbol{S}^u[10]$, $\boldsymbol{S}^u[11]$ and $\boldsymbol{S}^u[12]$ are -1, $+1$, -1 and $+1$, respectively.

The resultant 16 spread codeword symbols will then be mapped to the $N_c = 16$ subcarriers using the IDFT operation.

We assume that each channel component of our MC-CDMA-aided STSK system corresponding to user u is frequency-selective, and is described by its discrete-time channel impulse response (CIR), $\boldsymbol{h}^u_{n,m}, \quad n = 1, 2, \ldots, N, \quad m = 1, 2, \ldots, M$, whereas $\tilde{\boldsymbol{H}}^u$ denotes the corresponding $(N \times M)$-element FD channel transfer matrix.

3.3.1.1 Multiple-User Downlink Scenario

The multiuser DL transmitter model of our proposed scheme is depicted in Figure 3.8. Let us assume that a block of N_p STSK symbols are serial to parallel converted and each of the N_p symbols is spread by one of the user-specific S_f-chip spreading sequence, $c^u = [c^u_1 c^u_2 \ldots c^u_{S_f}],\ u = 1, 2, \ldots, U$, resulting in a total of $N_c = (N_p \times S_f)$ FD symbols. The N_c symbols of the U users generated in this manner at any particular AE m are then superimposed on each other, which results in the N_c-chip composite multi-user signal. These resultant sequences are then assigned to N_c sub-carriers by the IDFT-modulation block of Figure 3.8. Thus the DL signals transmitted from all the M AEs contain N_c subcarrier signals.

During DL transmissions, the desired signal and the interferring signals are received at any

MS through the same channel. The channel variables for all the users may thus be expressed as identical to those of the intended[1] user v for DL transmissions:

$$\boldsymbol{h}_{n,m}^{u} = \boldsymbol{h}_{n,m}^{v} \qquad \tilde{\boldsymbol{H}}^{u} = \tilde{\boldsymbol{H}}^{v} \qquad \forall u. \tag{3.6}$$

The signals emanating from the M transmit AEs contain the superposition of all the U users' signals. In the receiver of a particular user, the user detects his own signal impinging on the N receive AEs by despreading with the aid of his own spreading sequence. Since the cross-correlation between the sequences of different users is zero, each user is capable of recovering his own signal, provided that the orthogonality of the sequences was not destroyed.

3.3.1.2 Multi-User Uplink Scenario

In the multi-user UL scenario, the signals from the mobile stations (MSs) of different users are received at the base station's (BS) AEs through different channels. Hence the TD and the FD channel coefficients are independent between users.

3.3.2 The Receiver

Figure 3.9 illustrates the receiver architecture of our MC-CDMA aided STSK system. The received signal, after CP removal, is demodulated by Fourier-transforming it. Assuming perfect synchronization at the receiver, the discrete-time signal impinging on the n-th receive AE during time interval T_i can be expressed as [73]

$$\boldsymbol{y}_{n,T_i} = \sum_{u=1}^{U} \sum_{m=1}^{M} \boldsymbol{h}_{n,m}^{u} \circledast \boldsymbol{s}_{m,T_i}^{u} + \boldsymbol{v}_{n,T_i}, \tag{3.7}$$

where $\circledast$ denotes N_c-point circular convolution and $\boldsymbol{v}_{n,T_i}$ represents the additive white Gaussian noise (AWGN). After applying N_c-point discrete Fourier transform (DFT) denoted by $\mathrm{DFT}_{N_c}\{\cdot\}$, the FD MIMO output $\boldsymbol{Y}[n_c]$ is given by

$$\boldsymbol{Y}[n_c] = \sum_{u=1}^{U} \tilde{\boldsymbol{H}}^{u}[n_c]\boldsymbol{S}^{u}[n_c] + \boldsymbol{V}[n_c] \tag{3.8}$$

$$= \underbrace{\tilde{\boldsymbol{H}}^{v}[n_c]\boldsymbol{S}^{v}[n_c]}_{\text{contribution from desired signal}} + \underbrace{\sum_{\substack{u=1 \\ u\neq v}}^{U} \tilde{\boldsymbol{H}}^{u}[n_c]\boldsymbol{S}^{u}[n_c]}_{\text{multi-user interference}} + \underbrace{\boldsymbol{V}[n_c]}_{\text{additive noise}}, \tag{3.9}$$

for every $n_c = 1, 2, \ldots, N_c$, such that

$$\boldsymbol{Y}_{n,T_i} = \mathrm{DFT}_{N_c}\left\{\boldsymbol{y}_{n,T_i}\right\} \qquad \boldsymbol{Y}[n_c] \in \mathbb{C}^{N\times T}, \tag{3.10}$$

$$\boldsymbol{S}_{m,T_i}^{u} = \mathrm{DFT}_{N_c}\left\{\boldsymbol{s}_{m,T_i}^{u}\right\} \qquad \boldsymbol{S}^{u}[n_c] \in \mathbb{C}^{M\times T}, \tag{3.11}$$

$$\boldsymbol{V}_{n,T_i} = \mathrm{DFT}_{N_c}\left\{\boldsymbol{v}_{n,T_i}\right\} \qquad \boldsymbol{Y}[n_c] \in \mathbb{C}^{N\times T}, \tag{3.12}$$

[1] We use the notation u to represent the generalized user and v to denote the intended user.

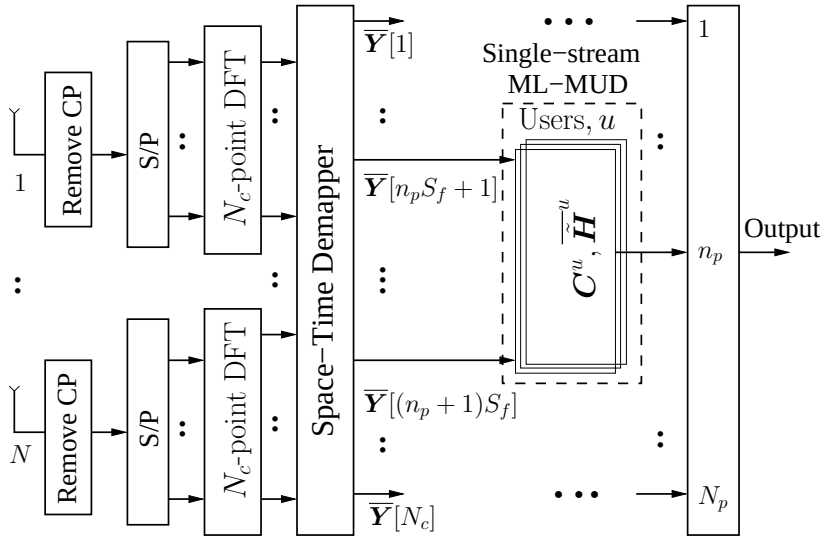

Figure 3.9: Receiver (DL/UL) architecture of the multi-user MC-CDMA aided STSK scheme employing the proposed ML-MUD.

and the FD channel transfer matrix $\tilde{\boldsymbol{H}}^u[n_c] \in \mathbb{C}^{N\times M}$ is expressed [18, 73] in terms of

$$\tilde{\boldsymbol{H}}^u_{n,m} = \text{diag}\{\tilde{h}^u_{n,m}[1], \tilde{h}^u_{n,m}[2], ..., \tilde{h}^u_{n,m}[N_c]\} \in \mathbb{C}^{N_c\times N_c}, \tag{3.13}$$

where $\tilde{\boldsymbol{h}}^u_{n,m} = \text{DFT}_{N_c}\left\{\boldsymbol{h}^u_{n,m}\right\}$.

The linearized system model of [32] reduces (3.8) to

$$\overline{\boldsymbol{Y}}[n_c] = \sum_{u=1}^{U} \overline{\tilde{\boldsymbol{H}}}^u[n_c]\boldsymbol{\chi}\left[c^u_{s_f}\boldsymbol{K}^u\right] + \bar{\boldsymbol{V}}[n_c], \quad s_f = 1, 2, \ldots, S_f \quad n_c = (n_pS_f + s_f), \tag{3.14}$$

where we have $\overline{\boldsymbol{Y}}[n_c] = vec(\boldsymbol{Y}[n_c]) \in \mathbb{C}^{NT\times 1}$ by using the vectorial stacking operator $vec(\cdot)$, $\overline{\tilde{\boldsymbol{H}}}^u[n_c] = \boldsymbol{I}_T \otimes \tilde{\boldsymbol{H}}^u[n_c] \in \mathbb{C}^{NT\times MT}$ is the stacked FD channel transfer matrix of user u, $\otimes$ denotes the Kronecker product and $\boldsymbol{I}_T$ represents the $(T \times T)$ identity matrix, and the linear transformation matrix or the dispersion character matrix (DCM)$\boldsymbol{\chi} \in \mathbb{C}^{N_TT\times Q}$ [32, 49] is given by $\boldsymbol{\chi} = [vec(\boldsymbol{A}_1), \ldots, vec(\boldsymbol{A}_Q)]$. Furthermore, $\bar{\boldsymbol{V}}[n_c] = vec(\boldsymbol{V}[n_c]) \in \mathbb{C}^{NT\times 1}$ is the AWGN vector, while the equivalent transmit signal vector $\boldsymbol{K}^u \in \mathbb{C}^{Q\times 1}$ is defined by [49]

$$\boldsymbol{K}^u = [\underbrace{0, ..., 0}_{q-1}, x^u, \underbrace{0, ..., 0}_{Q-q}]^T, \tag{3.15}$$

where a constellation symbol x^u exists only at position q, so that the q-th DM is activated.

Both SUDs and MUDs may be employed for the detection of the different users' signals [95]. Since the orthogonality between the different users' signals is destroyed by dispersive channels, MUI is imposed if a low-complexity single-user detector is used. The MUI degrades the resultant BER performance both in the DL and UL multiuser scenarios. By contrast, the MUD jointly detects the information of all the users and hence an improved BER performance may be

attained, albeit at the cost of imposing an increased decoding complexity. The single-user detector combines the different sub-carrier signals employing a combining method, such as orthogonality-restoring combining (ORC) [95], equal gain combining (EGC) [6,95] or maximal-ratio combining (MRC) [6,95]. Using MRC, the decision variables for the desired user v may be obtained from $\overline{\boldsymbol{z}}^v[n_d] = \overline{\text{vec}(z}^v[n_d])$ as [95]:

$$\boldsymbol{z}^v[n_p] = \sum_{s_f=1}^{S_f} \boldsymbol{g}^v[n_p S_f + s_f] \boldsymbol{Y}[n_p S_f + s_f], \tag{3.16}$$

where $\boldsymbol{g}^v[n_p S_f + s_f]$ is given by $\boldsymbol{g}^v[n_p S_f + s_f] = c^v_{s_f} \left[\tilde{\boldsymbol{H}}^v[n_p S_f + s_f]\right]^H$. Hence, the source bits of user v may be estimated as [49, 117]

$$\begin{aligned}(q^v[n_p], l^v_c[n_p]) &= \arg\min_{q^v, l^v_c} \left|\left| \overline{\boldsymbol{z}}^v[n_p] - \boldsymbol{\chi} \boldsymbol{K}^v_{q^v, l^v_c} \right|\right|^2 &(3.17)\\ &= \arg\min_{q^v, l^v_c} \parallel \overline{\boldsymbol{z}}^v[n_p] - (\boldsymbol{\chi})_{q^v} (s^v)_{l^v_c} \parallel^2. &(3.18)\end{aligned}$$

Below we will also propose a new single-stream maximum-likelihood multiuser detector (ML-MUD) for the joint detection of the user signals, which amalgamates both the single-stream maximum-likelihood (ML) detector of [49, 57] and the MUD of [95].

Since the source information of users in a particular space-time block indexed by n_p is spread over S_f number of outputs from $\overline{\boldsymbol{Y}}[n_p S_f + 1]$ to $\overline{\boldsymbol{Y}}[(n_p + 1) S_f]$, the ML-MUD is employed over these S_f number of matrices to jointly detect the information of the users corresponding to the specific block. The single-stream ML-MUD may hence be used for estimating the set of DM indices, $\boldsymbol{q}[n_p] = \left\{q^1[n_p], \ldots, q^U[n_p]\right\}$ and the constellation symbol indices, $\boldsymbol{l}_c[n_p] = \left\{l^1_c[n_p], \ldots, l^U_c[n_p]\right\}$. More explicitly, given the received signals of (3.14), the ML-MUD may thus be formulated as [57, 95]:

$$\begin{aligned}\left(\hat{\boldsymbol{q}}[n_p], \hat{\boldsymbol{l}}_c[n_p]\right) &= \arg\min_{\boldsymbol{q}, \boldsymbol{l}_c} \sum_{s_f=1}^{S_f} \left|\left| \overline{\boldsymbol{Y}}[n_p S_f + s_f] - \sum_{u=1}^{U} c^u_{s_f} \overline{\tilde{\boldsymbol{H}}}^u [n_p S_f + s_f] \boldsymbol{\chi} \boldsymbol{K}^u_{q^u, l^u_c} \right|\right|^2 \\ &= \arg\min_{\boldsymbol{q}, \boldsymbol{l}_c} \sum_{s_f=1}^{S_f} \left|\left| \overline{\boldsymbol{Y}}[n_p S_f + s_f] - \sum_{u=1}^{U} c^u_{s_f} s_{l^u_c} (\overline{\tilde{\boldsymbol{H}}}^u [n_p S_f + s_f] \boldsymbol{\chi})_{q^u} \right|\right|^2, &(3.19)\end{aligned}$$

where $\boldsymbol{K}^u_{q^u, l^u_c}$ denotes the equivalent transmit signal vector defined in (3.15) when the transmitted indices are q^u and l^u_c respectively, $s_{l^u_c}$ denotes the l^u_c-th constellation symbol of user u and $(\bullet)_{q^u}$ indicates the q^u-th column of the matrix '$\bullet$'. The computational complexity imposed by the ML-MUD of (3.19) is naturally very high.

More specifically, the complexity imposed by the detector of (3.18) quantified in terms of the number of RMOs per bit is evaluated as:

$$\text{Complexity}_{\text{SUD}} = \frac{10 M T Q \mathcal{L}}{\log_2(Q \cdot \mathcal{L})}, \tag{3.20}$$

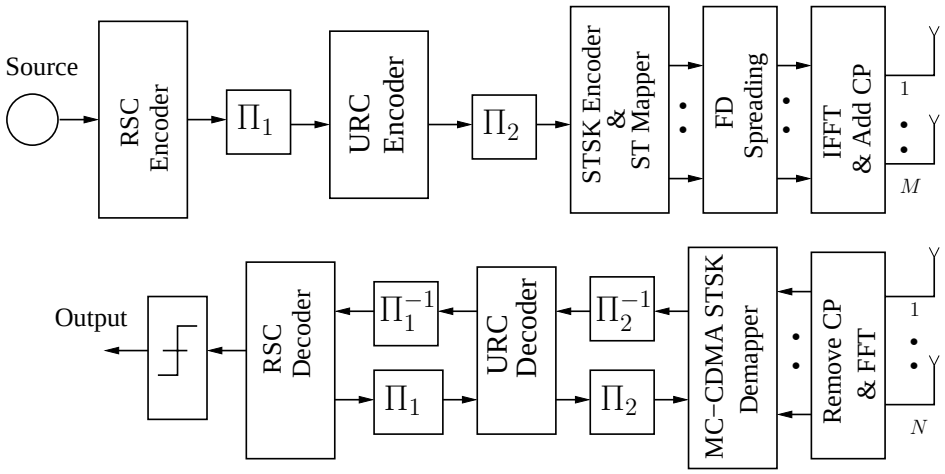

Figure 3.10: The channel-coded MC-CDMA STSK scheme.

whereas that imposed by the ML-MUD of (3.19) is found to be

$$\text{Complexity}_{\text{ML-MUD}} = \frac{S_f \left(4MNT^2QU + 5NTQ\mathcal{L}U + 2NTQ\mathcal{L}\right)}{\log_2(Q \cdot \mathcal{L})}. \tag{3.21}$$

Equations (3.7) - (3.14) and (3.19) are applicable for both the UL and DL scenarios and may be simplified further using (3.6) for downlink channels.

3.4 Channel-Coded Scheme

In this section, we propose a powerful iterative-detection aided MC-CDMA STSK transceiver as shown in Figure 3.10. We employ a recursive systematic convolutional (RSC) and unity-rate coding (URC) architecture, where the information bits, after being channel-encoded by the RSC code, are passed to the random bit interleaver Π_1. The URC has been used to beneficially spread the extrinsic information owing to its infinite impulse response [5], thus facilitating iterative convergence to extremely low bit-error rate (BER). After being randomly permuted, these bits are then URC encoded and after a second interleaving by Π_2, are transmitted through the MC-CDMA STSK scheme.

The received signals, after discarding the CP, are demodulated by the FD MC-CDMA demodulator. The symbols, after DFT processing at the demodulator, are input to the MC-CDMA STSK demapper block. Then, the three soft-decision decoders (the STSK demapper, the URC and the RSC decoder) start exchanging extrinsic information iteratively. The URC decoder generates extrinsic information employing the *a priori* information gleaned from the STSK demapper. More specifically, if the band of linearized FD signals from $\overline{\boldsymbol{Y}}[n_pS_f + 1]$ to $\overline{\boldsymbol{Y}}[(n_p + 1)S_f]$ contains B channel coded bits $b_1, b_2, ..., b_B$, then (3.22) formulates the extrinsic

logarithmic-likelihood ratio (LLR), $L_e(b_i)$ for the bit $b_i,\ i = 1, 2, \ldots, B$:

$$L_e(b_i) = \ln \frac{\sum\limits_{\boldsymbol{K}^u_{q^u,l^u_c} \in \boldsymbol{K}^i_1} \exp\left[-\sum\limits_{s_f=1}^{S_f} \left(\frac{\left|\left| \overline{\boldsymbol{Y}}[n_p S_f + s_f] - \sum\limits_{u=1}^{U} c^u_{s_f} \overline{\tilde{\boldsymbol{H}}}^u [n_p S_f + s_f] \boldsymbol{\chi} \boldsymbol{K}^u_{q^u,l^u_c} \right|\right|^2}{N_0} \right) + \sum\limits_{j \neq i} b_j L_a(b_j) \right]}{\sum\limits_{\boldsymbol{K}^u_{q^u,l^u_c} \in \boldsymbol{K}^i_0} \exp\left[-\sum\limits_{s_f=1}^{S_f} \left(\frac{\left|\left| \overline{\boldsymbol{Y}}[n_p S_f + s_f] - \sum\limits_{u=1}^{U} c^u_{s_f} \overline{\tilde{\boldsymbol{H}}}^u [n_p S_f + s_f] \boldsymbol{\chi} \boldsymbol{K}^u_{q^u,l^u_c} \right|\right|^2}{N_0} \right) + \sum\limits_{j \neq i} b_j L_a(b_j) \right]}, \tag{3.22}$$

as detailed in [5, 143]. In (3.22), $L_a(\bullet)$ refers to the *a priori* LLR for the bit '$\bullet$', $\boldsymbol{K}^i_1$ and $\boldsymbol{K}^i_0$ denote the subsets of the possible $\boldsymbol{K}^u$ vectors defined by (3.15) corresponding to the bit values $b_i = 1$ and $b_i = 0$, respectively, whereas other notations were defined earlier in Sec. 2.4.1. Equation (3.22) can be further simplified using the approximate-logarithmic-maximum *a posteriori* (Approx-log-MAP) algorithm [155], yielding

$$L_e(b_i) = \underset{\boldsymbol{K}^u_{q^u,l^u_c} \in \boldsymbol{K}^i_1}{\text{jac}}(d) - \underset{\boldsymbol{K}^u_{q^u,l^u_c} \in \boldsymbol{K}^i_0}{\text{jac}}(d), \tag{3.23}$$

where $\underset{\boldsymbol{K}^u_{q^u,l^u_c} \in \boldsymbol{K}^i_1}{\text{jac}}(d)$ and $\underset{\boldsymbol{K}^u_{q^u,l^u_c} \in \boldsymbol{K}^i_0}{\text{jac}}(d)$ represent the Jacobian logarithm of the expression 'd', when $\boldsymbol{K}^u_{q^u,l^u_c}$ is a member of $\boldsymbol{K}^i_1$ and $\boldsymbol{K}^i_0$, respectively and where 'd' is given by:

$$d = -\sum_{s_f=1}^{S_f} \left|\left| \overline{\boldsymbol{Y}}[n_p S_f + s_f] - \sum_{u=1}^{U} c^u_{s_f} \overline{\tilde{\boldsymbol{H}}}^u [n_p S_f + s_f] \boldsymbol{\chi} \boldsymbol{K}^u_{q^u,l^u_c} \right|\right|^2 / N_0 + \sum_{j \neq i} b_j L_a(b_j). \tag{3.24}$$

The RSC decoder, after several iterative exchange of extrinsic information, outputs the estimate of the information bits.

3.5 Results and Discussions

The performance of our MC-CDMA aided STSK scheme and the effects of the channels mentioned in Table 3.1 on our scheme are detailed in this section.

3.5.1 Performance of the Single-User MC-CDMA Aided STSK

The performance achievable by our MC-CDMA-aided STSK under a single-user scenario is illustrated in Figure 3.11. As expected, both the STSK and MC-CDMA STSK schemes exhibits a similar performance as in narrowband channels owing to the absence of ISI. Furthermore, the MC-CDMA STSK scheme is capable of maintaining its superior multiple antenna gain

Table 3.1: System parameters: MC-CDMA-aided STSK

Channel model	COST207-RA
	COST207-TU12
Fast fading envelope	Rayleigh
Normalized Doppler frequency	0.01
Spreading code	Walsh-Hadamard
No. of subcarriers, N_c	64
CP length	16
STSK (M, N, T, Q)	$(2, 2, 2, 2)$, BPSK
	$(2, 2, 2, 4)$, QPSK
Outer RSC en/decoder	Half-rate
	Constraint length=2
Generator polynomial	$(011, 010)_2$
Interleaver length	$240,000$ bits
Outer iterations, I_{outer}	7
Inner en/decoder	Unity Rate Code
Inner iterations, I_{inner}	2

in both the rural area (RA) scenario modelled by the COST207-RA channel as well as in the TU scenario characterized by the COST207-TU12 model. Furthermore, the single-user MC-CDMA aided STSK scheme shows improved performance upon increasing S_f both for the COST207-RA and COST207-TU12 channels owing to the fact that a FD spreading sequence may still remain recoverable, even when some of its chips are corrupted. The performance of the proposed MC-CDMA STSK ($M = 2, N = 2, T = 2, Q = 2$), BPSK and MC-CDMA STSK ($M = 2, N = 2, T = 2, Q = 4$), QPSK system in dispersive channels is also compared to that of the MC-CDMA based STBC $(M, N) = (2, 2)$, BPSK and STBC $(2, 2)$, QPSK respectively having similar throughput, which demonstrates the strength of the proposed scheme.

3.5.2 Performance of the Multiuser MC-CDMA Aided STSK DL/UL

Additionally, the performances of the multi-user MC-CDMA aided STSK scheme for the DL and the UL scenarios in the COST207-RA channel are characterized in Figure 3.12 and Figure 3.13 respectively, which were found to be more or less similar under the idealized conditions of perfect synchronization. Furthermore, the achievable performance improved upon increasing the S_f, while both the UL and the DL BER degraded under multiuser scenarios as a result of the increased MUI imposed by multiple users.

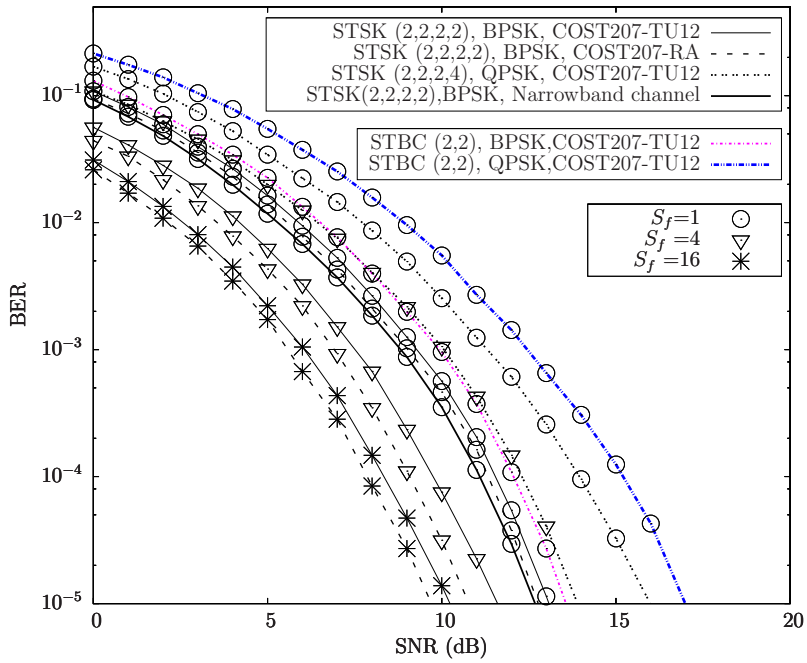

Figure 3.11: Performance of single-user uncoded MC-CDMA STSK system of Figure 3.5 using the parameters in Table 3.1 both in narrowband and in dispersive channels. The performance of the MC-CDMA aided $\mathcal{G}_2-$STBC $(M, N) = (2, 2)$, BPSK and $\mathcal{G}_2-$STBC $(2, 2)$, QPSK is also shown as benchmarker.

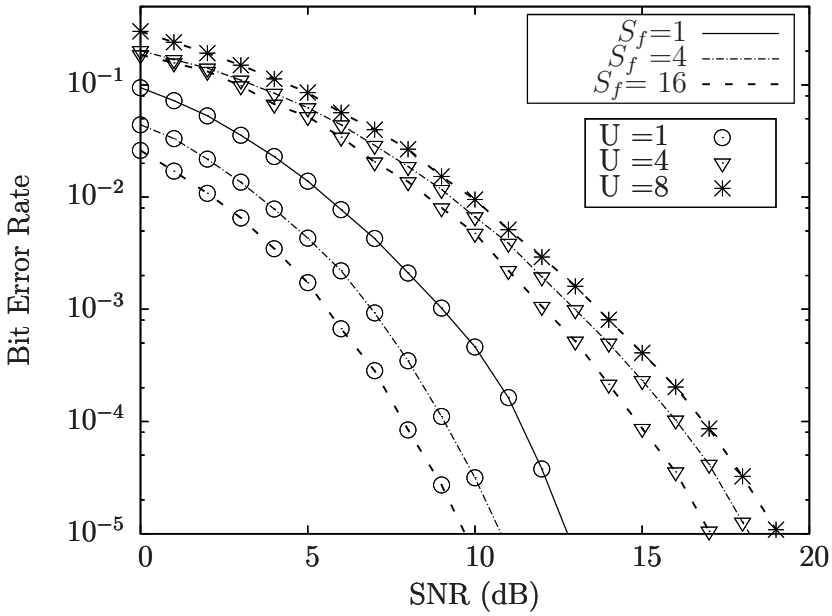

Figure 3.12: BER performance of MC-CDMA aided STSK $(M = 2, N = 2, T = 2, Q = 2)$, BPSK of Figure 3.8 using the parameters in Table 3.1 for the DL COST207-RA channel using different S_f supporting U users.

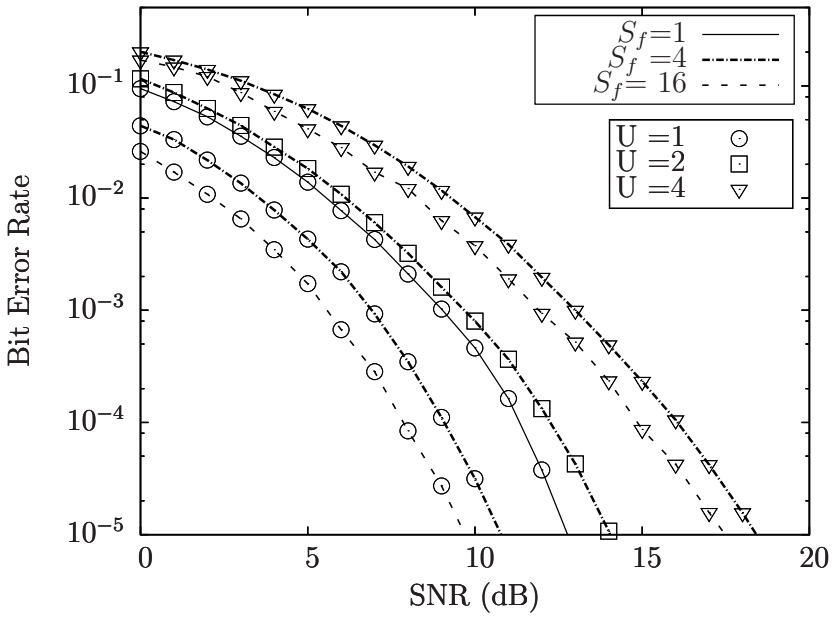

Figure 3.13: Performance of MC-CDMA STSK ($M = 2, N = 2, T = 2, Q = 2$), BPSK, UL of Figure 3.9 using the parameters in Table 3.1 for the COST207-RA channel using different S_f supporting U users.

3.5.3 Performance of the Channel-Coded MC-CDMA Aided STSK

Figure 3.14 characterizes the performance of the serially concatenated RSC- and URC-coded single-user MC-CDMA STSK ($M = 2, N = 2, T = 2, Q = 4$) scheme in conjunction with QPSK modulation communicating over broadband COST207-TU12 channel. The investigation of our channel-coded scheme was carried out using the simulation parameters of Table 3.1. Figure 3.14 demonstrates that the channel-coded scheme provides a sharp decrease in BER after a few iterations. The maximum achievable rates, where the scheme can still exhibit an extremely low BER, were computed using EXIT chart analysis and are shown as the ultimate benchmarker of the proposed scheme. Specifically, as discussed in [146], the area under the inner decoder's EXIT characteristic gives the maximum achievable rate for the specific scheme. The signal-to-noise ratios (SNRs), which provide maximum achievable rates for the MC-CDMA STSK ($M = 2, N = 2, T = 2, Q = 4$), QPSK schemes having spreading factors of $S_f = 1$ and $S_f = 4$ are computed and are shown in Figure 3.14. The scheme is observed to exhibit an infinitesimally low BER, especially with higher value of S_f, after a few outer iterations.

Figure 3.15 portrays the EXIT chart of the MC-CDMA aided STSK ($M = 2, N = 2, T = 2, Q = 4$), QPSK using $S_f = 4$, where the SNR was varied from -3.0 dB to 3.0 dB in steps of 1.0 dB. It can be seen in Figure 3.15 that all the inner decoder EXIT curves associated with $S_f = 4$ reached the point of perfect decoding convergence $(1.0, 1.0)$, which is the explicit benefit of employing URC precoding [5]. We also notice that an open EXIT tunnel was 'just' formed at SNR $= -2.0$ dB, and the EXIT curve at SNR $= -1$ dB was also confirmed by the corresponding

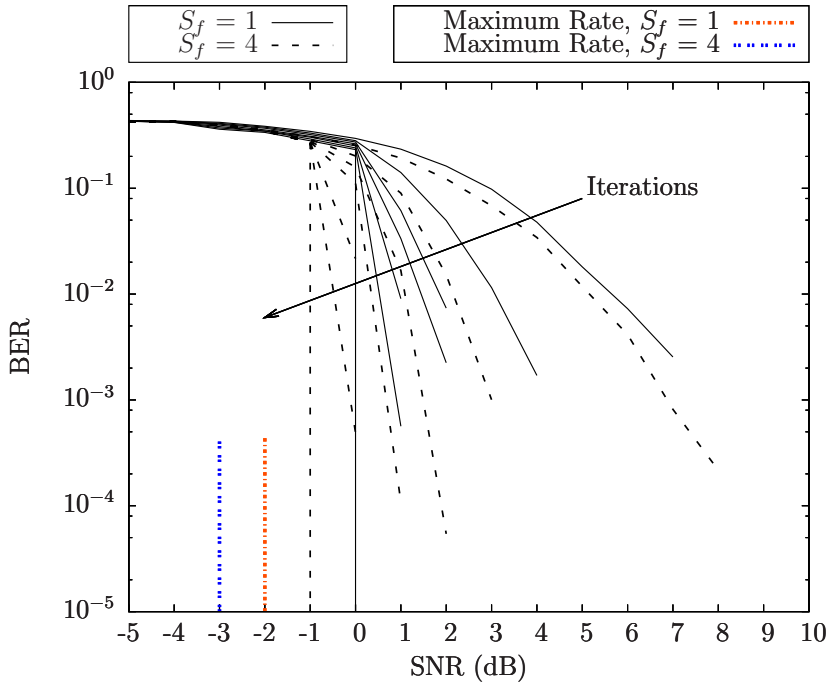

Figure 3.14: BER of our channel-coded single-user MC-CDMA STSK ($M = 2, N = 2, T = 2, Q = 4$), QPSK system of Figure 3.10 with $S_f = 1$ and $S_f = 4$ for the COST207-TU12 channel model of Table 3.1. The maximum achievable rates with $S_f = 1$ and $S_f = 4$ are also shown as the ultimate benchmarker of the scheme.

Monte-Carlo simulation based staircase-shaped decoding trajectory [147]. Therefore, it may be predicted that an infinitesimally low BER is achieved at SNR $= -1.0$ dB using $I_{outer} = 7$ outer iterations.

3.6 Chapter Summary and Conclusions

In Section 3.2, we provided a rudimentary introduction to the different multicarrier-based CDMA systems. Specifically, the FD-spread, the TD-spread and the multidimensional MC-based CDMA schemes were briefly compared. In Section 3.3, we proposed FD-spread MC-CDMA-aided STSK for improving the attainable frequency diversity of the OFDM-aided STSK system of Chapter 2, while facilitating multiuser transmissions. A novel single-stream ML-MUD was also proposed for jointly estimating the information of all the users. A channel-coded FD MC-CDMA-aided STSK scheme was conceived in Section 3.4. The performance of the scheme advovated was evaluated for transmission over frequency-selective channels in both uncoded and channel-coded scenarios in Section 3.5. The BER performance attainable by using our MC-CDMA-aided STSK scheme of Figure 3.5 as well as by our channel-coded MC-CDMA-aided STSK scheme of Figure 3.10 under both single-user and multiuser scenarios is summarized in Table 3.2. The results of our simulations demonstrated that the scheme

Table 3.2: Summary of the achievable BER performance of MC-CDMA-aided STSK

Scheme	*Schematic diagram*	*Figure number*	*SNR, dB* at BER		*SNR gain/difference, dB at BER (benchmark scheme)*	
			10^{-3}	10^{-4}	10^{-3}	10^{-4}
Single-user MC-CDMA STSK $(2,2,2,2)$, *BPSK COST207-TU12,* $S_f = 1$	Figure 3.5	Figure 3.11	9.4	12.0	0.4 ($\mathcal{G}_2$-STBC $(2,2), BPSK$)	1.0 ($\mathcal{G}_2$-STBC $(2,2), BPSK$)
Single-user MC-CDMA STSK $(2,2,2,2)$, *BPSK COST207-TU12,* $S_f = 4$	Figure 3.5	Figure 3.11	7.5	9.8	1.9 (Corresponding $S_f = 1$ scheme)	2.0 (Corresponding $S_f = 1$ scheme)
Single-user MC-CDMA STSK $(2,2,2,4)$, *QPSK COST207-TU12,* $S_f = 1$	Figure 3.5	Figure 3.11	12.4	14.0	0.8 ($\mathcal{G}_2$-STBC $(2,2), QPSK$)	1.0 ($\mathcal{G}_2$-STBC $(2,2), QPSK$)
Single-user MC-CDMA STSK $(2,2,2,4)$, *QPSK COST207-TU12,* $S_f = 4$	Figure 3.5	Figure 3.11	10.4	12.2	2.0 (Corresponding $S_f = 1$ scheme)	1.8 (Corresponding $S_f = 1$ scheme)
4-*user MC-CDMA STSK* $(2,2,2,2)$, *BPSK COST207-RA,* $S_f = 4$, *DL*	Figure 3.5	Figure 3.12	13.0	15.5	6.0 (Single-user scheme)	6.0 (Single-user scheme)
4-*user MC-CDMA STSK* $(2,2,2,2)$, *BPSK COST207-RA,* $S_f = 4$, *UL*	Figure 3.5	Figure 3.13	7.3	13.4	6.0 (Single-user scheme)	6.0 (Single-user scheme)
Channel-coded single-user MC-CDMA-aided STSK $(2,2,2,4)$, *QPSK* $S_f = 1$, *COST207-TU12*	Figure 3.10	Figure 3.14	0.0	0.0	2.0 (maximum achievable rate at BER ≈ 0)	
Channel-coded 4-*user MC-CDMA-aided STSK* $(2,2,2,4)$, *QPSK* $S_f = 4$, *COST207-TU12*	Figure 3.10	Figure 3.14	-1.0	-1.0	2.0 (maximum achievable rate at BER ≈ 0)	

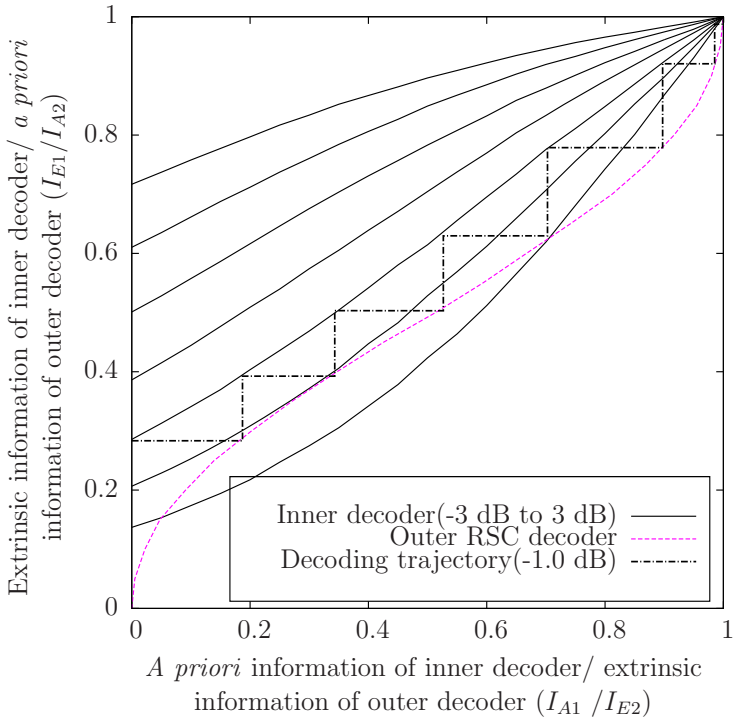

Figure 3.15: EXIT trajectory recorded at -1.0 dB of our three-stage turbo detected MC-CDMA STSK ($M = 2, N = 2, T = 2, Q = 4$), QPSK of Figure 3.10 using the parameters in Table 3.1 with $S_f = 4$ communicating over the COST207-TU12 channel ($f_d = 0.01$) together with the inner decoder EXIT curves from -3.0 to 3.0 dB in steps of 1.0 dB and the outer RSC decoder EXIT function.

portrayed in Figure 3.5 overcomes the channel impairments imposed by dispersive multi-path channels, as exemplified with the aid of Figure 3.11. Indeed, the scheme of Figure 3.10 exhibits a near-capacity performance in a channel-coded scenario, as illustrated by Figure 3.14 and Figure 3.15. Moreover, the attainable performance may be further improved upon increasing the spreading factor S_f, although as seen in Figure 3.12 and Figure 3.13, the system suffers from MUI in a multiuser scenario.

The performance degradation of single-carrier STSK system in broadband channels was efficiently mitigated by our OFDM-aided STSK system [119] of Chapter 2. For further improvement of the attainable frequency diversity provided by FD spreading, while facilitating multi-user communications, we have employed MC-CDMA in the system of Figure 3.5 relying on the single-stream ML-MUD illustrated in Figure 3.9.

The performance of our system crucially depends on the optimization of the DMs utilized. We have optimized the spreading matrices minimizing the pairwise symbol error probability by an exhaustive search, as detailed in [5, 32, 156], so that the power constraint of (2.29) used in [49] is satisfied. Furthermore, in order to reduce the computational complexity associated with the exhaustive search, genetic algorithm-aided DM optimization [131, 134] may also be

applied, as detailed in Chapter 2.

In Chapters 2 and 3, we proposed the novel OFDM-aided and MC-CDMA-aided STSK architectures of Figure 2.9 and Figure 3.5, respectively for mitigating the performance degradation of STSK system is dispersive wireless channels. These schemes also benefitted from additional FD diversity advantages. In the following chapter, we will further generalize the multicarrier STSK system employing OFDMA aided STSK in the DL and SC-FDMA aided STSK in the UL for exploiting the advantages of multicarrier systems, while facilitating multiuser communications.

Chapter 4

OFDMA/SC-FDMA Aided STSK for Dispersive Downlink/Uplink Scenarios

4.1 Introduction

Motivated by the recent concept of STSK [49] developed for striking a flexible diversity versus multiplexing gain trade-off as discussed in Chapter 2, in this chapter we propose a novel orthogonal frequency division multiple access (OFDMA)/ single-carrier frequency division multiple access (SC-FDMA) aided multi-user STSK scheme for frequency-selective channels. The proposed OFDMA/SC-FDMA STSK scheme is capable of providing an improved performance in dispersive channels, while supporting multiple users in a multiple antenna aided wireless system. Furthermore, the scheme has the inherent potential of benefitting from the employment of a low-complexity single-stream maximum-likelihood (ML) detector. Both an uncoded and a sophisticated near-capacity coded OFDMA/SC-FDMA STSK scheme will be studied and their performances will be compared in multiuser wideband MIMO scenarios. Explicitly, OFDMA/SC-FDMA aided STSK exhibits an excellent performance even in the presence of channel impairments due to the frequency-selectivity of wideband channels and proves to be a beneficial choice for high capacity multi-user MIMO systems.

In order to mitigate the performance degradation of STSK systems imposed by dispersive channels, we intrinsically amalgamated the OFDMA and SC-FDMA concept with the STSK system in this chapter. OFDMA/SC-FDMA aided STSK systems are capable of attaining a superb diversity-multiplexing tradeoff even in a multipath environment, whilst additionally supporting multiuser transmissions and maintaining a low peak-to-average power ratio (PAPR) in uplink SC-FDMA-aided STSK scenarios.

Hence OFDMA/SC-FDMA assisted STSK systems are advocated in this chapter, since

OFDMA and SC-FDMA have been adopted for the downlink (DL) and the uplink (UL) of the Long Term Evolution (LTE)-Advanced standard, respectively [157]. Before transmitting the signals from each of the transmit antenna elements (AEs) of our STSK system, either the discrete Fourier transformed (DFT) or the original frequency-domain (FD) symbols are mapped to a number of subcarriers, either in a contiguous subband-based fashion or by dispersing them right across the entire FD. The resultant signal is then transmitted after the inverse discrete Fourier transform (IDFT)-based modulation operation.

The transmitted signal of each subcarrier of the parallel modem experiences a non-dispersive, narrowband channel and the overall STSK based MIMO scheme exhibits a performance similar to that observed in narrowband channels, despite operating in a wideband scenario. The appropriate mapping of the users' symbols to subcarriers results in a flexible multi-user performance, while benefitting from our low-complexity single-stream based detection. In case of the SC-FDMA UL mode, we can use a minimum mean squared error (MMSE) or zero-forcing (ZF) based single-tap FD equalizer followed by single-stream based ML detection in the TD. Furthermore, the DFT-precoding based SC-FDMA scheme is capable of reducing the PAPR for the mobile's uplink transmissions. Finally, the performance of the proposed system relying on a three-stage concatenated recursive systematic convolutional (RSC) and unity rate coded (URC) scenario is characterized with the aid of extrinsic information transfer (EXIT) charts.

The remainder of this chapter is organised as follows. A comparative study of OFDMA and SC-FDMA as an UL multiple access scheme will be provided in Section 4.2. In Section 4.3, we present a brief overview of our proposed system, which relies on the linear dispersion matrix aided STSK scheme of Figure 4.6 and Figure 4.7 amalgamated with OFDMA/SC-FDMA transmission. A reduced-complexity detector is proposed for the OFDMA/SC-FDMA-aided STSK architecture in Section 4.4, which is detailed in Subsection 4.4.2. Its complexity is analyzed in Subsection 4.4.3. In Section 4.5, an OFDMA/SC-FDMA STSK scheme based on three-stage RSC-URC coded scenario similar to that of Figure 2.14 and Figure 3.10 is discussed. The OFDMA/SC-FDMA-aided STSK scheme and the channel-coded OFDMA/SC-FDMA-aided STSK scheme based on an EXIT chart assisted near capacity design is investigated in Section 4.6. Finally, in Section 4.7, we provide the summary and conclusions of this chapter.

4.2 A Brief Review of OFDMA and SC-FDMA

Again, OFDMA and SC-FDMA [101, 102] has been adopted by the Third-Generation Partnership Project (3GPP) for the DL and the UL of its next generation LTE-Advanced wireless standard, respectively. OFDMA is a multiple access version of OFDM, where a block of subcarriers are allocated to the different users in a frequency-division multiple access fashion. This facilitates having a low data rate for each subcarrier, which is subjected to narrowband fading.

SC-FDMA, on the other hand, is a transmission scheme, which employs single-carrier modulation (SCM) as an alternative to the multicarrier modulation scheme employed in OFDM, OFDMA and/or MC-CDMA.

The employment of SCM has been motivated by the idea of exploiting the low PAPR of the trasmit signals, which is beneficial for achieving improved power-amplifier efficiency. SCM is implemented in the SC-FDMA scheme by the DFT-precoding of the user symbols, before being mapped to the subcarriers. Unlike in OFDM or in OFDMA where each data symbol modulates individual subcarriers, the SC-FDMA transmitter spreads each data symbol across a group of subcarriers transmitted simultaneously. As each data symbol is spread across multiple subcarriers by using the DFT-operation, SC-FDMA offers frequency spreading and hence a frequency diversity gain. For this reason, as already mentioned in Section 1.3.3, SC-FDMA may be viewed as a DFT-precoded OFDMA system. However, it differs from the more generic 'Precoded OFDMA' scheme, where any precoding matrix such as the Walsh-Hadamard matrix may also be employed, for example, for the sake of spreading the data symbols across the frequency band. Naturally, the DFT matrix may also be interpreted as a precoding matrix and SC-FDMA may be termed as DFT-spread or frequency-spread OFDMA. But again, the main benefit of SC-FDMA in the uplink, however, is its low PAPR which is of vital importance for the low-power handset or user equipment (UE). SC-FDMA has the further benefit of flexible frequency allocation, whilst inheriting the multipath-resilience of OFDMA schemes, as detailed below.

The basic OFDMA/SC-FDMA transmission scheme is shown in Figure 4.1. From Figure 4.1, we may also explicitly infer the differences between SC-FDMA and OFDMA based communications. In OFDMA, the dotted block 'DFT size=N_d ' of the transmitter and the 'IDFT size=N_d ' block of the receiver do not exist. More specifically, the first 'Time domain' region at the left of the transmitter and the last 'Time domain' region at the right of the receiver are absent. Hence, OFDMA does not benefit from DFT-precoding. The information entering into and detected at the output of the OFDMA scheme is in the FD, whereas that in the SC-FDMA scheme is in the TD.

4.2.1 Subcarrier Mapping

The FD data symbols of the OFDMA system or the DFT outputs of the SC-FDMA system are mapped to a subset of subcarriers. In the LTE standard, the subcarrier mapping is categorized into two types: localized mapping or localized frequency division multiple access (LFDMA) and distributed mapping. In LFDMA, the symbols are mapped to a subset of consecutive subcarriers. By contrast, the symbols are mapped in a distributed fashion to subcarriers that are spread over the entire bandwidth in a distributed mapping method. A special case of

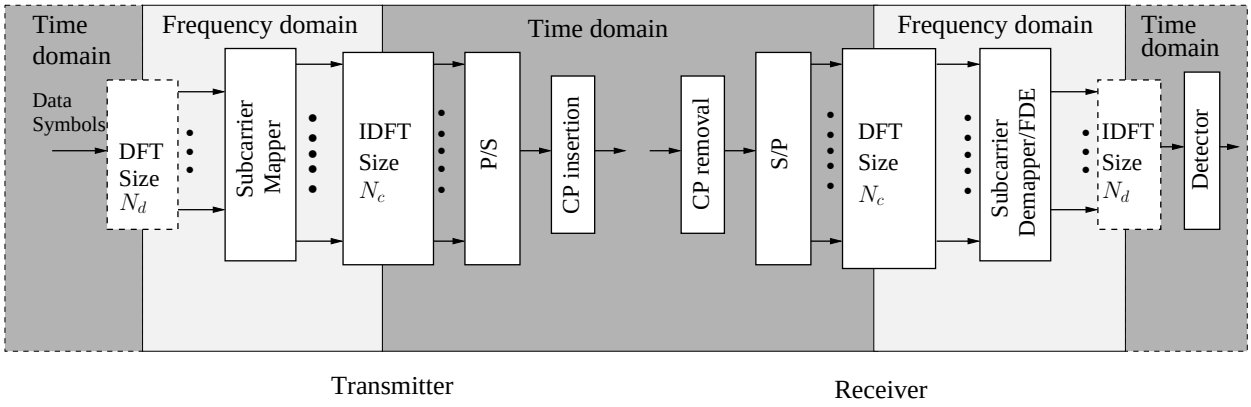

Figure 4.1: Typical transceiver architecture of OFDMA/SC-FDMA aided systems. In the OFDMA aided scheme the dotted block 'DFT size=N_d' at the left of the transmitter and the 'IDFT size=N_d' block at the right of the receiver do not exist. Explicitly, in OFDMA the information enters the transmitter and it is mapped directly to the subcarriers.

distributed subcarrier mapping is referred to as interleaved FDMA (IFDMA), where the subcarriers conveying consecutive input symbols are uniformly spaced over the entire bandwidth, which has the benefit of improved FD diversity in comparison to LFDMA. Both the localized and the distributed mapping of a fully-loaded $4-$user OFDMA/SC-FDMA scheme employing 16 subcarriers are illustrated in Figure 4.2.

For LFDMA, the subcarrier mapping operation of the users may be described as: user $1:\{1,2,3,4\}$, user $2:\{5,6,7,8\}$, user $3:\{9,10,11,12\}$, user $4:\{13,14,15,16\}$. By contrast, the subcarrier mapping using IFDMA may be represented as: user $1:\{1,5,9,13\}$, user $2:\{2,6,10,14\}$, user $3:\{3,7,11,15\}$, user $4:\{4,8,12,16\}$. Again, IFDMA maintains a higher FD separation between the subcarriers of a particular user and thus provides additional frequency diversity gain. Furthermore, IFDMA imposes a lower PAPR than LFDMA [158]. However, LFDMA in combination with channel-dependent scheduling, which is invoked for allocating frequencies to users depending on the channel conditions, is capable of providing multiuser diversity and a potentially higher sum rate in frequency-selective channels [159, 160].

4.2.2 Single-Carrier Modulation and Frequency Domain Equalization

In the aftermath of widespread multicarrier applications, single-carrier modulation (SCM) is enjoying a renaissance, especially in the context of UL scenarios [104]. This is because having a low PAPR is of salient importance for the sake of relaxing the power-amplifier linearity requirements, hence achieving an improved power efficiency. To elaborate a little further, SCM has the advantage that for a given signal power the PAPR of its signal is significantly lower than that of its multicarrier counterpart. As a result, its performance is less gravely affected by the transmitter power amplifier nonlinearities, which allows cost- and power-efficient amplifiers

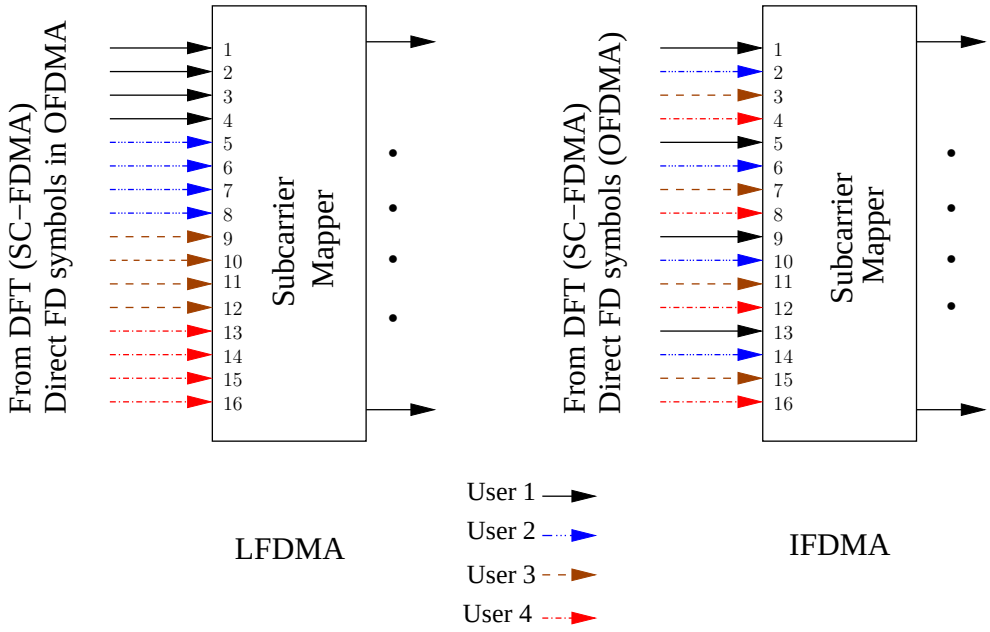

Figure 4.2: Localized versus distributed (interleaved) subcarrier mapping of a fully-loaded 4−user OFDMA/SC-FDMA scheme employing 16 subcarriers. In the OFDMA scheme, each user is allocated 4 subchannels, where 4 point DFT precoding is used for SC-FDMA scheme.

to be employed. A further benefit of SCM is its higher robustness to both carrier frequency offsets and phase noise than that of OFDM.

However, the question which may arise is, how SCM is implemented in the context of a SC-FDMA scheme, when multiple subcarriers are used? The answer might be revealed by a close inspection of Figure 4.3. Observe in Figure 4.3 that in contrast to OFDM/OFDMA, each data symbol transmitted in the SC-FDMA scheme is spread to a subset of subcarriers by using the DFT operation, rather than being directly mapped in a one-to-one fashion to the individual subcarriers. The subset of subcarriers which transmits a specific symbol is interpreted as a single carrier analogously to say single-carrier DS-CDMA, where each symbol is spread with the aid of a unique, user-specific spreading sequence. Hence the dotted portion of the SC-FDMA transmitter seen in Figure 4.3 may be viewed as a SCM scheme [104].

To elaborate a little further, the symbols at different stages of Figure 4.3 are shown in Figure 4.4 for both IFDMA and LFDMA. The symbols represented by x refer to the TD symbols, while those denoted by X are FD symbols. For IFDMA, the TD modulated symbols generated after sub-carrier mapping and inverse DFT of the FD symbols $\{\tilde{X}_{n_c}\}$ are given by [158]:

$$x_{n_c} = \frac{1}{U} x_{n_d} \tag{4.1}$$

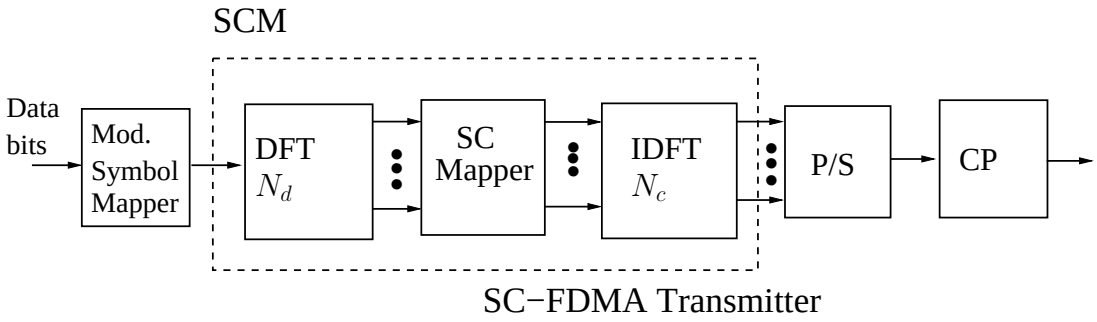

Figure 4.3: Illustration of the SCM block composed of the DFT, the subcarrier (SC) mapper and the IDFT blocks, which is shown dotted. Observe that DFT-based spreading takes place over N_d subcarriers, whilst the IDFT-operation assists in parallel transmission employing N_c subcarriers.

whereas for LFDMA they are expressed as [158]:

$$x_{n_c} = \frac{1}{U}(1 - e^{j2\pi\frac{u}{U}}) \cdot \frac{1}{N_d} \sum_{p=1}^{N_d} \frac{x_p}{1 - e^{j2\pi\left\{\frac{(n_d-p)}{N_d} + \frac{u}{N_d U}\right\}}}. \tag{4.2}$$

Figure 4.4 portrays both the FD symbols mapped to subcarriers both in the localized and in the interleaved fashion. The TD representation of the IDFT block's output is also shown in Figure 4.4. The $0'$s in the FD represent subcarrier symbols are either left blank or are assigned to another user's FD symbols, whereas '?'s indicate symbols represented by (4.2). As seen from Figure 4.4 and from (4.1), the TD symbols at the output of the IDFT block of Figure 4.3 are the exact replicas of the original symbols after the bit-to-symbol mapper of Figure 4.3 in IFDMA [158]. However, in LFDMA, the symbols are uniformly spaced in the same order as that of the original symbols. Hence again, the 'DFT-SC Mapper-IDFT' blocks of Figure 4.3 together may be interpreted as a SCM block.

Traditionally equalization has been performed in the TD for single carrier transmissions [161]. However, if the intersymbol interference (ISI) spreads over more than for example $30-50$ symbols, the signal processing complexity associated with this TD approach might become excessive [104]. As an alternative, FD equalization (FDE) was first studied in [99]. However, the full benefit of this method was gradually realized after it was proposed as a low-complexity solution to digital terrestrial TV broadcasting [100]. Later, Falconer *et al.* [101, 102] detalied the FDE concept in relation to SCM and compared it to OFDM. In simple terms one might argue that FDE is attractive, because instead of applying a high-complexity TD equalizer N_c times to N_c symbols, each of the N_c symbols is equalized by a low-complexity single-tap FDE. This is the explicit benefit facilitated by the efficient DFT/IDFT operation. The difference between FDE used in OFDMA and in SC-FDMA may be illustrated with the aid of Figure 4.5. The basic difference between FDE in OFDMA and that in SCM is that an additional 'IDFT' block transforms the SC signal back to the TD after FD equalization [96, 101]. The performance

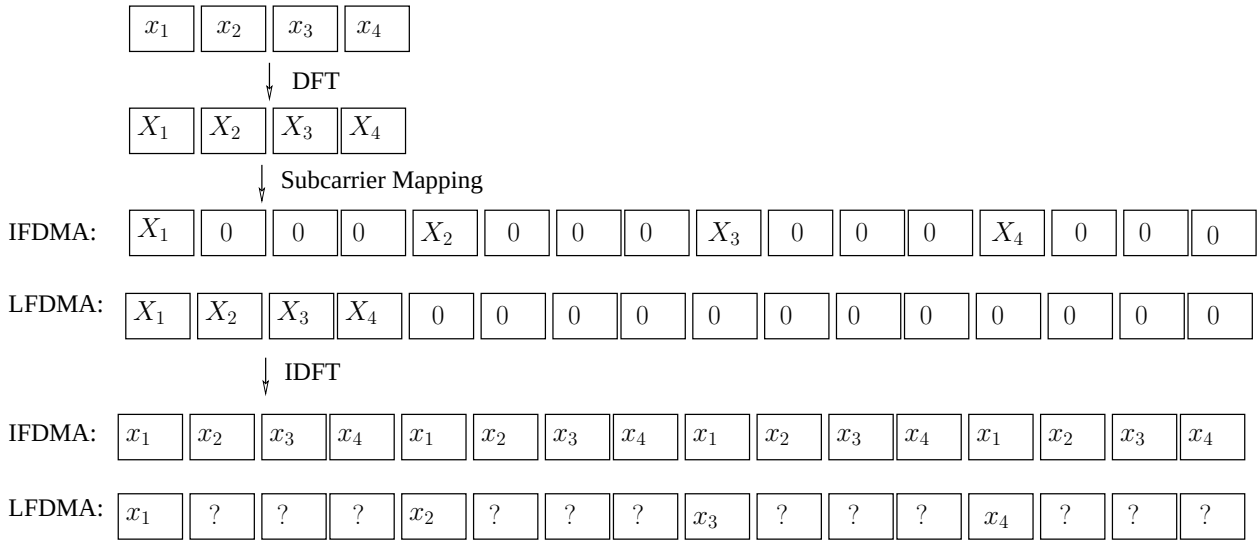

Figure 4.4: The transmit symbols at the output of the different stages of Figure 4.3 for both IFDMA and LFDMA. The symbols represented by x refer to the TD symbols, while those denoted by X are FD symbols. The TD symbols at the output of the 'IDFT N_c' block of IFDMA are the exact replicas of the original symbols, whereas those of LFDMA are the original symbols spaced uniformly in the same order - indicating single-carrier modulation [158]. The '0's in the FD represent subcarrier symbols are either left blank or are assigned to another user's FD symbols, whereas '?'s indicate symbols represented by (4.2).

of SC-FDMA is similar to that of OFDMA. However, FDE combined with SCM provides the following advantages [101]:

- It is less sensitive to nonlinear distortion, hence power-efficient and low-cost class A,B amplifiers may be used,
- It is less sensitive to carrier frequency offset.

In a nutshell, OFDMA is a multiple access scheme which benefits from multicarrier based communications providing high data-rate transmissions with protection against the frequency selectivity of dispersive channels. On the other hand, SC-FDMA gleans two main benefits from the employment of the DFT-precoder. Firstly, the DFT-precoding restores the single-carrier-like signal envelope, which reduces the PAPR of OFDMA signals. Secondly, the DFT performs a spreading operation - spreading each modulated symbol over a group of subcarriers. As a result, the scheme achieves additional frequency diversity. If a particular subcarrier is subject to deep fading, this would only affect a single sample of the FD signal and hence the original symbol may still be recoverable.

Having provided a brief overview of the OFDMA and the SC-FDMA system, let us now proceed to our OFDMA/SC-FDMA aided STSK system architecture in Section 4.3.

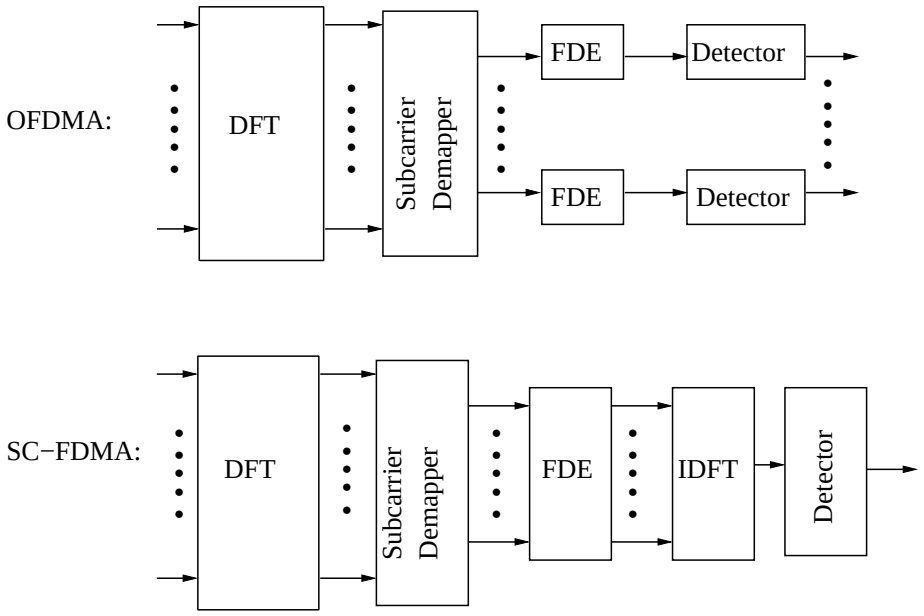

Figure 4.5: Equalization and detection of OFDMA and SC-FDMA scheme illustrating the difference between FDE applied to SCM and that applied to multicarrier system.

4.3 OFDMA/SC-FDMA Aided STSK: System Overview

We consider an OFDMA/SC-FDMA STSK system having M transmit and N receive AEs. The channel is assumed to be a frequency-selective Rayleigh fading medium, which can be modelled by a finite impulse response (FIR) filter with time-varying tap values [139, 140]. In our investigations of the system performance in section 4.6, we have utilized the COST207-TU12 channel specifications for the delay and the Doppler power spectral density to represent a typical urban (TU) scenario. The number of subcarriers employed for the transmission of N_d STSK blocks of a single user after N_d -point DFT processing is N_c.

4.3.1 Transmitter

The transmitter architecture of our OFDMA/SC-FDMA STSK system is shown in Figure 4.6. The signals are transmitted from different transmit AEs within T different symbol intervals after being mapped by the Space-Time (ST) mapper of the STSK block and after OFDMA/SC-FDMA based processing. To be specific, the STSK encoder of Figure 4.6 maps the source information of one of the U users to ST blocks $\boldsymbol{x}^u[n_d] \in \mathbb{C}^{M\times T}$, $n_d = 1, 2, \ldots, N_d$ according to [49]:

$$\boldsymbol{x}^u[n_d] = s^u[n_d]\boldsymbol{A}^u[n_d], \;\; u = 1, 2, \ldots, U, \tag{4.3}$$

where $s^u[n_d]$ and $\boldsymbol{A}^u[n_d]$ represent the u-th user's $\mathcal{L}$-PSK/QAM symbol and activated dispersion matrix (DM), respectively, from a set of Q such matrices $\boldsymbol{A}_q$ ($q = 1, 2...., Q$), which are pre-assigned in advance of transmissions. The DMs may be generated, for example, either by

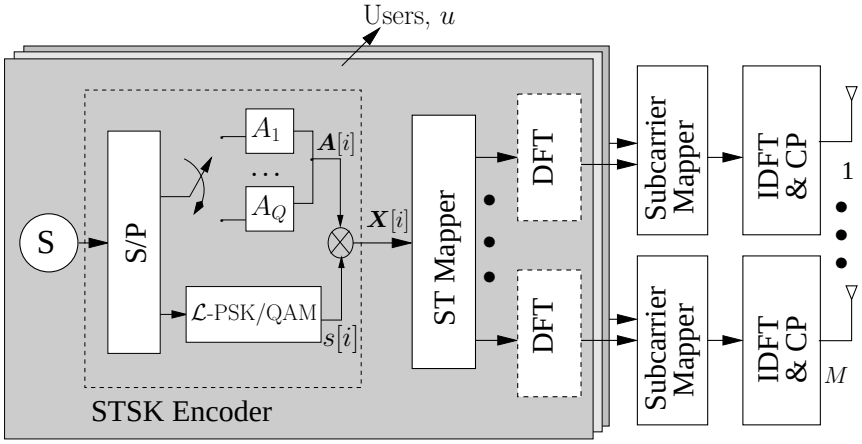

Figure 4.6: Transmission model of SC-FDMA aided STSK scheme. In OFDMA aided scheme the dotted block 'DFT N_d' in the transmitter does not exist. The STSK mapper selects one out of the Q dispersion matrices along with one constellation symbol and the resultant space-time codewords are passed in different time slots through the OFDMA or SC-FDMA based multi-user transmission system before being transmitted through the transmit AEs.

maximizing the continuous-input continuous-output memoryless channel (CCMC) capacity, or the discrete-input continuous-output memoryless channel (DCMC) capacity or alternatively, by minimizing the maximum pairwise symbol error probability (PSEP) under the power-constraint criterion [5, 32] of:

$$\mathrm{tr}(\boldsymbol{A}_q^H \boldsymbol{A}_q) = T \qquad \forall q. \tag{4.4}$$

Thus, a block of $\log_2(\mathcal{L} \cdot Q)$ number of bits are transmitted by the space-time (ST) mapper of Figure 4.6 per symbol interval, which forms an STSK ST-block and the STSK system of Figure 4.6 is uniquely specified by the parameters (M, N, T, Q) in conjunction with the $\mathcal{L}$-PSK or $\mathcal{L}$-QAM modulation scheme, where N is the number of receiver AEs.

After generating the space-time blocks $\boldsymbol{x}^u[n_d]$ for a particular user u, we employ frame based transmission. In particular, N_c sub-carriers are used for transmitting a frame, each frame consisting of N_d STSK blocks. To be specific, we define the transmit frame $\tilde{\boldsymbol{x}}^u \in \mathbb{C}^{MN_d \times T}$ for user u as

$$\tilde{\boldsymbol{x}}^u = \begin{pmatrix} \tilde{\boldsymbol{x}}^u_{1,1} & \tilde{\boldsymbol{x}}^u_{1,2} & \cdots & \tilde{\boldsymbol{x}}^u_{1,T} \\ \tilde{\boldsymbol{x}}^u_{2,1} & \tilde{\boldsymbol{x}}^u_{2,2} & \cdots & \tilde{\boldsymbol{x}}^u_{2,T} \\ \vdots & \vdots & \ddots & \vdots \\ \tilde{\boldsymbol{x}}^u_{M,1} & \tilde{\boldsymbol{x}}^u_{M,2} & \cdots & \tilde{\boldsymbol{x}}^u_{M,T} \end{pmatrix}, \tag{4.5}$$

where each $(N_d \times 1)$-element data vector $\tilde{\boldsymbol{x}}^u_{m,T_i}$, $(m = 1, 2, \ldots, M, \quad T_i = 1, 2, \ldots, T)$ can be

represented by

$$\tilde{\boldsymbol{x}}^{u}_{m,T_i} = \left[\boldsymbol{x}^{u}_{m,T_i}[1], \boldsymbol{x}^{u}_{m,T_i}[2], \cdots, \boldsymbol{x}^{u}_{m,T_i}[N_d]\right]^{T}, \tag{4.6}$$

which undergoes the N_d-point DFT operation.

To expound a little further, the data stream $\tilde{\boldsymbol{x}}^{u}_{m,T_i}$ to be transmitted from the transmit AE m at a specific time interval T_i is first DFT-precoded by the N_d-point DFT block; in case of OFDMA, however, this step is not required. Then, assuming a full-load system, the FD symbols $\boldsymbol{X}_{m,T_i} \in \mathbb{C}^{N_d \times 1}$ output from the N_d-point DFT block of the SC-FDMA STSK scheme (or the direct FD STSK codeword symbols of the OFDMA STSK scheme) are mapped to N_c sub-carriers with $N_c = (N_d \times U)$, where the sub-carrier allocation may be in contiguous (localized FDMA or LFDMA) [96] or in an interleaved (IFDMA) [96] fashion. Denoting the set of sub-carriers allocated to user u by $\mathcal{S}_u$, the sub-carrier allocation matrix, $\boldsymbol{P}^{u} \in \mathbb{C}^{N_c \times N_d}$ may be represented by [98]:

$$\boldsymbol{P}^{u}_{n_c,n_d} = \begin{cases} 1, & \text{if } n_c \in \mathcal{S}_u \text{ and sub-carrier } n_c \\ & \text{is allocated to } \boldsymbol{\mathcal{F}}_{N_d}\mathbf{x}^{u}_{m,T_i}[n_d] \\ 0, & \text{otherwise,} \end{cases} \tag{4.7}$$

where we have:

$$n_c = \begin{cases} (n_d \times U) + u, & \text{IFDMA} \\ (N_d \times u) + n_d, & \text{LFDMA,} \end{cases} \tag{4.8}$$

for all $n_c = 1, 2, \ldots, N_c$ and all $n_d = 1, 2, \ldots, N_d$.

Defining $\boldsymbol{C}_{add}(\bullet)$ as a matrix [105] which adds a TD cyclic prefix (CP) of length L_{cp} (which is higher than the channel's delay spread) to the N_c-length vector $(\bullet)$, the TD data vector after the IDFT operation may be written as:

$$\breve{\boldsymbol{x}}^{u}_{m,T_i} = \boldsymbol{C}_{add}\left(\boldsymbol{\mathcal{F}}^{H}_{N_c}\boldsymbol{P}^{u}\boldsymbol{\mathcal{F}}_{N_d}\boldsymbol{x}^{u}_{m,T_i}\right), \tag{4.9}$$

$$= \boldsymbol{C}_{add}\left(\boldsymbol{\mathcal{F}}^{H}_{N_c}\boldsymbol{P}^{u}\boldsymbol{X}_{m,T_i}\right), \tag{4.10}$$

Hence, the u-th user's transmit frame after IDFT operation can be formulated in a similar form as (4.5), yielding:

$$\breve{\boldsymbol{x}}^{u} = \begin{pmatrix} \breve{\boldsymbol{x}}^{u}_{1,1} & \breve{\boldsymbol{x}}^{u}_{1,2} & \cdots & \breve{\boldsymbol{x}}^{u}_{1,T} \\ \breve{\boldsymbol{x}}^{u}_{2,1} & \breve{\boldsymbol{x}}^{u}_{2,2} & \cdots & \breve{\boldsymbol{x}}^{u}_{2,T} \\ \vdots & \vdots & \ddots & \vdots \\ \breve{\boldsymbol{x}}^{u}_{M,1} & \breve{\boldsymbol{x}}^{u}_{M,2} & \cdots & \breve{\boldsymbol{x}}^{u}_{M,T} \end{pmatrix}, \tag{4.11}$$

where each vector $\breve{\boldsymbol{x}}^{u}_{m,T_i}$ is defined by (4.9) and (4.10) with

$$\breve{\boldsymbol{x}}^{u}_{m,T_i} \in \mathbb{C}^{(N_c+L_{cp})\times 1}, \tag{4.12}$$

and hence,

$$\breve{\boldsymbol{x}}^u \in \mathbb{C}^{(N_c+L_{cp})M\times T}. \tag{4.13}$$

Each link of the M transmit and N receive AE aided system is assumed to be frequency-selective, whose channel impulse respone (CIR) may be modelled as the ensemble of all the propagation paths [139, 140]:

$$h^u_{n,m}(t,\tau) = \sum_{l=1}^{L} a^u_l g^u_l(t)\delta(\tau-\tau^u_l), \tag{4.14}$$

for each $n = 1, 2, \ldots, N$, $m = 1, 2, \ldots, M$ and $u = 1, 2, \ldots, U$ and where L is the number of multipath components in the channel between the m-th transmit and the n-th receive AE, a^u_l, τ^u_l and $g^u_l(t)$ are the channel's envelope, delay and Rayleigh fading process exhibiting a particular normalized Doppler frequency f_d respectively, associated with the l-th path of user u.

Note that we use h and $\boldsymbol{H}$ to denote the CIR and the $(N \times M)$-element CIR matrix respectively, while $\tilde{h}$ and $\tilde{\boldsymbol{H}}$ denote the channel's FD channel transfer function (FDCHTF) and the $(N \times M)$-element FD channel transfer matrix (FDCHTM), respectively.

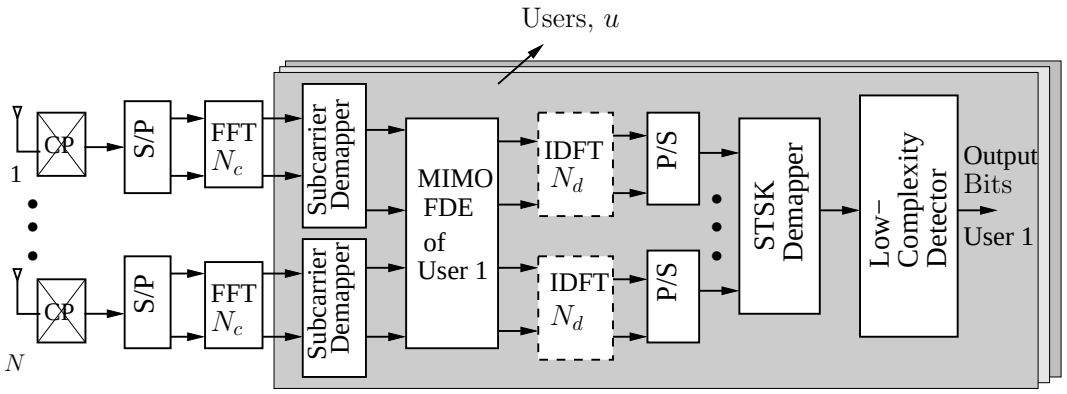

Figure 4.7: Receiver model of SC-FDMA aided STSK scheme. In OFDMA aided scheme the dotted block 'IDFT N_d' in the receiver does not exist. Since a single dispersion matrix is selected in one transmission block, a low-complexity single-stream ML detector can be employed.

4.3.2 Receiver

Assuming perfect synchronization at the receiver of Figure 4.7 and after removing the CP, the discrete-time input to the receiver's 'N_c-point IDFT ' block at the receive AE n at time slot T_i is given by [73]

$$\boldsymbol{y}_{n,T_i} = \sum_{u=1}^{U}\sum_{m=1}^{M} \boldsymbol{h}^u_{n,m} \circledast_{N_c} \breve{\boldsymbol{x}}^u_{m,T_i} + \mathbf{v}_{n,T_i}, \tag{4.15}$$

where $\circledast_{N_c}$represents the length-N_c circular convolution operator and $\boldsymbol{v}_{n,T_i}$ is the noise vector.

Defining the FDCHTM by $\tilde{\boldsymbol{H}}^u$, the FD transmit codeword matrix after sub-carrier mapping by $\tilde{\boldsymbol{X}}^u$ and the FD Additive White Gaussian Noise (AWGN) matrix by $\boldsymbol{V}$, the FD output matrix $\boldsymbol{Y}$ after the N_c-point DFT of our space-time (ST) architecture may be written as:

$$\boldsymbol{Y} = \sum_{u=1}^{U} \tilde{\boldsymbol{H}}^u \tilde{\boldsymbol{X}}^u + \boldsymbol{V}, \tag{4.16}$$

where each (n,m)-th component of $\tilde{\boldsymbol{H}}^u$ is formulated as

$$\tilde{\boldsymbol{H}}^u_{n,m} = \text{diag}\{\tilde{h}^u_{n,m}[1], \tilde{h}^u_{n,m}[2], ..., \tilde{h}^u_{n,m}[N_c]\} \in \mathbb{C}^{N_c \times N_c}, \tag{4.17}$$

where $\tilde{h}^u_{n,m}$ denotes the FDCHTF corresponding to user u and the components of $\tilde{\boldsymbol{X}}^u$, $\boldsymbol{V}$ and $\boldsymbol{Y}$ are defined by

$$\tilde{\boldsymbol{X}}^u_{m,T_i} = \boldsymbol{P}^u \boldsymbol{X}^u_{m,T_i} \in \mathbb{C}^{N_c \times 1}, \tag{4.18}$$

$$\boldsymbol{V}_{n,T_i} \in \mathbb{C}^{N_c \times 1}, \tag{4.19}$$

and

$$\boldsymbol{Y}_{n,T_i} \in \mathbb{C}^{N_c \times 1}. \tag{4.20}$$

Hence, the components of $\boldsymbol{Y}$ can be formulated from (4.16) as:

$$\boldsymbol{Y}_{n,T_i} = \sum_{u=1}^{U} \tilde{\boldsymbol{H}}^u_{n,m} \boldsymbol{P}^u \boldsymbol{X}^u_{m,T_i} + \boldsymbol{V}_{n,T_i} \tag{4.21}$$

$$= \sum_{u=1}^{U} \tilde{\boldsymbol{H}}^u_{n,m} \boldsymbol{P}^u \boldsymbol{\mathcal{F}}_{N_d} \tilde{\boldsymbol{x}}^u_{m,T_i} + \boldsymbol{V}_{n,T_i} \tag{4.22}$$

Now, after sub-carrier demapping and MIMO Frequency-Domain Equalization (FDE), the received symbols are passed through the 'N_d-point IDFT' block of user v. Defining $\tilde{\boldsymbol{P}}^u = [\boldsymbol{P}^u]^T$ as the sub-carrier demapping matrix and $\boldsymbol{W}^v$ as the weight matrix of the MIMO ZF or MMSE FDE of user v, which is given by [162]

$$\boldsymbol{W}^v = \begin{cases} [(\tilde{\boldsymbol{H}}^v)^H \tilde{\boldsymbol{H}}^v]^{-1} (\tilde{\boldsymbol{H}}^v)^H & \text{ZF} \\ [(\tilde{\boldsymbol{H}}^v)^H \tilde{\boldsymbol{H}}^v + \sigma_n^2 \boldsymbol{I}_M]^{-1} (\tilde{\boldsymbol{H}}^v)^H & \text{MMSE,} \end{cases} \tag{4.23}$$

where σ_n^2 denotes the variance of the additive noise, the elements of the TD output $\boldsymbol{z}^v$ of user v after the IDFT operation may be expressed as [98]:

$$\boldsymbol{z}^v_{m,T_i} = \boldsymbol{\mathcal{F}}^H_{N_d} \tilde{\boldsymbol{P}}^v \boldsymbol{W}^v_{m,n} \left(\tilde{\boldsymbol{H}}^v_{n,m} \boldsymbol{P}^v \boldsymbol{\mathcal{F}}_{N_d} \tilde{\boldsymbol{x}}^v_{m,T_i} + \sum_{\substack{u=1 \\ u \neq v}}^{U} \tilde{\boldsymbol{H}}^u_{n,m} \boldsymbol{P}^u \boldsymbol{\mathcal{F}}_{N_d} \tilde{\boldsymbol{x}}^u_{m,T_i} \right) + \tilde{\boldsymbol{v}}^v_{m,T_i}, \tag{4.24}$$

where $\boldsymbol{z}^{v}_{m,T_i}$ and $\boldsymbol{W}^{v}_{m,n}$ are the (m,T_i)-th and the (m,n)-th component of $\boldsymbol{z}^{v}$ and $\boldsymbol{W}^{v}$ respectively. Since each $\tilde{\boldsymbol{H}}^{u}_{n,m}$ is diagonal, we see from (4.23) that each $\boldsymbol{W}^{v}_{m,n}$ will also be diagonal. Due to the diagonal nature of both $\tilde{\boldsymbol{H}}^{u}_{n,m}$ and $\boldsymbol{W}^{v}_{m,n}$ and because

$$\tilde{\boldsymbol{P}}^{v}\boldsymbol{P}^{u} = \begin{cases} \boldsymbol{I}_{N_d}, & u = v \\ \boldsymbol{0}, & u \neq v \end{cases} \tag{4.25}$$

we have,

$$\boldsymbol{z}^{v}_{m,T_i} = \boldsymbol{\mathcal{F}}^{H}_{N_d}\tilde{\boldsymbol{P}}^{v}\boldsymbol{W}^{v}_{m,n}\tilde{\boldsymbol{H}}^{v}_{n,m}\boldsymbol{P}^{v}\boldsymbol{\mathcal{F}}_{N_d}\tilde{\boldsymbol{x}}^{v}_{m,T_i} + \tilde{\boldsymbol{v}}^{v}_{m,T_i}. \tag{4.26}$$

Observe from (4.26) that under the idealized assumption of perfect synchronization, perfect orthogonality of the users using different sub-carriers and by exploiting the perfectly diagonal nature of both $\boldsymbol{W}^{v}_{m,n}$ and of the FDCHTMs $\tilde{\boldsymbol{H}}^{v}_{n,m}$, our scheme becomes free from multiuser interferences (MUI). However, the symbols transmitted by a given user in the context of both the LFDMA and IFDMA scheme with MMSE equalization will experience some form of self-interference (SI) [98]. By contrast, the ZF scheme is capable of completely mitigating the SI and the DFT matrices $\boldsymbol{\mathcal{F}}^{H}_{N_d}$ and $\boldsymbol{\mathcal{F}}_{N_d}$, the sub-carrier mapping and de-mapping matrices, $\boldsymbol{P}^{v}$ and $\tilde{\boldsymbol{P}}^{v}$ as well as the FDCHTM $\tilde{\boldsymbol{H}}^{v}$ and the MMSE equalization matrix $\boldsymbol{W}^{\boldsymbol{v}}$ are absent in (4.26), albeit the scheme suffers from performance degradation due to the inherent noise enhancement process when a particular subcarrier experiences deep fading. Hence, following the FD equalization and the receiver's IDFT operation in Figure 4.6, the decision variable $\boldsymbol{z}^{\boldsymbol{v}}$ for the ZF scheme can be readily written as

$$\boldsymbol{z}^{v}[n_d] = \tilde{\boldsymbol{x}}^{v}[n_d] + \tilde{\boldsymbol{v}}^{v}[n_d], \tag{4.27}$$

where $\tilde{\boldsymbol{x}}^{v}[n_d] \in \mathbb{C}^{M\times T}$ and $\tilde{\boldsymbol{v}}^{v}[n_d] \in \mathbb{C}^{M\times T}$ for all $n_d = 1, 2, \ldots, N_d$.

The IFDMA principle, on the other hand, increases the FD separation between the subcarriers and thereby provides some additional diversity gain. Thus, the decision variable of our scheme using ZF or assuming mitigation of MMSE SI may be formulated, using the linearized sytem model of [32], as:

$$\overline{\boldsymbol{z}}^{v}[n_d] = \boldsymbol{\chi}\boldsymbol{k}^{v} + \bar{\mathbf{v}}^{v}[n_d], \tag{4.28}$$

where $\overline{\boldsymbol{z}}^{v}[n_d]$ is the $(MT\times 1)$-element matrix obtained by applying the vectorial stacking operation $vec(\cdot)$ to the received FD signal block $\boldsymbol{z}^{v}[n_d]$, while $\boldsymbol{\chi} = [vec(\boldsymbol{A}_1)\ldots vec(\boldsymbol{A}_Q)] \in \mathbb{C}^{MT\times Q}$ is the dispersion character matrix (DCM) [5], and finally, $\bar{\boldsymbol{v}}^{v}[n_d] = vec(\tilde{\boldsymbol{v}}^{v}[n_d]) \in \mathbb{C}^{MT\times 1}$ is the stacked AWGN vector. Still referring to (4.28), the equivalent transmit signal vector is represented by,

$$\boldsymbol{k}^{v} = [0,\ldots,0,s^{v},0,\ldots,0]^{T} \in \mathbb{C}^{Q\times 1}, \tag{4.29}$$

where $(q-1)$ and $(Q-q)$ number of zeros surround the $\mathcal{L}$-PSK or $\mathcal{L}$-QAM symbol s^v in the v-th user's equivalent transmit signal vector $\boldsymbol{k}^v$ and the symbol s^v is located exactly at the q-th position, where q is the index of the activated dispersion matrix.

We can now employ the single-stream based ML detection [49] to detect the indices q and l_c of the dispersion matrix activated and of the constellation symbol used, respectively. The estimates $(\hat{q}^v, \hat{l}_c^v)$ can be determined from

$$\left(\hat{q}^v, \hat{l}_c^v\right) = \arg\min_{q,l_c} \parallel \overline{\boldsymbol{z}}^v[n_d] - \boldsymbol{\chi}\boldsymbol{k}_{q,l_c}^v \parallel^2 \tag{4.30}$$

$$= \arg\min_{q,l_c} \parallel \overline{\boldsymbol{z}}^v[n_d] - (\boldsymbol{\chi})_q (s^v)_{l_c} \parallel^2, \tag{4.31}$$

where $(s^v)_{l_c}$ is the l_c-th $\mathcal{L}$-PSK or $\mathcal{L}$-QAM symbol, $(\boldsymbol{\chi})_q$ represents the q-th column of $\boldsymbol{\chi}$ and $\boldsymbol{k}_{q,l_c}^v$ is the equivalent transmit signal vector of (4.29) corresponding to user v at indices q and l_c.

In case of OFDMA, we have, $\boldsymbol{\mathcal{F}}_{N_d}^H = \boldsymbol{\mathcal{F}}_{N_d} = \boldsymbol{I}_{N_d}$. In other words, the blocks 'N_d-point DFT' and 'N_d-point IDFT' do not exist in OFDMA and as such, the OFDMA scheme cannot benefit from the potential diversity provided by the DFT based precoding stage. We can thus proceed with our ZF or MMSE weight matrix $\boldsymbol{W}^v$ as above. Alternatively, for the OFDMA STSK, the ML detector of [49] can directly be applied in the FD without employing the MIMO FDE. To be specific, in absence of the weight matrix $\boldsymbol{W}^v$and with the substitution $\boldsymbol{\mathcal{F}}_{N_d}^H = \boldsymbol{\mathcal{F}}_{N_d} = \boldsymbol{I}_{N_d}$, (4.26) reduces to $\boldsymbol{Z}_{m,T_i}^v = \tilde{\boldsymbol{H}}_{n,m}^v \tilde{\boldsymbol{x}}_{m,T_i}^v + \tilde{\boldsymbol{v}}_{m,T_i}^v$, where $\boldsymbol{z}_{m,T_i}^v$ is replaced by $\boldsymbol{Z}_{m,T_i}^v$ when the MIMO FDE is not employed. The direct ML detector of [49] for the OFDMA STSK scheme can thus be formulated as:

$$\left(\hat{q}^v, \hat{l_c}^v\right) = \arg\min_{q,l_c} \left\| \overline{\boldsymbol{Z}}^v[n_d] - (\overline{\tilde{\boldsymbol{H}}}^v[n_d]\boldsymbol{\chi})_q (s^v)_{l_c} \right\|^2, \tag{4.32}$$

where $\overline{\boldsymbol{Z}}^v[n_d] = vec(\boldsymbol{Z}^v[n_d])$ and the equivalent FDCHTM $\overline{\tilde{\boldsymbol{H}}}^v[n_d]$ is given by $\overline{\tilde{\boldsymbol{H}}}^v[n_d] = \boldsymbol{I}_T \otimes \tilde{\boldsymbol{H}}^v[n_d]$, whereas other notations are as used in (4.31).

In addition, we can see that our OFDMA/SC-FDMA STSK signal can be detected from (4.31) at a low complexity, because:

1. Equation (4.31) does not explicitly contain either the FD channel transfer function or the TD channel impulse response. Hence, data estimation using this equation involves a reduced number of multiplications and additions.

2. We can successfully employ the single-stream based ML detection relying on the linearized model of [32], because only a single dispersion matrix is activated at a given STSK block interval.

4.4 A Reduced-Complexity Detector

In this section, we propose a new detector which is particularly useful in the OFDMA/SC-FDMA aided STSK arrangement in dispersive channels. Since the SM and the SSK schemes activate only one antenna element (AE) during each symbol interval, the matched-filter (MF) [47], the maximal-ratio combining (MRC) [52] and the maximum-likelihood (ML) [52] detectors using the signal stream of a single AE can be employed, since no inter-element-interference (IEI) is experienced at the receiver. Hence, the STSK scheme may also employ a single-stream ML [49] detector. In order to mitigate the impairments due to the channel-induced dispersion imposed by wideband channels, OFDM-aided STSK [119] and OFDMA/SC-FDMA aided STSK [117] have been proposed for the single-user downlink (DL) and the multiuser downlink/uplink (DL/UL), respectively. All these schemes benefit from the employment of the single-stream ML detector proposed in [49]. To further reduce the complexity of STSK, especially when bandwidth-efficient quadrature amplitude modulation (QAM) is used, two further detectors modifying the MF detectors of [47] were proposed in [55].

Against this background, we propose a new detector, which further reduces the decoding complexity, especially in OFDMA/SC-FDMA-aided STSK arrangements. The proposed detector employs MIMO minimum mean square error (MMSE) equalization, followed by the estimation of the index of the DM activated and of the constellation symbol utilized for constructing the STSK codewords. The main contributions in this section are as follows.

1. We propose a novel detector for the STSK scheme, which is particularly suitable for the OFDMA/SC-FDMA-aided STSK DL/UL proposed in [117] without sacrificing the performance achieved.

2. The complexity of the scheme is quantified in terms of the number of real-valued multiplications and the scheme is found to have a low complexity.

We now provide a brief overview of the existing detectors and the motivation for conceiving a new detector.

4.4.1 Existing Detectors

In this subsection, we briefly describe the optimal ML detector [49, 52] and the two detectors proposed in [55]. In the following, we omit the block index i for the sake of notational simplicity.

The detectors estimate both the index of the activated dispersion matrix (DM) q and the index of the transmitted constellation symbol l_c corresponding to space-time block index i and thereby estimates the source information.

4.4.1.1 The Optimal ML Detector

The single-stream based ML detector finds the estimates $(\hat{q}, \hat{l}_c)$ from:

$$\left(\hat{q}, \hat{l}_c\right) = \arg\min_{q,l_c} \left\{ \left\| \bar{\boldsymbol{Y}} - \bar{\boldsymbol{H}}\boldsymbol{\chi}\boldsymbol{K}_{l_c,q} \right\|^2 \right\} \tag{4.33}$$

$$= \arg\min_{q,l_c} \left\{ \left\| \bar{\boldsymbol{Y}} - s_{l_c} \left(\bar{\boldsymbol{H}}\boldsymbol{\chi}\right)_q \right\|^2 \right\}, \tag{4.34}$$

where $\boldsymbol{K}_{l_c,q}$ represents the equivalent transmit symbol vector $\boldsymbol{K}$ defined in (4.46) when the $\mathcal{L}$-PSK/QAM symbol s_{l_c} is placed in the q -th position of the vector and $(\bullet)_q$ represents the q-th column of the matrix '$\bullet$'. An exhaustive search over the entire space of $(Q \cdot \mathcal{L})$ is essential for this optimal detector.

4.4.1.2 The Two Recent Detectors

Two detectors were proposed in [55] for reduced-complexity detection of STSK schemes, which we refer to as Detector I and Detector II in this paper.

Detector I Detector I normalizes each column $\bar{\boldsymbol{h}}_q$ of $\bar{\boldsymbol{H}}$ to generate the modified equivalent channels, $\boldsymbol{H}' = \left[\frac{\bar{\boldsymbol{h}}_1}{\| \bar{\boldsymbol{h}}_1 \|}, \ldots, \frac{\bar{\boldsymbol{h}}_Q}{\| \bar{\boldsymbol{h}}_Q \|}\right]$ and exhaustively searches through $\boldsymbol{Z} = [z_1, \ldots z_Q]^T = \boldsymbol{H}'\bar{\boldsymbol{Y}}$ to yield [55]:

$$\begin{aligned} \hat{q} \;=\; \arg\max_{q,\forall l'} \Bigg[& 2 \parallel \bar{\boldsymbol{h}}_q \parallel \Big\{ \mid \Re(z_q) \mid\mid \Re(s_{l'_c}) \mid \\ & + \mid \Im(z_q) \mid\mid \Im(s_{l'_c}) \mid \Big\} - \parallel \bar{\boldsymbol{h}}_q \parallel^2 \mid s_{l'_c} \mid^2 \Bigg], \end{aligned} \tag{4.35}$$

where $s_{l'_c}$ $(l'_c = 1, 2, \ldots, \mathcal{L}^1)$ represents the constellation points in the first quadrant only. Having estimated the DM index $\hat{q}$ using (4.35), the constellation symbol index is estimated from [55]:

$$\hat{l}_c \;=\; \arg\min_{l_c} \left| z_{\hat{q}} - \parallel \bar{\boldsymbol{h}}_{\hat{q}} \parallel s_{l_c} \right|. \tag{4.36}$$

Thus the search space for (4.35) of this two-stage detector is $Q\mathcal{L}^1$, which is one-fourth of the search space $Q\mathcal{L}$ for optimal ML detector. This detector, however, has an additional search space of $\mathcal{L}$ to calculate $\hat{l}_c$ from (4.36).

Detector II Detector I was further modified in [55] for simplifying (4.35) as:

$$\hat{q} \;=\; \arg\max_{q,\forall v} \left[\mid \Re(z_q) \mid x_{v,I} + \mid \Im(z_q) \mid x_{v,Q} \right], \tag{4.37}$$

while (4.36) invoked for estimating $\hat{l}_c$ remains unchanged. Note that $x_{v,I}$ and $x_{v,Q}$ indicate the real and imaginary parts of the unit vectors having the same phase angles as those of the first-quadrant constellation points respectively.

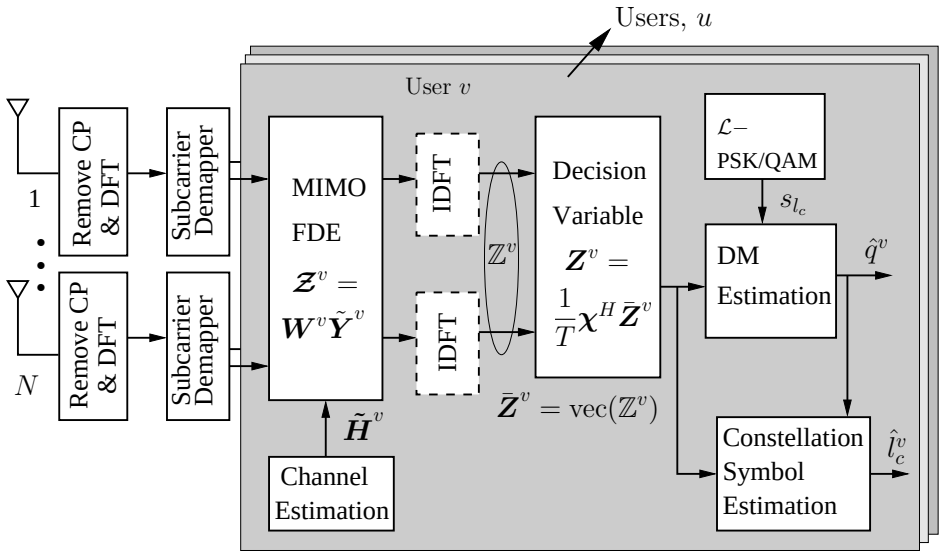

Figure 4.8: The receiver architecture of the OFDMA/SC-FDMA-aided STSK employing the proposed reduced-complexity detector. The dotted 'IDFT' block does not exist in the OFDMA-aided STSK receiver.

The detectors mentioned above are designed for non-dispersive channels, where FDE is not essential. They impose a considerably reduced complexity, especially in case of a high channel coherence interval and higher order QAM constellation. However, in an OFDMA or SC-FDMA aided STSK, MIMO FDE has to be employed and the resulting data estimation does not explicitly involve the channel transfer matrix. Hence detection complexity quantified in terms of the number of multiplications required is considerably reduced [117]. Against this background, we conceived a modified reduced-complexity detector, which estimates the DM index and contellation index after MIMO FDE and is particularly useful for STSK transmissions in dispersive channels.

4.4.2 The Proposed Reduced-Complexity Detector

The schematic diagram of the OFDMA/SC-FDMA-aided STSK receiver employing the proposed detector is shown in Figure 4.8. After the discrete Fourier transform (DFT) operation and subcarrier demapping at the receive AEs, the detector employs MIMO MMSE FDE and then separately estimates the indices of the activated DM, q^v and of the constellation symbol, l_c^v corresponding to a particular user v.

To be specific, the detector first invokes the MIMO MMSE FDE in an attempt to minimize the average squared error. The MIMO ZF detector suffers from a performance degradation due to the noise enhancement when a subcarrier is in deep fade and hence is not used in the proposed scheme.

Let the space-time codewords corresponding to user u $(u = 1, 2, \ldots, U)$ of the SC-FDMA-aided STSK in Figure 4.6 be denoted by $\boldsymbol{X}^u$, and the transmit blocks obtained by DFT operation of the codeword symbols be represented by $\tilde{\boldsymbol{X}}^u$. For the OFDMA-aided STSK, the DFT-precoding block in Figure 4.6 does not exist and we have, $\tilde{\boldsymbol{X}}^u = \boldsymbol{X}^u$.

The block-based FD output $\tilde{\boldsymbol{Y}}$ in Figure 4.8 obtained after DFT operation at the receive antennas may be expressed as [117]:

$$\tilde{\boldsymbol{Y}} = \sum_{u=1}^{U} \tilde{\boldsymbol{H}}^u \tilde{\boldsymbol{X}}^u + \tilde{\boldsymbol{V}} \tag{4.38}$$

where $\tilde{\boldsymbol{H}}^u$ represents the FD MIMO channel transfer matrix corresponding to user u and $\tilde{\boldsymbol{V}}$ denotes the additive white Gaussian noise (AWGN) matrix.

In order to estimate the transmit blocks $\tilde{\boldsymbol{X}}^v$ of user v, the subcarriers are first demapped and the demapped signal $\tilde{\boldsymbol{Y}}^v$ is then multiplied by the MMSE weight matrix $\boldsymbol{W}^v$, which minimizes $\mathcal{E}\left\{\left[\boldsymbol{W}^v\tilde{\boldsymbol{Y}}^v - \tilde{\boldsymbol{X}}^v\right]\left[\boldsymbol{W}^v\tilde{\boldsymbol{Y}}^v - \tilde{\boldsymbol{X}}^v\right]^H\right\}$, yielding [117, 162]:

$$\boldsymbol{W}^v = \left[\left(\tilde{\boldsymbol{H}}^v\right)^H \tilde{\boldsymbol{H}}^v + \sigma_n^2 \boldsymbol{I}_M\right]^{-1} \left(\tilde{\boldsymbol{H}}^v\right)^H, \tag{4.39}$$

where σ_n^2 indicates the noise variance. The MMSE codeword estimate $\boldsymbol{\mathcal{Z}}^v$ of user v can then be expressed as [98]

$$\boldsymbol{\mathcal{Z}}^v = \boldsymbol{W}^v\tilde{\boldsymbol{Y}}^v. \tag{4.40}$$

After MIMO FDE, the received signal is passed through the 'IDFT' block, which results in the space-time blocks $\mathbb{Z}^v$. In case of the OFDMA-aided STSK, however, the 'IDFT' block does not exist and we have, $\mathbb{Z}^v = \boldsymbol{\mathcal{Z}}^v$.

Under the idealized assumption of perfect orthogonality of the subcarriers and of perfect synchronization, the scheme is decontaminated from multiuser interference (MUI), albeit the MMSE-based scheme imposes self-interference (SI). Assuming the SI to be low, the decision variable corresponding to user v can be expressed as

$$\mathbb{Z}^v = \boldsymbol{X}^v + \tilde{\boldsymbol{V}}^v. \tag{4.41}$$

Upon applying the vectorial stacking operation $\mathrm{vec}(\cdot)$ to both sides of (4.41), we have

$$\bar{\boldsymbol{Z}}^v = \boldsymbol{\chi}\boldsymbol{K}^v + \bar{\boldsymbol{V}}^v, \tag{4.42}$$

where

$$\bar{\boldsymbol{Z}}^v = \mathrm{vec}(\mathbb{Z}^v) \in \mathbb{C}^{MT\times 1}, \tag{4.43}$$

$$\bar{\boldsymbol{V}}^v = vec(\tilde{\boldsymbol{V}}^v) \in \mathbb{C}^{MT\times 1}, \tag{4.44}$$

and $\boldsymbol{\chi}$ and $\boldsymbol{K}^v$ are defined as

$$\boldsymbol{\chi} \triangleq [\mathrm{vec}\left(\boldsymbol{A}_1\right), \cdots, \mathrm{vec}\left(\boldsymbol{A}_Q\right)] \in \mathbb{C}^{MT \times Q}, \tag{4.45}$$

$$\boldsymbol{K}^v\left[i\right] \triangleq [\underbrace{0, \cdots, 0}_{q^v-1}, s^v\left[i\right], \underbrace{0, \cdots, 0}_{Q-q^v}]^T \in \mathbb{C}^{Q \times 1}, \tag{4.46}$$

respectively.

The decision variable $\boldsymbol{Z}^v$ is now obtained by multiplying (4.42) by $\frac{1}{T}\boldsymbol{\chi}^H$ as:

$$\boldsymbol{Z}^v = \frac{1}{T}\boldsymbol{\chi}^H \bar{\boldsymbol{Z}}^v = \left[z_1^v, \ldots z_Q^v\right]^T \in \mathbb{C}^{Q \times 1}. \tag{4.47}$$

We now perform an exhaustive search for the estimates $(\hat{q}^v, \hat{l}_c^v)$:

$$(\hat{q}^v, \hat{l}_c^v) = \arg\min_{q, l_c} \parallel \boldsymbol{Z}^v - \boldsymbol{K}_{l_c,q} \parallel^2 \tag{4.48}$$

$$= \arg\min_{q,l} \left(\mid z_q^v - s_l \mid^2 + \sum_{q' \neq q} \mid z_{q'}^v \mid^2 \right)$$

$$= \arg\min_{q,l_c} \left(\mid z_q^v - s_{l_c} \mid^2 + \parallel \boldsymbol{Z}^v \parallel^2 - \mid z_q^v \mid^2 \right)$$

$$= \arg\max_{q,l_c} \left(\mid z_q^v \mid^2 - \mid z_q^v - s_{l_c} \mid^2 \right)$$

$$= \arg\max_{q,l_c} \left[2\Big\{ \mid \Re(z_q^v) \mid\mid \Re(s_{l_c}) \mid + \mid \Im(z_q^v) \mid\mid \Im(s_{l_c}) \mid \Big\} - \mid s_{l_c} \mid^2 \right]. \tag{4.49}$$

Assuming the $\mathcal{L}$-PSK/QAM constellation to be symmetric about the I- and Q-axis, we can rewrite (4.49) to estimate the index of the activated dispersion matrix q^v as:

$$\hat{q}^v = \arg\max_{q\ \forall l'} \left[2\Big\{ \pm \mid \Re(z_q^v) \mid\mid \Re(s_{l'_c}) \mid \pm \mid \Im(z_q^v) \mid\mid \Im(s_{l'_c}) \mid \Big\} - \mid s_{l'_c} \mid^2 \right]$$

$$= \arg\max_{q\ \forall l'_c} \left[2\Big\{ \mid \Re(z_q^v) \mid\mid \Re(s_{l'_c}) \mid + \mid \Im(z_q^v) \mid\mid \Im(s_{l'_c}) \mid \Big\} - \mid s_{l'_c} \mid^2 \right], \tag{4.50}$$

where l'_c denotes the index of the constellation symbol $s_{l'_c}$ that lies in the first quadrant only [55].

The index of the constellation symbol used in forming the STSK codeword can be estimated from:

$$\hat{l}_c^v = \arg\min_{l_c} \mid z_{\hat{q}}^v - s_{l_c} \mid . \tag{4.51}$$

The rationale of multiplying $\bar{\boldsymbol{Z}}^v$ by the term $\frac{1}{T}\boldsymbol{\chi}^H$ in (4.47) is outlined as follows. Substituting the value of $\bar{\boldsymbol{Z}}$ from (4.42) into (4.47), we have

$$\boldsymbol{Z}^v = \frac{1}{T}\boldsymbol{\chi}^H \bar{\boldsymbol{Z}}^v \tag{4.52}$$

$$= \frac{1}{T}\boldsymbol{\chi}^H \left[\boldsymbol{\chi}\boldsymbol{K}^v + \bar{\boldsymbol{V}}^v\right]$$

$$= \frac{1}{T}\boldsymbol{\chi}^H (\boldsymbol{\chi})_{q^v} s_{l_c^v} + \bar{\boldsymbol{V}}_0, \tag{4.53}$$

where $(\boldsymbol{\chi})_{q^v}$ denotes the q^v-th column of the matrix '$\boldsymbol{\chi}$' and we have, $\bar{\boldsymbol{V}}_0 \in \mathbb{C}^{Q\times 1}$.

Now we have $\boldsymbol{\chi}^H = [\text{vec}(\boldsymbol{A}_1), \cdots, \text{vec}(\boldsymbol{A}_Q)]^H \in \mathbb{C}^{Q\times MT}$ and $(\boldsymbol{\chi})_{q^v} = [\text{vec}(\boldsymbol{A}_{q^v})] \in \mathbb{C}^{MT\times 1}$, and hence,

$$\begin{aligned} \boldsymbol{\chi}^H(\boldsymbol{\chi})_{q^v} &= [z'_1, z'_2, \cdots, \underset{\substack{\uparrow \\ q-th\, position}}{\text{tr}(\boldsymbol{A}^H_{q^v}\boldsymbol{A}_{q^v})}, \cdots, z'_Q]^T \\ &= [z'_1, z'_2, \cdots, \underset{\substack{\uparrow \\ q-th\, position}}{T}, \cdots, z'_Q]^T, \end{aligned} \tag{4.54}$$

where $z'_i = \text{tr}(\boldsymbol{A}^H_i \boldsymbol{A}_{q^v})$, $i = 1, 2, \ldots, Q$ with $i \neq q^v$ and $\text{tr}(\boldsymbol{A}^H_{q^v}\boldsymbol{A}_{q^v}) = T$ according to (4.4). Thus we obtain,

$$\boldsymbol{Z}^v = [z'_1, z'_2, \cdots, \underset{\substack{\uparrow \\ q^v-th\, position}}{s_{l^v_c}}, \cdots, z'_Q]^T + \bar{\boldsymbol{V}}_0. \tag{4.55}$$

Equation (4.55) demonstrates that the ML search of (4.48) can be simplified to obtain the detection rules of (4.50) and (4.51).

We note that the optimal ML detector [49], Detector I and Detector II [55] were conceived mainly for non-dispersive MIMO channels. By contrast, the proposed detector is designed for realistic dispersive scenarios. Detector I and Detector II are capable of reducing the complexity of the optimal ML detector at the cost of a modest performance penalty. In case of OFDMA-aided STSK, the existing detectors can be employed using the FD channel transfer matrix [117], but imposing a higher complexity. However, none of them can be directly employed in the SC-FDMA-aided STSK scheme, because the TD data estimation has to be preceded by equalization in FD. In this context, the OFDMA/SC-FDMA-aided STSK scheme and a low-complexity ML detector were proposed in [117] under multiuser scenarios.

We observe that a single-stream ML detector becomes feasible for the STSK-based system, because a single DM is activated in any signalling interval. The coherent scheme requires channel state information (CSI) for the detection of source information. However, after MIMO equalization in FD, the search for the user information given by (4.50) and (4.51) in our proposed scheme does not explicitly involve the channel transfer function for calculating $\hat{q}^v$ and $\hat{l}^v$. Hence the number of multiplications and additions involved is significantly lower than that required by the existing detectors.

Following the above-mentioned elaborations on the detector's operation obeying the architecture portrayed in Figure 4.8, each of the steps followed by the detector may be summarized as follows in Algorithm 4.1.

Algorithm 4.1 The reduced-complexity detector proposed for OFDMA/SC-FDMA-aided STSK

1) Given the STSK parameters $(M, N, T, Q, \mathcal{L})$ and the DMs in terms of the dispersion character matrix (DCM) $\boldsymbol{\chi}$, the signals received by the AEs are input to MIMO FDE after OFDM demodulation and subcarrier demapping;

2) After multiplication by the MMSE weight matrix $\boldsymbol{W}^v$, the signal is passed through the 'IDFT' block of Figure 4.8. For OFDMA, there is no 'IDFT' block, as seen in Figure 4.8;

3) The vectorial stacking based linearization of [32] is employed: $\bar{\boldsymbol{Z}}^v = \text{vec}(\mathbb{Z}^v)$;

4) The decision variable is then obtained as: $\boldsymbol{Z}^v = \frac{1}{T}\boldsymbol{\chi}^H \bar{\boldsymbol{Z}}^v$;

5) The index $\hat{q}^v$ of the DM activated and the index $\hat{l}^v$ of the constellation symbol are computed separately;

6) The index $\hat{q}^v$ of the DM activated is evaluated as:

$$\hat{q}^v = \arg\max_{q\ \forall l'_c} \left[2\left\{ \mid \Re(z_q^v) \mid\mid \Re(s_{l'_c}) \mid + \mid \Im(z_q^v) \mid\mid \Im(s_{l'_c}) \mid \right\} - \mid s_{l'_c} \mid^2 \right]; \tag{4.56}$$

5) The index $\hat{l}^v$ of the constellation symbol is found by evaluating:

$$\hat{l}^v = \arg\min_{l} \mid z_{\hat{q}}^v - s_l \mid; \tag{4.57}$$

6) Thereby the source bits of user v have now been estimated.

4.4.3 Complexity Analysis

We quantify the complexity of the proposed scheme in terms of the number of real-valued multiplications required per bit of information and summarize it in Table 4.1 in order to compare with the complexity imposed by the existing detectors. Note that a single complex-valued multiplication is treated as equivalent to four real-valued multiplications.

The complexity associated with our multiple-antenna-based MMSE FDE is given by[1],

$$\text{comp}\left[\left[\left(\tilde{\boldsymbol{H}}^v\right)^H \tilde{\boldsymbol{H}}^v + \sigma_n^2 \boldsymbol{I}_M\right]^{-1} \left(\tilde{\boldsymbol{H}}^v\right)^H\right] = 4MN + 4M^2N. \tag{4.58}$$

[1]The complexity associated with the inversion of the $(M \times M)$ matrix at this stage is $O\left(M^{2.807}\right)$, if Strassen algorithm is used. This has not been included in our complexity calculation, because we quantify complexity in terms of the number of real-valued multiplications. The proposed scheme, however, has a significantly reduced complexity, even if the complexity associated with this matrix inversion is also taken into account.

Table 4.1: Complexity of the detection schemes

Detection Scheme	Complexity per Bit
ML	$\frac{4MNT^2Q+4NTQ\mathcal{L}+2NTQ\mathcal{L}}{log_2(Q\cdot\mathcal{L})}$
Detector I	$\frac{4MNT^2Q+8NTQ+4Q\mathcal{L}^1+4\mathcal{L}}{log_2(Q\cdot\mathcal{L})}$
Detector II	$\frac{4MNT^2Q+8NTQ+2VQ+4\mathcal{L}}{log_2(Q\cdot\mathcal{L})}$
Proposed detector	$\frac{4M^2N+8MN+4MTQ+2Q\mathcal{L}^1+Q+2\mathcal{L}}{log_2(Q\cdot\mathcal{L})}$

The complexity imposed by computing $\boldsymbol{\mathcal{Z}}^v = \boldsymbol{W}^v\tilde{\boldsymbol{Y}}^v$ may be written as

$$\text{comp}\left[\boldsymbol{\mathcal{Z}}^v = \boldsymbol{W}^v\tilde{\boldsymbol{Y}}^v\right] = 4MN. \tag{4.59}$$

Similarly, we have:

$$\text{comp}\left[\boldsymbol{Z}^v = \frac{1}{T}\boldsymbol{\chi}^H\bar{\boldsymbol{Z}}^v\right] = 4MTQ + Q. \tag{4.60}$$

$$\text{comp}\left[\arg\max_{q\ \forall l'_c}\left\{2\big(\mid\Re(z_q^v)\mid\mid\Re(s_{l'_c})\mid+\mid\Im(z_q^v)\mid\mid\Im(s_{l'_c})\mid\big) - \mid s'_{l'_c}\mid^2\right\}\right] = 2Q\mathcal{L}^1, \tag{4.61}$$

and

$$\text{comp}\left[\arg\min_{l_c}\mid z_{\hat{q}}^v - s_{l_c}\mid\right] = 2\mathcal{L}. \tag{4.62}$$

The overall complexity of the proposed detector for estimating $\log_2(Q\cdot\mathcal{L})$ bits of source information carried by any transmit block is thus given by

$$\text{Complexity} = 4M^2N + 8MN + 4MTQ + 2Q\mathcal{L}^1 + Q + 2\mathcal{L}.$$

From the numerical expressions in Table 4.1, we can see that our scheme exhibits a substantially reduced complexity.

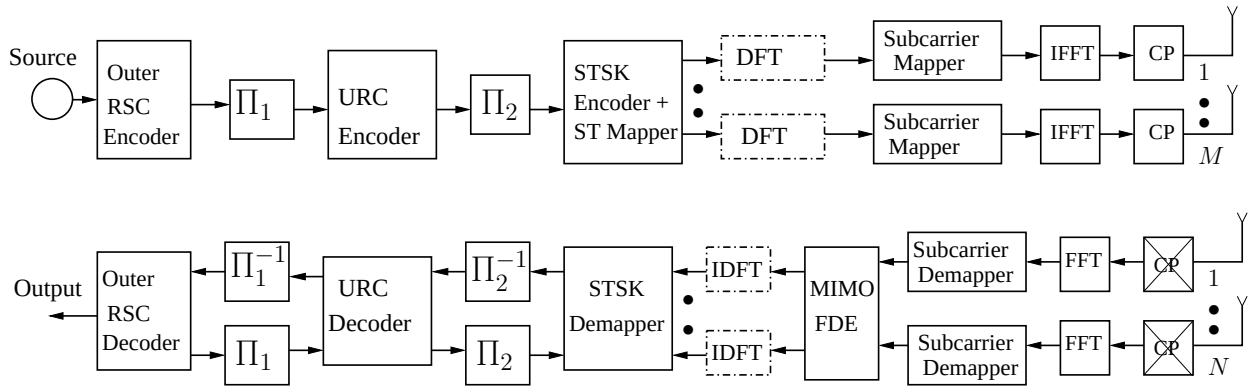

Figure 4.9: Three stage RSC-URC coded OFDMA/SC-FDMA STSK transceiver. The dotted 'DFT' block in the transmitter and the 'IDFT' block in the receiver do not appear in coded OFDMA STSK.

4.5 Channel-Coded OFDMA/SC-FDMA Aided STSK

In this section we investigate the three-stage parallel concatenated Recursive Systematic Convolutional (RSC) coded OFDMA/SC-FDMA STSK scheme of Figure 4.9. The source bits are first convolutionally encoded and then interleaved by a random bit interleaver Π_1. A (2,1,2) RSC code is employed and following channel interleaving, the symbols are precoded by a Unity Rate Coding (URC) scheme, which was shown to be beneficial, since it efficiently spreads the extrinsic information, as a benefit of its infinite impulse response [5]. Then the precoded bits are further interleaved by a second interleaver Π_2 in Figure 4.9 and the interleaved bits are then transmitted by the OFDMA/SC-FDMA STSK scheme in the TD using an M-element MIMO transmitter.

As seen at the receiver of Figure 4.9, after removing the CP, the received symbols are passed through the FFT unit and the resultant FD symbols are then de-allocated in an inverse fashion according to the IFDMA/LFDMA scheme used. The demapped symbols of a user are then equalized by the MIMO FDE, passed through another IDFT unit of Figure 4.9 in accordance with the DFT precoding used, before they are then fed to the STSK demapper. We note that the equivalent received signal $\overline{\boldsymbol{z}}^v$ carries B^v channel-coded bits $b^v = [b_1^v, b_2^v, ..., b_B^v]$ and the extrinsic log likelihood ratio (LLR) of b_k^v, $k = 1, ..., B^v$ can be expressed as [5]:

$$L_e(b_k^v) = \ln \frac{\sum_{\boldsymbol{k}_{q,l_c}^v \in \boldsymbol{k}_1^v} e^{-\|\overline{\boldsymbol{z}}^v - \boldsymbol{\chi}\boldsymbol{k}_{q,l_c}^v\|^2/N_0 + \sum_{j\neq k} b_j^v L_a(b_j^v)}}{\sum_{\boldsymbol{k}_{q,l_c}^v \in \boldsymbol{k}_0^v} e^{-\|\overline{\boldsymbol{z}}^v - \boldsymbol{\chi}\boldsymbol{k}_{q,l_c}^v\|^2/N_0 + \sum_{j\neq k} b_j^v L_a(b_j^v)}}, \tag{4.63}$$

where $L_a(\bullet)$ denotes the *a priori* LLR of the bits corresponding to '$\bullet$' and $\boldsymbol{k}_1^v$ and $\boldsymbol{k}_0^v$ refer to the sets of the possible equivalent transmit signal vectors $\boldsymbol{k}^v$ of user v when $b_k^v = 1$ and $b_k^v = 0$, respectively. As a further advance, the extrinsic LLR can be found by using the Jacobian

logarithm [144, 145], yielding:

$$L_e(b_k^v) = \text{jac}_{\boldsymbol{k}_{q,l_c}^v \in \boldsymbol{k}_1^v} \left[-\| \overline{\boldsymbol{z}}^v - \boldsymbol{\chi} \boldsymbol{k}_{q,l_c}^v \|^2 / N_0 + \sum_{j \neq k} b_j^v L_a(b_j^v) \right] - \text{jac}_{\boldsymbol{k}_{q,l_c}^v \in \boldsymbol{k}_0^v} \left[-\| \overline{\boldsymbol{z}}^v - \boldsymbol{\chi} \boldsymbol{k}_{q,l_c}^v \|^2 / N_0 + \sum_{j \neq k} b_j^v L_a(b_j^v) \right], \quad (4.64)$$

where $\text{jac}_{\boldsymbol{k}_{q,l_c}^v \in \boldsymbol{k}_1^v}[\bullet]$ and $\text{jac}_{\boldsymbol{k}_{q,l_c}^v \in \boldsymbol{k}_0^v}[\bullet]$ represents the Jacobian logarithm of '$\bullet$', when the equivalent transmit symbol vector is a subset corresponding to k-th bits of 1 and 0, respectively.

Then the URC decoder of Figure 4.9 processes the information provided by the STSK demapper, in conjunction with the *a priori* information, in order to generate the *a posteriori* probability. The URC generates extrinsic information for both the RSC decoder and the demapper of Figure 4.9. The RSC channel decoder, which can be termed as the external decoder, exchanges extrinsic information with the URC decoder and after a number of iterations, outputs the estimated bits. It is noteworthy here that for each of the outer iterations between the RSC decoder and the URC, there are a number of inner iterations between the URC and the STSK demapper.

4.6 Performance of the Proposed OFDMA/SC-FDMA-aided STSK Scheme

We have investigated both the OFDMA DL and the SC-FDMA aided UL STSK scheme for both the IFDMA and LFDMA algorithms using the simulation parameters of Table 4.2.

4.6.1 Performance of the OFDMA/SC-FDMA Aided STSK Scheme

Observe in Figure 4.10 that the SC-FDMA STSK scheme employing MMSE equalization operating in an uncoded scenario exhibits a better bit error ratio (BER) performance than that of OFDMA STSK, which is a benefit of the additional FD diversity attained by the DFT-precoding of Figure 4.6. The performance of IFDMA is seen to be better than that of the LFDMA due to the higher FD separation between the sub-carriers of the same user, which hence results in independent FD fading. The multi-user performance attained is also investigated and is more or less similar to that of the single-user scenario due to the absence of MUI because of the diagonal nature of the weight matrix $\boldsymbol{W}_{m,n}^{u'}$ in (4.26). Observe furthermore from Figure 4.10 that SC-FDMA STSK exhibits a better performance than OFDMA STSK in both the LFDMA and IFDMA regime employing MMSE based FD equalization and ML detection. The achievable performance is, however, degraded, when ZF is used due to the noise enhancement imposed. The performance of the proposed STSK based scheme is also compared

Table 4.2: Simulation parameters for OFDMA/SC-FDMA-aided STSK

Simulation parameter	*Value*
Fast fading model	Corr. Rayleigh fading
Normalized Doppler frequency, f_d	0.01
Channel specification	COST207-TU12
No. of subcarriers	64
N_d-point DFT precoder	16
Length of cyclic prefix	32
No. of Tx AE, M	2
No. of Rx AE, N	2
No. of Tx time slots, T	2
No. of dispersion matrices	$Q = 2, 4$
STSK specification	$(M = 2, N = 2, T = 2, Q = 2, 4)$
Modulation order	2, 4
Outer decoder	RSC $(2, 1, 2)$
Generator polynomials	$(g_r, g) = (3, 2)_8$
Size of interleavers	240,000 bits
Outer decoding iterations	9
Inner decoder	URC
Inner decoding iterations	2

to those of the V-BLAST [17] and $\mathcal{G}_2$-STBC [8,9] aided OFDMA/SC-FDMA schemes using the same number of transmit and receive AEs (M, N) and the same throughput per block interval in Figure 4.10, which demonstrates the efficacy of the proposed scheme.

4.6.2 Peak-to-Average-Power Ratio

The SC-FDMA design has been conceived for alleviating the high PAPR of multicarrier-based systems [163], especially in the uplink, since the MS's battery consumption would suffer from the low power efficiency of high-linearity class-A amplifiers. In this section, we will investigate the PAPR of OFDMA and SC-FDMA based STSK schemes of Figure 4.6 relying on the LFDMA or IFDMA arrangements.

Observe from (4.1) that for IFDMA, the transmitted TD symbols are simply the repeated symbols. By contrast, TD LFDMA signals have exact copies of the input symbols in the N_d-spaced TD sample positions, but the signals between these samples are constituted by different complex-valued weighted sums of the input symbols. Hence, although the SC modulation principle of SC-FDMA aided STSK results in lower PAPR values than OFDMA aided STSK,

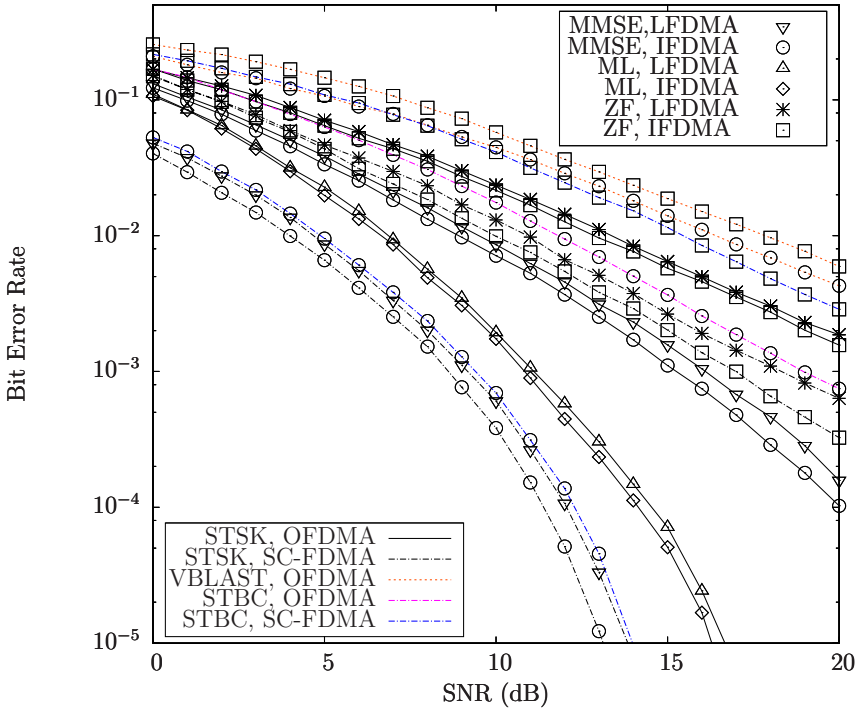

Figure 4.10: Performance of the single-user OFDMA/SC-FDMA STSK (2,2,2,4) system of Figure 4.6 with QPSK modulation in dispersive COST207-TU12 channel with different allocation scheme and with ZF and MMSE FDE and with ML detector of [49]. The performance of the scheme is also compared against V-BLAST $(M, N) = (2, 2)$, OFDMA, QPSK and $\mathcal{G}_2$-STBC $(M, N) = (2, 2)$, OFDMA/SC-FDMA, QPSK benchmarker under the same channel condition. The remaining system parameters are listed in Table 4.2.

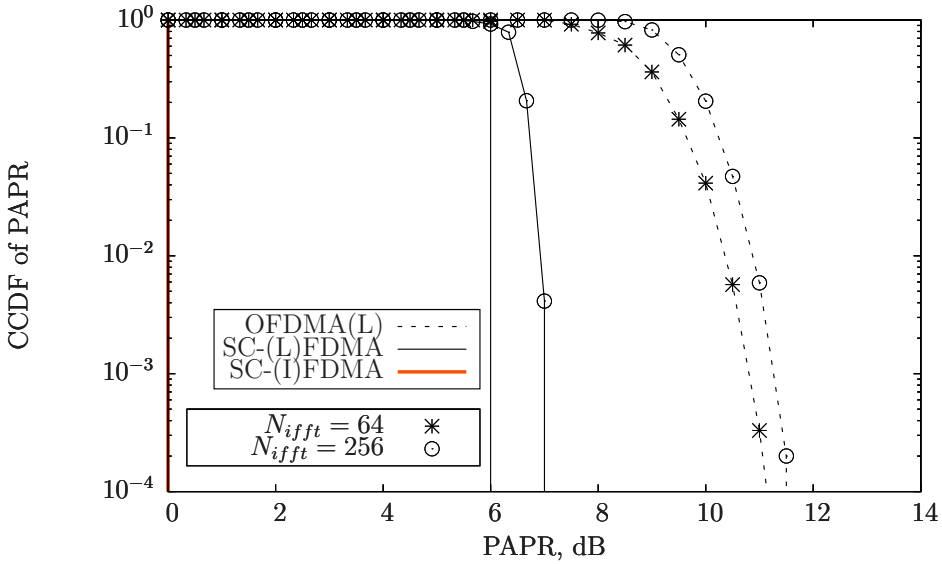

Figure 4.11: CCDF of PAPR in OFDMA STSK and SC-FDMA STSK of Figure 4.6 with contiguous and distributed allocation and with different number of sub-carriers. SC-FDMA STSK with interleaved allocation, as expected, shows the lowest envelope fluctuations. The remaining system parameters are listed in Table 4.2.

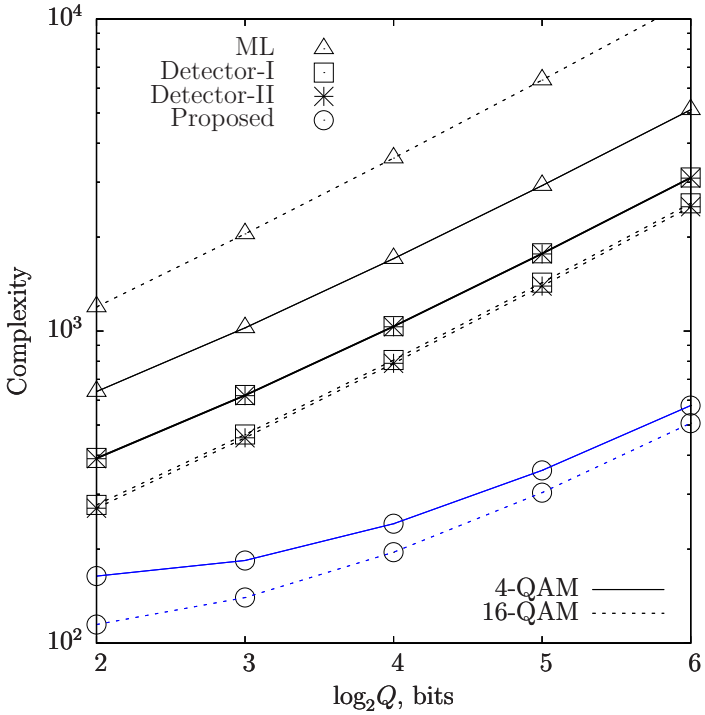

Figure 4.12: Complexity of the detection algorithms for the OFDMA STSK and the SC-FDMA STSK of Figure 4.6 considered as a function of the number of DMs. The parameters are: $M = 4, N = 4$, with $T = 4$. The remaining system parameters are listed in Table 4.2.

LFDMA STSK fails to attain as high a PAPR reduction, as the IFDMA allocation.

In Figure 4.11, we have quantified the PAPR of the transmitted OFDMA STSK and SC-FDMA STSK signals without using pulse shaping. Observe in Figure 4.11 that SC-FDMA STSK transmission always has a more beneficial complimentary cumulative distribution function (CCDF) than its OFDMA STSK counterpart, where the OFDMA STSK scheme relied on the contiguous allocation of sub-carriers to users. By contrast, SC-FDMA STSK was characterized in both the contiguous and in the distributed allocation scenarios. Again, Figure 4.11 demonstrates for two different IFFT lengths N_{fft} that the SC-FDMA STSK scheme exhibits only modest peak variations for the interleaved allocation strategy. In case of the localized allocation, however, the peak fluctuations exhibit higher values, as shown in Figure 4.11 and demonstrated by Eq.(4.2). The envelope fluctuations of the OFDMA STSK scheme are seen to be higher as a result of the multiple carrier modulation employed.

4.6.3 Performance and Complexity of the Reduced-Complexity Detector

We have further investigated the performance and the complexity of our reduced-complexity detector proposed in Section 4.4, which were compared to those of the existing detectors in Figures 4.12, 4.13 and 4.14, upon varying the number of dispersion matrices Q and the number

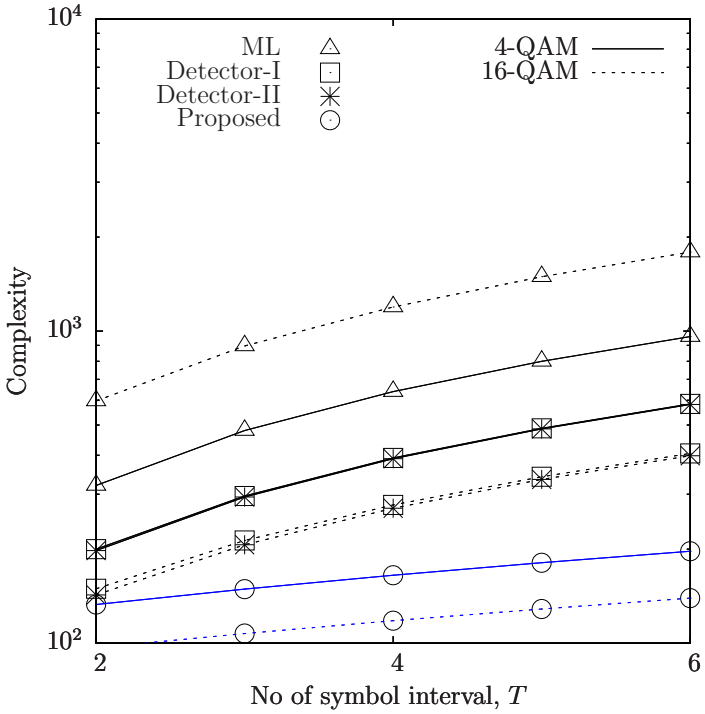

Figure 4.13: Complexity of the detection algorithms for the OFDMA STSK and the SC-FDMA STSK of Figure 4.6 considered as a function of the number of symbol intervals. The parameters are: $M = 4, N = 4$, with $Q = 4$. The remaining system parameters are listed in Table 4.2.

of symbol intervals T in conjunction with $M = 4$, $N = 4$ and employing both the 4-QAM and 16-QAM. We observe that Detector I and Detector II impose an identical complexity and both exhibit a lower complexity than the optimal ML detector on OFDMA STSK, albeit their complexity is not significantly reduced for lower-order constellations. On the other hand, our proposed detector exhibits a more significantly reduced complexity for all the scenarios, where we have included the complexity of the MIMO FDE stage in the overall complexity calculation of the proposed detector.

The bit-error ratio (BER) performance of our reduced-complexity scheme was also investigated for OFDMA/SC-FDMA-aided single-user STSK ($M = 2, N = 2, T = 2, Q = 4$) employing QPSK modulation for transmission over the COST 207-TU12 dispersive channel model employing 64 subcarriers. We note that Detector I and Detector II cannot be directly employed for the SC-FDMA-aided STSK scheme, because the scheme has to perform MIMO FDE and the source information has to be detected in the TD. In case of OFDMA, however, both the ML detector and the proposed detector can be employed, as mentioned in [117]. We observe that our proposed scheme exhibits a performance comparable to the detector proposed in [117], but at a substantially reduced complexity. While the ML detector for the OFDMA STSK scheme provides better performance, the proposed scheme is sufficiently reduced in complexity.

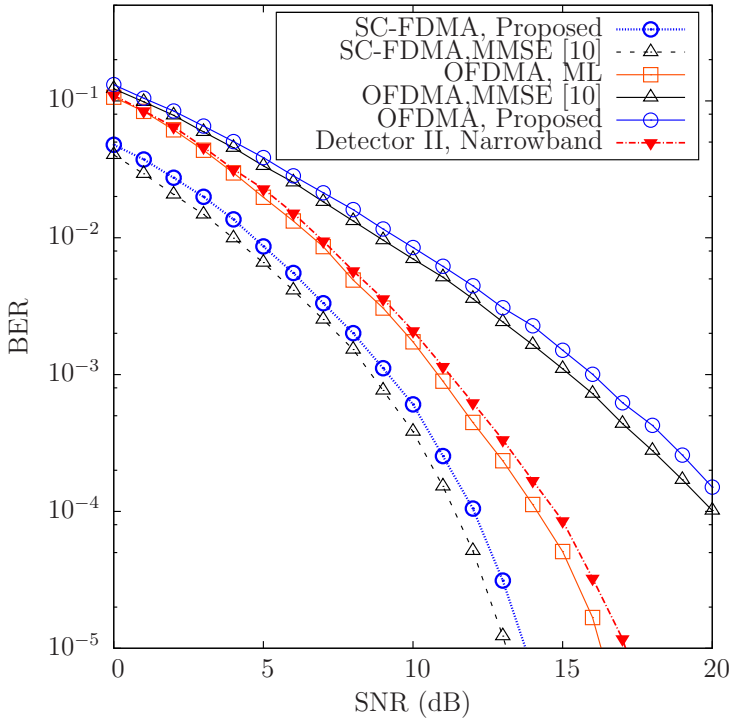

Figure 4.14: BER performance of OFDMA/SC-FDMA aided single-user STSK ($M = 2, N = 2, T = 2, Q = 4$) scheme for the OFDMA STSK and the SC-FDMA STSK of Figure 4.6 employing QPSK modulation in COST 207-TU12 channel model and the different detectors. The remaining system parameters are listed in Table 4.2. The performance of Detector II in narrowband STSK ($M = 2, N = 2, T = 2, Q = 4$), QPSK is also shown as a fair comparison.

The performance of Detector II for transmission over narrowband channels is also shown in Figure 4.14 for a fair comparison with other schemes. Observe that the proposed detector as well as the detector advocated in [117] for SC-FDMA-aided transmission even over dispersive channel outperforms Detector II in narrowband channel. This is because a beneficial frequency-domain diversity is provided by the DFT-based precoding in our SC-FDMA aided STSK scheme. Thus it can be inferred that the proposed detector reduces the complexity of the existing detector without sacrificing its performance, especially in the SC-FDMA aided STSK uplink.

4.6.4 Performance of the Channel-Coded Scheme

In Figure 4.15 and Figure 4.17, we also characterized the achievable BER performance of the three-stage RSC- and URC-coded OFDMA/SC-FDMA STSK ($M = 2, N = 2, T = 2, Q = 4$) QPSK scheme relying on interleaved subcarrier allocation strategy in the context of the wideband COST207-TU12 channel [139], where we employed a half-rate RSC code having a constraint length of $k_c = 2$ and the octrally represented generator polynomials of $(g_r, g) = (3, 2)_8$ as well as two random interleavers having a memory of 240,000 bits. The number of inner and

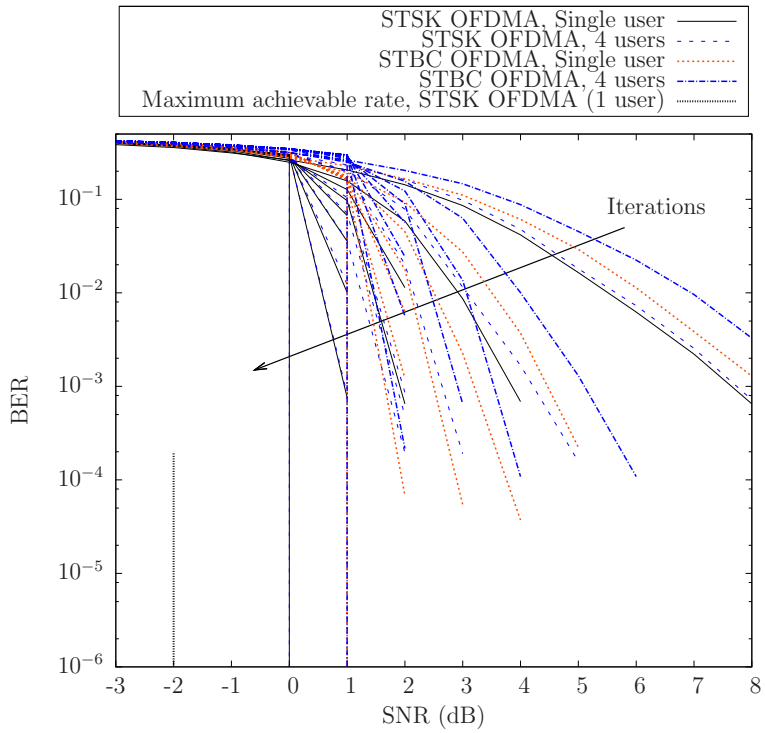

Figure 4.15: BER performance of our channel coded MMSE equalization based OFDMA STSK($M = 2, N = 2, T = 2, Q = 4$) of Figure 4.9 employing QPSK modulation in dispersive COST207-TU12 channel and that of the corresponding $\mathcal{G}_2$-STBC scheme. Maximum achievable rate for the corresponding scheme for single-user computed using the EXIT chart's area property is also shown. The remaining system parameters are listed in Table 4.2.

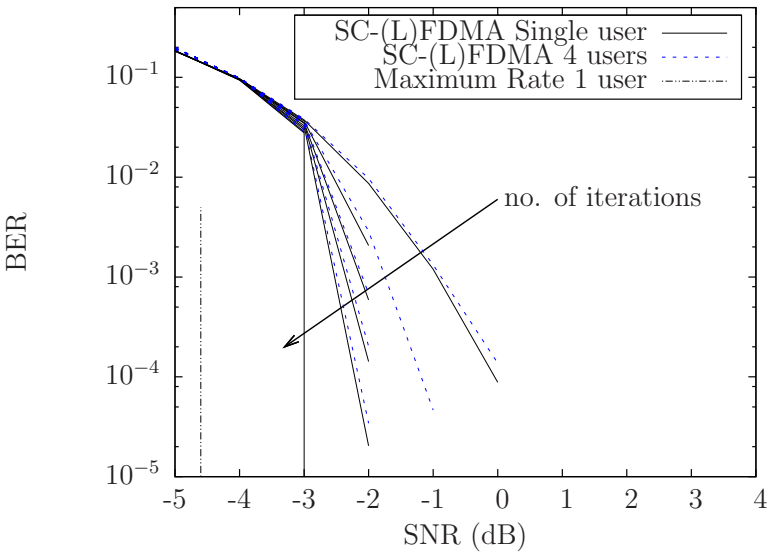

Figure 4.16: Achievable BER performance of our channel coded MMSE based SC-(L)FDMA STSK($M = 2, N = 2, T = 2, Q = 4$) of Figure 4.9 with QPSK modulation in COST207-TU12 channel. Maximum achievable rate of the corresponding scheme with single user is also shown. The remaining system parameters are listed in Table 4.2.

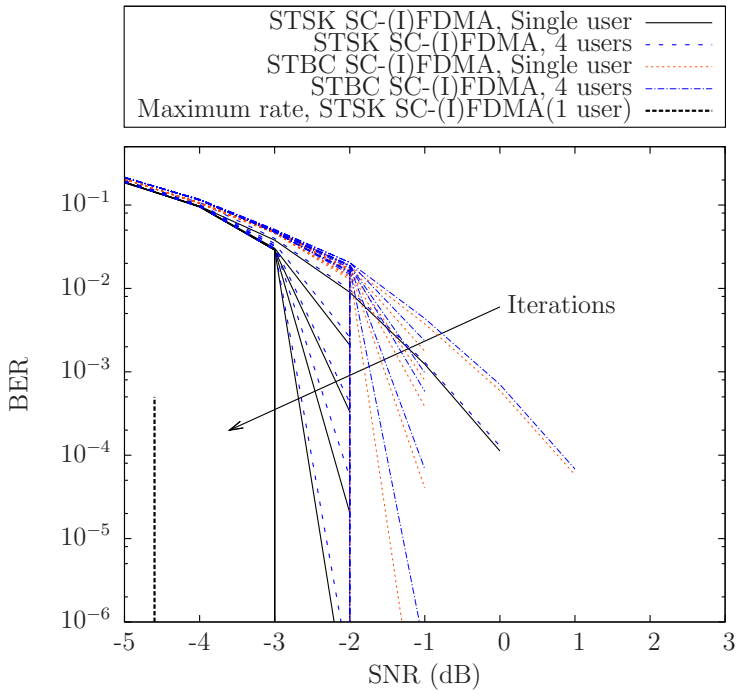

Figure 4.17: Achievable BER performance of our channel coded MMSE based SC-(I)FDMA STSK($M = 2, N = 2, T = 2, Q = 4$) of Figure 4.9 with QPSK modulation in COST207-TU12 channel and that of the corresponding $\mathcal{G}_2$-STBC scheme with similar parameters. Maximum achievable rate of the corresponding scheme with single user is also shown. The remaining system parameters are listed in Table 4.2.

outer decoder iterations was set to $I_{inner} = 2$ and $I_{outer} = 9$, respectively. We also investigated the performance of SC-(L)FDMA-aided STSK scheme and the performance was observed to be similar to SC-IFDMA in coded scenario as seen in Figure 4.16. The performance of both the OFDMA STSK and SC-(I)FDMA STSK has been compared against the corresponding $\mathcal{G}_2$-STBC benchmarkers. The maximum achievable rates of our schemes were also calculated by exploiting the so-called area property of EXIT charts. To be specific, it was shown in [146, 147, 164] that the area under the inner decoder's EXIT curve at certain SNR quantifies the maximum achievable rate of the system, where an infinitesimally low BER may be achieved. The SNRs corresponding to the maximum achievable rates of the schemes are also shown in Figure 4.15 and Figure 4.17.

Figure 4.18 portrays the EXIT chart of the SC-FDMA STSK ($M = 2, N = 2, T = 2, Q = 4$) arrangement combined with QPSK modulation and the IFDMA strategy, where the SNR was varied from -5 dB to 1 dB in steps of 0.5 dB. It can be seen that an open EXIT tunnel is formed at SNR $=-4.0$ dB using an interleaver depth of $240,000$ bits. The corresponding staircase-shaped decoding trajectory [147] based on bit-by-bit Monte Carlo simulations conducted at -3.0 dB is also shown. Thus it can be inferred that an infinitesimally low BER may be achieved at SNR $= -3.0$ dB in an uplink scenario after $I_{outer} = 6$ iterations.

Table 4.3: Summary of the achievable BER performance of schemes proposed in in Chapter 4

Scheme	*Schematic diagram*	*Figure number*	*SNR, dB at BER*		*SNR gain/difference, dB at BER (benchmark)*	
			10^{-3}	10^{-4}	10^{-3}	10^{-4}
SC-(I)FDMA-aided STSK $(2,2,2,4)$, *QPSK, MMSE*	Figure 4.6 & Figure 4.7	Figure 4.10	4.0	11.5	0.8 (SC-(I)FDMA, $\mathcal{G}_2$-STBC)	1.0 (SC-(I)FDMA, $\mathcal{G}_2$-STBC)
SC-(L)FDMA-aided STSK $(2,2,2,4)$, *QPSK, MMSE*	Figure 4.6 & Figure 4.7	Figure 4.10	4.8	12.3	0.2 (SC-(I)FDMA, $\mathcal{G}_2$-STBC)	0.2 (SC-(I)FDMA, $\mathcal{G}_2$-STBC)
OFDMA-aided QPSK STSK $(2,2,2,4)$, *MMSE, IFDMA*	Figure 4.6 & Figure 4.7	Figure 4.10	8.5	> 20.0	3.5 (O(I)FDMA, $\mathcal{G}_2$-STBC)	–
OFDMA-aided QPSK STSK $(2,2,2,4)$, *LFDMA, MMSE*	Figure 4.6 & Figure 4.7	Figure 4.10	9.0	> 20.0	3.0 (O(I)FDMA, $\mathcal{G}_2$-STBC)	–
OFDMA-aided QPSK STSK $(2,2,2,4)$, *IFDMA, ML*	Figure 4.6 & Figure 4.7	Figure 4.10	7.0	13.0	2.5 (SC-(I)FDMA, $\mathcal{G}_2$-STBC)	3.0 (SC-(I)FDMA, $\mathcal{G}_2$-STBC)
OFDMA-aided QPSK STSK $(2,2,2,4)$, *LFDMA, ML*	Figure 4.6 & Figure 4.7	Figure 4.10	7.3	13.4	2.8 (SC-(I)FDMA, $\mathcal{G}_2$-STBC)	3.3 (SC-(I)FDMA, $\mathcal{G}_2$-STBC)
SC-(I)FDMA QPSK STSK $(2,2,2,4)$, *reduced-complexity*	Figure 4.6 & Figure 4.8	Figure 4.14	4.7	12.5	2.0 (Detector II, Narrowband)	2.2 (Detector II, Narrowband)
O(I)FDMA QPSK STSK $(2,2,2,4)$, *reduced-complexity*	Figure 4.6 & Figure 4.8	Figure 4.14	9.8	> 20.0	2.2 (Detector II, Narrowband)	3.3 (SC-(I)FDMA $\mathcal{G}_2$-STBC)
Channel-coded OFDMA STSK $(2,2,2,4)$ *QPSK, MMSE*	Figure 4.9	Figure 4.15	0.0	0.0	2.0 (maximum achievable rate at BER ≈ 0)	
Channel-coded QPSK SC-(I)FDMA STSK $(2,2,2,4)$ *MMSE*	Figure 4.9	Figure 4.17	-3.0	-3.0	1.7 (maximum achievable rate at BER ≈ 0)	

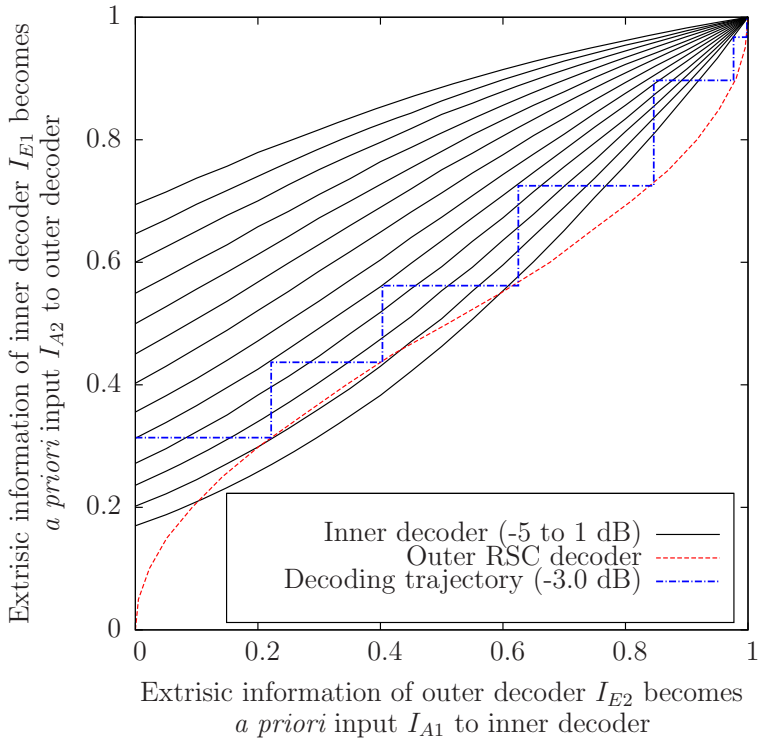

Figure 4.18: EXIT trajectory of our three-stage turbo detected MMSE based SC-(I)FDMA STSK($M = 2, N = 2, T = 2, Q = 4$) of Figure 4.9 with QPSK modulation applied in a COST207-TU12 dispersive channel model with $f_d = 0.01$ and remaining parameters as listed in Table 4.2. The EXIT trajectory at -3.0 dB is mapped on inner decoder EXIT curves from -5 to 1 dB in steps of 0.5 dB and the outer RSC decoder EXIT function.

4.7 Chapter Summary and Conclusions

In this chapter, the OFDM-aided STSK scheme of Chapter 2 has been extended to an OFDMA or SC-FDMA aided STSK scheme for the sake of facilitating multiuser STSK DL/UL communications. In Section 4.2, we started out with a brief review of OFDMA as well as SC-FDMA-aided communications, listing their pros and cons. In line with the physical layer specifications of the 3GPP LTE-Advanced standard, we have proposed an OFDMA/SC-FDMA aided STSK scheme in Section 4.3, which overcomes the impairments of realistic dispersive channels, while facilitating multi-user transmissions. The scheme benefits from a flexible diversity versus multiplexing gain trade-off offered by the recently developed STSK scheme relying on low-complexity single-stream based ML detection. In Section 4.4, we proposed a reduced-complexity detector, which further reduces the complexity of the single-stream ML detector of OFDMA/SC-FDMA aided STSK formulated in (4.31). The complexity quantified in terms of the RMOs per bit is compared to that of the previous detectors in Table 4.1. Furthermore, a channel-coded near-capacity OFDMA/SC-FDMA-aided STSK scheme was proposed in Section 4.5. The performance of both our uncoded and channel-coded STSK arrangement was investigated and

compared to existing benchmark schemes in Section 4.6 using the system parameters listed in Table 4.2. The PAPR of both OFDMA as well as of SC-FDMA using both the localized and interleaved subcarrier mapping schemes of Section 4.3 was investigated in Figure 4.11. The performance versus complexity of our reduced-complexity detector of Section 4.4 was characterized and compared to that of the previously designed detectors in Section 4.6. The BER performance shown in Figures 4.10, 4.14, 4.15 and 4.17 for the schemes portrayed in Figures 4.6, 4.7, 4.8 and 4.9 is summarized in Table 4.3. As seen in Table 4.3, the proposed schemes emplying SC-FDMA exhibit a better performance than its OFDMA counterpart. The scheme employing the interleaved subcarrier allocation strategy benefits from a better BER performance than its localized counterpart as a result of the additional frequency diversity attained by using increased separation between the subcarriers. The reduced-complexity detector is characterized in Figures 4.12 and 4.13. The channel-coded scheme of Figure 4.9 exhibits an infinitesimally low BER at 1.7 and 2.0 dB higher SNRs, when compared to the maximum achievable rate benchmarkers.

We quantified the relative merits of OFDMA and SC-FDMA, when combined with STSK and advocated the SC-FDMA based STSK scheme of Figure 4.9 relying on the interleaved subcarrier allocation in the uplink scenario, as a benefit of its low PAPR. The effects of the spatial correlation between the different AEs of a multiple antenna-aided uplink, however, have to be further investigated and will be included in our future study. It is worth mentioning here that the dispersion matrices invoked for constructing our STSK system were optimized by an exhaustive search to minimize the maximum PEP under the power constraint of (4.4). The EXIT curves of the proposed scheme seen in Figure 4.18 succeeded in reaching the $(1.0, 1.0)$ point of perfect convergence to a vanishingly low BER after a few iterations, thus indicating a sharp decrease of the BER curve in Figure 4.17.

The reduced-complexity detector proposed in Section 4.4 for both the OFDMA-aided STSK DL and for the SC-FDMA-aided STSK UL is inherently immune to inter-element interference (IEI) as a benefit of activating a single DM and it has a reduced complexity compared to the existing detectors. It is a promising candidate for employment in OFDMA/SC-FDMA-aided STSK transmissions over frequency-selective channels even under multiuser scenarios in terms of its performance versus complexity tradeoff.

We have intrinsically amalgamated the OFDM, MC-CDMA and SC-FDMA systems with the STSK multiple-antenna architecture in Chapters 2, 3 and 4 for employment in realistic dispersive wireless channels. In order to exploit the cooperative diversity of distributed relaying protocols, we propose a successive relaying aided coherent versus non-coherent multicarrier STSK scheme in Chapter 5. Successive relaying assists in recovering the typical 50% throughput loss of the half-duplex relaying scheme, while MC-CDMA provides protection against the frequency-selectivity of the channel and mitigates the successive relaying induced interferences.

Chapter 5

Cooperative Multicarrier STSK Employing Successive Relaying

5.1 Introduction

In Chapters 2, 3 and 4, we have investigated novel schemes incorporating OFDM, MC-CDMA and OFDMA/SC-FDMA based transmissions of the multiple-antenna signals relying on the recently proposed STSK system. However, in these chapters, we have focussed our attention on co-located MIMO scenarios, where multiple antennas are employed both at the transmitter as well as the receiver. The co-located MIMO schemes are potentially susceptible to the detrimental effects of inter-antenna correlation due to the insufficient separation among the antennas. For the sake of mitigating the deleterious effects imposed by the inter-antenna correlation, in this chapter, we consider cooperative relaying aided multicarrier STSK schemes. More explicitly, we propose successive relaying (SR) aided cooperative multicarrier STSK for transmission over frequency-selective channels. We invoke SR for mitigating the typical 50% throughput loss of conventional half-duplex relaying schemes, whilst MC-CDMA is used for circumventing the dispersive effects of wireless channels as well as for reducing the SR-induced interferences. The distributed relay terminals form a pair of virtual antenna arrays (VAAs) and the source node (SN) successively transmits its frequency-domain (FD) spread signals to one of the VAAs in addition to it directly transmitting to the destination node (DN). The constituent relay nodes (RNs) of each VAA activate cyclic redundancy checking (CRC) based selective decode-and-forward (DF) relaying. The DN can jointly detect the signals received via the SN-to-DN and the VAA-to-DN links using a low-complexity single-stream based joint maximum-likelihood (ML) detector. We also propose a differentially encoded cooperative MC-CDMA STSK scheme for facilitating communications over hostile dispersive channels without requiring channel estimation (CE). The ability to dispense with CE

is important, since the relays cannot be expected to altruistically estimate the SN-to-RN links for simply supporting the source. Furthermore, we invoke the soft-decision aided serially concatenated recursive systematic convolutional (RSC) coded and unity-rate coded (URC) system of Figure 3.10 in the context of our cooperative multicarrier STSK in Figure 5.7 and Figure 5.8 and investigate its performance in both coherent and non-coherent scenarios.

Thus, in this chapter, we propose coherent versus noncoherent SR-aided cooperative MC-STSK employing both hard-decision as well as soft-decision decoding. The remainder of this chapter is organised as follows. We commence with the rationale, problem statement and outline of our contributions in Section 5.2. In Section 5.3, we present an overview of the proposed system. The joint detection of the signals arriving from the SN-DN and VAA-DN links is discussed in Section 5.4. The proposed differential multi-carrier cooperative STSK and the channel-coded soft-decision-based multi-carrier cooperative STSK schemes are outlined in Section 5.5 and Section 5.6, respectively. In Section 5.7, the attainable performance of the proposed scheme is investigated. Finally, we conclude in Section 5.8.

5.2 Background and Problem Statement

As discussed in the previous chapters, MIMO schemes allow us to mitigate the fundamental limitations of SISO systems. MIMO systems relying on multicarrier STSK [117,119] are capable of ensuring link reliability for transmission over realistic dispersive channels, while simultaneously providing a multiplexing gain at a low decoding complexity. To be specific, STSK combines the appealing simplicity of SM [47] and of SSK [48] with the attractive the rate versus diversity tradeoffs provided by linear dispersion codes (LDCs) [11,32]. LDCs constitute a generic MIMO family subsuming both space-time block codes [9] as well as the Bell Laboratories layered space-time (BLAST) [15] arrangement and the vertical-BLAST (V-BLAST) [17, 122] schemes. As a benefit, they are capable of outperforming both STBCs and BLAST/V-BLAST schemes, albeit at the cost of a higher decoding complexity. Thus STSK is capable of retaining the benefits of LDCs, while relying on a low-complexity design [55]. However, the antenna elements of a co-located STSK system typically suffer from spatially correlated large-scale fading imposed by the ubiquitous shadowing effects [165]. For the sake of mitigating this correlation-induced diversity-gain erosion, the concept of cooperative space-time processing [166, 167] has become popular in recent years owing to its benefits accruing from the geographically distributed nature of relay nodes (RNs), where the relays may be viewed as the distributed elements of a MIMO system, with each element experiencing uncorrelated fading. Additionally, this cooperative MIMO architecture enables us to avoid the physical limitations of installing multiple antennas on a mobile handset.

Recently, the concept of cooperative STSK [54] was proposed for frequency-flat Rayleigh

fading channels in order to benefit from MS-cooperation, although naturally, this scheme suffers from the usual throughput loss imposed by the relaying strategy employed. The introduction of successive relaying (SR) [114], on the other hand, is potentially capable of mitigating the half-duplex multiplexing loss. Specifically, it was shown in [114] that SR mitigates the typical 50% throughput loss of conventional half-duplex relaying, without eroding its diversity gain. This recovery of the multiplexing loss is attained, however, at the expense of incurring some SR-induced interference. SR provides significant performance advantages over the conventional relaying protocols, especially when the SR-induced interference can be efficiently mitigated. SR was successfully used in [115] as a near-capacity cooperative space-time coding architecture. Furthermore, a non-coherent detection based scheme employing both multiple-symbol differential sphere decoding (MSDSD) and SR was conceived in [168, 169]. However, the SR-induced interferences encountered both at the RNs and at the destination nodes (DNs) [114] inevitably limit its performance. A differential STSK aided successive-relay-assisted DF scheme was proposed for cooperative multiuser code-division multiple-access (CDMA) systems [170], which mitigates the throughput loss imposed by half-duplex relaying. However, this scheme is only applicable to non-dispersive MIMO scenarios.

To exploit the diversity benefits of cooperative schemes as well as to circumvent the channel-induced dispersion, while mitigating the throughput loss imposed by half-duplex relaying, we propose a novel SR based DF cooperative multi-carrier (MC) STSK scheme. We will demonstrate in Section 5.7 that the coherent SR-aided MC-CDMA STSK scheme performs well, but it might be unrealistic to expect that the RNs altruistically estimate the SN-to-RN channels. The estimation of the SN-RN as well as the RN-DN channels would become extremely challenging under high-mobility scenarios. As a potential remedy, we propose a noncoherent cooperative MC STSK scheme. The novel contributions of this chapter are as follows.

1. We intrinsically amalgamate for the first time multi-carrier transmissions with a cooperative STSK system for the sake of communicating reliably over hostile multipath channels. More particularly, we propose MC-CDMA based cooperative STSK for achieving an improved diversity gain to recover the original input sequence. Although orthogonal frequency division multiplexing/multiple access (OFDM/OFDMA) or single-carrier frequency division multiple access (SC-FDMA) can be employed for mitigating the channel-induced dispersion in our STSK based system [117, 119], MC-CDMA is capable of providing the additional benefit of frequency-domain (FD) diversity. The incorporation of MC-CDMA has the further benefit of substantially reducing both the SR-induced inter-relay interference (IRI) and co-channel interference (CCI) [114], when employing the specific SR regime of [168].

2. We propose an SR aided cyclic redundancy checking (CRC) based selective DF cooperative

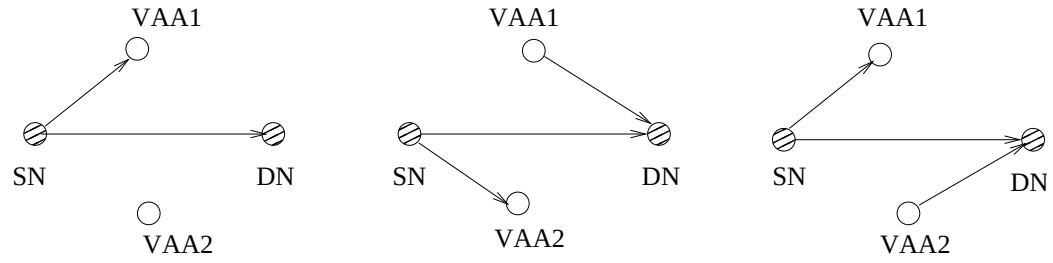

(a) Time slot 1 (b) Time slot 2 (c) Time slot 3

Figure 5.1: Transmission protocol of successive relaying (SR) aided cooperation during different time slots.

STSK scheme. The SR invoked in this context assists us in recovering the multiplexing loss of conventional half-duplex relaying schemes.

3. We also propose a new modality for the joint detection [54, 168] of the FD-despread signals gleaned from two successively arriving frames at the DN via the source node (SN)-to-DN and the virtual antenna array (VAA)-to-DN links by using the single-stream based maximum likelihood (ML) detector of [52]. The joint detector takes advantage of the inter-stream interference-free nature of STSK schemes, since always a single dispersion matrix is activated.

4. A new non-coherent cooperative multi-carrier STSK arrangement using unitary DMs, rather than using the nonlinear Cayley transform [49, 171] is proposed.

5. We propose a powerful serially concatenated turbo-detection based channel-coded cooperative multi-carrier scheme, where the DN iteratively exchanges soft information between the component decoders, before finally outputting the estimated source information. The performance of the scheme is evaluated both in the context of the coherent as well as the differential schemes and compared against the corresponding maximum achievable capacity benchmarker, using our EXIT chart based semi-analytical method.

Having briefly described the background of the proposed scheme and having outlined the contributions of this chapter, let us now proceed to the system model of our coherent cooperative MC STSK arrangement in the following section.

5.3 System Overview of the Coherent Scheme

This section describes our SR-aided coherent cooperative multicarrier STSK scheme. The typical four-node network topology and transmission protocol of the classic SR scheme [114] is portrayed in Figure 5.1, while the overall system architecture of our proposed scheme is

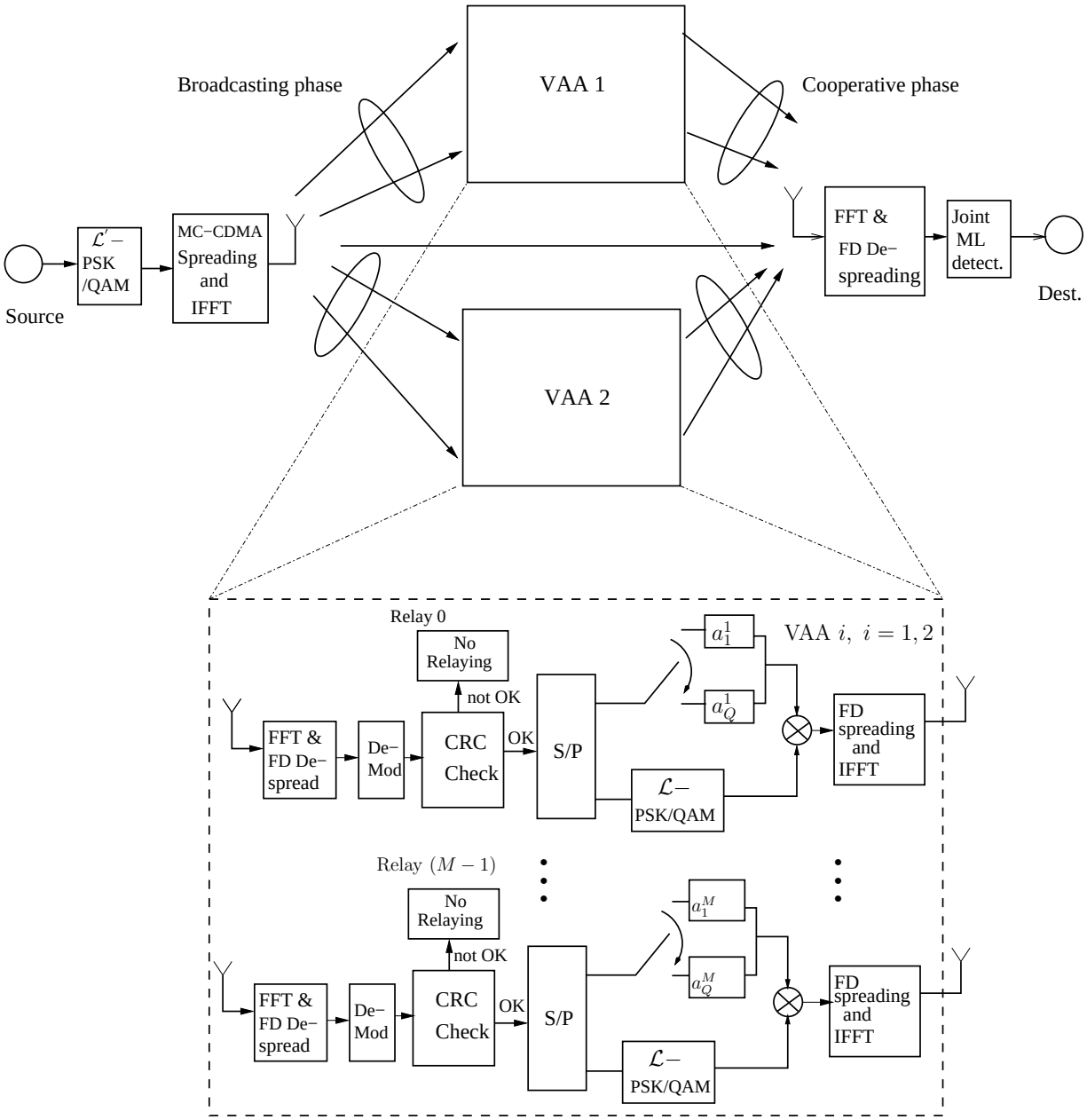

Figure 5.2: Transmission model of SR aided STSK employing FD-spreading/despreading and inverse fast Fourier transform (IDFT)/fast Fourier transform (DFT)-based MC-CDMA modem. As an extension to Figure 5.1, each of the two VAAs consists of M number of RNs which activate relaying depending on the outcome of CRC. The chip-waveform based spread-despread paradigm overcomes SR induced interferences, whereas the scheme is benefitted from the joint single-stream based ML detector.

depicted in Figure 5.2, where the SN, DN and the two VAAs taking part in SR are explicitly labelled. Additionally, for the sake of enabling the CRC at the RNs, frame-based rather than symbol-based transmissions are adopted. We assume that the distances between the different RNs of the same VAA are negligible with respect to the distance between the SN and the DN (or between the SN and the VAA). Accordingly, a VAA is assumed to exhibit a unitary nature, when considering the geometric relationship amongst the SN s, the i -th VAA v_i, and the DN d. The average path-loss gains of the SN-VAA and VAA-DN links with respect to the SN-DN links are denoted by $G_{sv_i} = \left(\frac{D_{sd}}{D_{sv_i}}\right)^{\alpha}, \quad i = 1, 2$ and $G_{v_id} = \left(\frac{D_{sd}}{D_{v_id}}\right)^{\alpha}, \quad i = 1, 2$ respectively, where α is the path-loss exponent and $D_{aa'}, \quad a, a' \in \{s, v_i, d\}$ represents the distance between the nodes a and a'. Furthermore, we assume a symmetric structure, where D_{sv_1}, D_{v_1d}, G_{sv_1} and G_{v_1d} are identical to D_{sv_2}, D_{v_2d}, G_{sv_2} and G_{v_2d}, respectively. Furthermore, all the possible channel paths are assumed to be frequency-selective Rayleigh fading channels.

5.3.1 The Source Node's Transmission Model

The SN first attaches the CRC bits to its information bits and transmits them both to the M RNs of a VAA as well as to the DN in each of its broadcast phases, as seen from Figure 5.2. To be specific, the CRC-protected bits are first mapped to the $\mathcal{L}'$-PSK or $\mathcal{L}'$-QAM symbol blocks [54] according to $\boldsymbol{S}_s(k) \triangleq [s_1(k), \ldots, s_b(k)]^T \in \mathbb{C}^{b\times 1}$, where k $(1, 2, \ldots)$ represents the block index and each block carries $(b \cdot \log_2 \mathcal{L}')$ bits. Let us also define the frame length L_f as the number of $(b \cdot \log_2 \mathcal{L}')$-bit signal blocks transmitted in each frame and hence the block index k is related to the l_f-th block of the n-th frame by $k = (n \times L_f + l_f)$.

We divide all the frames into two sets. The frame being broadcast when VAA1 of Figure 5.1 is receiving is referred to as frame-A, which is spread by the spreading sequence $\boldsymbol{C}_A^u$ for user $u, \quad (u = 1, 2, ..., U)$. By contrast, the frame being broadcast when VAA2 is receiving is referred to as frame-B, which is spread by $\boldsymbol{C}_B^u$, where both $\boldsymbol{C}_A^u = [C_A^u(1), C_A^u(2), \ldots, C_A^u(S_f)]$ and $\boldsymbol{C}_B^u = [C_B^u(1), C_B^u(2), \ldots, C_B^u(S_f)]$ have a spreading factor of S_f. Both the spreading sequences $\boldsymbol{C}_A^u$ and $\boldsymbol{C}_B^u$ are S_f-length vectors whose chips are denoted by $C_A^u(s_f), \quad s_f = 1, 2, \ldots, S_f$ and $C_B^u(s_f), \quad s_f = 1, 2, \ldots, S_f$, respectively. The block index k $(1, 2, \ldots)$ of the signal block $\boldsymbol{S}_s(k)$ is related to the index k' $(1, 2, \ldots)$ of the spread blocks, e.g. $\boldsymbol{S}_c(k') = [C_A^u(s_f)\boldsymbol{S}_s(k)] \in \mathbb{C}^{b\times 1}$ by $k' = k \times S_f + s_f \quad s_f = 1, 2, \ldots, S_f$, while the spread blocks are generated using the spreading sequence $C_A^u(s_f)$ or $C_B^u(s_f)$, depending on whether frame-A or frame-B is being transmitted. We assume that a particular spread block is transmitted over b time intervals and the fading envelope during the transmission of a block of b symbols remains constant. For the sake of readability, we omit the user index u in the following, except in (5.32) and in (5.34) where the multiuser scenario is specifically considered. The different users are separated by their mutually orthogonal user-specific spreading sequences, albeit the multiuser scenario

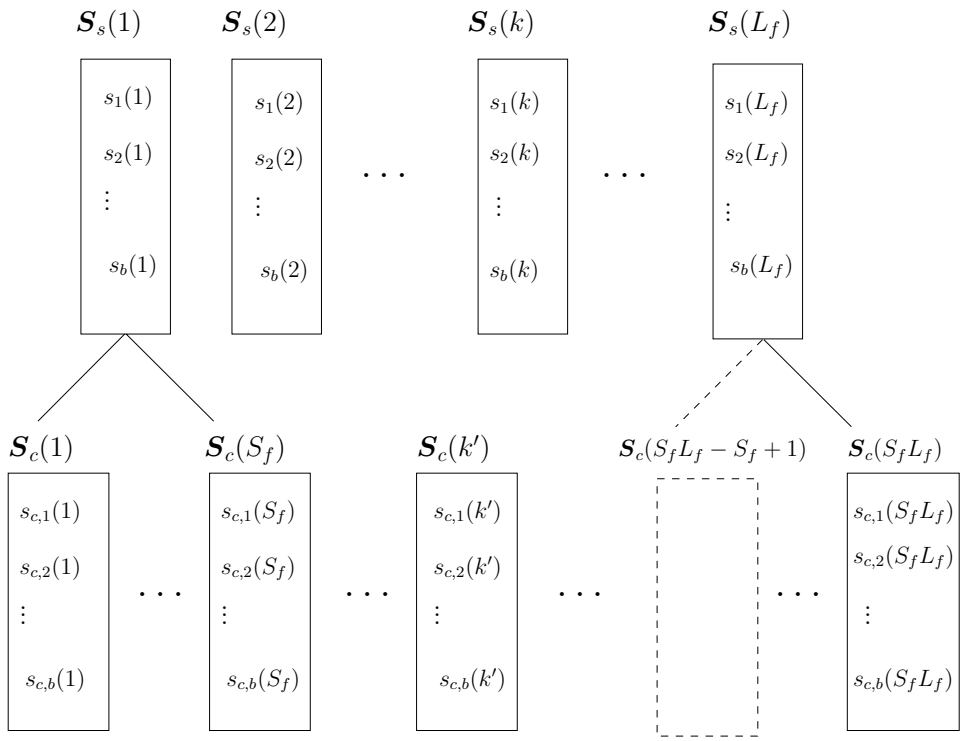

Figure 5.3: Illustration of the transmission protocol of the SN of Figure 5.2. The L_f transmit blocks $\boldsymbol{S}_s(k)$ of a transmission frame are spread in FD by the MC-CDMA modem using the user-specific spreading sequence $\boldsymbol{C}_A^u$ or $\boldsymbol{C}_B^u$ depending on whether frame-A or frame-B is being transmitted, which results in S_fL_f spread blocks $\boldsymbol{S}_c(k')$. Note that the initial transmit blocks are indexed by k, while the spread blocks are indexed by k'.

is not shown explicitly in Figure 5.2 for avoiding obfuscation. Assuming the spread frame length $(L_f \times S_f)$ to be a multiple of the number N_c of subcarriers, while N_c is equal to or a multiple of S_f, each frame is mapped to the N_c subcarriers using the N_c-point inverse discrete Fourier transform (IDFT). Then the cyclic prefices (CPs), which are designed to be longer than the channel's delay-spread are attached to avoid any inter-symbol interference (ISI).

In order to further illustrate the transmission protocol of the SN, in Figure 5.3 we further augment the formation of a transmit frame consisting of L_f transmit blocks, while the frame will contain S_fL_f spread blocks. Each of the blocks to be transmitted from the SN denoted by $\boldsymbol{S}_s(k)$ is a $(b \times 1)-$element vector, where each element of the vector is a $\mathcal{L}'$-PSK/QAM symbol. Before being mapped to the subcarriers, these symbols are spread in the FD by the user-specific spreading sequences. We note that the symbols of a specific block will be spread in the FD by the same spreading sequence. Furthermore, in general, the symbols mapped to the same subcarrier will be subjected to frequency-flat fading and will be multiplied by the same FD channel transfer gain. By contrast, the symbols mapped to a different subcarrier will be multiplied by a different FD channel transfer gain. Hence a particular block $\boldsymbol{S}_s(k)$ will result in S_f number of spread blocks, each of which can be denoted by $[C_A^u(s_f)\boldsymbol{S}_s(k)]$ for

$s_f = 1, 2, ..., S_f$. The index of these spread blocks is represented by k', which is related to k by $k' = k \times S_f + s_f \quad s_f = 1, 2, \ldots, S_f$. Note that the spread block $[C_A^u(s_f)\boldsymbol{S}_s(k)]$ is also a $(b \times 1)-$ element column vector, like the $\boldsymbol{S}_s(k)$ block, since the spread block is generated with the aid of FD spreading of the $\boldsymbol{S}_s(k)$ block by a single chip of the spreading code. Since a single $\boldsymbol{S}_s(k)$ block gives rise to S_f number of spread blocks $[C_A^u(s_f)\boldsymbol{S}_s(k)], \quad s_f = 1, 2, \ldots, S_f$, a frame consisting of L_f number of $\boldsymbol{S}_s(k) \quad k = 1, 2, ..., L_f$ blocks contains $(L_f \times S_f)$ spread blocks.

After FD spreading of the block symbols, N_c symbols assembled from N_c different spread blocks are mapped to the N_c subcarriers of our MC-CDMA based parallel modem in order to form an MC-CDMA symbol. All the b symbols of a particular block are mapped to the same subcarrier, but are transmitted in b different signalling intervals. Thus the N_c spread blocks may be viewed as being mapped to the N_c subcarriers. Hence, a particular spread block $[C_A^u(s_f)\boldsymbol{S}_s(k)]$ is assigned to a specific subcarrier and it is multipled by the channel gain $\tilde{h}_{sv_1}^m(k')$, whereas another spread block indexed by a different k' (which is expressed by s_f), will be subjected to another channel gain. In this manner, the symbols of the N_c different spread blocks will experience N_c different channel gains and the combination of these N_c spread blocks may be viewed as constituting an MC-CDMA symbol block.

Since N_c spread blocks are assigned to N_c subcarriers, the total number of spread blocks corresponding to a transmit frame is $(L_f \times S_f)$, which has to be a multiple of N_c. On the other hand, N_c is a multiple of the spreading factor S_f for the sake of ensuring that the N_c subcarriers carry an integer number of $\boldsymbol{S}_s(k)$ blocks. Since a single spread block $[C_A^u(s_f)\boldsymbol{S}_s(k)] \in \mathbb{C}^{b\times 1}$ is multipled by a single channel gain $\tilde{h}_{sv_1}^m(k')$, after CP removal and FFT, the received FD spread block at the m-th relay node (RN) of VAA1, which is denoted by $\boldsymbol{Y}_{sv1}^m(k')$ is also a $(b \times 1)-$element column vector.

The linear convolution between the time-domain (TD) channel input signals and the channel impulse response (CIR) is transformed into scalar multiplication in the FD [73]. Hence, the FD signals $\boldsymbol{Y}_{sd}^A(k') \in \mathbb{C}^{b\times 1}$ and $\boldsymbol{Y}_{sd}^B(k') \in \mathbb{C}^{b\times 1}$ received at the DN from the direct SN-DN link of a particular user and $\boldsymbol{Y}_{sv_i}^m(k') \in \mathbb{C}^{b\times 1}, \quad i = 1, 2$ at the m-th RN of each VAA are given, after

CP removal and discrete Fourier transform (DFT), by

$$\boldsymbol{Y}_{sv_1}^{m}(k') = \sqrt{G_{sv_1}}\tilde{h}_{sv_1}^{m}(k')\left[C_A(s_f)\boldsymbol{S}_s(k)\right] + \tilde{\boldsymbol{V}}_{v_1}^{m}(k') \quad \text{(Frame-A)} \tag{5.1}$$

$$\boldsymbol{Y}_{sv_2}^{m}(k') = \sqrt{G_{sv_2}}\tilde{h}_{sv_2}^{m}(k')\left[C_B(s_f)\boldsymbol{S}_s(k)\right] + \tilde{\boldsymbol{V}}_{v_2}^{m}(k') \quad \text{(Frame-B)} \tag{5.2}$$

$$\boldsymbol{Y}_{sd}^{A}(k') = \tilde{h}_{sd}(k')\left[C_A(s_f)\boldsymbol{S}_s(k)\right] + \tilde{\boldsymbol{V}}_{d}(k') \quad \text{(Frame-A)} \tag{5.3}$$

$$\boldsymbol{Y}_{sd}^{B}(k') = \tilde{h}_{sd}(k')\left[C_B(s_f)\boldsymbol{S}_s(k)\right] + \tilde{\boldsymbol{V}}_{d}(k') \quad \text{(Frame-B)} \tag{5.4}$$

where $\tilde{h}_{sv_i}^{m}$ and $\tilde{h}_{sd}$ denote the FD channnel coefficients between the SN and the m-th RNs of VAA i as well as between the SN and DN, respectively, obeying the complex-valued Gaussian distributions of $\mathcal{CN}(0, \sigma_{sv_i}^2)$ and $\mathcal{CN}(0, \sigma_{sd}^2)$ respectively. Each component of the noise vectors $\tilde{\boldsymbol{V}}_{v_i}^{m}$ and $\tilde{\boldsymbol{V}}_{d}$ in (5.1) - (5.4) is a complex-valued Gaussian variable of $\mathcal{CN}(0, N_0)$, with N_0 representing the noise variance.

5.3.2 The Virtual Antenna Array

As already mentioned, each of the two VAAs taking part in the SR paradigm is composed of M RNs and operates on the principle of the CRC-enabled selective DF strategy of [54, 172]. The signal received at each RN of a VAA is decoded following FD MC-CDMA despreading. For a scenario supporting multiple users, the source information of different users are jointly detected by a ML-multiuser detector (ML-MUD) as discussed in [95]. If the signal at any RN of the VAA is deemed to be correctly decoded by the CRC, then that specific RN is allowed to engage in relaying. The same RN re-encodes the decoded bits, similarly to the classic STSK structure of [49]. Explicitly, according to the relationship of $b \cdot \log_2 \mathcal{L}' = \log_2(\mathcal{L} \cdot Q)$, the $\log_2 \mathcal{L}$ bits of source information are mapped to an $\mathcal{L}$-PSK or $\mathcal{L}$-QAM symbol $s(k)$, while the remaining $\log_2 Q$ bits select the m-th row vector $\boldsymbol{a}_q^m(k)$ of the q-th matrix from the set of Q pre-assigned DMs, $\boldsymbol{A}_q \in \mathbb{C}^{M\times T}$, $(q = 1, 2...., Q)$. The DMs are generated under the power constraint, as detailed in [5, 49]: $\mathrm{tr}(\boldsymbol{A}_q^{\mathrm{H}}\boldsymbol{A}_q) = T$, $(q = 1, 2...., Q)$, where T represents the number of time slots used in the specific STSK structure considered and $\mathrm{tr}(\bullet)$ and $\bullet^H$ denote the trace and the Hermitian transpose of the matrix '$\bullet$', respectively. Specifically, the m-th RN maps the decoded bits to a symbol vector $\boldsymbol{S}_{v_i}^{m}(k) \in \mathbb{C}^{1\times T}$, $i = 1, 2$, which is given by $\boldsymbol{S}_{v_i}^{m}(k) = s(k)\boldsymbol{a}_q^m(k)$. Additionally, the activation/deactivation of the m-th RN may be represented by the parameter $\alpha_m \in \{0, 1\}$, where we have $\alpha_m = 0$, if a decoding error is identified by the CRC, hence resulting in the termination of relaying and we have $\alpha_m = 1$, otherwise. Note that the source bit-dependent selection of a dispersion vector out of Q such vectors provides an additional

Table 5.1: Example of the bit-to-vector mapping of relay node m in the cooperative MC-STSK scheme of Figure 5.2 for 3 bits per block, employing $Q = 2$ dispersion matrices and a QPSK constellation.

Input bits		$Q = 2$ $\mathcal{L} = 4$		
		$\boldsymbol{a}_q^m(k)$	$s(k)$	$\boldsymbol{S}_{v_i}^m(k)$
0	00	$\boldsymbol{a}_1^m$	1	$\boldsymbol{a}_1^m$
0	01	$\boldsymbol{a}_1^m$	$e^{j\frac{\pi}{2}}$	$j\boldsymbol{a}_1^m$
0	10	$\boldsymbol{a}_1^m$	$e^{j\frac{2\pi}{2}}$	$-\boldsymbol{a}_1^m$
0	11	$\boldsymbol{a}_1^m$	$e^{j\frac{3\pi}{2}}$	$-j\boldsymbol{a}_1^m$
1	00	$\boldsymbol{a}_2^m$	1	$\boldsymbol{a}_2^m$
1	01	$\boldsymbol{a}_2^m$	$e^{j\frac{\pi}{2}}$	$j\boldsymbol{a}_2^m$
1	10	$\boldsymbol{a}_2^m$	$e^{j\frac{2\pi}{2}}$	$-\boldsymbol{a}_2^m$
1	11	$\boldsymbol{a}_2^m$	$e^{j\frac{3\pi}{2}}$	$-j\boldsymbol{a}_2^m$

means of transmitting $\log_2 Q$ bits, as in the co-located STSK scheme [49, 57]. For the sake of providing further insight on the bit-to-vector mapping of a relay node m, we elaborate the bit-to-vector mapping of the cooperative MC-STSK employing $Q = 2$ and $\mathcal{L} = 4$ in Table 5.1. However, for the transmission of 3−bits per block, there are several potential combinations of Q and $\mathcal{L}$ given by $(Q, \mathcal{L}) = (8, 1), (4, 2), (2, 4)$ and $(1, 8)$. Furthermore, the resultant cooperative STSK scheme is unambiguously described by the (M, T, Q) parameters in conjunction with the associated $\mathcal{L}$-PSK or $\mathcal{L}$-QAM modulation. Note that whereas the STSK schemes relying on co-located antennas were specified by the (M, N, T, Q) parameters, the distributed MC STSK is specified by (M, T, Q), because we consider an SR aided cooperative scheme relying on a single DN.

5.3.3 The Receiver Model at Destination

In this section, we describe the decoding principle of the receiver at the DN with the aid of the double-frame matched filter of [168] for a particular user u. To be specific, a filter matched to C_A^u is employed during frame-A, whereas a filter matched to C_B^u is employed during the next consecutive frame-B transmission. Application of this strategy helps to detect signals during a particular frame, considerably suppressing the SR-induced interferences, especially with high spreading factor. Considering the FD representations of the signals and the FD channel response rather than the CIR, the signal received at the DN from the VAA-DN link

during the frame-A and frame-B transmissions are given by [54, 168]

$$\begin{aligned}\boldsymbol{Y}^{A}_{v_2d}(k') =& \sum_{m=1}^{M}\left[\sqrt{G_{v_2d}}\alpha_m\tilde{h}^{m}_{v_2d}(k')\left[C_B(s_f)\boldsymbol{S}^{m}_{v_2}(k-L_f)\right]\right] + \tilde{\boldsymbol{V}}'_{v_2d}(k') \\ =& \sqrt{G_{v_2d}}\tilde{\boldsymbol{H}}'_{v_2d}(k')\left[C_B(s_f)\boldsymbol{A}_q(k-L_f)s(k-L_f)\right] + \tilde{\boldsymbol{V}}'_{v_2d}(k'), \end{aligned} \tag{5.5}$$

$$\begin{aligned}\boldsymbol{Y}^{B}_{v_1d}(k') =& \sum_{m=1}^{M}\left[\sqrt{G_{v_1d}}\alpha_m\tilde{h}^{m}_{v_1d}(k')\left[C_A(s_f)\boldsymbol{S}^{m}_{v_1}(k-L_f)\right]\right] + \tilde{\boldsymbol{V}}'_{v_1d}(k') \\ =& \sqrt{G_{v_1d}}\tilde{\boldsymbol{H}}'_{v_1d}(k')\left[C_A(s_f)\boldsymbol{A}_q(k-L_f)s(k-L_f)\right] + \tilde{\boldsymbol{V}}'_{v_1d}(k'), \end{aligned} \tag{5.6}$$

where we have

$$\tilde{\boldsymbol{H}}'_{v_id}(k') \triangleq [\alpha_1\tilde{h}^{1}_{v_id}(k'), \ldots, \alpha_M\tilde{h}^{M}_{v_id}(k')] \in \mathbb{C}^{1\times M},\ i=1,2 \tag{5.7}$$

and

$$\boldsymbol{A}_q(k-L_f) = \begin{bmatrix} \boldsymbol{a}^{1}_q(k-L_f) \\ \vdots \\ \boldsymbol{a}^{M}_q(k-L_f) \end{bmatrix} \in \mathbb{C}^{M\times T}. \tag{5.8}$$

The FD channel coefficients $\tilde{h}^{m}_{v_id}(k')$ and the noise components $\tilde{\boldsymbol{V}}'_{v_id}(k')$ for $i=1,2$ and $m=1,2,\ldots,M$ obey the complex-valued Gaussian distributions of $\mathcal{CN}(0,\sigma^2_{v_id})$ and $\mathcal{CN}(0,N_0)$, respectively.

Applying the vectorial stacking operation $vec(\cdot)$ to both sides of (5.5) and (5.6), we arrive at the linearized VAA-DN link output signals, similarly to the LDCs of [32],

$$\bar{\boldsymbol{Y}}^{A}_{v_2d}(k') = \sqrt{G_{v_2d}}\bar{\boldsymbol{H}}'_{v_2d}(k')C_B(s_f)\boldsymbol{\chi}\boldsymbol{K}(k-L_f) + \bar{\boldsymbol{V}}'_{v_2d}(k'), \tag{5.9}$$

$$\bar{\boldsymbol{Y}}^{B}_{v_1d}(k') = \sqrt{G_{v_1d}}\bar{\boldsymbol{H}}'_{v_1d}(k')C_A(s_f)\boldsymbol{\chi}\boldsymbol{K}(k-L_f) + \bar{\boldsymbol{V}}'_{v_1d}(k'), \tag{5.10}$$

where we have

$$\bar{\boldsymbol{Y}}^{A}_{v_2d}(k') = vec(\boldsymbol{Y}^{A}_{v_2d}(k')) \in \mathbb{C}^{T\times 1} \tag{5.11}$$

$$\bar{\boldsymbol{Y}}^{B}_{v_1d}(k') = vec(\boldsymbol{Y}^{B}_{v_1d}(k')) \in \mathbb{C}^{T\times 1} \tag{5.12}$$

$$\boldsymbol{\chi} \triangleq [vec(\boldsymbol{A}_1), \cdots, vec(\boldsymbol{A}_Q)] \in \mathbb{C}^{MT\times Q} \tag{5.13}$$

$$\bar{\boldsymbol{H}}'_{v_id}(k') \triangleq \sqrt{G_{v_id}}\left[\boldsymbol{I}_T \otimes \tilde{\boldsymbol{H}}'_{v_id}(k')\right] \in \mathbb{C}^{T\times MT},\ i=1,2 \tag{5.14}$$

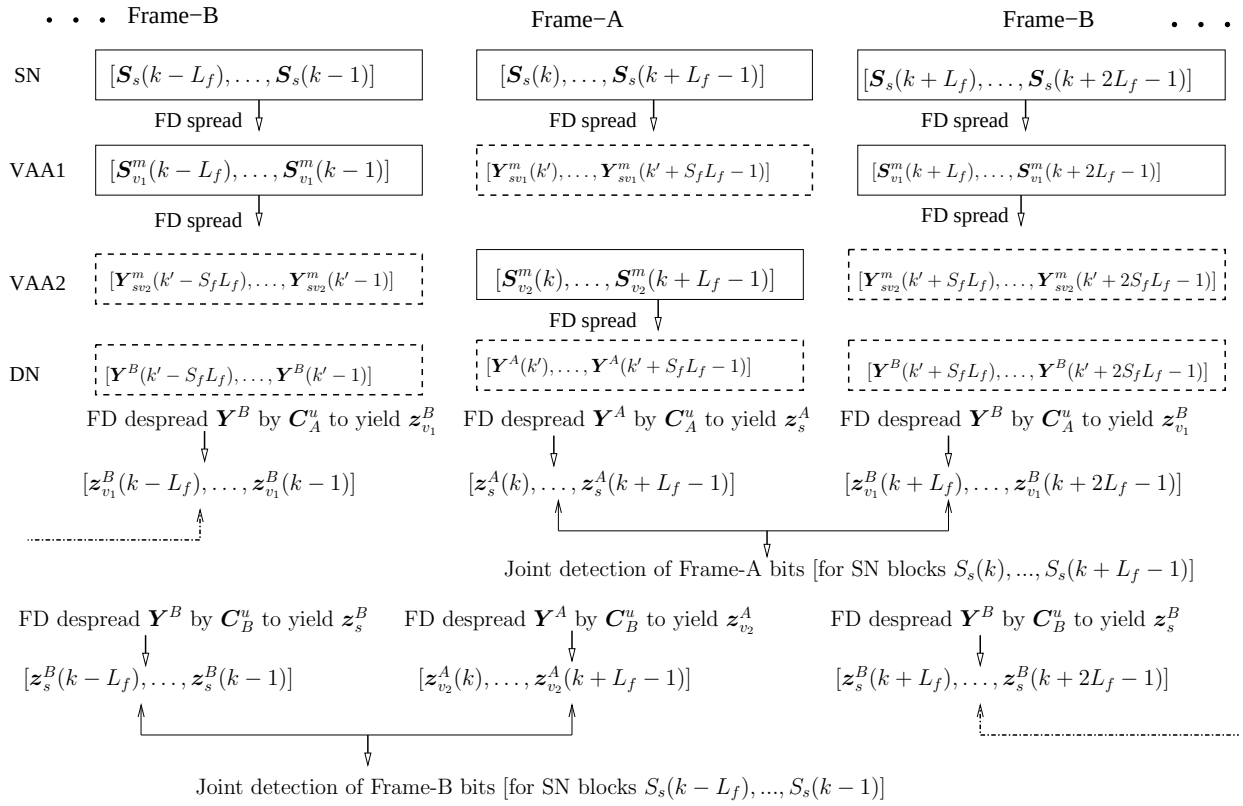

Figure 5.4: Illustration of the proposed SR based cooperative STSK protocol of Figure 5.2 in order to conceive the joint ML detector using the different transmitted and received symbol blocks of the corresponding frames. The solid box represents that the related node is transmitting, while signal reception at a particular node is indicated by the dashed box.

$$\boldsymbol{K}(k-L_f) \triangleq [\underbrace{0,\cdots,0}_{q-1}, s(k-L_f), \underbrace{0,\cdots,0}_{Q-q}]^T \in \mathbb{C}^{Q\times 1} \tag{5.15}$$

$$\bar{\boldsymbol{V}}'_{v_i d}(k') = vec(\tilde{\boldsymbol{V}}'_{v_i d}(k')) \in \mathbb{C}^{T\times 1},\ i=1,2. \tag{5.16}$$

Here the equivalent signal vector $\boldsymbol{K}(k-L_f)$ has only a single non-zero symbol component $s(k-L_f)$ placed in the q-th position, $\boldsymbol{I}_T \in \mathbb{C}^{T\times T}$ is the identity matrix and $\otimes$ represents the Kronecker product, while $\bullet^T$ denotes the transpose of the matrix '$\bullet$'.

The combined received signal at the DN during both the frame-A and frame-B transmissions is constituted by the superposition of the signals arriving from the SN-DN link and the VAA-DN links, which can be expressed as [168]:

$$\begin{aligned}\boldsymbol{Y}^A(k') = {} & \tilde{h}_{sd}(k')C_A(s_f)\boldsymbol{S}_s(k) + \tilde{\boldsymbol{V}}_d(k') \\ & + \sqrt{G_{v_2 d}}\tilde{\boldsymbol{H}}'_{v_2 d}(k')C_B(s_f)\boldsymbol{A}_q(k-L_f)s(k-L_f) + \tilde{\boldsymbol{V}}'_{v_2 d}(k'),\end{aligned} \tag{5.17}$$

and

$$\boldsymbol{Y}^B(k') = \tilde{h}_{sd}(k')C_B(s_f)\boldsymbol{S}_s(k) + \tilde{\boldsymbol{V}}_d(k') + \sqrt{G_{v_1d}}\tilde{\boldsymbol{H}}'_{v_1d}(k')C_A(s_f)\boldsymbol{A}_q(k-L_f)s(k-L_f) + \tilde{\boldsymbol{V}}'_{v_1d}(k'). \tag{5.18}$$

Now, employing the double-frame matched-filter based despreading and defining the equivalent SN-DN channel transfer function by

$$\bar{h}_{sd}(k) \triangleq \frac{1}{S_f}\left[\tilde{h}_{sd}(k') + \tilde{h}_{sd}(k'+1) + \cdots + \tilde{h}_{sd}(k'+S_f-1)\right] \tag{5.19}$$

and the equivalent VAA2-DN channel matrix by

$$\bar{\boldsymbol{H}}_{v_2d}(k) \triangleq \frac{1}{S_f}\left[\bar{\boldsymbol{H}}'_{v_2d}(k') + \bar{\boldsymbol{H}}'_{v_2d}(k'+1) + \cdots + \bar{\boldsymbol{H}}'_{v_2d}(k'+S_f-1)\right] \tag{5.20}$$

where k is related to k' by $k = \left\lceil \frac{k'}{S_f} \right\rceil$ and $\lceil\cdot\rceil$ denotes the ceiling $(\cdot)$ operator, the pair of despread signals gleaned from the SN-DN and the VAA2-DN links can be extracted from $\boldsymbol{Y}^A(k')$ during the transmission of frame-A, which is given by

$$\boldsymbol{z}_s^A(k) = \bar{h}_{sd}(k)\boldsymbol{S}_s(k) + \boldsymbol{I}_{v_2}(k) + \boldsymbol{V}_d(k) \tag{5.21}$$

$$\bar{\boldsymbol{z}}_{v_2}^A(k) = \bar{\boldsymbol{H}}_{v_2d}(k)\boldsymbol{\chi}\boldsymbol{K}(k-L_f) + \boldsymbol{I}_s(k) + \boldsymbol{V}_{v_2d}(k). \tag{5.22}$$

Similarly, the despread signals from $\boldsymbol{Y}^B(k')$ during frame-B's transmission may be expressed as

$$\boldsymbol{z}_s^B(k) = \bar{h}_{sd}(k)\boldsymbol{S}_s(k) + \boldsymbol{I}_{v_1}(k) + \boldsymbol{V}_d(k) \tag{5.23}$$

$$\bar{\boldsymbol{z}}_{v_1}^B(k) = \bar{\boldsymbol{H}}_{v_1d}(k)\boldsymbol{\chi}\boldsymbol{K}(k-L_f) + \boldsymbol{I}_s(k) + \boldsymbol{V}_{v_1d}(k) \tag{5.24}$$

where $\bar{\boldsymbol{z}}_{v_2}^A(k)$ and $\bar{\boldsymbol{z}}_{v_2}^A(k)$ are the vectorially stacked despread signal from the VAA-DN links, $\boldsymbol{I}_s(k)$, $\boldsymbol{I}_{v_1}(k)$ and $\boldsymbol{I}_{v_2}(k)$ are the interference terms that are substantially mitigated by the specific spread-despread regime, especially at a high S_f and $\boldsymbol{V}_d(k)$, $\boldsymbol{V}_{v_1d}(k)$ and $\boldsymbol{V}_{v_2d}(k)$ are the AWGN terms imposed on the corresponding signals. We note that owing to the employment of SR in our scheme, the information is received by the DN from the direct SN-DN link as well as from the VAA-DN link during both the broadcast and the cooperation phase. This leads to the total normalized throughput of

$$R = \frac{b\cdot\log_2\mathcal{L}' + T\log_2(\mathcal{L}\cdot Q)}{b+T} = \frac{2\log_2(\mathcal{L}\cdot Q)}{b+T}\,[\text{bits/symbol duration}]\,, \tag{5.25}$$

which is twice that of the corresponding half-duplex scheme[1] [54]. This benefit, however, is achieved at the cost of supporting less users, because the available number of spreading sequences becomes less as a consequence of employing SR.

[1]We note that when invoking an MC-CDMA spreading factor of S_f, this throughput is commensurately reduced. However, when supporting $U = S_f$ users in a fully-loaded CDMA system, this throughput reduction is compensated.

5.4 Joint Single-Stream ML Detection of the Proposed Cooperative Scheme

The joint single-stream ML detector of our scheme detects the source information from the signals received from both the SN-DN and the VAA-DN links as detailed in [54,167], but takes the delay of the relayed frame due to both SR and the double-frame FD despreading [168] into account.

The different stages of the joint detection procedure appropriately combining the components of the transmitted, received and despread signals during the different transmission frames are visualized in Figure 5.4. It is plausible that due to the inherent nature of SR, the two replicas of the same frame, which are broadcast through the direct SN-DN link during the broadcast phase - with its counterpart forwarded by the VAA through the VAA-DN link in the consecutive cooperative phase - cannot arrive at the DN at the same time. Hence, as seen from Figure 5.4, joint detection of the transmitted information has to be carried out over two consecutive frames of the FD despread received signals.

Thus, the joint detection of the source information of a user broadcast by the SN during Frame-A is performed by combining the above-mentioned two replicas. This combination yields the Frame-A received sequence $\boldsymbol{Z}^A(k)$, which may be formally expressed as [54,167]:

$$\begin{aligned}\boldsymbol{Z}^A(k) &\triangleq \begin{bmatrix} \boldsymbol{z}_s^A(k) \\ \bar{\boldsymbol{z}}_{v_1}^B(k+L_f) \end{bmatrix} \\ &= \boldsymbol{H}_J^A(k)\bar{\boldsymbol{S}}_s(k) + \boldsymbol{V}_J(k) \in \mathbb{C}^{(b+T)\times 1} \end{aligned} \tag{5.26}$$

where we have

$$\bar{\boldsymbol{S}}_s(k) \triangleq \begin{bmatrix} \boldsymbol{S}_s(k) \\ \boldsymbol{K}(k) \end{bmatrix} \in \mathbb{C}^{(b+Q)\times 1} \tag{5.27}$$

$$\boldsymbol{N}_J(k) = \begin{bmatrix} \boldsymbol{I}_{v_2}(k) + \boldsymbol{V}_d(k) \\ \boldsymbol{I}_s(k+L_f) + \boldsymbol{V}_{v_1 d}(k+L_f) \end{bmatrix} \in \mathbb{C}^{(b+T)\times 1} \tag{5.28}$$

and the combined FD channel transfer matrix

$$\boldsymbol{H}_J(k) \triangleq \left[\begin{array}{c:c} \bar{h}_{sd}(k)\boldsymbol{I}_b & \boldsymbol{0}_{b\times Q} \\ \hdashline \boldsymbol{0}_{T\times b} & \bar{\boldsymbol{H}}_{v_1 d}(k+L_f)\boldsymbol{\chi} \end{array}\right] \in \mathbb{C}^{(b+T)\times(b+Q)}, \tag{5.29}$$

has two submatrices expressed by $\bar{h}_{sd}(k)\boldsymbol{I}_b \in \mathbb{C}^{b\times b}$ and $\bar{\boldsymbol{H}}_{v_1 d}(k+L_f)\boldsymbol{\chi} \in \mathbb{C}^{T\times Q}$ respectively and two zero-matrices.

Additionally, the equivalent transmit signal vector of the k-th block $\boldsymbol{K}(k)$ in (5.27) using the q-th DM and the l_c-th constellation symbol s_{l_c} may be expressed by

$$\boldsymbol{K}_{l_c,q} = \Big[\underbrace{0,\cdots,0}_{q-1}, s_{l_c}, \underbrace{0,\cdots,0}_{Q-q}\Big]^T \in \mathbb{C}^{Q\times 1}, \tag{5.30}$$

where s_{l_c} is placed exactly at the q-th position.

If the SR-imposed interference components $\boldsymbol{I}_{v_2}$ and $\boldsymbol{I}_s$ are approximated by noise processes, the equivalent noise process $\boldsymbol{V}_J$ can be assumed to be Gaussian-distributed having the same variance as $\boldsymbol{I}_{v_2}$ and $\boldsymbol{I}_s$.

The joint ML detector conceived for our cooperative scheme estimates the source information during Frame-A transmission of a particular user based on the FD despread direct SN-DN frame and on the FD despread frame arriving via the VAA1-DN link, which may be formulated as [52, 54]:

$$\begin{aligned}\left[\hat{q}(k), \hat{l_c}(k)\right] &= \arg\min_{q,l_c}\left\{\left|\left|\boldsymbol{Z}^A(k) - \boldsymbol{H}_J^A(k)\bar{\boldsymbol{S}}_s^{q,l_c}\right|\right|^2\right\} \\ &= \arg\min_{q,l_c}\left\{\left|\left|\boldsymbol{z}_s^A(k) - \bar{h}_{sd}(k)\boldsymbol{S}_s^{q,l_c}\right|\right|^2 + \left|\left|\bar{\boldsymbol{z}}_{v_1}^B(k+L_f) - s_{l_c}\left(\bar{\boldsymbol{H}}_{v_1d}(k+L_f)\boldsymbol{\chi}\right)_q\right|\right|^2\right\},\end{aligned} \tag{5.31}$$

where $\| \bullet \|$ represents the Euclidean norm of the matrix '$\bullet$', $\boldsymbol{S}_s^{q,l_c}$ and $\bar{\boldsymbol{S}}_s^{q,l_c}$ are the legitimate values of the symbol blocks $\boldsymbol{S}_s(k)$ and $\bar{\boldsymbol{S}}_s(k)$ specified by the indices (q, l_c), while $(\bar{\boldsymbol{H}}_{v_1d}(k+L_f)\boldsymbol{\chi})_q$ indicates the q-th column of $\bar{\boldsymbol{H}}_{v_1d}(k+L_f)\boldsymbol{\chi}$. As seen from Figure 5.4, the joint ML detector for the next consecutive frame can be formulated from $\boldsymbol{z}_s^B(k+L_f)$ and $\boldsymbol{z}_{v_2}^A(k+2L_f)$. Since the signal vectors received from the RNs during the VAA's cooperation phase are composed of the row vectors from a single DM, the joint detection scheme remains immune to the inter-stream interferences.

In a multiuser scenario the received sequence will be the superposition of the sequences corresponding to the individual users. Since the orthogonality of the spreading sequences of different users is destroyed by the dispersive channels, multiuser interference (MUI) is imposed. Upon reinstating the user index u, we can formulate the superposed destination signal with the aid of (5.3) and (5.10) in a form similar to (5.26), which has the additional MUI term seen below:

$$\begin{aligned}\boldsymbol{Y}^A(k') &= \sum_{u=1}^{U}\begin{bmatrix}\boldsymbol{Y}_{sd}^{A,u}(k') \\ \bar{\boldsymbol{Y}}_{v_1d}^{B,u}(k'+L_f\cdot S_f)\end{bmatrix} \\ &= \underbrace{\boldsymbol{H}_{J'}^{A,v}(k')\bar{\boldsymbol{S}}_c^v(k')}_{\text{desired user's signal}} + \underbrace{\sum_{\substack{u=1\\u\neq v}}^{U}\boldsymbol{H}_{J'}^{A,u}(k')\bar{\boldsymbol{S}}_c^u(k')}_{\text{MUI}} + \underbrace{\boldsymbol{V}_J^u(k')}_{\text{additive noise}}\end{aligned} \tag{5.32}$$

where $\bar{\boldsymbol{S}}_c^u(k')$, $\boldsymbol{N}_J^u(k')$ and $\boldsymbol{H}_{J'}^{A,u}(k')$ are defined similar to $\bar{\boldsymbol{S}}_s(k)$, $\boldsymbol{N}_J(k)$ and $\boldsymbol{H}_J^A(k)$ in (5.27), (5.28) and (5.29) respectively, but refer to the transmission of the spread symbol block indexed by k' of user u. Furthermore, the desired user has been denoted by v, the generalized user by u, whereas $u \neq v$ represents the interferring user.

A multiuser detector (MUD) [95,173] combined with the single-stream ML detector of [49,57] may be used in the multiuser scenario for jointly detecting the information of the different users. Since the source information of users in the k-th symbol block $\boldsymbol{S}_s^u(k)$ is spread over S_f blocks from $\boldsymbol{Y}^A(kS_f+1)$ to $\boldsymbol{Y}^A([k+1]S_f)$, the ML-MUD may be formulated as:

$$\left[\hat{\boldsymbol{q}}(k), \hat{\boldsymbol{l}}_{\boldsymbol{c}}(k)\right] = \arg\min_{\boldsymbol{q},\boldsymbol{l_c}} \sum_{s_f=1}^{S_f} \left\{ \left\| \boldsymbol{Y}_{sd}^{A,u}(k\cdot S_f+s_f) - \sum_{u=1}^{U} \tilde{h}_{sd}^u(k\cdot S_f+s_f) C_A^u(s_f) \boldsymbol{S}_s^{q^u,l_c^u} \right\|^2 + \left\| \bar{\boldsymbol{Y}}_{v_{1d}}^{B,u}([k+L_f]\cdot S_f+s_f) - \sum_{u=1}^{U} C_B^u(s_f) s_{l_c^u} \left(\bar{\boldsymbol{H}}_{v_1 d}^u([k+L_f]\cdot S_f+s_f)\boldsymbol{\chi}\right)_{q^u} \right\|^2 \right\} \quad (5.34)$$

in order to jointly estimate the set of indices for the DM, $\boldsymbol{q}(k) = \left\{q^1(k), \ldots, q^U(k)\right\}$ and the constellation symbol, $\boldsymbol{l_c}(k) = \left\{l_c^1(k), \ldots, l_c^U(k)\right\}$. In (5.34), the transmitted indices for the u-th user are represented by q^u and l_c^u respectively, $s_{l_c^u}$ denotes the l_c^u-th constellation symbol of user u and $(\bullet)_{q^u}$ indicates the q^u-th column of the matrix '$\bullet$'.

Equation (5.32) and (5.34) explicitly portray the MUI, but the MUD complexity escalates upon increasing the number of users, despite the fact that each user activates a single DM at a time, as indicated by the q^u-th column of the dispersion character matrix (DCM) $\boldsymbol{\chi}$ in (5.34).

5.5 Design of a Cooperative Noncoherent Multicarrier STSK Scheme

In this section, we introduce our differentially-encoded and non-coherently detected multicarrier cooperative STSK scheme relying on SR dispensing with any channel estimation. Figure 5.5 depicts the schematic of our cooperative differential MC STSK scheme. This arrangement retains all the benefits of its coherent counterpart, but typically requires a 3 dB higher power. As in the cooperative coherent MC STSK scheme of Figure 5.2, we assume two identical VAA arrangements whose architectures are shown explicitly in the dashed box of Figure 5.5.

Regarding our differential encoding scheme, the following points are worth mentioning with special emphasis:

1. The dispersion matrices we use for the differential cooperative STSK scheme are directly generated unitary matrices $\boldsymbol{A}_q\,(q=1,...,Q)$, which allow us to avoid the nonlinear Cayley transform of [49].

2. The differential encoding requires satisfying the STSK-related condition of relying on $M=T$, so that the resultant STSK signalling blocks are $(T\times T)$-element square matrices.

3. Differential encoding of the multicarrier based system can be performed either in the TD (differential encoding across the consecutive symbols of the same sub-carrier) or in the

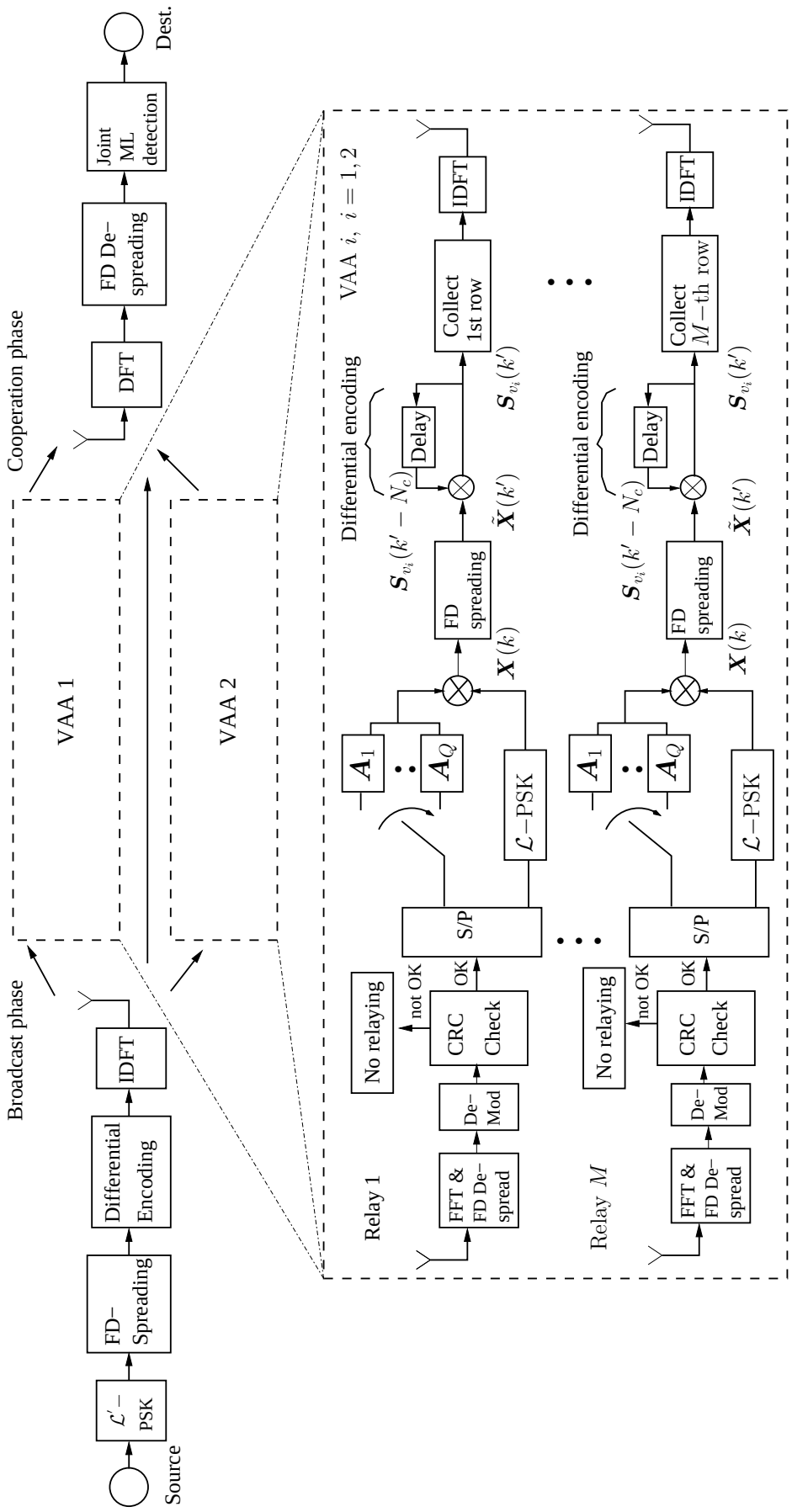

Figure 5.5: Schematic of our distributed MC DSTSK employing CRC-based selective DF relaying, which was developed from the cooperative coherent MC STSK scheme of Figure 5.2.

FD (differential encoding across the symbols of the adjacent sub-carriers of the same MC-CDMA block). We opted for invoking the TD approach, because our scheme was conceived for frequency-selective channels, which exhibit flat fading for the individual sub-carriers, while the FD channel envelope of the adjacent sub-carriers might be different.

5.5.1 The Source Node's Transmission Protocol

In the differential scheme we utilize $\mathcal{L}'-$ary differential phase-shift keying ($\mathcal{L}'$-DPSK) modulation at the SN. The SN's transmit blocks $\boldsymbol{S}_s(k) \triangleq [s_1(k), \ldots, s_b(k)]^T \in \mathbb{C}^{b\times 1}\, k = 1, 2, \ldots, L_f$ are spread in the FD in the same manner as in the coherent scheme of Subsection 5.3.1. The spread blocks $\boldsymbol{S}_c(k') = [s_{c,1}(k'), \ldots, s_{c,b}(k')]^T$ are obtained from $\boldsymbol{S}_s(k)$ according to $\boldsymbol{S}_c(k') = [C_A(s_f)\boldsymbol{S}_s(k)]$ or using $\boldsymbol{S}_c(k') = [C_B(s_f)\boldsymbol{S}_s(k)]$, where we have $s_f = 1, 2, \ldots, S_f$ and $k' = k \times S_f + s_f$, depending on which frame is being transmitted. The consecutive spread blocks under the same sub-carrier are placed N_c blocks apart in any transmission frame, where N_c is the number of sub-carriers. Hence, the differentially encoded transmit block $\boldsymbol{S}'_s(k') \in \mathbb{C}^{b\times 1}$ for $k' = -(N_c - 1), \ldots, 0, 1, 2, \ldots, S_f L_f$ at the SN of each transmission frame is related to $\boldsymbol{S}_c(k')$ by

$$\boldsymbol{S}'_s(k') = \begin{cases} [s'_1(k'), \ldots, s'_b(k')]^T & k' = 1, 2, \ldots, S_f L_f, \\ [\underbrace{1, 1, \ldots, 1}_{b}]^T & k' = -(N_c - 1), \ldots, 1, 0, \end{cases} \tag{5.35}$$

where we have:

$$s'_j(k') = s'_j(k' - N_c)s_{c,j}(k'), \quad j = 1, 2, \ldots, b. \tag{5.36}$$

The TD differential encoding process at the SN may be further explained with the aid of Figure 5.6. As noted, the consecutive symbols under the same sub-carrier of the spread blocks are placed N_c blocks apart. Hence, as shown in Figure 5.6, differential encoding is performed over these blocks, for example, over the blocks $\boldsymbol{S}_c(1)$, $\boldsymbol{S}_c(N_c + 1)$, $\boldsymbol{S}_c(2N_c + 1)$ etc. The differentially encoded transmit blocks $\boldsymbol{S}'_s(k')$ are generated using the differential encoding rules specified by (5.35) and (5.36) and are also shown in Figure 5.6.

Let us define the b_j-th symbol ($b_j = 1, 2, \ldots, b$) of the $k'-$th spread block $\boldsymbol{S}_c(k')$ by $S_c(k', b_j)$. Taking the TD differential en-/decoding operation into consideration, the FD signals $\boldsymbol{Y}^A_{sd}(k') \in \mathbb{C}^{b\times 1}$ and $\boldsymbol{Y}^B_{sd}(k') \in \mathbb{C}^{b\times 1}$ received at the DN from the direct SN-DN link during frame-A and frame-B may be expressed as [171]

$$\boldsymbol{Y}^A_{sd}(k') = \begin{bmatrix} Y^A_{sd}(k', 1) \\ Y^A_{sd}(k', 2) \\ \vdots \\ Y^A_{sd}(k', b) \end{bmatrix} = \begin{bmatrix} Y^A_{sd}(k' - N_c, 1)S_c(k', 1) \\ Y^A_{sd}(k' - N_c, 2)S_c(k', 2) \\ \vdots \\ Y^A_{sd}(k' - N_c, b)S_c(k', b) \end{bmatrix} + \begin{bmatrix} \tilde{V}^A_{sd}(k', 1) \\ \tilde{V}^A_{sd}(k', 2) \\ \vdots \\ \tilde{V}^A_{sd}(k', b) \end{bmatrix} \tag{5.37}$$

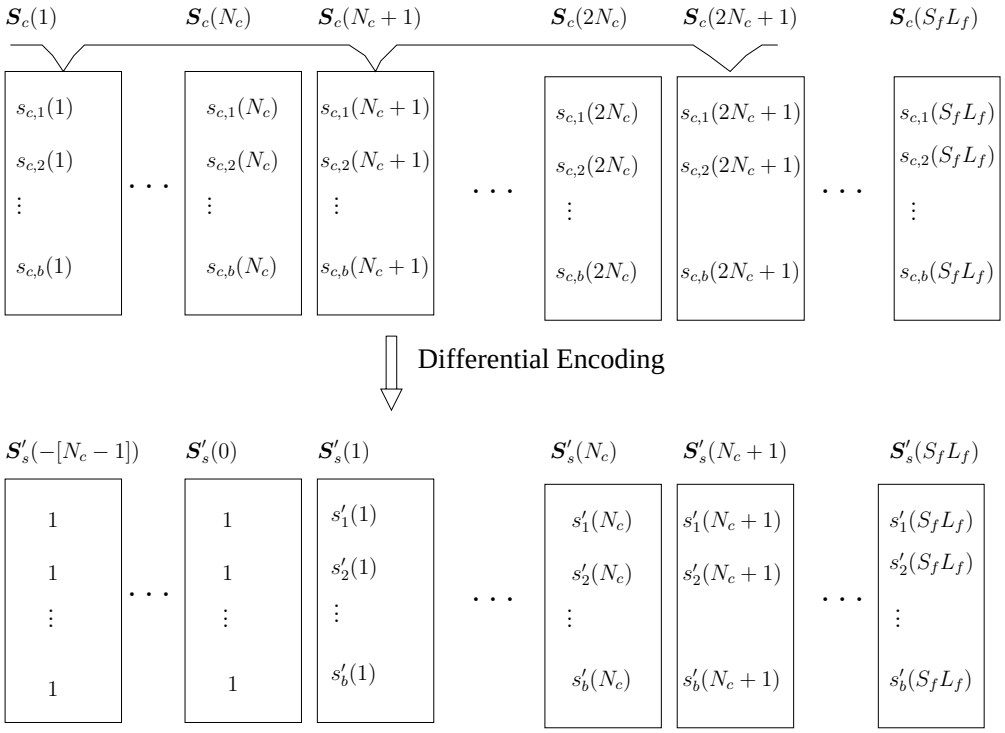

Figure 5.6: Illustration of the TD differential encoding process at the SN of our differential cooperative MC STSK arrangement shown in Figure 5.5. The FD-spread transmit blocks $\boldsymbol{S}_c(k')$ of a transmission frame are then differentially encoded across the same subcarrier blocks, which results in the final transmit blocks specified by $\boldsymbol{S}'_s(k')$, and generated using (5.35) and (5.36).

and

$$\boldsymbol{Y}^B_{sd}(k') = \begin{bmatrix} Y^B_{sd}(k',1) \\ Y^B_{sd}(k',2) \\ \vdots \\ Y^B_{sd}(k',b) \end{bmatrix} = \begin{bmatrix} Y^B_{sd}(k'-N_c,1)S_c(k',1) \\ Y^B_{sd}(k'-N_c,2)S_c(k',2) \\ \vdots \\ Y^B_{sd}(k'-N_c,b)S_c(k',b) \end{bmatrix} + \begin{bmatrix} \tilde{V}^B_{sd}(k',1) \\ \tilde{V}^B_{sd}(k',2) \\ \vdots \\ \tilde{V}^B_{sd}(k',b) \end{bmatrix}, \tag{5.38}$$

respectively, where $\tilde{\boldsymbol{V}}^A_{sd}(k') \in \mathbb{C}^{b\times 1}$ and $\tilde{\boldsymbol{V}}^A_{sd}(k') \in \mathbb{C}^{b\times 1}$ are the corresponding AWGN vectors.

Equations (5.37) and (5.38) may be rewritten as

$$\boldsymbol{Y}^A_{sd}(k') = \begin{bmatrix} Y^A_{sd}(k'-N_c,1) & 0 & \cdots & 0 \\ 0 & Y^A_{sd}(k'-N_c,2) & \cdots & 0 \\ \vdots & \vdots & \ddots & \vdots \\ 0 & 0 & \cdots & Y^A_{sd}(k'-N_c,b) \end{bmatrix} \begin{bmatrix} S_c(k',1) \\ S_c(k',2) \\ \vdots \\ S_c(k',b) \end{bmatrix} + \begin{bmatrix} \tilde{V}^A_{sd}(k',1) \\ \tilde{V}^A_{sd}(k',2) \\ \vdots \\ \tilde{V}^A_{sd}(k',b) \end{bmatrix} \tag{5.39}$$

and

$$\boldsymbol{Y}_{sd}^{B}(k') = \begin{bmatrix} Y_{sd}^{B}(k'-N_c,1) & 0 & \cdots & 0 \\ 0 & Y_{sd}^{B}(k'-N_c,2) & \cdots & 0 \\ \vdots & \vdots & \ddots & \vdots \\ 0 & 0 & \cdots & Y_{sd}^{B}(k'-N_c,b) \end{bmatrix} \begin{bmatrix} S_c(k',1) \\ S_c(k',2) \\ \vdots \\ S_c(k',b) \end{bmatrix} + \begin{bmatrix} \tilde{V}_{sd}^{B}(k',1) \\ \tilde{V}_{sd}^{B}(k',2) \\ \vdots \\ \tilde{V}_{sd}^{B}(k',b) \end{bmatrix}, \quad (5.40)$$

respectively. Defining $\boldsymbol{H}_{sd}^{A}(k')$ and $\boldsymbol{H}_{sd}^{B}(k')$ by

$$\boldsymbol{H}_{sd}^{A}(k') = \text{diag}\left\{Y_A'\left(k'-N_c,1\right),...,Y_A'\left(k'-N_c,b\right)\right\} \in \mathbb{C}^{b\times b} \quad (5.41)$$

and

$$\boldsymbol{H}_{sd}^{B}(k') = \text{diag}\left\{Y_B'\left(k'-N_c,1\right),...,Y_B'\left(k'-N_c,b\right)\right\} \in \mathbb{C}^{b\times b}, \quad (5.42)$$

respectively, where the notation $\text{diag}\left\{a_1,...,a_b\right\}$ represents a $(b\times b)-$element diagonal matrix having diagonal entries of $a_1,\ldots,a_b$, (5.39) and (5.40) reduce to

$$\boldsymbol{Y}_{sd}^{A}(k') = \boldsymbol{H}_{sd}^{A}(k')\left[C_A(s_f)\boldsymbol{S}_s(k)\right] + \tilde{\boldsymbol{V}}_{sd}^{A}(k') \quad (5.43)$$

and

$$\boldsymbol{Y}_{sd}^{B}(k') = \boldsymbol{H}_{sd}^{B}(k')\left[C_B(s_f)\boldsymbol{S}_s(k)\right] + \tilde{\boldsymbol{V}}_{sd}^{B}(k'), \quad (5.44)$$

respectively, where we have

$$\boldsymbol{S}_c(k') = \begin{cases} C_A(s_f)\boldsymbol{S}_s(k), & \text{Frame-A transmission,} \\ C_B(s_f)\boldsymbol{S}_s(k). & \text{Frame-B transmission.} \end{cases} \quad (5.45)$$

5.5.2 The Virtual Antenna Array

The RN m of VAA i transmits only the m-th row of the differentially encoded STSK codeword, while the STSK signalling block $\boldsymbol{X}(k) = s(k)\boldsymbol{A}_q(k) \in \mathbb{C}^{T\times T}$ is created from the correctly decoded bits at the RN by activating a single DM, $\boldsymbol{A}_q(k)\,(q=1,...,Q)$ for the transmission of the $\mathcal{L}$-PSK or $\mathcal{L}$-QAM symbol, $s(k)=s_l$. The STSK space-time codeword $\boldsymbol{X}(k)$ is further FD spread to $\tilde{\boldsymbol{X}}(k') = C_A(s_f)\boldsymbol{X}(k) \in \mathbb{C}^{T\times T} \quad s_f = 1,2,\ldots,S_f$ or to $\tilde{\boldsymbol{X}}(k') = C_B(s_f)\boldsymbol{X}(k) \in \mathbb{C}^{T\times T} \quad s_f = 1,2,\ldots,S_f$, depending on which frame is being transmitted, where $k = \left\lceil \frac{k'}{S_f} \right\rceil$ and $s_f = \left([k']_{S_f}\right)$ ('$[\cdot]_{S_f}$' denotes the modulo-S_f operator). So for the VAA-DN link, we have the

differentially encoded codeword $\boldsymbol{S}_{v_i}(k') \in \mathbb{C}^{T\times T}$ expressed by

$$\boldsymbol{S}_{v_i}(k') = \begin{cases} \boldsymbol{S}_{v_i}(k'-N_c)\tilde{\boldsymbol{X}}(k') & k' = 1, 2, \ldots, S_f L_f, \\ \boldsymbol{I}_T & k' = -(N_c-1), \ldots, 1, 0 \end{cases} \tag{5.46}$$

for each transmit frame, where $\boldsymbol{I}_T \in \mathbb{C}^{T\times T}$ denotes the identity matrix.

5.5.3 Joint Detection at The Destination Node

Defining the signals received via the VAA-DN links $\boldsymbol{Y}^A_{v_2d}(k') \in \mathbb{C}^{1\times T}$ and $\boldsymbol{Y}^B_{v_1d}(k') \in \mathbb{C}^{1\times T}$ in terms of the relay activation parameter α_m as in (5.5) and (5.6), we have

$$\boldsymbol{Y}^A_{v_2d}(k') = \boldsymbol{Y}^A_{v_2d}(k'-N_c)C_B(s_f)\boldsymbol{X}(k-L_f) + \bar{\boldsymbol{V}}'_{v_2d}(k') \tag{5.47}$$

$$\boldsymbol{Y}^B_{v_1d}(k') = \boldsymbol{Y}^B_{v_1d}(k'-N_c)C_A(s_f)\boldsymbol{X}(k-L_f) + \bar{\boldsymbol{V}}'_{v_1d}(k') \tag{5.48}$$

where $\bar{\boldsymbol{V}}'_{v_2d}(k') \in \mathbb{C}^{1\times T}$ and $\bar{\boldsymbol{V}}'_{v_1d}(k') \in \mathbb{C}^{1\times T}$ are the corresponding AWGN vector.

Replacing $\boldsymbol{Y}^A_{v_2d}(k'-N_c)$ and $\boldsymbol{Y}^B_{v_1d}(k'-N_c)$ by $\mathbb{H}_{v_2d}(k')$ and $\mathbb{H}_{v_1d}(k')$ respectively for the differential scheme, the equivalent received signals $\bar{\boldsymbol{Y}}^A_{v_2d}(k') = vec\left[\boldsymbol{Y}^A_{v_2d}(k')\right] \in \mathbb{C}^{T\times 1}$ and $\bar{\boldsymbol{Y}}^B_{v_1d}(k') = vec\left[\boldsymbol{Y}^B_{v_1d}(k')\right] \in \mathbb{C}^{T\times 1}$ may be expressed as:

$$\bar{\boldsymbol{Y}}^A_{v_2d}(k') = \boldsymbol{H}_{v_2d}(k')C_B(s_f)\boldsymbol{\chi}\boldsymbol{K}(k-L_f) + \breve{\boldsymbol{V}}'_{v_2d}(k') \tag{5.49}$$

$$\bar{\boldsymbol{Y}}^B_{v_1d}(k') = \boldsymbol{H}_{v_1d}(k')C_A(s_f)\boldsymbol{\chi}\boldsymbol{K}(k-L_f) + \breve{\boldsymbol{V}}'_{v_1d}(k') \tag{5.50}$$

where

$$\boldsymbol{H}_{v_2d}(k') = \sqrt{G_{v_id}}[\boldsymbol{I}_T \otimes \mathbb{H}_{v_2d}(k')] \in \mathbb{C}^{T\times MT}, \tag{5.51}$$

$$\boldsymbol{H}_{v_1d}(k') = \boldsymbol{I}_T \otimes \mathbb{H}_{v_1d}(k')] \in \mathbb{C}^{T\times MT}, \tag{5.52}$$

$$\breve{\boldsymbol{V}}'_{v_2d}(k') = vec\left[\bar{\boldsymbol{N}}'_{v_2d}(k')\right] \in \mathbb{C}^{T\times 1}, \tag{5.53}$$

$$\breve{\boldsymbol{V}}'_{v_1d}(k') = vec\left[\bar{\boldsymbol{N}}'_{v_1d}(k')\right] \in \mathbb{C}^{T\times 1} \tag{5.54}$$

and

$$M = T. \tag{5.55}$$

Applying FD double-frame matched filter based despreading at the DN, we obtain

$$\boldsymbol{z}^A_s(k) = \bar{\boldsymbol{H}}^A_{sd}(k)\boldsymbol{S}_s(k) + \boldsymbol{I}_{v_2}(k) + \boldsymbol{V}^A_{sd}(k) \tag{5.56}$$

$$\bar{\boldsymbol{z}}^A_{v_2}(k) = \breve{\boldsymbol{H}}_{v_2d}(k)\boldsymbol{\chi}\boldsymbol{K}(k-L_f) + \boldsymbol{I}_s(k) + \boldsymbol{V}_{v_2d}(k) \tag{5.57}$$

$$\boldsymbol{z}^B_s(k-L_f) = \bar{\boldsymbol{H}}^B_{sd}(k-L_f)\boldsymbol{S}_s(k-L_f) + \boldsymbol{I}_{v_1}(k-L_f) + \boldsymbol{V}^B_{sd}(k-L_f) \tag{5.58}$$

$$\bar{\boldsymbol{z}}^B_{v_1}(k+L_f) = \breve{\boldsymbol{H}}_{v_1d}(k+L_f)\boldsymbol{\chi}\boldsymbol{K}(k) + \boldsymbol{I}_s(k+L_f) + \boldsymbol{V}_{v_1d}(k+L_f) \tag{5.59}$$

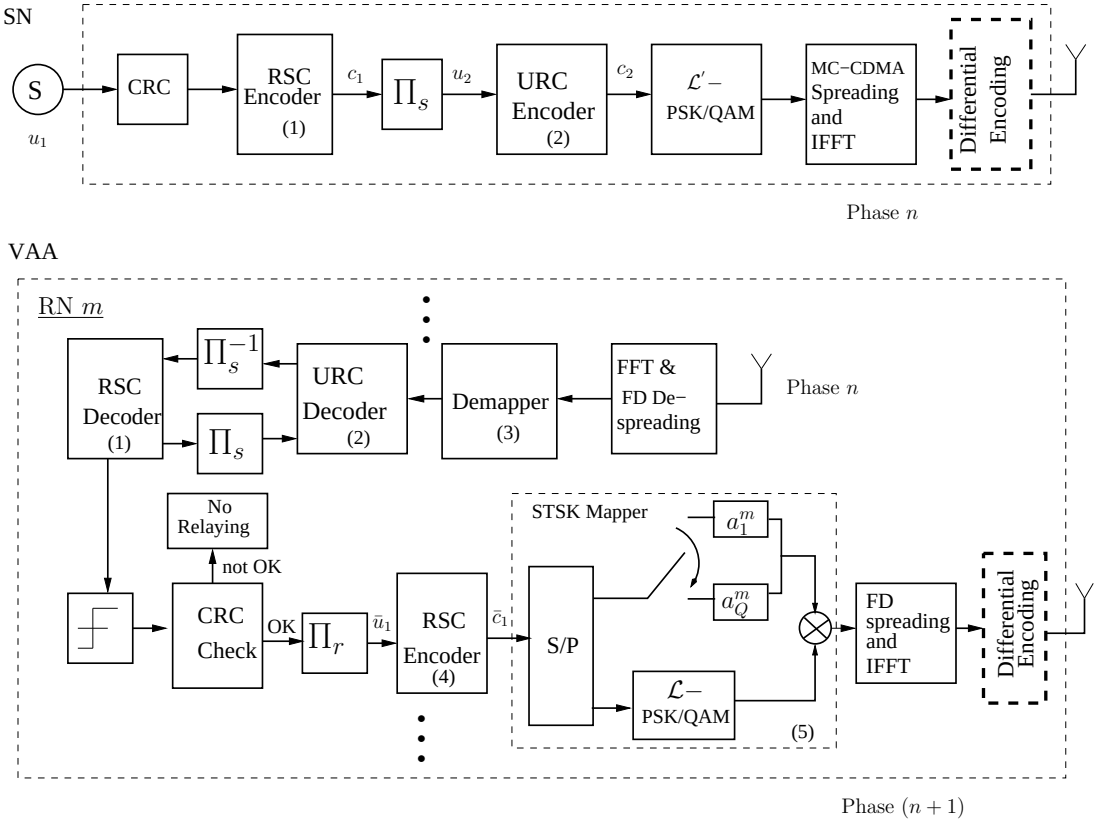

Figure 5.7: Transmission model of near-capacity RSC and URC-aided SN and RNs of the cooperative multi-carrier scheme between two VAAs.

where $\bar{\boldsymbol{H}}_{sd}^{A}(k)$, $\bar{\boldsymbol{H}}_{sd}^{B}(k)$, $\breve{\boldsymbol{H}}_{v_1d}(k)$ and $\breve{\boldsymbol{H}}_{v_2d}(k)$ are related to $\boldsymbol{H}_{sd}^{A}(k')$, $\boldsymbol{H}_{sd}^{B}(k')$, $\boldsymbol{H}_{v_1d}(k')$ and $\boldsymbol{H}_{v_2d}(k')$, respectively in a similar manner as in (5.19) and (5.20).

The joint ML detector of (5.31) can now be applied, employing $\boldsymbol{z}_s^A(k)$, $\bar{\boldsymbol{z}}_{v_1}^B(k+L_f)$, $\bar{\boldsymbol{H}}_{sd}^{A}(k)$ and $\breve{\boldsymbol{H}}_{v_2d}(k+L_f)$ to estimate the Frame-A information. For the estimation of Frame-B signal, the joint ML detector of (5.31) has to be applied employing $\boldsymbol{z}_s^B(k-L_f)$, $\bar{\boldsymbol{z}}_{v_2}^A(k)$, $\bar{\boldsymbol{H}}_{sd}^{B}(k-L_f)$ and $\breve{\boldsymbol{H}}_{v_2d}(k)$.

5.6 Soft-Decision SR Multicarrier Cooperative STSK

In this section, we propose the powerful channel-coded cooperative scheme illustrated in Figure 5.7 and Figure 5.8, which employs soft-decision based iterative detection. As demonstrated in Figure 5.7, our transmitter consists of a three-stage serially concatenated recursive systematic convolutional (RSC) and unity-rate coding (URC)-aided $\mathcal{L}$-PSK/QAM mapper followed by the MC-CDMA FD spreader plus the IFFT module based modulator. At each of the RNs of each VAA, the same two-component serially concatenated RSC-URC scheme is amalgamated with our multi-carrier based STSK despread/spread and de/encode regime. The blocks Π_s and Π_r in Figure 5.7 represent the random bit interleavers used both at the SN and at each RN

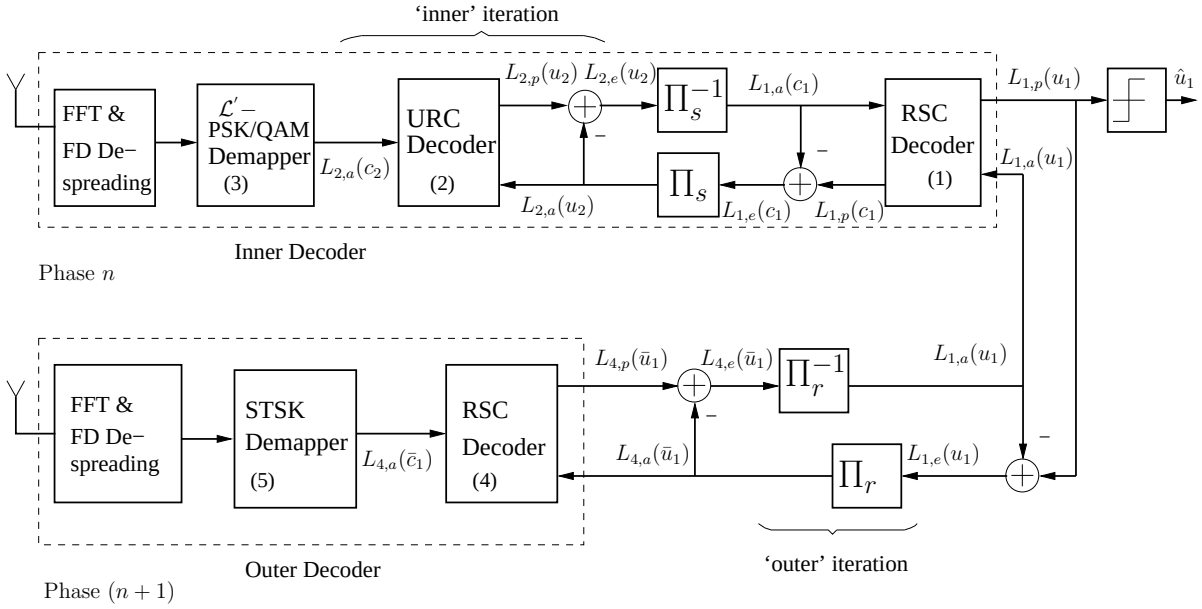

Figure 5.8: The three-stage iterative detector at destination.

of each VAA. Our soft-decision based scheme can be employed for both the coherent and for the differential cooperative multi-carrier STSK arrangement, where the latter has a differential encoding block before the transmit antenna. The differential encoding block is shown dotted in Figure 5.7.

The iterative receiver of the destination in our three-stage cooperative arrangement is portrayed in Figure 5.8. The signals received after FFT and FD despreading during phase n at the destination node (DN) are detected iteratively. Except for the first and last phase of the $(N+1)$-phase relaying protocol, the DN jointly detects the information of phase n gleaned from the signals received from the SN in addition to that acquired via the VAA during phase $(n+1)$. As such, the relayed signal of frame $(n+1)$ is jointly detected with the SN's signal of frame n, while that from the relayed frame n is treated as interference.

The conditional probability $P\left(\boldsymbol{Z}^A(k) \mid \bar{\boldsymbol{S}}_s^{q,l_c}, \boldsymbol{H}_J(k)\right)$ can be deduced according to the system model described by (5.26) as:

$$P\left(\boldsymbol{Z}^A(k) \mid \bar{\boldsymbol{S}}_s^{q,l_c}, \boldsymbol{H}_J(k)\right) = \frac{1}{(\pi N_0)^{b+T}} e^{-\frac{\left\|\boldsymbol{Z}^A(k) - \boldsymbol{H}_J^A(k)\bar{\boldsymbol{S}}_s^{q,l_c}\right\|^2}{N_0}} \tag{5.60}$$

where

$$\left\|\boldsymbol{Z}^A(k) - \boldsymbol{H}_J^A(k)\bar{\boldsymbol{S}}_s^{q,l_c}\right\|^2 = \left\| \begin{bmatrix} \boldsymbol{z}_s^A(k) \\ \bar{\boldsymbol{z}}_{v_1}^B(k+L_f) \end{bmatrix} - \begin{bmatrix} \bar{h}_{sd}(k)\boldsymbol{S}_s^{q,l_c} \\ \bar{\boldsymbol{H}}_{v_1 d}(k+L_f)\boldsymbol{\chi}\boldsymbol{K}_{l_c,q} \end{bmatrix} \right\|^2 \tag{5.61}$$

and $\boldsymbol{S}_s^{q,l_c}(k)$ and $\bar{\boldsymbol{S}}_s^{q,l_c}(k)$ represent the symbol blocks as discussed in Section 5.4 and specified by the indices (q, l_c). For the differential scheme, the substitutions detailed in Section 5.5 have

to be made.

We note that if at stage n, the equivalent FD received signal $\boldsymbol{z}_s^A(k)$ received directly from the SN carries B channel-coded bits $b = [b_1, b_2, ..., b_B]$, then the extrinsic logarithmic-likelihood ratio (LLR) of bits, $b_k,\ k = 1, ..., B$ gleaned from the demapper can be expressed as [5, 143]:

$$L_{3,e}(b_k) = \ln \frac{\sum_{\boldsymbol{S}_s^{q,l_c} \in \boldsymbol{S}_1} \exp\left[-\frac{\left\| \boldsymbol{z}_s^A(k) - \bar{h}_{sd}(k) \boldsymbol{S}_s^{q,l_c} \right\|^2}{N_0} + \sum_{j \neq k} b_j L_{3,a}(b_j) \right]}{\sum_{\boldsymbol{S}_s^{q,l_c} \in \boldsymbol{S}_0} \exp\left[-\frac{\left\| \boldsymbol{z}_s^A(k) - \bar{h}_{sd}(k) \boldsymbol{S}_s^{q,l_c} \right\|^2}{N_0} + \sum_{j \neq k} b_j L_{3,a}(b_j) \right]} \tag{5.62}$$

where $\boldsymbol{S}_1$ and $\boldsymbol{S}_0$ represent the subsets of the legitimate signal vectors transmitted directly by the SN-DN link $\boldsymbol{S}_s(k)$ corresponding to bits $b_k = 1$ and $b_k = 0$, respectively and $L_{3,a}(b_j)$ is the *a priori* LLR corresponding to the "inner" decoder bits b_j.

Similarly the $(n+1)$ stage LLRs acquired from the VAA demapper for the same bits $b_k,\ k = 1, ..., B$ obtained from $\boldsymbol{z}_{v_1}^B(k + L_f)$ can be formulated as:

$$L_{5,e}(b_k) = \ln \frac{\sum_{\boldsymbol{K}_{l_c,q} \in \boldsymbol{K}_1} \exp\left[-\frac{\left\| \boldsymbol{z}_{v_1}^B(k+L_f) - \bar{\boldsymbol{H}}_{v_1 d}(k+L_f) \boldsymbol{\chi} \boldsymbol{K}_{l_c,q} \right\|^2}{N_0} + \sum_{j \neq k} b_j L_{5,a}(b_j) \right]}{\sum_{\boldsymbol{K}_{l_c,q} \in \boldsymbol{K}_0} \exp\left[-\frac{\left\| \boldsymbol{z}_{v_1}^B(k+L_f) - \bar{\boldsymbol{H}}_{v_1 d}(k+L_f) \boldsymbol{\chi} \boldsymbol{K}_{l_c,q} \right\|^2}{N_0} + \sum_{j \neq k} b_j L_{5,a}(b_j) \right]}, \tag{5.63}$$

where $\boldsymbol{K}_1$ and $\boldsymbol{K}_0$ represent the subspaces of the possible equivalent transmit vectors $\boldsymbol{K}$ for $b_k = 1$ and $b_k = 0$, respectively, while $L_{5,a}(b_j)$ is the *a priori* LLR of the "outer" decoder corresponding to bits b_j.

Equations (5.62) and (5.63) can be re-written using the approximate-logarithmic-maximum *a posteriori* (Approx-log-MAP) algorithm [145, 155] as

$$\begin{aligned} L_{3,e}(b_k) \quad = \quad & \underset{\boldsymbol{S}_s^{q,l_c} \in \boldsymbol{S}_1}{\text{jac}} \left[-\frac{\left\| \boldsymbol{z}_s^A(k) - \bar{h}_{sd}(k) \boldsymbol{S}_s^{q,l_c} \right\|^2}{N_0} + \sum_{j \neq k} b_j L_{3,a}(b_j) \right] \\ & - \underset{\boldsymbol{S}_s^{q,l_c} \in \boldsymbol{S}_0}{\text{jac}} \left[-\frac{\left\| \boldsymbol{z}_s^A(k) - \bar{h}_{sd}(k) \boldsymbol{S}_s^{q,l_c} \right\|^2}{N_0} + \sum_{j \neq k} b_j L_{3,a}(b_j) \right], \end{aligned} \tag{5.64}$$

and

$$\begin{aligned} L_{5,e}(b_k) \quad = \quad & \underset{\boldsymbol{K}_{l_c,q} \in \boldsymbol{K}_1}{\text{jac}} \left[-\frac{\left\| \boldsymbol{z}_{v_1}^B(k+L_f) - \bar{\boldsymbol{H}}_{v_1 d}(k+L_f) \boldsymbol{\chi} \boldsymbol{K}_{l_c,q} \right\|^2}{N_0} + \sum_{j \neq k} b_j L_{5,a}(b_j) \right] \\ & - \underset{\boldsymbol{K}_{l_c,q} \in \boldsymbol{K}_0}{\text{jac}} \left[-\frac{\left\| \boldsymbol{z}_{v_1}^B(k+L_f) - \bar{\boldsymbol{H}}_{v_1 d}(k+L_f) \boldsymbol{\chi} \boldsymbol{K}_{l_c,q} \right\|^2}{N_0} + \sum_{j \neq k} b_j L_{5,a}(b_j) \right], \end{aligned} \tag{5.65}$$

respectively, where $\underset{\boldsymbol{S}_s^{q,l_c}\in\boldsymbol{S}_1}{\text{jac}}[\bullet]$, $\underset{\boldsymbol{S}_s^{q,l_c}\in\boldsymbol{S}_o}{\text{jac}}[\bullet]$, $\underset{\boldsymbol{K}_{l_c,q}\in\boldsymbol{K}_1}{\text{jac}}[\bullet]$ and $\underset{\boldsymbol{K}_{l_c,q}\in\boldsymbol{K}_0}{\text{jac}}[\bullet]$ represent the Jacobian logarithm of the expression '$\bullet$' under the conditions specified by $\boldsymbol{S}_s^{q,l_c} \in \boldsymbol{S}_1$, $\boldsymbol{S}_s^{q,l_c} \in \boldsymbol{S}_0$, $\boldsymbol{K}_{l_c,q} \in \boldsymbol{K}_1$ and $\boldsymbol{K}_{l_c,q} \in \boldsymbol{K}_0$, respectively. We repeat here that the substitutions detailed in Section 5.5 have to be made for the differential scheme.

Now the exchange of extrinsic information takes place between the DN's demapper-URC-RSC decoder processing frame n (which may be referred to as the "inner" decoder) and the STSK demapper-URC block detecting the VAA frame $(n+1)$ (treated as the "outer" decoder). The extrinsic LLR is apprpriately interleaved and deinterleaved by the SN as well as by the VAA interleavers and deinterleavers Π_s, Π_s^{-1}, Π_r and Π_r^{-1} respectively, for the sake of generating the appropriate *a priori* LLRs for the next iteration. During the last "outer" iteration, the LLR values $L_{1,p}(u_1)$ of the original information bits u_1 are passed to the hard-decision block of Figure 5.8 for estimating the source information. The source information of the next frame is detected in the same manner, processing the frame received directly from the SN by the DN and the relayed frame received during the consecutive cooperative frame from the other VAA. This process continues, until the detection of the last frame is completed.

5.7 Performance of the Proposed Cooperative Scheme

In this section, the performance of our cooperative multi-carrier STSK scheme relying on the parameters of Table 5.2 is investigated and compared to that of our benchmark schemes. The performance of the STSK based scheme, especially its diversity-multiplexing tradeoff depends mainly on the specific objective function (OF) used for the optimization of the DMs utilized [57]. More explicitly, the pre-assigned spreading matrices can be optimized using different OFs, as detailed in [5, 32]. We have employed an exhaustive search over 10^6 candidate DM sets for minimizing the pairwise symbol error probability (PSEP) under the power constraint as mentioned in Subsection 5.3.2 for the optimization of the DMs used in our proposed scheme. Further detailed discussions on the spreading matrix design can be found in [131, 132, 134].

5.7.1 BER Performance of the Coherent Cooperative MC STSK

Figure 5.9 shows the bit-error ratio (BER) performance of the coherent cooperative multi-carrier STSK(2,2,4) scheme employing QPSK modulation and compares the performances of different DF schemes in the dispersive typical-urban (TU) scenario characterized by the COST 207-TU12 channel model. The detailed power delay profile of the 12 taps which determine the coherence bandwidth and/or delay spread of this channel model may be found in [139] and in [141]. The delay spread of the channel is found to be $\sigma_\tau = 1.0\,\mu s$, which determines

Table 5.2: Simulation parameters adopted for SR-aided MC STSK scheme

Simulation Parameter	*Adopted Value*
Fast fading model	Correlated Rayleigh fading
Doppler frequency	0.01
Channel specification	COST 207-TU12, 12-tap channel delay-spread = 1.0 μs [141]
No. of subcarriers	64, 256 (used only for $S_f = 256$)
Length of cyclic prefix	32
Symbol duration, $\mathcal{T}$	$500\,ns$
CRC code	CRC - 4
Path loss co-efficient, α	4
No. of RNs in a VAA, M	2
No. of Tx time slots, T	2
Distance of VAA from SN	1/3 of SN-DN distance
No. of dispersion matrices	$Q = 2, 4$
Distributed STSK specification	$(M = 2, T = 2, Q = 2, 4)$
Modulation order	2, 4
Spreading codes	Walsh-Hadamard
Spreading factor	16, 64, 256
RSC code	$(2, 1, 2)$
Generator polynomials	$(g_r, g) = (3, 2)_8$
Size of interleavers	$240,000$ bits
Inner decoding iterations	2
Outer decoding iterations	6

the coherence bandwidth according to [174]: $B_c = \dfrac{1}{(2\pi) \cdot \sigma_\tau} \approx 160$ KHz, where the value of the constant $\alpha = 2\pi$ is assumed according to [175]. These channel parameters and the overall system's symbol duration of $\mathcal{T} = 500\,ns$ demonstrate that the individual subchannels experience frequency-flat fading and the length of cyclic prefices adopted in Table 5.2 ensures the absence of ISI. The different DF schemes compared in our investigations, however, are: 1) the perfect DF scheme, 2) the proposed scheme assuming perfect interference cancellation, 3) the proposed SR scheme employing CRC based selective DF and 4) the conventional DF scheme. The perfect DF scheme represents the proposed scheme assuming perfect decoding at the RNs i.e. where all the RNs of each VAA take part in cooperation, while the conventional DF schemes allow re-transmissions from the VAA RNs without checking whether any decoding error has occurred at the RNs or not. Finally, the perfect interference cancellation oriented

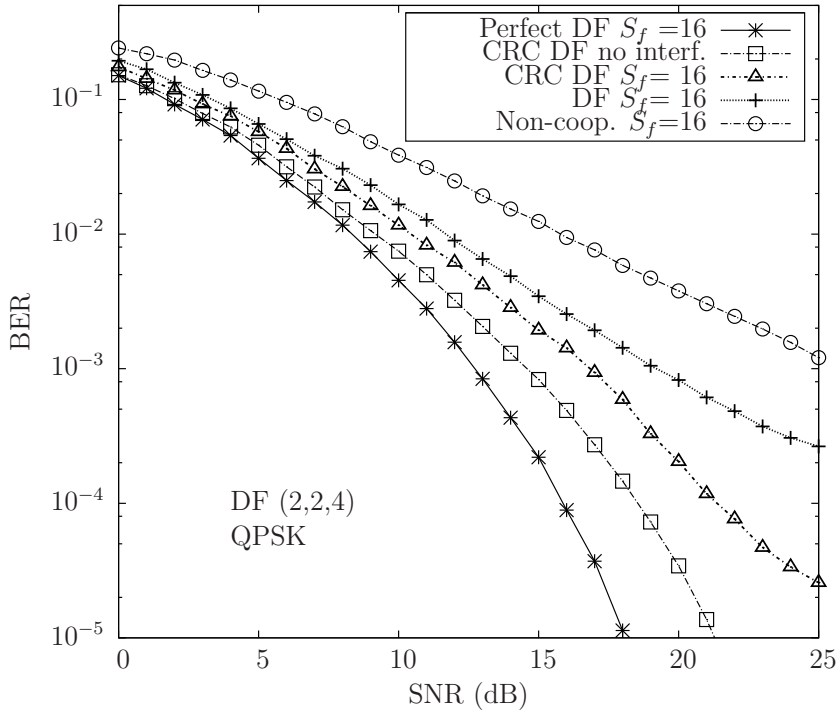

Figure 5.9: BER performance of our single user selective SR multicarrier cooperative coherent STSK ($M = 2, T = 2, Q = 4$), QPSK scheme of Figure 5.2 with $S_f = 16$ in the dispersive COST207-TU12 channel and other parameters as shown in Table 5.2 compared against different scenarios, such as the perfect DF scheme, CRC based scheme assuming perfect interference cancellation, cooperative DF scheme without CRC activation and against the non-cooperative QPSK scenario.

scheme assumes that no SR-induced interference is imposed. The BER performance of the non-cooperative scenario employing QPSK modulation and the same parameters is also shown in Figure 5.9. We observe that the proposed CRC-activated scheme can benefit from a higher diversity gain than either the conventional DF or the non-cooperative schemes and attains an increased throughput as a benefit of using SR.

In order to investigate the performance of the interference mitigation process using a double-frame matched-filter, the scheme was further studied using spreading codes having different spreading factors. To be specific, the investigations were carried out using the CRC-activated cooperative multi-carrier STSK ($M = 2, T = 2, Q = 2$) scheme employing BPSK modulation relying on $S_f = 16$, 64, 256 and the parameters of Table 5.2. The corresponding performance results are presented in Figure 5.10. The performance of the proposed scheme is again compared against those of the four different DF schemes as in Figure 5.9 and of the non-cooperative BPSK scenario. Observe in Figure 5.10 that our MC-CDMA based scheme succeeds in circumventing the channel-induced dispersion and exhibits an improved performance upon increasing the spreading factor. Upon increasing S_f, the scheme provides additional FD diversity gains and the specific FD despreading mitigates the SR-induced interferences.

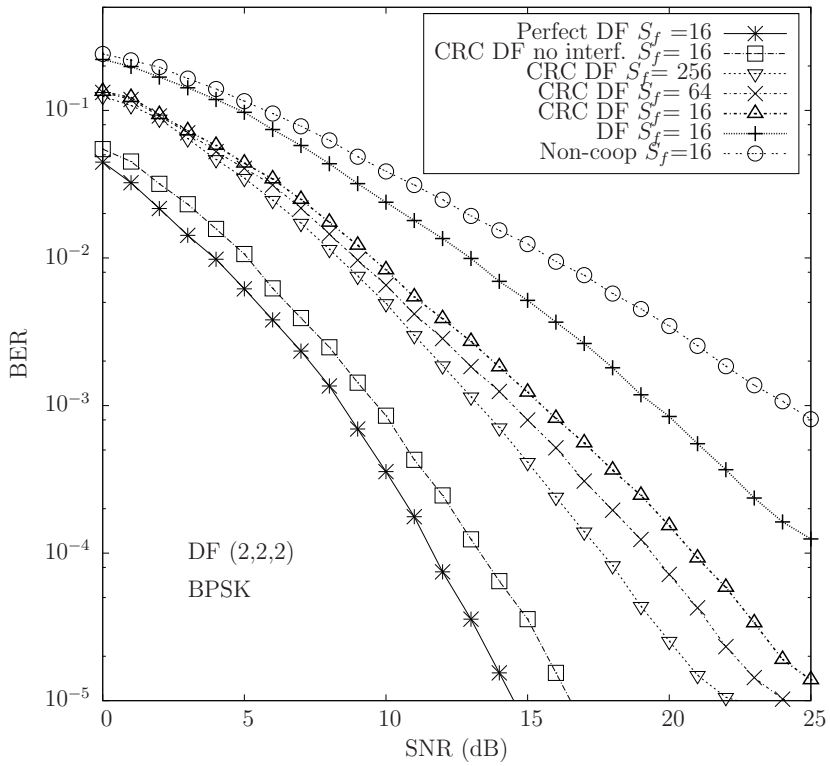

Figure 5.10: Achievable BER performance of the proposed ($M = 2, T = 2, Q = 2$) scheme of Figure 5.2 in conjunction with BPSK modulation having $S_f = 16$, 64, 256, under single user scenario in dispersive COST 207-TU12 channel using other parameters listed in Table 5.2. The performance is compared against those with the perfect DF cooperation and with the scheme having complete interference cancellation. The non-cooperative benchmarker having the same parameters and the same throughput is also shown.

5.7.2 Effect of VAA Location and Multiuser Performance

The performance of the proposed cooperative MC-CDMA STSK ($M = 2, T = 2, Q = 2$) scheme employing BPSK modulation associated with $S_f = 256$ and recorded for different geographical positions of the VAAs is shown in Figure 5.11, together with the achievable multiuser performance. The shapes of the performance curves in single-user scenarios were observed to be shifted towards higher or lower SNRs owing to the location-related reduced or increased channel gains, respectively. The performance achieved when supporting $U = 4$ users and a SN-VAA distance of 1/3 relative to the direct SN-DN link is shown in Figure 5.11, which is observed to be degraded by MUI. The performance erosion may, however, be mitigated by employing a MUD formulated in (5.34). The scheme employing OFDMA and SC-FDMA using FD minimum mean square error (MMSE) equalization and localized subcarrier allocation supporting $U = 4$ users, on the other hand, exhibits a further degraded performance as shown in Figure 5.11. This degradation is a consequence of the SR-induced IRI and CCI, demonstrating the benefits of MC-CDMA compared to other candidate multicarrier systems.

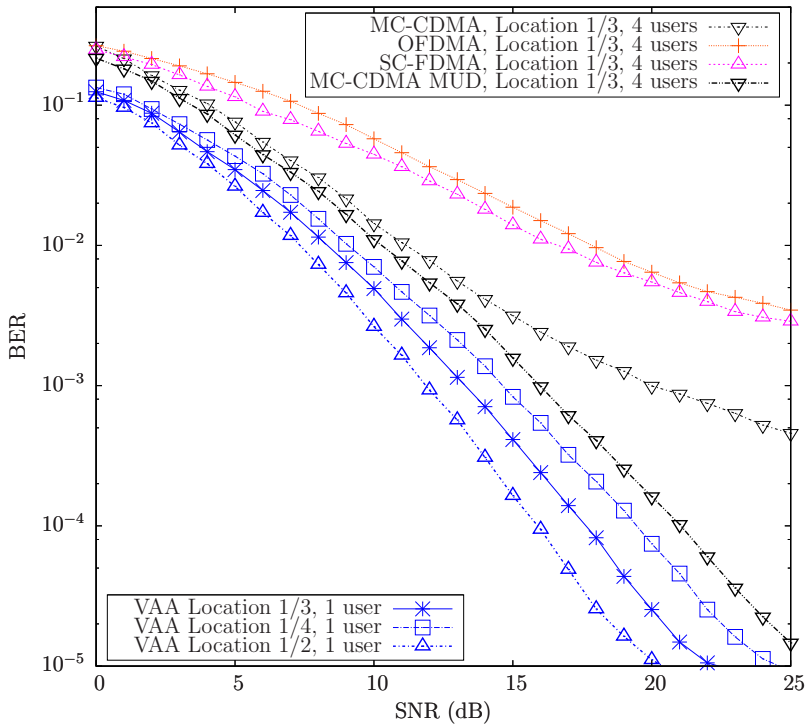

Figure 5.11: Performance of the single user cooperative MC-CDMA STSK ($M = 2, T = 2, Q = 2$) scheme employing BPSK modulation of Figure 5.2 under different SN-VAA distances relative to the direct SN-DN distance employing the simulation parameters listed in Table 5.2. Achievable performance employing different multicarrier systems namely, MC-CDMA with $S_f = 256$, OFDMA, SC-FDMA using FD MMSE equalization supporting $U = 4$ users and 1/3 relative SN-VAA distance is also shown, together with the MC-CDMA performance of the ML-MUD as proposed in (5.34).

5.7.3 BER Performance of the Noncoherent Cooperative MC STSK

The performance of our cooperative differential STSK ($M = 2, T = 2, Q = 2$) scheme relying on BPSK modulation having $S_f = 256$ is characterized in Figure 5.12, which may be directly compared to its coherent counterpart. The effects of the channel state information (CSI) estimation error associated with the coherent scheme are also investigated. More particularly, we assume the channel estimation errors to be Gaussian distributed and the level of CSI errors is quantified in terms of an equivalent CSI-error signal-to-noise ratio (SNR) of $\omega = -10$ and -5 dB below the received signal power. For example, the perfect CSI scenario corresponds to $\omega = -\infty$ dB, while $\omega = -10$ dB represents a CSI error power, which is one-tenth of the received signal power. Observe from Figure 5.12 that the differential scheme suffers from a performance penalty of about 3 dB compared to the perfect-CSI aided coherent scheme owing to the inherent noise doubling process of differential encoding. By contrast, the cooperative coherent scheme's performance was degraded severely by the inevitable CSI estimation errors. The FD spreading renders our scheme less susceptible to CSI errors, because a bit might still become recoverable

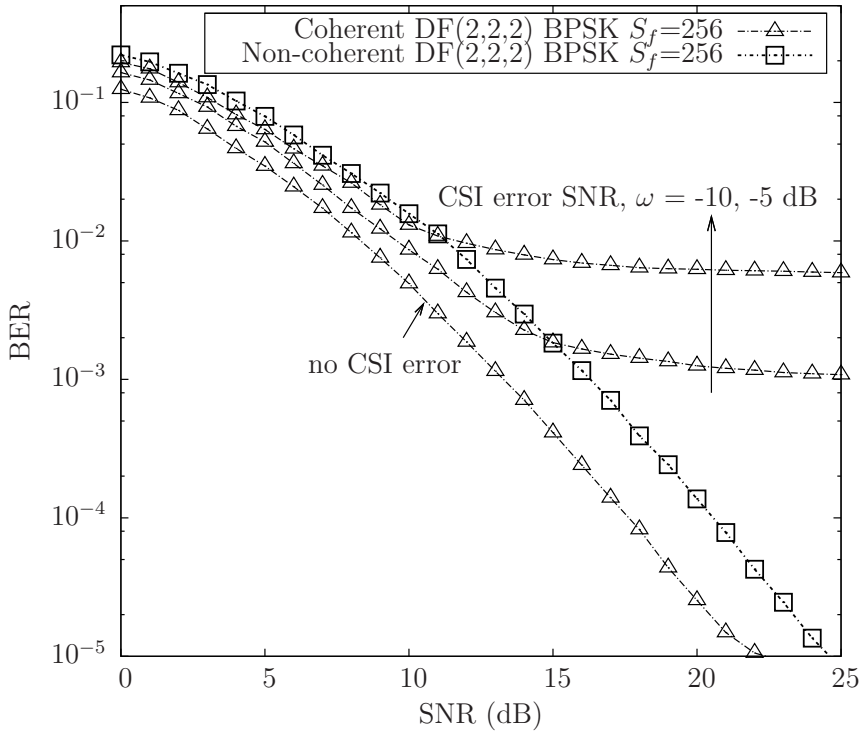

Figure 5.12: BER performance of the proposed multi-carrier SR BPSK modulated coherent scheme of Figure 5.2 and the differential STSK ($M = 2, T = 2, Q = 2$) scheme of Figure 5.5 with $S_f = 256$, single user in COST 207-TU12 channel. Other system parameters are listed in Table 5.2. The differential scheme suffers from -3 dB performance penalty compared to its coherent counterpart. The effects of the channel estimation errors for the coherent scheme is characterized by the assumed Gaussian CSI estimation error SNR of $\omega = -10$ and -5 dB.

if some of the spreading-code chips become corrupted. Nonetheless, the coherent scheme is seen to exhibit a considerable error floor in Figure 5.12. Moreover, the coherent scheme requires the transmission of pilot symbols in addition to the CRC overhead. In the light of the above-mentioned impediments of the coherent scheme, the differential multi-carrier STSK system may be deemed an attractive candidate for cooperative MIMO-aided multi-carrier communications.

5.7.4 Performance of the Channel-Coded Cooperative MC STSK

Figure 5.13 characterizes the achievable BER performance of the soft-decision aided channel-coded cooperative MC-CDMA STSK ($M = 2, T = 2, Q = 4$), QPSK scheme using $S_f = 16$ in the context of wideband channels, where we have employed a half-rate RSC code having a constraint length of $k = 2$ and the generator polynomials of $(g_r, g) = (3, 2)_8$ as well as two random interleavers of length $240,000$ bits. Both the coherent and the differential cooperative schemes are benchmarked against the non-cooperative scheme and against the cooperative arrangement employing no SR schemes. As observed from Figure 5.13, the non-coherent scheme

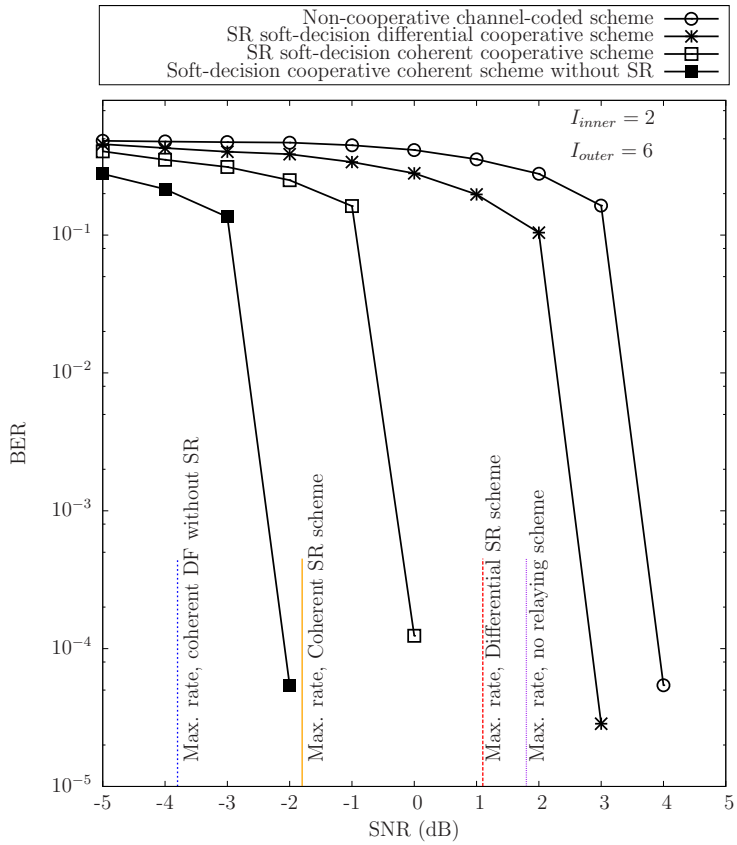

Figure 5.13: Achievable performance of the soft-decision three-stage turbo cooperative MC-CDMA STSK ($M = 2, T = 2, Q = 4$), scheme of Figure 5.7 and Figure 5.8 employing QPSK modulation with $S_f = 16$, single user communicating over the COST207-TU12 channel ($f_d = 0.01$) using system parameters listed in Table 5.2. The performance of both the coherent and differentially encoded SR scheme is provided with that of the direct non-cooperative and half-duplex cooperative benchmarkers. The maximum achievable rates of the corresponding schemes, computed by the EXIT chart based analysis are also provided.

exhibits a slight performance degradation compared to its coherent counterpart. But the non-coherent scheme has the potential advantage of dispensing with channel estimation. The non-cooperative scheme exhibits a substantially eroded performance, while the half-duplex scheme shows a somewhat better performance, albeit this is achieved at the cost of a severe thoughput loss. The number of inner and outer decoder iterations was set to $I_{\text{inner}}= 2$ and $I_{\text{outer}}= 6$, respectively. The maximum achievable rates were estimated by evaluating the area under the EXIT chart of the corresponding inner decoder, which are shown in Figure 5.13. To be more specific, we exploited using the area property of EXIT charts, as discussed in [146, 176], which states that the maximum achievable rate is determined by the area under the inner decoder's EXIT curve, whereas the maximum capacity $C_{\max}$ may be formulated as

$$C_{\max}(\text{SNR}) \approx R \cdot A_{\text{inner}}(\text{SNR}), \tag{5.66}$$

where A_{inner} is the the above-mentioned area corresponding to a ceratin SNR value and R is the number of bits per symbol.

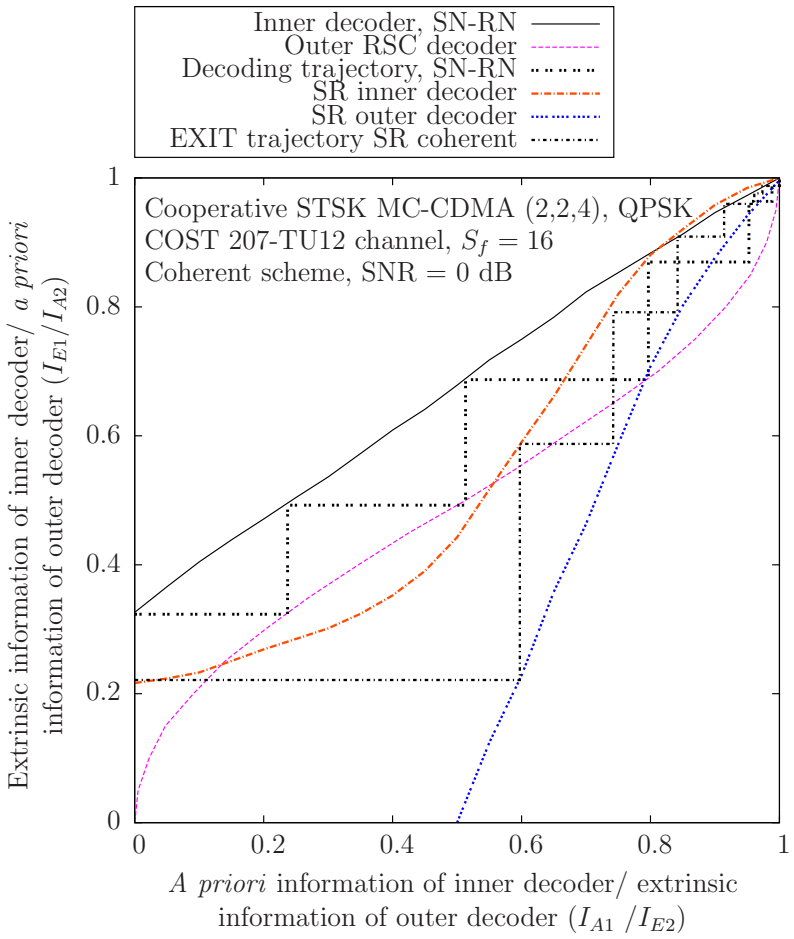

Figure 5.14: EXIT trajectory recorded at 0 dB of our three-stage turbo detected SR aided cooperative MC-CDMA STSK ($M = 2, T = 2, Q = 4$), scheme of Figure 5.7 and Figure 5.8 employing QPSK modulation with $S_f = 16$, single user communicating over the COST207-TU12 channel ($f_d = 0.01$) together with the inner decoder EXIT curves at 0 dB and the outer decoder EXIT function. The remaining system parameters are listed in Table 5.2.

Figure 5.14 shows the EXIT chart of the SR aided cooperative MC-CDMA STSK ($M = 2, T = 2, Q = 4$), QPSK scheme using $S_f = 16$ at a channel SNR of 0 dB. It can be seen in Figure 5.14 that the inner decoder's EXIT curve reached the point of perfect decoding convergence $(1.0, 1.0)$, which is the explicit benefit of employing URC precoding [5].

We also observe that an open EXIT tunnel was formed at SNR = 0 dB, and the EXIT curve at SNR =0 dB was also confirmed by the corresponding Monte-Carlo simulation based staircase shaped decoding trajectory [147]. Therefore, it may be predicted that an infinitesimally low BER is achieved at SNR = 0 dB using I_{outer}= 6 outer iterations.

Table 5.3: Main contributions in Chapter 5 on distributed multicarrier STSK

	Coherent scheme	*Noncoherent scheme*	*Channel-Coded scheme*
Section	Section 5.3	Section 5.5	Section 5.6
Schematic diagram	Figure 5.2	Figure 5.5	Figure 5.7 and Figure 5.8
Detection	Coherent	Noncoherent	Both is possible
Channel estimation	Required	Not required	Dependent on the scheme
Multicarrier scheme	MC-CDMA	MC-CDMA	MC-CDMA
Dispersion matrices	Unitary or non-unitary	unitary	Dependent on the scheme
Channel model	Dispersive	Dispersive	Dispersive

5.8 Chapter Summary and Conclusions

Motivated by the cooperative space-time architectures proposed in [54,166,167], in this chapter a novel distributed multicarrier STSK scheme using selective DF and SR was conceived for recovering the half-duplex multiplexing loss. The scheme is capable of striking a flexible diversity versus multiplexing gain tradeoff (DMT) with the aid of the STSK concept of Section 2.2.7 at a low decoding complexity. The contributions of this chapter may be summarized as shown in Table 5.3. In Section 5.2, we briefly outlined the background and our new contributions in this chapter. Coherent detection aided cooperative MC STSK employing SR was detailed in Section 5.3. The source node's transmission model, as well as the STSK-based DF relaying used at the VAAs constituted by the RNs and the signals received at the DN were also described in this section. The joint single-stream ML detection of the signals arriving at the DN from the direct SN-DN link as well as via the VAAs were elaborated on in Section 5.4. For the sake of dispensing with channel estimation, a novel noncoherent distributed MC-STSK arrangement was proposed in Section 5.5, which invoked differential en-/decoding across the STSK codewords mapped to the same subcarrier of consecutive OFDM symbols for ensuring frequency-flat fading over the differentially encoded symbols. The scheme proposed in Section 5.5 also utilized directly generated unitary dispersion matrices for avoiding the nonlinear Cayley transform used in [49, 54]. For achieving a near-capacity performance, in Section 5.6 we proposed a serially concatenated recursive systematic convolutional and unity-rate coded cooperative MC STSK arrangement for both the coherent and noncoherent scenarios. Finally, we investigated the performance of the proposed schemes in Section 5.7. The performance achievable by the schemes proposed in this chapter employing the system parameters listed in Table 5.2 is summarized in Table 5.4. As seen in Table 5.4, both the coherent and the differential cooperative scheme of Figure 5.2 and Figure 5.5 exhibit improved performance with increased S_f and with increased SN-DN distance. The channel-coded cooperative CSTSK $(2, 2, 4)$ employing QPSK modulation scheme and the corresponding noncoherent scheme of Figure 5.7 and Figure 5.8

Table 5.4: Summary of the achievable BER performance of schemes proposed in Chapter 5

Scheme	*Schematic diagram*	*Figure number*	*SNR (dB) at BER*		*SNR difference (dB) at BER (benchmark)*	
			10^{-3}	10^{-4}	10^{-3}	10^{-4}
Cooperative MC CSTSK $(2,2,4)$, *QPSK,* $S_f = 16$, $D_{sv_i} = 1/3D_{sd}$	Figure 5.2	Figure 5.9	17.0	21.5	4.0 (Perfect DF $S_f = 16$)	5.5 (Perfect DF $S_f = 16$)
Cooperative MC CSTSK $(2,2,2)$, *BPSK,* $S_f = 256$ $D_{sv_i} = 1/3D_{sd}$	Figure 5.2	Figure 5.10	12.5	16.5	3.5 (Perfect DF $S_f = 16$)	5.5 (Perfect DF $S_f = 16$)
Cooperative MC CSTSK $(2,2,2)$, *BPSK,* $S_f = 256$ $D_{sv_i} = 1/2D_{sd}$	Figure 5.2	Figure 5.11	11.5	15.5	2.5 (Perfect DF $S_f = 16$)	4.5 (Perfect DF $S_f = 16$)
Cooperative MC CSTSK $(2,2,2)$, *BPSK,* $S_f = 256$ $D_{sv_i} = 1/4D_{sd}$	Figure 5.2	Figure 5.11	13.5	17.5	4.5 (Perfect DF $S_f = 16$)	6.5 (Perfect DF $S_f = 16$)
Cooperative MC DSTSK $(2,2,2)$, *BPSK,* $S_f = 256$ $D_{sv_i} = 1/3D_{sd}$	Figure 5.5	Figure 5.12	15.5	19.5	3.0 (DF CSTSK of Figure 5.2)	3.0 (DF CSTSK of Figure 5.2)
Channel-coded Coop. MC CSTSK $(2,2,4)$, *QPSK,* $S_f = 16$ $D_{sv_i} = 1/3D_{sd}$	Figure 5.7 & Figure 5.8	Figure 5.13	-0.6	0	1.8 (maximum achievable rate at BER ≈ 0)	
Channel-coded Coop. MC DSTSK $(2,2,4)$, *QPSK,* $S_f = 16$ $D_{sv_i} = 1/3D_{sd}$	Figure 5.7 & Figure 5.8	Figure 5.13	2.5	2.8	2.0 (maximum achievable rate at BER ≈ 0)	

exhibit infinitesimally low BER at 1.8 dB and 2.0 dB away from the corresponding maximum achievable rate benchmarkers.

The SR regime used in the proposed schemes assists in recovering the half-duplex throughput loss at the cost of imposing inter-VAA interference and inter-stream interference at the DN [114, 115]. The problem of Inter-VAA interference is eliminated by invoking the proposed CRC based selective DF cooperation along with the specific FD despreading regime used, while the inter-stream interference is mitigated by using our double-frame-based chip-waveform matched filter [168] along with the proposed joint single-stream based ML decoding.

Furthermore, to overcome the performance degradation imposed by channel estimation errors, we proposed a cooperative multicarrier DSTSK scheme, which retained all the fundamental benefits of the coherent scheme. As a further advance, we also conceived a serially concatenated channel-coded and soft-decision based iteratively decoded cooperative STSK architecture of Figure 5.7 and Figure 5.8. In a nutshell, the scheme has the inherent design flexibility of adaptively selecting the number of RNs in the VAAs as well as the ability to strike a flexible rate-diversity tradeoff depending on the near-instantaneous channel conditions, while providing protection against the frequency selectivity of the channel.

Chapter 6

MSDSD Aided Multicarrier Space-Time Shift Keying

6.1 Introduction

HARD-decision as well as soft-decision multiple-symbol differential sphere decoding (MSDSD) is invoked in this chapter for multicarrier (MC) differential space-time shift keying (DSTSK)-aided transmission over frequency-selective channels. Specifically, the DSTSK signalling blocks are generated by the channel-encoded source information and the space-time (ST) blocks are appropriately mapped to a number of orthogonal frequency division multiplexing (OFDM) subcarriers. After OFDM-demodulation, the DSTSK signal is noncoherently detected by our soft-decision-aided MSDSD detector. A novel soft-MSDSD detector is designed in this chapter and the associated decision rule is derived for the DSTSK scheme, which might be a promising candidate for employment in the cooperative regime for the sake of dispensing with channel estmation.

The remainder of this chapter is organized as follows. Section 6.2 outlines the problem formulation and the main contributions in this chapter. In Section 6.3, an overview of the proposed hard-decision assisted MC DSTSK scheme is provided, while its soft-MSDSD-aided MC DSTSK counterpart is discussed in Section 6.4. In Section 6.5 The associated DM design criterion is described and the complexity imposed by the system is quantified. The performance of the soft-MSDSD aided DSTSK scheme is investigated in Section 6.6. Finally, we conclude this chapter in Section 6.7.

6.2 Problem Formulation and Contributions

We have developed co-located multicarrier space-time shift keying (MC STSK) in Chapters 2, 3 and 4 and distributed MC STSK in Chapter 5. The previous STSK studies of [49, 57] and of our Chapter 5 demonstrate that coherent STSK performs well in conjunction with perfect channel state information (CSI), but exhibits a severe error floor in the presence of channel estimation (CE) errors.

Differential STSK (DSTSK) employing conventional differential detection (CDD) has also been proposed for the sake of dispensing with the CE [49] and thus to eliminate the potentially high Doppler-dependent pilot overhead. However, CDD suffers from a typical 3 dB performance penalty in low-Doppler scenarios. Furthermore, an irreducible error floor may be observed in a high-mobility scenario characterized by a high Doppler frequency [177]. To circumvent the performance degradation of CDD, multiple-symbol differential detection (MSDD) was proposed for differential phase-shift keying (DPSK) in [178]. MSDD uses the fading-plus-noise statistics of the channel for jointly detecting $(N_w - 1)$ information symbols from N_w number of consecutively received symbols, where N_w is usually referred to as the *observation window size*. The performance improvement of MSDD is, however, achieved at the cost of an increased complexity, which increases exponentially with N_w. For mitigating this potentially excessive complexity, sphere decoding was invoked for MSDD in the context of multiple-symbol differential sphere decoding (MSDSD) in [179, 180]. Hard-decision MSDSD was conceived in [171] for a DSTSK scheme operating in non-dispersive channels. As a further advance, inspired by the near-capacity performance of turbo detection [147, 181], a soft-MSDSD scheme was also designed for DPSK in [182]. Furthermore, the concept of differential space-frequency modulation (DSFM) employing MSDSD in conjunction with a specific subcarrier allocation was proposed in [183] for exploiting both the achievable spatial- and frequency-domain diversity. However, the conception of the soft-MSDSD-aided DSTSK designed for realistic dispersive scenarios constitutes an unexplored open problem.

Against this background, we conceive a novel ML-MSDSD and soft-decision MSDSD for OFDM based MC DSTSK operating in frequency-selective channels. The main contributions of this paper are:

1. A novel soft-decision aided MSDSD is proposed for OFDM-aided DSTSK operating in dispersive channels. The decision rule of the soft-MSDSD is deduced by considering the construction of DSTSK codewords based on the DMs, the Doppler frequency, the OFDM system parameters and the generation of soft information.

2. A lower bound of the detection complexity is deduced, which is verified by simulations.

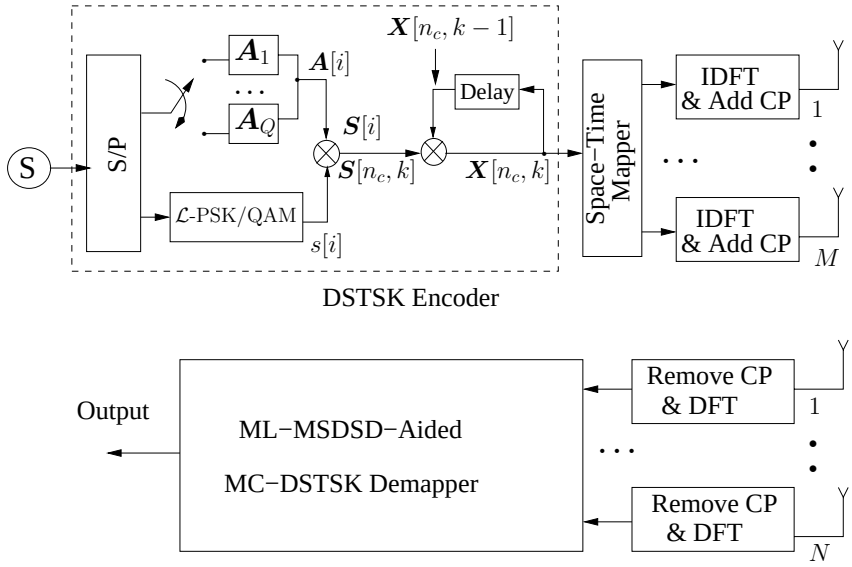

Figure 6.1: Transceiver architecture of the proposed hard-decision ML-MSDSD-aided MC DSTSK scheme. The space-time codewords generated from the source bits are differentially encoded in TD and the differentially encoded codewords are then transmitted in a manner similar to the OFDM-aided STSK architecture of Figure 2.9. The received signal is OFDM-demodulated similarly to Figure 2.9, but employs our ML-MSDSD-based demapper rather than using the ML detector of Figure 2.9.

6.3 System Model of the Hard-Decision ML-MSDSD-Aided DSTSK

In this section, we provide an overview of the hard-decision-based ML-MSDSD-aided MC DSTSK transceiver architecture shown in Figure 6.1.

6.3.1 DSTSK Architecture and OFDM Layout

The STSK encoder generates space-time (ST) codewords from the source information by activating a single DM in any symbol duration in conjunction with the classic modulated symbols for transmission over T time slots using M transmit AEs [49,57]. More specifically, each STSK signalling block $\boldsymbol{S}[i] \in \mathbb{C}^{T\times M}$ is created from $\log_2(\mathcal{L}\cdot Q)$ source bits according to [49, 57]

$$\boldsymbol{S}[i] = s[i]\boldsymbol{A}[i], \tag{6.1}$$

where $s[i]$ is an $\mathcal{L}$-ary constellation symbol represented by $\log_2 \mathcal{L}$ bits and $\boldsymbol{A}[i] \in \mathbb{C}^{T\times M}$ is the specific DM activated from the set of Q DMs $\boldsymbol{A}_q$ $(q = 1, ..., Q)$, as determined by the remaining $\log_2 Q$ bits. The DMs may be generated by using a variety of optimization methods [5, 32], as detailed in Subsection 6.5.1. The resultant STSK system is uniquely and unambiguously described by the parameters (M, N, T, Q) in conjunction with the $\mathcal{L}-$ary modulation.

We observe that the STSK codeword $\boldsymbol{S}[i]$ belongs to a set $\boldsymbol{\mathcal{S}}$ of $(\mathcal{L}\cdot Q)$ codeword matrices

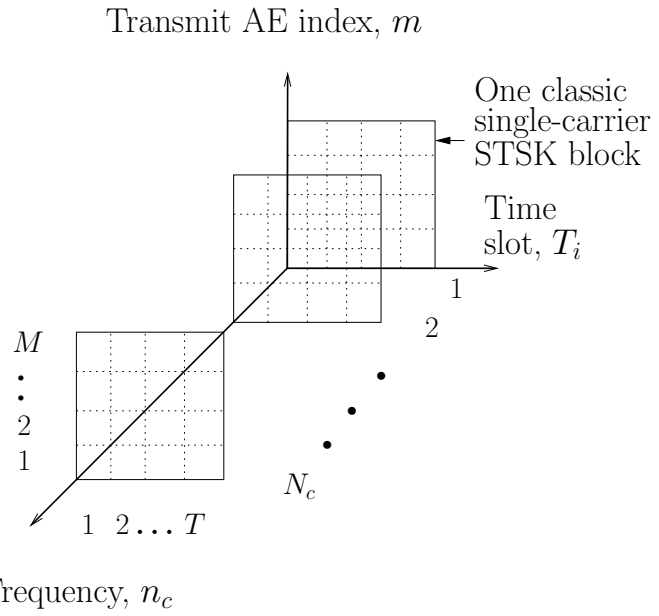

Figure 6.2: Mapping of the STSK codewords of Figure 6.3 to N_c parallel OFDM subcarriers before proper TD differential encoding and transmission over dispersive channels by M transmit AEs over T time-slots.

defined by

$$\boldsymbol{\mathcal{S}} \triangleq \{s_l \boldsymbol{A}_q \mid (q \in \{1, ..., Q\}, l \in \{1, ..., \mathcal{L}\})\}. \tag{6.2}$$

The STSK codewords are mapped to N_c parallel subcarriers, as illustrated in Figure 6.2, before being differentially encoded. We may represent the codeword $\boldsymbol{S}[i]$ by $\boldsymbol{S}[n_c, k]$, so that the overall codeword index i is related to the OFDM frame index k and the subcarrier index n_c by $i = kN_c + n_c, \quad n_c = 1, 2, \ldots, N_c$. Additionally, we invoke differential encoding in the TD, i.e. differential encoding is performed across the the same subcarrier of the consecutive OFDM symbols. In order to facilitate convenient differential encoding, we assume $M = T$. Furthermore, directly generated unitary DMs are used in the proposed scheme for avoiding the nonlinear Cayley transform [49, 171]. The codewords $\boldsymbol{S}[n_c, k]$ are thus differentially encoded to form the transmit blocks $\boldsymbol{X}[n_c, k] \quad (k = 0, 1, 2, \ldots)$ according to [183]

$$\boldsymbol{X}[n_c, k] = \begin{cases} \boldsymbol{X}[n_c, k-1]\boldsymbol{S}[n_c, k], & k = 1, 2, \ldots \\ \boldsymbol{I}_T & k = 0. \end{cases} \tag{6.3}$$

The DSTSK codewords are then transmitted after the N_c-point inverse discrete Fourier transform (IDFT) operation and appropriate CP incorporation.

6.3.2 Channel Model

Each link between the m-th transmit and n-th receive AE is assumed to be a frequency-selective channel, but as a benefit of OFDM-based transmission, each dispersive channel is

then partitioned into N_c low-rate parallel frequency-flat subchannels [20, 119]. The complex-valued fading gain $h_{m,n}[n_c, k]$ $(m = 1, 2, \ldots, M, \quad n = 1, 2, \ldots, N)$ obeys the distribution $\mathcal{CN}(0, 1)$ associated with an autocorrelation function based on Clarke's model [184]:

$$\varphi_{hh}[n_c, \kappa] \triangleq \mathcal{E}\left\{h_{m,n}[n_c, k]h^*_{m,n}[n_c, k + \kappa]\right\} = J_0\left(2\pi\kappa f_d\right), \tag{6.4}$$

where J_0 denotes the zeroth-order Bessel function of the first kind, and $f_d = f_m\mathcal{T}$ is the normalized maximum Doppler frequency, while f_m and $1/\mathcal{T}$ represent the maximum Doppler frequency and the symbol rate, respectively. The fading is assumed to be quasi-static, i.e. the channel's complex-valued envelope remains approximately constant during the transmission of an OFDM STSK frame.

Given the above-mentioned assumptions, the received signal $\boldsymbol{Y}[n_c, k] \in \mathbb{C}^{T\times N}$ obtained after CP removal and discrete Fourier transform (DFT) may be expressed by [119, 183]

$$\boldsymbol{Y}[n_c, k] = \boldsymbol{X}[n_c, k]\boldsymbol{H}[n_c, k] + \boldsymbol{V}[n_c, k], \tag{6.5}$$

where $\boldsymbol{X}[n_c, k] \in \mathbb{C}^{T\times M}$ represents the codeword transmitted and $\boldsymbol{H}[n_c, k] \in \mathbb{C}^{M\times N}$ denotes the FD channel transfer matrix, with its (m, n)-th entry given by $h_{m,n}[n_c, k]$. Furthermore, $\boldsymbol{V}[n_c, k] \in \mathbb{C}^{T\times N}$ is the AWGN with entries of $v_{T_i,n}[n_c, k] \sim \mathcal{CN}(0, \sigma_n^2)$.

6.3.3 ML-MSDSD for OFDM-Aided DSTSK

The ML-MSDD processes N_w consecutively received space-time blocks corresponding to the n_c-th subcarrier given by $\boldsymbol{Y}^w[n_c, k] \triangleq \left[\boldsymbol{Y}^T[n_c, k - N_w + 1], \ldots, \boldsymbol{Y}^T[n_c, k]\right]^T$ and finds the ML estimates $\hat{\boldsymbol{X}}^w[n_c, k]$ of the corresponding N_w transmitted blocks as defined by [180, 185]

$$\boldsymbol{X}^w[n_c, k] = \left[\boldsymbol{X}^T[n_c, k - N_w + 1], \ldots, \boldsymbol{X}^T[n_c, k]\right]^T. \tag{6.6}$$

Since the differentially encoded blocks $\boldsymbol{X}[n_c, k]$ are related to the STSK codewords by the one-to-one relationship expressed by (6.3), the ML-MSDD in turn estimates the $(N_w - 1)$ STSK codewords $\boldsymbol{S}[n_c, k-N_w+2], \ldots, \boldsymbol{S}[n_c, k]$, which further estimates the source information mapped to the STSK codewords.

Let us define the block-diagonal matrix $\boldsymbol{X}^w_D[n_c, k]$ by

$$\boldsymbol{X}^w_D[n_c, k] \triangleq diag\left\{\boldsymbol{X}[n_c, k - N_w + 1], \ldots, \boldsymbol{X}[n_c, k]\right\}, \tag{6.7}$$

$$\boldsymbol{H}^w[n_c, k] \triangleq \left[\boldsymbol{H}^T[n_c, k - N_w + 1], \ldots, \boldsymbol{H}^T[n_c, k]\right]^T, \tag{6.8}$$

and

$$\boldsymbol{V}^w[n_c,k] \triangleq \left[\boldsymbol{V}^T[n_c,k-N_w+1],\ldots,\boldsymbol{V}^T[n_c,k]\right]^T. \tag{6.9}$$

The N_w-block received sequence can then be expressed by [180, 185]

$$\boldsymbol{Y}^w[n_c,k] = \boldsymbol{X}_D^w[n_c,k]\boldsymbol{H}^w[n_c,k] + \boldsymbol{V}^w[n_c,k], \tag{6.10}$$

where

$$\begin{aligned} \boldsymbol{Y}^w[n_c,k] &\in \mathbb{C}^{N_wM\times N} \qquad \boldsymbol{V}^w[n_c,k] \in \mathbb{C}^{N_wM\times N} \\ \boldsymbol{H}^w[n_c,k] &\in \mathbb{C}^{N_wM\times N} \qquad \boldsymbol{X}_D^w[n_c,k] \in \mathbb{C}^{N_wM\times N_wM}. \end{aligned}$$

For the sake of clarity, we omit the subcarrier index and time index $[n_c,k]$ in the following and refer to the μ-th submatrix of a block-matrix, e.g. $\boldsymbol{B}$ by the subscripted matrix $\boldsymbol{B}_\mu$. Under the assumption that $h_{m,n}$ and $v_{T_i,n}$ $(m = T_i = 1,2,\ldots,M, \quad n = 1,2,\ldots,N)$ are zero-mean Gaussian random processes, the probability distribution function (pdf) of $\boldsymbol{Y}^w$ conditioned on $\boldsymbol{X}_D^w$ is given [186, 187] by

$$P\left(\boldsymbol{Y}^w \mid \boldsymbol{X}_D^w\right) = \frac{1}{\left(\pi^{N_wM}\det\left[\boldsymbol{\Lambda}_Y\right]\right)^N}\exp\left\{-\mathrm{tr}\left(\left[\boldsymbol{Y}^w\right]^H\boldsymbol{\Lambda}_Y^{-1}\boldsymbol{Y}^w\right)\right\}, \tag{6.11}$$

where $\boldsymbol{\Lambda}_Y$ is defined by $\boldsymbol{\Lambda}_Y \triangleq \mathcal{E}\left\{\boldsymbol{Y}^w\left[\boldsymbol{Y}^w\right]^H \mid \boldsymbol{X}_D^w\right\}$. The ML estimate $\hat{\boldsymbol{X}^w}$ under the assumption of quasi-static fading and unitary $\bar{\boldsymbol{X}}_D$ reduces to [186]

$$\hat{\boldsymbol{X}^w} = \arg\max_{\tilde{\boldsymbol{X}}^w} P\left(\boldsymbol{Y}^w \mid \boldsymbol{X}_D^w\right) = \arg\min_{\tilde{\boldsymbol{X}}^w}\left\{\mathrm{tr}\left(\left[\boldsymbol{Y}^w\right]^H\boldsymbol{\Lambda}_Y^{-1}\boldsymbol{Y}^w\right)\right\}. \tag{6.12}$$

Here the conditional covariance matrix $\boldsymbol{\Lambda}_Y$ is related to the channel parameters [186, 187] by

$$\boldsymbol{\Lambda}_Y^{-1} = \frac{1}{N}\boldsymbol{X}_D^w\left(\boldsymbol{\Lambda}^{-1}\otimes\boldsymbol{I}_M\right)\left[\boldsymbol{X}_D^w\right]^H, \tag{6.13}$$

where we have $\boldsymbol{\Lambda} \triangleq (\boldsymbol{\psi}_{hh} + \sigma_n^2\boldsymbol{I}_{N_w})$ and $\boldsymbol{\psi}_{hh} \triangleq toeplitz\left\{\varphi_{hh}[n_c,0],\ldots,\varphi_{hh}[n_c,(N_w-1)]\right\}$ with the component autocorrelation functions $\varphi_{hh}[n_c,\kappa]$ being identical for all spatial channels. The subcarrier index and the time index have been reinstated in this definition for better understanding. Applying the Cholesky factorization of $\boldsymbol{\Lambda}^{-1} = \boldsymbol{U}^H\boldsymbol{U}$ with the upper triangular matrix $\boldsymbol{U}$ and considering the identity $\mathrm{tr}\left(\boldsymbol{\mathcal{X}}\boldsymbol{\mathcal{X}}^H\right) = \| \boldsymbol{\mathcal{X}} \|^2$ for any matrix $\boldsymbol{\mathcal{X}}$, the ML-MSDD decision rule can be deduced from (6.11), yielding [180]

$$\hat{\boldsymbol{X}^w} = \arg\min_{\tilde{\boldsymbol{X}}^w}\left\{\sum_{\mu=1}^{N_w}\left\|\boldsymbol{Y}_{\mu,\mu}^H\tilde{\boldsymbol{X}}_\mu + \sum_{\nu=\mu+1}^{N_w}\left(\boldsymbol{Y}_{\mu,\nu}^H\tilde{\boldsymbol{X}}_\nu\right)\right\|^2\right\}, \tag{6.14}$$

where $\boldsymbol{Y}_{\mu,\nu}^H$ is defined by

$$\boldsymbol{Y}_{\mu,\nu}^H \triangleq \boldsymbol{Y}_\nu u_{\mu,\nu} \tag{6.15}$$

and $u_{\mu,\nu}$ represents the (μ,ν)-th element of $\boldsymbol{U}$. Still referring to (6.14), $\hat{\boldsymbol{X}^w}$ denotes the *estimate* of $\boldsymbol{X}_D^w$, whereas $\tilde{\boldsymbol{X}}_\mu$ refers to the μ-th *candidate* submatrix of $\boldsymbol{X}_D^w$.

Since the ML metric of (6.14) is invariant to a phase shift common to all elements of $\tilde{\boldsymbol{X}}_\mu$ $\forall\mu$ corresponding to the same $\boldsymbol{S}$ $\left(\boldsymbol{S}_\lambda^T \in \boldsymbol{\mathcal{S}}\ \forall\lambda\right)$, the accumulated differential matrices may be expressed as [182]

$$\boldsymbol{\mathcal{A}}_\nu = \begin{cases} \prod_{\lambda=\nu}^{N_w-1} \boldsymbol{S}_\lambda^H, & 1 \leqslant \nu \leqslant (N_w-1) \\ \boldsymbol{I}_T, & \nu = N_w. \end{cases} \tag{6.16}$$

For the sake of reducing the complexity associated with an exhaustive search, we employ MSDSD similar to [179,180] in order to search through the candidate set lying within a sphere of radius ρ_s:

$$\sum_{\mu=1}^{N_w} \left\| \boldsymbol{Y}_{\mu,\mu}^H \boldsymbol{\mathcal{A}}_\mu + \sum_{\nu=\mu+1}^{N_w} \left(\boldsymbol{Y}_{\mu,\nu}^H \boldsymbol{\mathcal{A}}_\nu\right) \right\|^2 \leq \rho_s^2. \tag{6.17}$$

Similar to the MSDSD principle described in [179], the ML-MSDSD is initialized with $\mu = (N_w - 1)$ and then proceeds by applying the search criterion of (6.17) until $\mu = 1$, where the search radius is updated to $\rho^2 = d_1^2$ and the search is repeated by commencing from $\mu = 2$ until $\mu = (N_w - 1)$ is reached. If the new search does not provide a better estimate, the previous estimate is retained. The estimate of the codewords obtained by the ML-MSDSD may be used to obtain the estimated source bits employing the single-stream ML detector of (4.31).

6.4 Soft-Decision MSDSD Receiver

In this section, we consider a three-stage recursive systematic convolutional (RSC) coded and unity-rate coded (URC) OFDM-aided DSTSK transceiver employing M transmit and N receive antenna elements (AEs), as illustrated in Figure 6.3. The source bits are first channel-encoded by the RSC code and the encoded bits are then interleaved by a random bit interleaver Π_1. Following URC-precoding, the interleaved bits are further interleaved by a second interleaver Π_2. The resultant bits are then mapped to STSK codewords, which are mapped to N_c parallel subcarriers and differentially encoded in the time-domain (TD). The DSTSK codewords generated are then OFDM-modulated, whilst incorporating appropriate cyclic prefices (CPs).

The signal received is first OFDM-demodulated and then input to the DSTSK soft-MSDSD demapper. Extrinsic soft information is then iteratively exchanged between the three soft-in soft-out components, namely the DSTSK demapper, the URC decoder and the RSC decoder, before finally outputting the estimated bits [5,117].

This section introduces the maximum *a posteriori*- MSDSD (MAP-MSDSD) algorithm and the generation of the logarithmic-likelihood ratios (LLRs) for the soft-MSDSD-aided MC DSTSK.

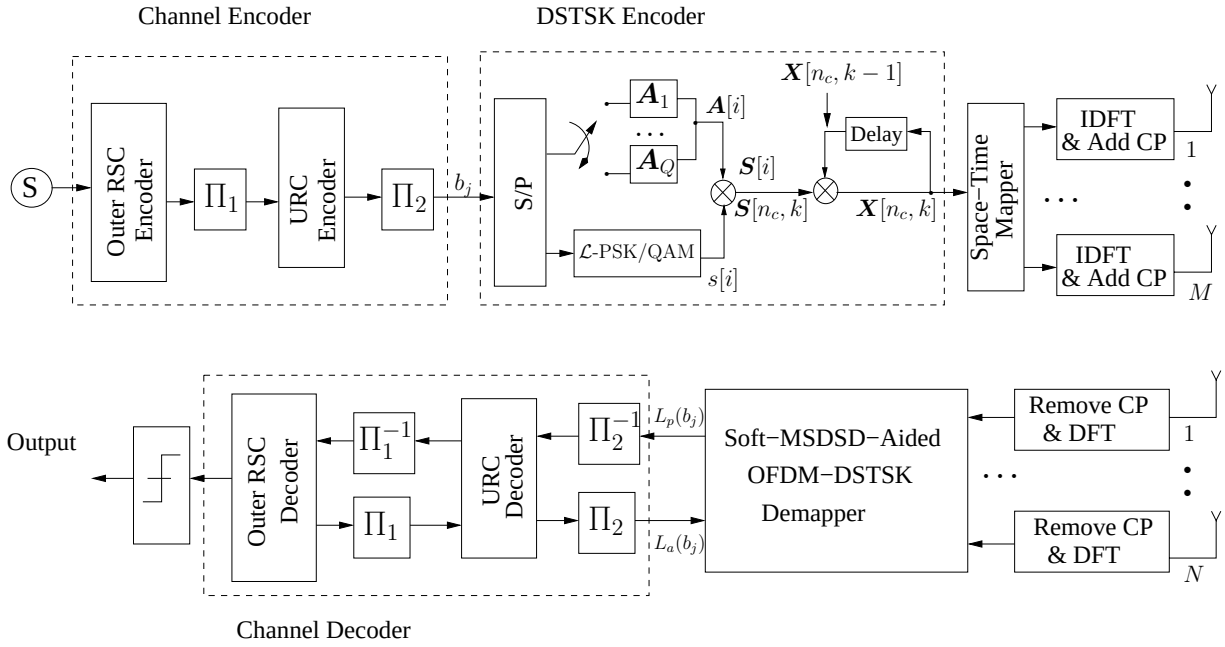

Figure 6.3: Transceiver architecture of the proposed soft-MSDSD-aided concatenated channel-codedd DSTSK scheme.

6.4.1 MAP-MSDSD

Assuming the STSK codewords to be mutually independent, (6.11) and (6.14) yields:

$$\begin{aligned} -\ln\left(P\left(\boldsymbol{S}^w \mid \boldsymbol{Y}^w\right)\right) &\propto -\ln\left(P\left(\boldsymbol{Y}^w \mid \boldsymbol{S}^w\right)\right) - \ln\left(P\left(\boldsymbol{S}^w\right)\right) \\ &\propto \sum_{\mu=1}^{N_w} \left\{ \left\| \boldsymbol{Y}_{\mu,\mu}^H \boldsymbol{\mathcal{A}}_\mu + \sum_{\nu=\mu+1}^{N_w} \boldsymbol{Y}_{\mu,\nu}^H \boldsymbol{\mathcal{A}}_\nu \right\|^2 - \ln\left(P\left(\boldsymbol{S}_\mu\right)\right) \right\} \end{aligned} \tag{6.18}$$

The MAP-MSDSD may thus be expressed as

$$\sum_{\mu=1}^{(N_w-1)} \left(\left\| \sum_{\nu=\mu}^{N_w} \left(\boldsymbol{Y}_{\mu,\nu}^H \boldsymbol{\mathcal{A}}_\nu \right) \right\|^2 - \ln\left(P\left(\boldsymbol{S}_\mu\right)\right) \right) \leq \rho_s^2 - \left\| u_{N_w,N_w} \boldsymbol{Y}_{N_w} \right\|^2 \triangleq \rho^2. \tag{6.19}$$

Clearly, the codeword $\boldsymbol{S}_\mu$ obeys the specific distance criterion [171, 179] that the current partial Euclidean distance (PED) d_μ^2 is the sum of the previous PED $d_{\mu+1}^2$ and the distance

increment $\triangle_\mu^2$:

$$\begin{aligned} d_\mu^2 &\triangleq \triangle_\mu^2 + d_{\mu+1}^2 \\ &= \underbrace{\left\| u_{\mu,\mu} \boldsymbol{Y}_\mu \boldsymbol{\mathcal{A}}_{\mu+1} \boldsymbol{S}_\mu^H + \sum_{\nu=\mu+1}^{N_w} u_{\mu,\nu} \boldsymbol{Y}_\nu \boldsymbol{\mathcal{A}}_\nu \right\|^2 - \ln\left(P\left(\boldsymbol{S}_\mu\right)\right)}_{\triangle_\mu^2} \\ &\quad + \underbrace{\sum_{\iota=\mu+1}^{(N_w-1)} \left(\left\| \sum_{\nu=\iota}^{N_w} u_{\iota,\nu} \boldsymbol{Y}_\nu \boldsymbol{\mathcal{A}}_\nu \right\|^2 - \ln\left(P\left(\boldsymbol{S}_\iota\right)\right) \right)}_{d_{\mu+1}^2}. \end{aligned} \tag{6.20}$$

Example 6.1: Decomposition of the Decision Metric for MAP-MSDSD [182,188]: $N_w = 4$

For the sake of exemplifying the relationship between the current PED d_μ^2 and the components of the MAP-MSDSD [182, 188] decision metric defined in (6.19), let us decompose the decision metric having $N_w = 4$ in terms of the current and previous PEDs.

For $N_w = 4$, from (6.20) we have:

$$\begin{aligned} d_\mu^2 &= \sum_{\iota=\mu}^{3} \left(\left\| \sum_{\nu=\iota}^{4} \left(\boldsymbol{Y}_{\iota,\nu}^H \boldsymbol{\mathcal{A}}_\nu \right) \right\|^2 - \ln\left(P\left(\boldsymbol{S}_\iota\right)\right) \right) \\ &= \sum_{\iota=1}^{\mu} \left(\left\| \sum_{\nu=\iota}^{4} \left(\boldsymbol{Y}_{\iota,\nu}^H \boldsymbol{\mathcal{A}}_\nu \right) \right\|^2 - \ln\left(P\left(\boldsymbol{S}_\iota\right)\right) \right) + \sum_{\iota=\mu+1}^{3} \left(\left\| \sum_{\nu=\iota}^{4} \left(\boldsymbol{Y}_{\iota,\nu}^H \boldsymbol{\mathcal{A}}_\nu \right) \right\|^2 - \ln\left(P\left(\boldsymbol{S}_\iota\right)\right) \right) \end{aligned} \tag{6.21}$$

Hence,

$$\begin{aligned} d_1^2 &= \left\| \sum_{\nu=1}^{4} \left(\boldsymbol{Y}_{1,\nu}^H \boldsymbol{\mathcal{A}}_\nu \right) \right\|^2 - \ln\left(P\left(\boldsymbol{S}_1\right)\right) + \sum_{\iota=2}^{3} \left(\left\| \sum_{\nu=\iota}^{4} \left(\boldsymbol{Y}_{\iota,\nu}^H \boldsymbol{\mathcal{A}}_\nu \right) \right\|^2 - \ln\left(P\left(\boldsymbol{S}_\iota\right)\right) \right) \\ &= \left\| \sum_{\nu=1}^{4} \left(\boldsymbol{Y}_{1,\nu}^H \boldsymbol{\mathcal{A}}_\nu \right) \right\|^2 - \ln\left(P\left(\boldsymbol{S}_1\right)\right) + d_2^2. \end{aligned} \tag{6.22}$$

Upon exploiting that we have $\boldsymbol{Y}_{\mu,\nu}^H \triangleq \boldsymbol{Y}_\nu u_{\mu,\nu}$ from (6.15), the PED d_1^2 in (6.22) may be expressed as:

$$\begin{aligned} d_1^2 &= \left\| \sum_{\nu=1}^{4} \left(\boldsymbol{Y}_\nu u_{1,\nu} \boldsymbol{\mathcal{A}}_\nu \right) \right\|^2 - \ln\left(P\left(\boldsymbol{S}_1\right)\right) + d_2^2 \\ &= \left\| u_{1,1} \boldsymbol{Y}_1 \boldsymbol{\mathcal{A}}_1 \right\|^2 + \left\| u_{1,2} \boldsymbol{Y}_2 \boldsymbol{\mathcal{A}}_2 \right\|^2 + \left\| u_{1,3} \boldsymbol{Y}_3 \boldsymbol{\mathcal{A}}_3 \right\|^2 + \left\| u_{1,4} \boldsymbol{Y}_4 \boldsymbol{\mathcal{A}}_4 \right\|^2 - \ln\left(P\left(\boldsymbol{S}_1\right)\right) + d_2^2 \\ &= \underbrace{\left\| u_{1,1} \boldsymbol{Y}_1 \boldsymbol{\mathcal{A}}_2 \boldsymbol{S}_1^H \right\|^2 + \left\| u_{1,2} \boldsymbol{Y}_2 \boldsymbol{\mathcal{A}}_2 \right\|^2 + \left\| u_{1,3} \boldsymbol{Y}_3 \boldsymbol{\mathcal{A}}_3 \right\|^2 + \left\| u_{1,4} \boldsymbol{Y}_4 \boldsymbol{\mathcal{A}}_4 \right\|^2 - \ln\left(P\left(\boldsymbol{S}_1\right)\right)}_{\triangle_1^2} + d_2^2 \end{aligned} \tag{6.23}$$

where from (6.16) we have:

$$\boldsymbol{\mathcal{A}}_4 = \boldsymbol{I}_T \tag{6.24}$$

Similarly to (6.23), we may calculate the other PEDs as:

$$\begin{aligned} d_2^2 &= \triangle_2^2 + d_3^2 = \left\|u_{2,2}\boldsymbol{Y}_2\boldsymbol{\mathcal{A}}_3\boldsymbol{S}_2^H\right\|^2 + \left\|u_{2,3}\boldsymbol{Y}_3\boldsymbol{\mathcal{A}}_3\right\|^2 + \left\|u_{2,4}\boldsymbol{Y}_4\boldsymbol{\mathcal{A}}_4\right\|^2 \\ &\qquad -\ln\left(P\left(\boldsymbol{S}_2\right)\right) + d_3^2 \qquad (6.25) \\ d_3^2 &= \triangle_3^2 + d_4^2 = \left\|u_{3,3}\boldsymbol{Y}_3\boldsymbol{\mathcal{A}}_4\boldsymbol{S}_3^H\right\|^2 + \left\|u_{3,4}\boldsymbol{Y}_4\boldsymbol{\mathcal{A}}_4\right\|^2 - \ln\left(P\left(\boldsymbol{S}_3\right)\right) + d_4^2 \qquad (6.26) \\ d_4^2 &= \triangle_4^2 + 0 = \left\|u_{4,4}\boldsymbol{I}_T\right\|^2 - 0 + 0. \qquad (6.27) \end{aligned}$$

Equations (6.23)−(6.27) may thus be used to visualize the decomposition of the MAP-MSDSD decision metric into different PEDs and the corresponding PED increments as shown in Figure 6.4.

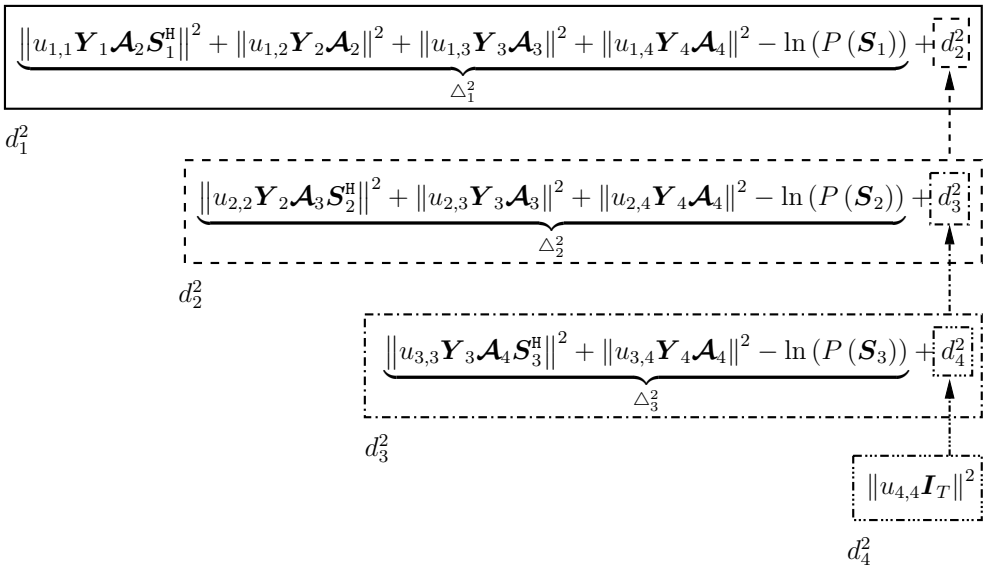

Figure 6.4: Decomposition of the entire MAP-MSDSD decision metric of (6.19) for $N_w = 4$ into different PEDs and the corresponding PED increments. The direction of the arrows corresponds to the sequence of the PED computations in the MAP-MSDSD algorithm.

Upon the application of the sphere decoding rule (6.19), the distance criterion of (6.20) reduces to:

$$\begin{aligned} d_\mu^2 &\triangleq \left\|u_{\mu,\mu}\boldsymbol{Y}_\mu\boldsymbol{\mathcal{A}}_{\mu+1}\boldsymbol{S}_\mu^H + \sum_{\nu=\mu+1}^{N_w} u_{\mu,\nu}\boldsymbol{Y}_\nu\boldsymbol{\mathcal{A}}_\nu\right\|^2 - \ln\left(P\left(\boldsymbol{S}_\mu\right)\right) \\ &\quad + \sum_{\iota=\mu+1}^{(N_w-1)} \left(\left\|\sum_{\nu=\iota}^{N_w} u_{\iota,\nu}\boldsymbol{Y}_\nu\boldsymbol{\mathcal{A}}_\nu\right\|^2 - \ln\left(P\left(\boldsymbol{S}_\iota\right)\right)\right) \leq \rho^2. \end{aligned} \tag{6.28}$$

Again, the MAP-MSDSD is initialized with $\mu = (N_w - 1)$ and then proceeds by applying the search criterion of (6.20) until $\mu = 1$, where the search radius is updated to $\rho^2 = d_1^2$ and the

search is repeated by commencing from $\mu = 2$ until $\mu = (N_w - 1)$ is reached. If the new search does not provide a better estimate, the previous estimate is retained.

6.4.2 Log-Likelihood Ratio (LLR) and Soft-MSDSD Aided MC DSTSK

The soft demapper relies on the *a priori* information gleaned from the URC decoder and the MAP-MSDSD. A high interleaver depth is assumed so that the permuted bits may be treated as being independent. The log-likelihood ratio (LLR) corresponding to the bit b_j interleaved by the interleaver Π_2 of Figure 6.3 is defined by [189]: $L_a(b_j) \triangleq \ln \frac{P(b_j = b)}{P(b_j = \bar{b})}$, where $b \in \{0, 1\}$ and the j-th bit $b_j = b$ corresponds to the MAP-MSDSD estimate $\hat{\boldsymbol{S}}^{w^b}$, while $\bar{b}$ indicates its complement. The *a posteriori* LLR $L_p(\cdot)$ of b_j may then be approximated by the maximum-logarithmic-MAP (max-log-MAP) algorithm [181, 182]:

$$
\begin{aligned}
L_p(b_j) &= \ln \frac{P(b_j = b \mid \boldsymbol{Y})}{P(b_j = \bar{b} \mid \boldsymbol{Y})} \\
&\approx \ln \frac{\max_{\tilde{\boldsymbol{S}}: b_j = b} \left[-\sum_{\mu=1}^{N_w} \left\| \sum_{\nu=\mu}^{N_w} \left(\boldsymbol{Y}_{\mu,\nu}^H \hat{\boldsymbol{\mathcal{A}}}_\nu \right) \right\|^2 + \ln \left(P\left(\hat{\tilde{\boldsymbol{S}}} \right) \right) \right]}{\max_{\tilde{\boldsymbol{S}}: b_j = b} \left[-\sum_{\mu=1}^{N_w} \left\| \sum_{\nu=\mu}^{N_w} \left(\boldsymbol{Y}_{\mu,\nu}^H \hat{\boldsymbol{\mathcal{A}}}_\nu \right) \right\|^2 + \ln \left(P\left(\hat{\tilde{\boldsymbol{S}}} \right) \right) \right]} \\
&= -\sum_{\mu=1}^{N_w} \left\| \sum_{\nu=\mu}^{N_w} \left(\boldsymbol{Y}_{\mu,\nu}^H \hat{\boldsymbol{\mathcal{A}}}_\nu^b \right) \right\|^2 + \ln \left(P\left(\hat{\boldsymbol{S}}^{w^b} \right) \right) + \sum_{\mu=1}^{N_w} \left\| \sum_{\nu=\mu}^{N_w} \left(\boldsymbol{Y}_{\mu,\nu}^H \hat{\boldsymbol{\mathcal{A}}}_\nu^{\bar{b}} \right) \right\|^2 - \ln \left(P\left(\hat{\boldsymbol{S}}^{w^{\bar{b}}} \right) \right)
\end{aligned}
\tag{6.29}
$$

where $\hat{\boldsymbol{S}}^{w^b}$ and $\hat{\boldsymbol{S}}^{w^{\bar{b}}}$ represent the MAP-MSDSD estimate and the constrained estimate associated with $b_j = \bar{b}$, respectively.

The extrinsic LLR $L_e(\cdot)$ for b_j is now evaluated by combining the *a posteriori* and *a priori* LLR: $L_e(b_j) = L_p(b_j) - L_a(b_j)$. The extrinsic information extracted from the soft-MSDSD demapper is iteratively exchanged with the URC decoder of Figure 6.3, which forms the *inner* iteration, while the exchange of extrinsic information between the URC and the RSC decoder of Figure 6.3 may be termed as the *outer* iteration. Note that for each outer iteration between the RSC and the URC decoder, several inner iterations may be invoked between the URC and the soft-MSDSD-aided DSTSK demapper [5, 49]. Finally, the RSC decoder generates *a posteriori* LLRs, from which the source bits are estimated.

6.5 Design Criterion and Complexity Metric

In this section, the DM design criterion and the complexity of the proposed scheme are detailed.

6.5.1 DM Optimization

For the MC DSTSK scheme, unitary DMs $\boldsymbol{A}_q (q = 1, ..., Q)$ are generated in the spirit of [32,130] by employing an exhaustive search for optimizing a specific objective function (OF) under the power constraint [49] expressed by $\text{tr}(\boldsymbol{A}_q^H \boldsymbol{A}_q) = T \quad \forall q$. As detailed in [32, 130], different OFs may be employed for the optimization of the DMs. Capacity-optimal designs rely on maximizing the continuous input continuous output memoryless channel (CCMC) capacity [5] or maximizing the discrete input continuous output memoryless channel (DCMC) capacity [127], whereas the minimum error-probability based designs aim for minimizing the pairwise error probability (PEP). The capacity-optimal designs do not necessarily minimize the error probability - indeed, the joint optimization of the capacity and the PEP is a challenging task [32]. A near-optimal design may, however, be attained [32], when relying on the specific configuration of $Q = MT$, leading to capacity optimization, while the PEP may be minimized by a search based on the rank and determinant criterion of [10]. In our design we randomly generate 10^6 unitary candidate matrices, which obey the power constraint mentioned above and rely on an exhaustive search for optimizing the DMs in order to minimize the average PEP of the codeword $\boldsymbol{X}$ being wrongly decoded as $\boldsymbol{X}'$, which is given [32, 49] by (2.24) and which may also be rewritten [10] as (2.25) mentioned in Chapter 2, where γ denotes the average signal-to-noise ratio (SNR) at each receive antenna, $\boldsymbol{X}_\Delta = (\boldsymbol{X} - \boldsymbol{X}')(\boldsymbol{X} - \boldsymbol{X}')^H$, while r and λ_i indicate the rank and the non-zero eigenvalues of $\boldsymbol{X}_\Delta$, respectively. The diversity and the coding advantage of the design is determined by the minimum product rN and $\prod_{i=1}^{r} \lambda_i$, respectively. Further insights on the optimization of the DMs are detailed in [5, 131].

6.5.2 Complexity

Equation (6.2) shows that there exists $(\mathcal{L} \cdot Q)$ legitimate codeword matrices for each $\log_2(\mathcal{L} \cdot Q)$ bits of source information. The exhaustive search based solution to (6.14) involves a search in a $(\mathcal{L} \cdot Q)^{(N_w - 1)}$-element space of candidate matrices $\tilde{\boldsymbol{X}}$ corresponding to all possible choices of $\tilde{\boldsymbol{S}}$. The ML-MSDSD associated with chosen sphere radius ρ imposes an average complexity, which is lower bounded by [180]

$$C \geq \frac{(\mathcal{L} \cdot Q)^{N_w \zeta - 1} - (\mathcal{L} \cdot Q)}{(\mathcal{L} \cdot Q) - 1}, \text{ where } \quad \zeta \triangleq \frac{\sigma_n^2 (1 + \epsilon)}{2 (1 + \sigma_n^2)} \quad \rho^2 = (1 + \epsilon) NMN_w \quad \epsilon > 0. \tag{6.30}$$

In order to quantify the complexity of the MAP-MSDSD scheme, we consider the number of real-valued multiplication operations (RMOs) required for obtaining a single soft-output value, which is used as our complexity metric. The lower bound of the complexity may be obtained, if the number of RMOs required for computing the soft-outputs corresponding to the first codeword estimate $\hat{\tilde{\boldsymbol{S}}}^b$ is counted and if a single constrained estimate $\hat{\tilde{\boldsymbol{S}}}^{\bar{b}}$ is taken into

account [182]. Considering the upper diagonal nature of the matrix $\boldsymbol{U}$, we observe that $\boldsymbol{Y}^H_{\mu,\nu}$ is defined only for $\nu \geq \mu$ in the context of (6.14), although each $\boldsymbol{Y}^H_{\mu,\nu}$ is an $(N \times T)$-element matrix, where $T = M$. The computation of the $\boldsymbol{Y}^H_{\mu,\nu}$ terms in (6.29) thus involves a total of $2MN\left[1+2+\cdots+N_w\right] = MNN_w\left(N_w+1\right)$ RMOs, assuming real-valued autocorrelation functions of $\varphi_{hh}[n_c,\kappa]$. In order to compute the *a posteriori* LLRs given by (6.29), the number of RMOs associated with the computation of each $\left\|\sum_{\nu=\mu}^{N_w}\left(\boldsymbol{Y}^H_{\mu,\nu}\hat{\boldsymbol{\mathcal{A}}}^b_\nu\right)\right\|^2$ is $4M^2N(N_w-\mu+1)+2$. The number of RMOs required for generating $\log_2(\mathcal{L}\cdot Q)$ soft-outputs corresponding to a single codeword estimate $\hat{\hat{\boldsymbol{S}}}^b$ is thus given by

$$\begin{aligned}\text{RMO}\left[\hat{\boldsymbol{S}}^{\hat{w}\,b}\right] &= MNN_w\left(N_w+1\right)+\sum_{\mu=1}^{N_w}\left[4M^2N(N_w-\mu+1)+2\right]\\ &= MN\left(2M+1\right)N_w\left(N_w+1\right)+2N_w. \end{aligned} \tag{6.31}$$

On the other hand, the number of RMOs related to each bit $\bar{b}$ of the constrained estimate $\hat{\hat{\boldsymbol{S}}}^{\bar{b}}$ is found to be $2N_w\left[M^2N\left(N_w+1\right)+1\right]$. The lower bound for the number of RMOs associated with the generation of a single soft-output is thus $\left[MN\left(2M+1\right)/\log_2(\mathcal{L}\cdot Q)+2M^2N\right]N_w^2$ for large N_w. The complexity of the scheme, however, depends on a number of parameters, such as the channel SNR, the autocorrelation function of the channel's fading-plus-noise and most importantly, on the *a priori* mutual information I_A of the inner decoder [182]. In Section 6.6, the complexity of the scheme will be investigated as a function of the observation window width N_w parameterized by the available *a priori* information I_A.

6.6 Performance Results

In this section, the performance of the proposed scheme is investigated using the parameters listed in Table 6.1. The detailed power delay profile characterizing the 12 taps of the channel model used may be found in [139, 141]. As mentioned in Table 6.1, we employ an RSC $(2,1,2)$ outer code having generator polynomials of $(g_r,g)=(3,2)_8$ as well as two random interleavers of length $240,000$ bits.

6.6.1 BER Performance of ML-MSDSD and Soft-MSDSD Aided MC DSTSK

Figure 6.5 characterizes the achievable bit-error ratio (BER) of the ML-MSDSD-aided QPSK-modulated MC DTSK $(M=2,N=2,T=2,Q=4)$ scheme of Figure 6.1, while that of soft-MSDSD-aided OFDM DSTSK scheme associated with different observation window sizes of $N_w=2,4,6,10$ is investigated in Figures 6.6 and 6.7. As seen in Figure 6.5, upon increasing the window size N_w, the BER performance difference between the coherent and noncoherent

Table 6.1: Main simulation parameters for ML-MSDSD- and soft-MSDSD-aided DSTSK of Figure 6.1 and Figure 6.3

Parameter	*Value*
Dispersive channel model	COST207-TU12
Fast fading envelope	Correlated Rayleigh
Normalized Doppler spread, f_d	0.01
Number of subcarriers, N_c	128
Length of cyclic prefix	32
Overall symbol duration	300 ns
STSK (M, N, T, Q)	$(M = 2, N = 2, T = 2, Q = 4)$
Modulation order, $\mathcal{L}$	4
RSC encoder and decoder	Half rate
	Constraint length=2
Generator polynomial	$(011, 010)_2$
Length of interleavers	240,000 bits
Outer iterations, I_{outer}	11
Inner iterations, I_{inner}	2

scheme is reduced. The BER of the proposed ML-MSDSD and soft-MSDSD-aided OFDM DSTSK schemes is compared furthermore to that of the corresponding coherent scheme relying on perfect CSI in Figure 6.5 and in Figure 6.7. We observe that the proposed scheme has the benefit of dispensing with CE due to differential encoding, while mitigating the dispersion-induced performance erosion of classic STSK by employing OFDM. Furthermore, the multiple-symbol detection partially mitigates the inherent performance penalty imposed by noncoherent detection. We observe in Figure 6.7 that as N_w increases, the BER performance gradually approaches that of the perfect CSI-oriented coherent scheme. Note that all the performance characteristics converge to a vanishingly low BER after $I_{\text{outer}} = 9$ iterations, which is the explicit benefit of using the URC in the system. The URC is a low-complexity recursive code, which has an infinite impulse response (IIR) and hence assists the inner decoder in efficiently spreading the soft information [5, 49]. As a result, the extrinsic information transfer (EXIT) charts of Figure 6.8 and Figure 6.9 converge to the $(1.0, 1.0)$ point of perfect decoding convergence, leading to a vanishingly low BER, thus eliminating the system's error floor. The maximum achievable rates for the corresponding scheme, where the scheme still exhibits an infinitesimally low BER were computed by exploiting the area property of EXIT charts [117,190] and are shown in Figure 6.7 as the ultimate benchmark of the scheme.

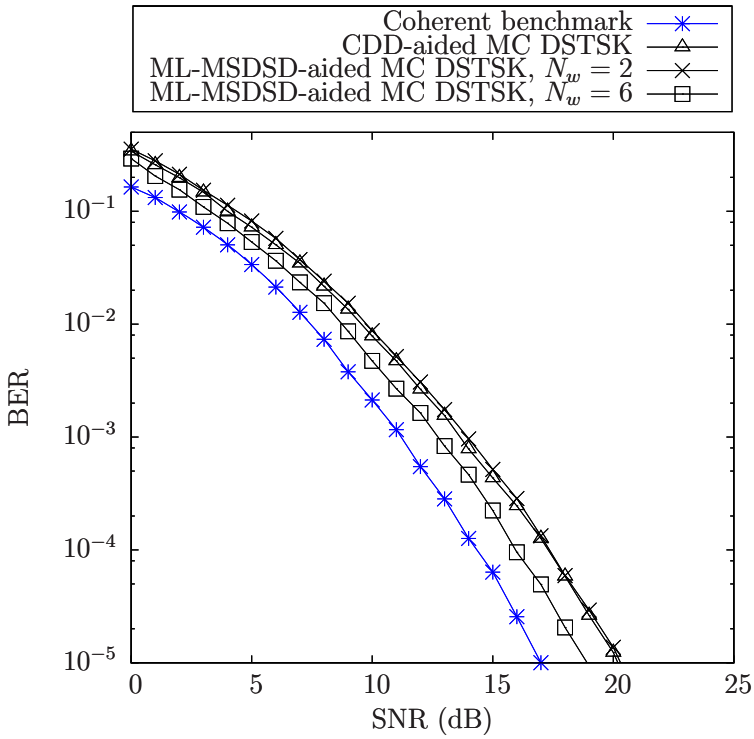

Figure 6.5: Simulated BER performance of the ML-MSDSD aided QPSK-modulated MC DSTSK ($M = 2, N = 2, T = 2, Q = 4$) scheme of Figure 6.1 for transmission over dispersive COST207-TU12 channel with normalized Doppler frequency $f_d = 0.01$ and observation window sizes of $N_w = 2$ and $N_w = 6$. The remaining system parameters are listed in Table 6.1. The difference in BER performance between coherent and noncoherent scheme decereases with increasing value of N_w.

6.6.2 EXIT Charts of the Soft-MSDSD Aided MC DSTSK

To elaborate further, Figure 6.8 and Figure 6.9 portray the EXIT charts of our proposed scheme at SNR=1.0 dB and 4.0 dB, respectively. We observe in Figure 6.8 that the inner decoder's EXIT charts recorded at SNR=1.0 dB for $N_w = 2, 4$ are 'pinched-off', i.e. there remains no 'open' EXIT tunnel, indicating a high residual BER. By contrast, the BER associated with $N_w = 6, 10$ may be expected to decrease sharply at this SNR after $I_{\text{outer}} = 9$ outer iterations, which is confirmed by the staircase-shaped Monte Carlo simulation based decoding trajectory [117, 147]. Figure 6.9, on the other hand, depicts the EXIT charts at SNR=4.0 dB, where all the curves associated with $N_w = 2, 4, 6, 10$ exhibit an open EXIT tunnel, implying an infinitesimally low BER after $I_{\text{outer}} = 9$ iterations. The EXIT charts of the soft-MSDSD-aided MC DSTSK recorded both for SNR=1.0 dB and SNR=4.0 dB are further compared in Figure 6.8 and Figure 6.9 to the ultimate benchmark of the coherent detector assuming perfect CSI at the receiver.

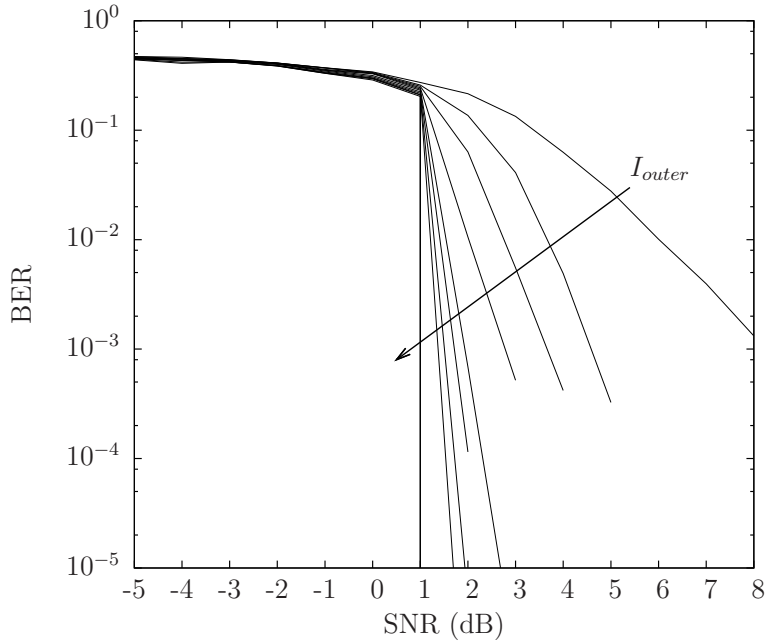

Figure 6.6: Simulated BER performance of the soft-MSDSD aided QPSK-modulated MC DSTSK ($M = 2, N = 2, T = 2, Q = 4$) scheme of Figure 6.3 for transmission over dispersive COST207-TU12 channel with normalized Doppler frequency $f_d = 0.01$ and different observation window size $N_w = 6$. The remaining system parameters are listed in Table 6.1. The performance curve converges to vanishingly low BER after $I_{outer} = 9$ outer iterations as a benefit of employing the URC.

6.6.3 Computational Complexity of the MAP-MSDSD Algorithm

Figure 6.10 characterizes the complexity associated with the MAP-MSDSD of the QPSK-modulated MC DTSK ($M = 2, N = 2, T = 2, Q = 4$) scheme at SNR=4.0 dB as a function of the window size N_w, parameterized by the *a priori* information I_A provided by the outer decoder for the demapper of Figure 6.3. The *a priori* information I_A is measured by the average mutual information (MI) [147] between the *a priori* LLR $L_a(b_j)$ and the *a posteriori* LLR $L_p(b_j)$ of Figure 6.3. The influence of the *a priori* information I_A on the complexity may be beneficially exploited in the context of adaptive system design [182], where N_w may be adaptively selected depending on the quality of the soft input. To be specific, the value of I_A increases during the consecutive decoding iterations and we can flexibly increase N_w when the value of I_A is higher. The theoretical lower bound of the complexity quantified by the number of RMOs in Subsection 6.5.2 is also shown as a benchmarker in Figure 6.10. As expected, the complexity rapidly escalates upon increasing N_w, albeit it does not become excessively high, provided that the *a priori* information gleaned from the outer decoder is in the range of $I_A \geq 0.8$.

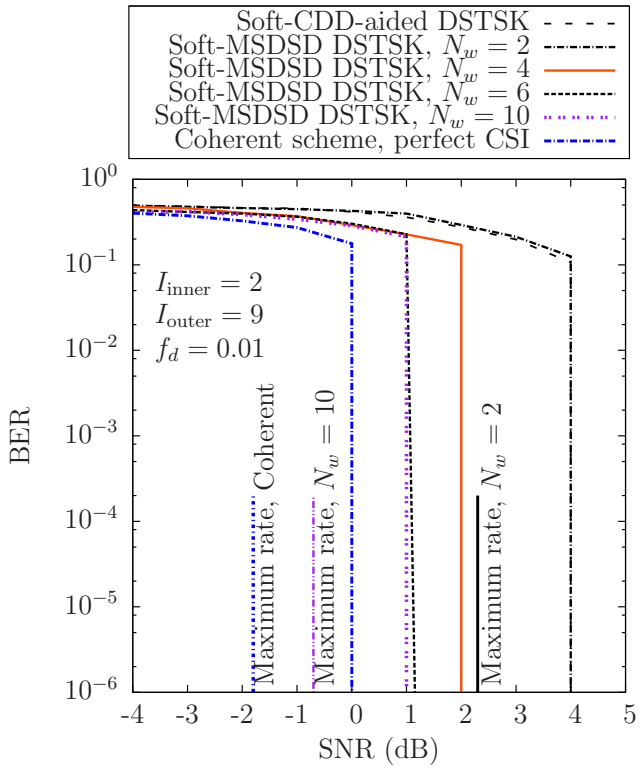

Figure 6.7: Simulated BER performance of the soft-MSDSD aided QPSK-modulated MC DSTSK ($M = 2, N = 2, T = 2, Q = 4$) scheme of Figure 6.3 for transmission over dispersive COST207-TU12 channel with normalized Doppler frequency $f_d = 0.01$ and different observation window size $N_w = 2, 4, 6, 10$. The remaining system parameters are listed in Table 6.1. The BER falls sharply after $I_{outer} = 9$ outer iterations as a benefit of employing the URC and the performance approaches that of the coherent scheme with perfect CSI with increasing value of N_w.

6.7 Chapter Summary and Conclusions

Motivated by the ability of the differential scheme of Section 5.5 to dispense with CE and of the MSDSD scheme of [182, 185] to mitigate the performance loss in CDD-aided transmissions at reduced complexity, in this chapter we proposed a hard-decision-aided and soft-MSDSD-aided multicarrier DSTSK scheme for communications over wideband channels. In Section 6.2, we described the background and ratinale of our work in this chapter and enunciated our contributions. We provided a brief overview of our system model in Section 6.3 and formulated the ML- and MAP-MSDSD algorithm for the MC DSTSK scheme in Section 6.4. The design criteria of the DMs used and the complexity associated with the MAP-MSDSD were explained in Section 6.5, whereas the performance as well as the complexity of MAP-MSDSD was investigated in Section 6.6. The OFDM-aided DSTSK provides a flexible diversity versus multiplexing gain tradeoff by spreading the source information across both the spatial- and time-dimensions, while mitigating the potential performance degradation imposed by the frequency-selectivity

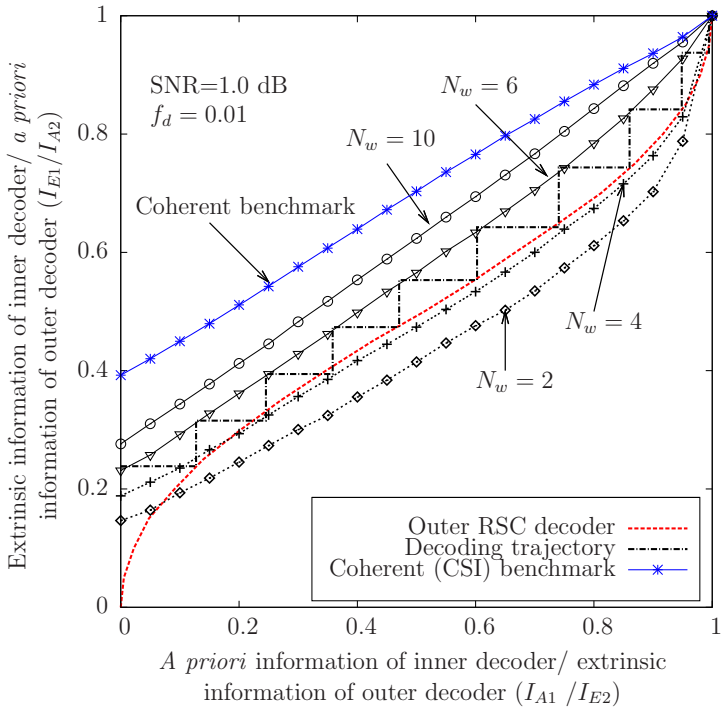

Figure 6.8: EXIT charts of the inner decoders of the soft-MSDSD aided QPSK-modulated MC DSTSK ($M = 2, N = 2, T = 2, Q = 4$) scheme of Figure 6.3 at SNR=1.0 dB with normalized Doppler frequency $f_d = 0.01$ and different observation window size $N_w = 2, 4, 6, 10$ and of the corresponding coherent system having perfect CSI at the receiver. The remaining system parameters are listed in Table 6.1. At this SNR, we observe the inner EXIT charts with $N_w = 6, 10$ have open EXIT tunnel and converge to the $(1.0, 1.0)$ point of perfect convergence, indicating sharp fall in the BER curve after $I_{\text{outer}} = 9$ outer iterations, which is confirmed by the decoding trajectory for $N_w = 6$. The EXIT charts with $N_w = 2, 4$ are, however, "pinched-off" and thus the BER at this SNR do not converge.

of the channel. The turbo principle based soft-MSDSD facilitates joint decisions over a number of DSTSK codewords, while exploiting the fading-plus-noise statistics of the channel. We have demonstrated that the proposed soft-MSDSD-aided DSTSK scheme provides a substantial flexibility at a moderate complexity owing to dispensing with CE. Furthermore, the MSDSD mitigates the performance degradation inflicted by the CDD scheme without an undue increase in computational complexity. The performance achievable by the schemes proposed in this chapter employing the system parameters listed in Table 6.1 is summarized in Table 6.2. Observe from Table 6.2 that the performance of both the hard-decision aided MC DSTSK scheme of Figure 6.1 and the soft-MSDSD-aided MC DSTSK scheme of Figure 6.3 improves with increasing window size N_w and gradually approaches the performance achievable by the coherent benchmarker.

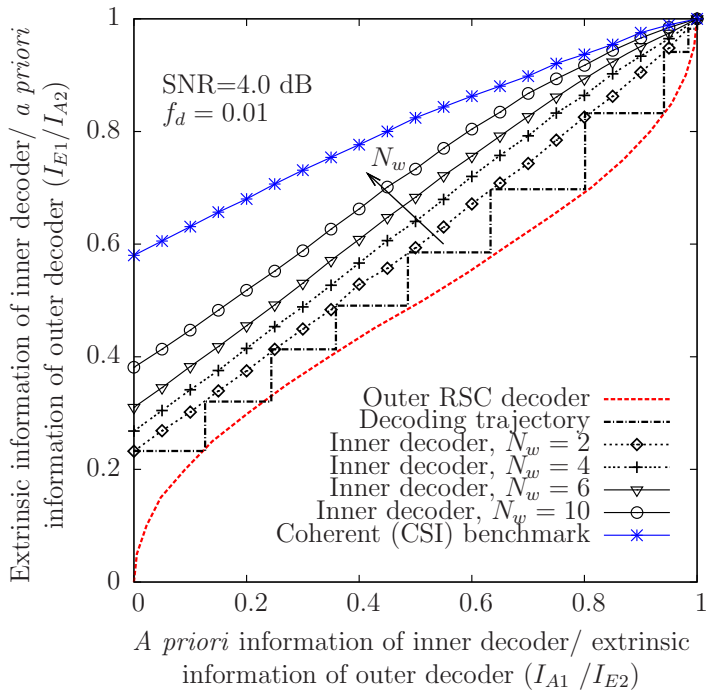

Figure 6.9: EXIT charts of the inner decoders of the soft-MSDSD aided QPSK-modulated MC DSTSK ($M = 2, N = 2, T = 2, Q = 4$) scheme of Figure 6.3 at SNR=4.0 dB with normalized Doppler frequency $f_d = 0.01$ and different observation window size $N_w = 2, 4, 6, 10$ and that of of the corresponding coherent inner decoder as benchmark. The remaining system parameters are listed in Table 6.1. All the EXIT charts have quite open EXIT tunnel at this SNR and converge to the $(1.0, 1.0)$ point as a benefit of employing the URC, indicating sharp fall in the BER curve after $I_{\text{outer}} = 9$ outer iterations, which is confirmed by the decoding trajectory.

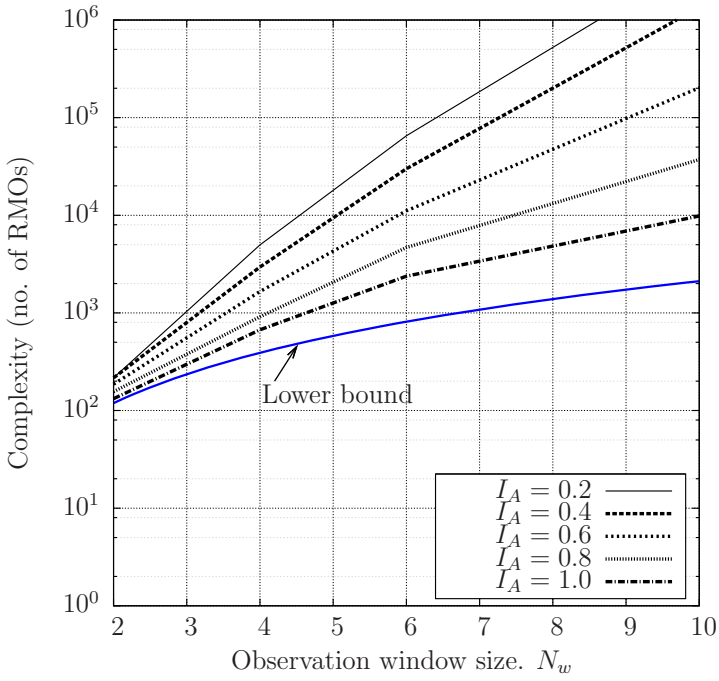

Figure 6.10: Complexity in terms of the numbers of RMOs associated with the MAP-MSDSD for the proposed QPSK-modulated MC DSTSK ($M = 2, N = 2, T = 2, Q = 4$) scheme of Figure 6.3 at SNR=4.0 dB using the parameters of Table 6.1 as a function of observation window size N_w parameterized against the *a priori* mutual information of the inner decoder I_A. The complexity shoots up with $N_w > 6$, although the rate of increase in complexity slows down with increased *a priori* information.

Table 6.2: Summary of the achievable BER performance of schemes proposed in Chapter 6

Scheme	*Schematic diagram*	*Figure number*	*SNR (dB) at BER*		*SNR difference (dB) at BER (benchmark)*	
			10^{-3}	10^{-4}	10^{-3}	10^{-4}
ML-MSDSD-aided MC DSTSK $(2,2,2,4)$ *QPSK* $N_w = 2$	Figure 6.1	Figure 6.5	17.0	20.2	3.0 (Coherent scheme)	3.0 (Coherent scheme)
ML-MSDSD-aided MC DSTSK $(2,2,2,4)$ *QPSK* $N_w = 6$	Figure 6.1	Figure 6.5	15.8	18.5	1.8 (Coherent scheme)	1.3 (Coherent scheme)
Soft-MSDSD-aided MC DSTSK $(2,2,2,4)$ *QPSK* $N_w = 2$	Figure 6.3	Figure 6.7	3.0	3.0	1.8 dB (maximum achievable rate at BER ≈ 0)	
Soft-MSDSD-aided MC DSTSK $(2,2,2,4)$ *QPSK* $N_w = 6$	Figure 6.3	Figure 6.7	1.0	1.0	1.7 dB (maximum achievable rate at BER ≈ 0)	
Soft-MSDSD-aided MC DSTSK $(2,2,2,4)$ *QPSK* $N_w = 10$	Figure 6.3	Figure 6.7	1.0	1.0	1.7 dB (maximum achievable rate at BER ≈ 0)	

Chapter 7

Conclusions and Future Research

In this concluding chapter, we will provide our overall summary and conclusions in Section 7.1. This will be followed by a range of research topics concerning potential future studies in Section 7.2.

7.1 Summary and Conclusions

In this thesis, we have provided detailed transceiver designs for the family of STSK-based MIMO-multicarrier systems for transmissions over dispersive wireless channels. More specifically, we proposed OFDM, MC-CDMA, OFDMA and SC-FDMA aided MIMO systems employing the STSK concept of Section 2.2.7. Furthermore, we proposed the successive DF relaying aided cooperative multicarrier STSK scheme of Chapter 5 for eliminating the effects of correlated fading often experienced in non-cooperative scenarios, while mitigating the typical throughput loss of classic half-duplex relaying schemes. Furthermore, we proposed the OFDM-aided DSTSK arrangement of Figure 6.3 for the sake of dispensing with channel estimation, while simultaneously reducing the decoding complexity imposed.

- **Chapter 1**: In Chapter 1, we provided a generic review of both classic MIMO arrangements as well as of the family of multicarrier systems and portrayed their historical development, as briefly summarized in Tables $1.1 - 1.6$. More specifically, in Section 1.1 we provided a detailed classification of the MIMO systems according to the applications they are employed in. These included the family of transmit diversity techniques, multiplexing schemes, multiple access methods and beamforming as well as multi-functional MIMO arrangements. The multicarrier systems, namely OFDM, MC-CDMA, MC DS-CDMA and SC-FDMA systems, were briefly reviewed in Section 1.3. Both SISO-OFDM and MIMO-OFDM systems were described in Subsection 1.3.1, while the main developments of these

systems are summarized in Table 1.4 and Table 1.5, respectively. In Subsection 1.3.1, we demonstrated in the context of (1.19) and Figure 1.5 that OFDM-based multicarrier transmission decomposes a dispersive channel into a number of non-dispersive frequency-flat subchannels. The study of OFDM in Subsection 1.3.1 was extended to a concise review of the multicarrier-based CDMA systems and of the SC-FDMA system in Subsection 1.3.2 and in Subsection 1.3.3 respectively. Section 1.4 provided an outline of the cooperative space-time systems. Finally, the organization of the thesis as well as its main findings were highlighted in Section 1.5.

- **Chapter 2** [119]: In Chapter 2, the OFDM-aided STSK concept was proposed for facilitating STSK transmissions over dispersive channels, whose transceiver architecture is shown in Figure 2.9. After generating the STSK codewords, the codewords representing the different ST blocks are mapped to N_c subcarriers. Thus the original high-rate serial datastream is transmitted over N_c parallel, orthogonal and low-rate subchannels. Each subcarrier symbol experiences frequency-flat fading, hence the typical broadband channel impairments imposed by dispersion are mitigated, while striking a flexible trade-off between the diversity- and the multiplexing-gain provided by the STSK systems. We briefly reviewed the different families of MIMO systems in Section 2.2 in order to provide both the motivation and rationale for the development of the STSK system. Specifically, Section 2.2 describes spatial division multiplexing (SDM) such as the classic BLAST and the V-BLAST schemes as well as diversity-oriented schemes such as the STBCs, STTCs, LDCs and the novel family of SM and SSK schemes. Specifically, the SDM family was described in Subsection 2.2.1, where it was shown that a SDM-aided channel may be decomposed into r_H independent parallel channels, where r_H denotes the rank of the channel matrix, which hence may be viewed as a set of parallel channels. Therefore the system exhibits a beneficial throughput gain. The spatial diversity type MIMOs, such as the STBC and STTC arrangements were described in Subsection 2.2.2, whereas the desirable property of simultaneously achieving both a multiplexing- as well as a diversity-gain was mentioned in Subsection 2.2.3. To be more specific, the diversity-multiplexing trade-off (DMT) was formalized in [126] and the corresponding mathematical definitions of multiplexing gain and diversity order were provided in Subsection 2.2.3. As a further advance, in Subsection 2.2.4 we provided an overview of LDCs, which strike a flexible DMT, albeit at a substantially increased decoding complexity. Both the CCMC capacity-optimal and the DCMC capacity-optimal designs of the LDC DMs were discussed, while the differentially encoded LDCs (DLDCs) were summarized in Subsection 2.2.5. The class of low-complexity SM and SSK architectures was briefly reviewed in Subsection 2.2.6. The STSK scheme, which also inherits the attractive DMT of LDCs and combines it with the low-complexity design of SM/SSK, was presented in Subsection 2.2.7. The optimiza-

tion of the DMs utilized in the STSK system was described in Section 2.3, where both the capacity-optimal and the PEP-optimal designs as well as the optimization procedure were presented based on [32, 49, 156]. As a new paradigm, in this section we presented the genetic algorithm (GA)-aided DM optimization based on [131, 134] and compared the performance of GA-aided search to that of the exhaustive random search technique employed for finding the optimal DM sets to be used in STSK. In particular, we demonstrated in Figure 2.7 that the genetically optimized DMs designed under the determinant criterion might be found at the cost of a significantly lower number of OF evaluations than that required by the random search method. This is achieved without any performance penalty. However, all the previous STSK studies were based on narrowband channels, whereas the realistic wireless channels are dispersive by nature. Hence the wideband channel model used was described in Subsection 2.3.4. The performance of the STSK scheme under dispersive wideband channel conditions was also investigated in Subsection 2.3.5 using the system parameters listed in Table 2.3. We observed in Figure 2.8 that although STSK provided excellent gains in narrowband scenarios, it exhibited a severe error floor in dispersive channels. The performance erosion of the STSK scheme in realistic dispersive propagation scenarios constituted the motivation for amalgamating multicarrier modulation with STSK transmissions. Hence in Chapter 2, we introduced the OFDM-aided STSK concept. In Section 2.4, we provided the design recipes for OFDM modulation of the STSK codewords and proposed two different strategies for mapping the STSK codewords to the orthogonal OFDM subcarriers. Furthermore, in Section 2.5 we proposed the three-stage serially concatenated convolutional coded OFDM-STSK architecture of Figure 2.14 for the sake of achieving a near-capacity performance. Finally, Section 2.6 characterized the achievable performance of our OFDM-aided STSK system. The performance of the scheme was investigated both in uncoded and in channel-coded scenarios. Our performance results of Figure 2.15, Figure 2.16 and Figure 2.17 reveal that our OFDM-aided STSK arrangement is capable of striking an attractive DMT at a low complexity, while exhibiting resilience against the frequency-selectivity of the channel. The performance achievable by our OFDM-aided STSK scheme of Figure 2.9 as well as by our channel-coded OFDM-STSK arrangement of Figure 2.14 is summarized in Table 2.5.

- **Chapter 3** [121]: In Figure 3.5 and Figure 3.9, we introduced MC-CDMA aided STSK for transmission over dispersive MIMO channels. Apart from mitigating the dispersion-induced performance degradation, this allows us to facilitate multiuser transmissions as well as to exploit the benefits accruing from FD spreading. In Figure 3.6, we detailed the mapping of the STSK space-time blocks to different sub-carriers of the MC-CDMA system. Furthermore, in Section 3.4 we designed the near-capacity three-stage concatenated recursive systematic convolutional (RSC)- and unity rate coded (URC) MC-CDMA STSK

arrangement Figure 3.10. We commenced with a brief review of different multicarrier-based CDMA systems in Section 3.2. More specifically, we classified the family of multicarrier based CDMA systems and presented a comparative study of the FD-spread and TD-spread multicarrier based CDMA. Then in Section 2.4.1 we presented the transmitter architecture of our FD-spread MC-CDMA aided STSK in Figure 3.5 and the channel model employed. In Section 3.3.2, we proposed a new single-stream ML-MUD for jointly detecting the information of all the users. Our transceiver architecture shown in Figure 3.5 and Figure 3.9 supports both uplink and downlink scenarios. Section 3.4 presents the design of our three-stage concatenated channel-coded MC-CDMA aided STSK scheme portrayed in Figure 3.10. Section 3.5 characterizes the performance of both uncoded and of channel-coded MC-CDMA-aided STSK both in single-user and in multiuser scenarios, as seen in Figure 3.11, Figure 3.12, Figure 3.13 and Figure 3.14. Observe in Figure 3.11 that the performance of the proposed scheme improves upon increasing the spreading factor S_f. Our investigations portrayed in Figure 3.12 and Figure 3.13 show that MC-CDMA aided STSK systems are capable of attaining a superb DMT even in dispersive multi-path environments, while supporting multi-user transmissions. Nonetheless, as expected, the system suffers from MUI in multiuser scenarios. The EXIT chart of Figure 3.15 recorded for the channel-coded scheme of Figure 3.10 reaches the $(1.0, 1.0)$ point of perfect convergence. Hence observe in Figure 3.14 that the system attains an infinitesimally low BER after a few iterations. The performance achievable by our MC-CDMA-aided STSK scheme of Figure 3.5 as well as by our channel-coded MC-CDMA-aided STSK arrangement of Figure 3.10 is summarized in Table 3.2.

- **Chapter 4** [117,118]: In Figure 4.6 and Figure 4.7, we proposed an OFDMA-aided multiuser STSK downlink arrangement and a SC-FDMA-aided multiuser STSK uplink architecture for dispersive channels. Furthermore, a novel reduced-complexity detector was conceived in Section 4.4 for the proposed OFDMA/SC-FDMA aided STSK arrangement. In Section 4.2, we commenced with a short discourse on the OFDMA based multicarrier DL scheme and on the SC-FDMA based single-carrier multiple access UL scheme. In Figure 4.2, we highlighted both the localized as well as the distributed subcarrier mapping concept and in Section 4.2.2 we briefly described the single-carrier concept invoking FDE for facilitating protection against channel dispersion, while benefitting from a low PAPR. In Figure 4.6 and Figure 4.7 of Section 4.3, we proposed the OFDMA/SC-FDMA-aided STSK concept and detailed its transmission as well as detection principles. The proposed reduced-complexity detector of Figure 4.8 was detailed in Section 4.4. In Figure 4.9 of Section 4.5, we also proposed an improved three-stage serially concatenated convolutional coded OFDMA/SC-FDMA-aided STSK arrangement. Finally, in Section 4.6 the performance of the proposed scheme of Figure 4.6 relying both on the localized and on

the interleaved sub-carrier allocation regimes was characterized in Figure 4.10 and Figure 4.11. The proposed reduced-complexity detector of Figure 4.8 was shown to be capable of reducing the complexity, as shown in Table 4.1 and in Figure 4.12 as well as in Figure 4.13. The achievable BER performance using the reduced-complexity detector was compared to that of the benchmark schemes in Figure 4.14 of Subsection 4.6.3. The BER performance of the channel-coded OFDMA/SC-FDMA-aided STSK scheme of Figure 4.9 employing interleaved subcarrier allocation was investigated in Figure 4.15 and Figure 4.17 in multiuser scenarios. We observed in Figure 4.15 and Figure 4.17 that the multiuser performance is comparable to the single-user performance. This is because the SC-FDMA aided STSK is potentially free from multiuser interferences (MUI) [98], as a benefit of the diagonal nature of both the weight matrix $\boldsymbol{W}_{n,m}^{v}$ of (4.23) and of the frequency-domain channel transfer matrix $\tilde{\boldsymbol{H}}_{n,m}^{v}$ of (4.17), as mentioned in Subsection 4.3.2. Furthermore, our OFDMA/SC-FDMA STSK signal can be detected at a low complexity using (4.31), because: 1) the coherent detector relies on accurate channel estimation, but the detection process does not explicitly use either the FD channel transfer function or the TD channel impulse response; 2) we can successfully employ the single-stream based ML detector of (4.31) relying on the linearized model of [32], because only a single dispersion matrix is activated at a given STSK block interval. The EXIT curve of the proposed scheme seen in Figure 4.18 reaches the $(1.0, 1.0)$ point of perfect convergence to a vanishingly low BER, as explicitly demonstrated in Figure 4.17, after a few iterations. The performance achievable by our OFDMA/SC-FDMA-aided STSK scheme of Figure 4.6 and Figure 4.7 as well as by our reduced-complexity detector of Figure 4.8 is summarized in Table 4.3.

- **Chapter 5** [116]: In Chapters 2, 3 and 4, efficient OFDM, MC-CDMA and OFDMA/SC-FDMA arrangements were combined with the STSK based co-located multiple-antenna system. For the sake of exploiting the cooperative diversity potential accruing from the independently fading channels of the geographically distributed relay nodes (RNs) communicating over frequency-selective channels, in Section 5.3 we proposed the successive relaying (SR) aided cooperative multicarrier STSK scheme of Figure 5.2. We invoke SR of Figure 5.1 for recovering the typical 50% throughput loss associated with the conventional half-duplex relaying. MC-CDMA is employed in Figure 5.2 for alleviating the performance degradation imposed by a single-carrier based STSK system as well as for mitigating both the SR-induced inter-relay interference (IRI) and the co-channel interference (CCI). In Section 5.5 and Section 5.6, the differential multi-carrier cooperative STSK regime of Figure 5.5 and the near-capacity channel-coded cooperative STSK arrangement of Figure 5.7 and Figure 5.8 were conceived. Section 5.3 elaborated on the transmission protocol of the coherent cooperative multicarrier STSK scheme of Figure 5.2 based on CRC-aided selective DF relaying. Furthermore, in Section 5.4 we proposed the joint detection of the

FD-despread signals gleaned from two successively arriving frames at the DN, which were received via the SN-to-DN and the VAA-to-DN links by using the appropriately adapted ML detector of [52]. As illustrated in Figure 5.4, the above-mentioned joint detector takes advantage of the inter-stream interference-free nature of STSK [49,57], since always a single dispersion matrix is activated. The coherent cooperative STSK scheme of Figure 5.2 is capable of performing well under the assumption of perfect CSI, as illustrated in Figure 5.9, Figure 5.10 and Figure 5.11. However, its performance degrades in the presence of channel estimation errors, as seen in Figure 5.12. Moreover, it is unrealistic to expect that the RNs altruistically estimate the SN-to-RN channels. As a potential remedy, in Section 5.5 we designed the noncoherent cooperative multicarrier STSK arrangement of Figure 5.5. Our differential encoding scheme of Figure 5.5 uses the directly generated unitary matrices $\boldsymbol{A}_q\,(q = 1, ..., Q)$ in the spirit of [32, 49, 171], while satisfying the STSK-related condition of relying on $M = T$, so that the resultant STSK signalling blocks are $(T \times T)$-element square matrices, which allow us to avoid employing the nonlinear Cayley transform of [49, 171]. In the architecture of Figure 5.5, we invoked the time-domain (TD) approach of differential encoding across the consecutive MC-CDMA symbols of the same sub-carrier, rather than the frequency-domain (FD) approach of differential encoding across the symbols of the adjacent sub-carriers of the same MC-CDMA block. The associated pros and cons were discussed in Section 5.5. Furthermore, in Section 5.6 we proposed the soft-decision based cooperative multicarrier STSK system of Figure 5.7 and Figure 5.8, which exhibits a superior performance, when communicating over dispersive channels, while maintaining the flexible DMT of the STSK scheme. The associated performance characteristics were shown in Figure 5.9 and Figure 5.10 for the uncoded coherent scheme of Figure 5.2 and in Figure 5.12 for the uncoded differential scheme of Figure 5.7. The corresponding channel-coded scheme of Figure 5.7 and Figure 5.8 was characterized in Figure 5.13. The BER performance of Figure 5.13 was verified by the EXIT chart based performance predictions depicted in Figure 5.14. The achievable performance of our SR-aided cooperative CSTSK scheme of Figure 5.2, of our SR-aided cooperative DSTSK scheme of Figure 5.5 as well as of our channel-coded soft-decision assisted coherent as well as noncoherent schemes of Figure 5.7 and Figure 5.8 was summarized in Table 5.4.

- **Chapter 6** [120]: As we discussed in Section 5.2, the cooperative multicarrier DSTSK of Figure 5.5 is particularly useful, because we cannot expect the RNs to estimate the source-to-relay channels simply for supporting the SNs. Furthermore, channel estimation errors result in an irreducible error floor in the BER performance characteristic of the cooperative MC CSTSK of Figure 5.2. For the sake of dispensing with channel estimation and for attaining an improved performance even in high-mobility dispersive channels while imposing a reduced complexity, we proposed the hard-decision as well as soft-decision

based MSDSD-aided DSTSK arrangement of Figure 6.1 and Figure 6.3, respectively. More specifically, Section 6.3 elaborated on the concept of ML-MSDSD-aided OFDM DSTSK. In Section 6.4, we proposed the soft-MSDSD-aided MC DSTSK scheme of Figure 6.3 and the associated maximum *a posteriori* MSDSD (MAP-MSDSD) philosophy. The design criterion used for optimizing the DMs employed and the complexity of the MAP-MSDSD were discussed in Section 6.5. Section 6.6 characterized the achievable performance of both the hard-decision and of the soft-decision MSDSD-aided MC DSTSK of Figure 6.1 and Figure 6.3 with the aid of Figure 6.5, Figure 6.6 and Figure 6.7. The EXIT chart aided prediction of the BER characteristics of Figure 6.6 and Figure 6.7 was then verified with the aid of Figure 6.8 and Figure 6.9, respectively, while Figure 6.10 characterized the complexity imposed by the MAP-MSDSD scheme. The achievable performance of our hard-decision MSDSD-aided OFDM-DSTSK scheme of Figure 6.1 versus that of our soft-MSDSD-aided OFDM-STSK scheme of Figure 6.3 is summarized in Table 6.2.

The design guidelines of our MC STSK schemes relying on the (M, N, T, Q) parameters in conjunction with the $\mathcal{L}-$ary constellation of the STSK system as a function of the number of subcarriers N_c, the spreading factor S_f, the DFT-spreading length N_d and the CP-length L_{cp} are summarized as follows:

- The values of (M, N) specify the number of transmit and receive AEs.
- The values of $(Q, \mathcal{L}, T)$, i.e. the number of DMs, the modulation order and the number of symbol intervals are chosen in any space-time block so as to satisfy the desirable DMT characterized by the rate $R = \log_2(\mathcal{L} \cdot Q)/T$ and the achievable diversity order of $N \cdot \min(M, N)$.
- For all the possible combinations of $(\mathcal{L}, Q)$, the Q DMs are computed based-on either the DCMC capacity-optimal or the PEP-optimal design procedure [32, 130].
- The best set of $(\mathcal{L}, Q)$ may be found by predicting the BER performance with the aid of the corresponding EXIT charts.
- The number of sub-carriers is chosen to ensure that the codeword symbols of each subcarrier experience frequency-flat fading. To be specific, the multicarrier modulation scheme is designed by ensuring that the coherence bandwidth of the channel is higher than the subcarrier symbol rate. Additionally, the length of the CP adopted ensures the absence of ISI between the consecutive OFDM symbols.
- In the MC-CDMA aided STSK scheme, the number of subcarriers N_c has to be equal to or a multiple of the spreading factor S_f, where increasing S_f provides a higher FD diversity gain.

- In the OFDMA/SC-FDMA aided STSK arrangement, the number of subcarriers N_c is usually a multiple of the DFT-spreading length N_d, whereas for a fully-loaded system supporting U users, we have $N_c = (N_d \times U)$.

- In the coherent SR aided cooperative MC-STSK arrangement, the parameters used are designed so as to support the date rate of $R = \frac{2\log_2(\mathcal{L} \cdot Q)}{b+T}$ [bits/symbol duration] , where b represents the number of symbols in the SN's transmit blocks.

- The differential cooperative MC STSK and the soft-MSDSD aided MC-STSK are designed using directly generated unitary matrices, while satisfying the relationship of $M = T$.

Let us now compare our OFDM-aided coherent STSK (CSTSK) scheme of Chapter 2, the MC-CDMA-aided CSTSK regime of Chapter 3, the OFDMA/SC-FDMA-aided CSTSK arrangement of Chapter 4, the MC-CDMA-aided cooperative CSTSK and DSTSK architecture of Chapter 5 and the soft-MSDSD-aided MC DSTSK scheme of Chapter 6. For this comparison, we tabulated some of their main features in Table 7.1, while the achievable performance of the individual schemes was tabulated at the end of the corresponding chapters, namely in Table 2.5, Table 3.2, Table 4.3, Table 5.4 and Table 6.2. We note that all our schemes mitigate the performance degradation imposed by the channel-induced dispersion, but as a further benefit, the MC-CDMA-aided STSK and the SC-FDMA-aided STSK are capable of providing additional FD diversity gains. Under the assumption of perfect orthogonality amongst the subcarriers, the SC-FDMA-aided scheme remains free from MUI, whereas the MUI imposed on the MC-CDMA-aided scheme can only be mitigated by a suitable MUD. The complexity associated with the employment of a MUD is typically high. The decoding complexity of the different schemes proposed in this treatise is summarized in Table 7.2. In addition to the low decoding complexity imposed by the SC-FDMA-aided scheme, it has the additional benefit of providing a low PAPR, and hence it is particularly suitable for uplink transmissions. It is also worth noting that our distributed MC STSK scheme has been investigated in the context of a single DN, but these studies may be readily extended to multiple DNs.

In a nutshell, the basic motivation of our designs was that of improving the overall quality of wireless systems by striking a compelling compromise among the conflicting design factors, such as the effective throughput, the coding as well as diversity gain, the implementational complexity etc. To outline the rationale of our work and to summarize our main contributions, we conclude as follows:

1. STSK has the benefit of striking a flexible DMT by using single-stream ML detection, as mentioned for example in [49, 56, 57]. However, all the previous studies apart from [148] investigated STSK in non-dispersive scenarios.

2. In order to retain all the benefits of STSK over dispersive channels, we need either a

Table 7.1: Comparative analysis of the OFDM-aided coherent STSK (CSTSK) scheme of Chapter 2, the MC-CDMA-aided CSTSK scheme of Chapter 3, the OFDMA/SC-FDMA-aided CSTSK scheme of Chapter 4, the MC-CDMA-aided cooperative CSTSK and DSTSK schemes of Chapter 5 and soft-MSDSD-aided MC DSTSK scheme of Chapter 6 for transmissions over the dispersive COST 207-TU12 channel. Co-located STSK $(M = 2, N = 2, T = 2, Q = 4)$, QPSK and distributed STSK $(M = 2, T = 2, Q = 4)$, QPSK schemes are considered.

	OFDM-aided CSTSK	MC-CDMA-aided CSTSK	OFDMA/SC-FDMA-aided CSTSK	Distributed MC CSTSK	Distributed MC DSTSK	MSDSD-aided OFDM-DSTSK
Schematic of the uncoded scheme	Figure 2.9	Figure 3.5 and 3.9	Figure 4.6 and 4.7 Figure 4.8 (Reduced-complexity)	Figure 5.2	Figure 5.5	Figure 6.1
Schematic of the channel-coded scheme	Figure 2.14	Figure 3.10	Figure 4.9	Figure 5.7 and 5.8	Figure 5.7 and 5.8	Figure 6.3
Parameter table	Table 2.4	Table 3.1	Table 4.2	Table 5.2	Table 5.2	Table 6.1
CSI required?	yes	yes	yes	yes	no	no
Detector	Single-stream ML detector of (2.53)	SUD of (3.18) & ML-MUD of (3.19)	Single-stream ML detector of (4.31) Reduced-complexity detector of (4.50) and (4.51)	Joint ML detector of (5.31)	Joint ML detector of (5.31) using (5.56)-(5.59)	The soft-MSDSD of (6.29)
SNR at BER=10^{-5} (uncoded scheme)	16 dB	16 dB ($S_f = 1$) 13.5 dB ($S_f = 4$)	16 dB (OFDMA, ML) 13.5 dB (SC-FDMA, MMSE)	16 dB ($N = 1$)	19 dB ($N = 1$)	18.0 dB ($N_w = 6$)
SNR at infinitesimally low BER (channel-coded scheme)	0 dB	0 dB ($S_f = 1$) -1 dB ($S_f = 4$)	0 dB (OFDMA) -3 dB (SC-FDMA, IFDMA)	0 dB ($N = 1$)	3.0 dB ($N = 1$)	1 dB ($N_w = 6$)

Table 7.2: Decoding complexity of the schemes proposed. The complexity is quantified in terms of the RMOs required for estimating a bit or for obtaining a single soft-output value of the soft-MSDSD-aided MC DSTSK scheme.

Decoding Scheme	Complexity
ML detector of (2.53) for OFDM-aided CSTSK	$\frac{4MNT^2Q + 6NTQ\mathcal{L}}{\log_2(Q \cdot \mathcal{L})}$
The detector of (3.18) for MC-CDMA-aided CSTSK	$\frac{10MTQ\mathcal{L}}{\log_2(Q \cdot \mathcal{L})}$
ML-MUD of (3.19) for MC-CDMA-aided CSTSK	$\frac{S_f\left(4MNT^2QU + 5NTQ\mathcal{L}U + 2NTQ\mathcal{L}\right)}{\log_2(Q \cdot \mathcal{L})}$
ML detector of (4.31) for SC-FDMA-aided CSTSK	$\frac{10MTQ\mathcal{L}}{\log_2(Q \cdot \mathcal{L})}$
ML detector of (4.32) for SC-FDMA-aided CSTSK	$\frac{4MNT^2Q + 6NTQ\mathcal{L}}{\log_2(Q \cdot \mathcal{L})}$
Reduced-complexity detector of (4.50) and (4.51) for OFDMA/SC-FDMA-aided CSTSK	$\frac{4M^2N + 8MN + 4MTQ + 2Q\mathcal{L}^1 + Q + 2\mathcal{L}}{\log_2(Q \cdot \mathcal{L})}$
Joint ML detector of (5.31) for cooperative MC-CSTSK as well as cooperative MC-DSTSK	$\frac{4MQT^2 + 6TQ\mathcal{L} + 4\mathcal{L}' + 2bQ\mathcal{L}}{\log_2(Q \cdot \mathcal{L})}$
MAP-MSDSD of (6.29) for soft-MSDSD-aided DSTSK	$\geq \left[MN\left(2M+1\right)/\log_2(\mathcal{L} \cdot Q) + 2M^2N\right] N_w^2$

space-time equalizer or OFDM/MC-CDMA, both of which, converts a dispersive channel into reduced-rate parallel non-dispersive channels [119, 121].

3. To maintain the benefits of OFDM-based transmission while facilitating multiuser communications, OFDMA/SC-FDMA aided STSK systems [117] were proposed. In order to further mitigate the decoding complexity of the single-stream ML detector, a reduced-complexity detector was proposed in [118].

4. The transmit power may be reduced with the aid of relaying, especially by DF relaying, where the plausible benefit is that in the absence of decoding errors, the relay retransmits to the DN from a reduced distance.

5. Albeit relaying is highly beneficial, it requires both a broadcast and a cooperation slot, which potentially halves the achievable throughput.

6. This disdavantage may be mitigated with the aid of successive relaying, which is achieved at the cost of reducing the number of users supported.

7. We proposed a SR-aided coherent versus noncoherent cooperative MC STSK arrangement in [116]. To be specific, we quantified the pros and cons of coherent versus noncoherent

detection. Explicitly, in practical terms, it is more realistic to use noncoherent detection dispensing with channel estimation at the relay nodes.

8. Differential STSK employing soft-MSDSD was proposed in [120] for the sake of dispensing with the channel estimation and thus to eliminate the potentially high Doppler-dependent pilot overhead, while benefitting from the low-complexity imposed by sphere decoding and from the iterative exchange of soft-information during detection.

7.2 Future Work

In this section, we briefly discuss a range of potential future research ideas.

7.2.1 Irregular Precoded MC STSK Scheme

For the sake of employing a suitable forward error correction (FEC) code in our MC STSK scheme, we chose the turbo principle based serially concatenated RSC-URC coded arrangement for attaining a near-capacity performance. The performance of the schemes may be improved by employing the irregular convolutional codes (IR-CC) of [191] as the outer en-/decoder. The design of these codes was detailed in [5, 192]. To be a bit more specific, the IR-CC incorporates a number of component convolutional codes (CCs) having different coding rates, each of which encodes an appropriately selected fraction of the source bits. The code has the design flexibility of adjusting the fractions of the information bits to be encoded by the different-rate component encoders with the aid of EXIT charts. This process is invoked for the sake of shaping the inverted EXIT chart of the composite IR-CC scheme for ensuring that it remains close to the inner decoder's EXIT curve throughout the entire mutual information interval of $[0, 1]$, whilst guaranteeing that they never cross. In this way, the "turbo-cliff" point may approach the associated system capacity quite closely. An irregular precoded LDC (IR-PLDC) was proposed in [193] employing a set of irregular inner codes corresponding to a set of LDCs for attaining near-capacity performance over a wide range of SNRs, while maintaining an infinitesimally low BER. Motivated by the benefits of this IR-PLDC architecture, irregular precoded MC STSK (IRP-MC STSK) may be conceived, which might have the potential of providing near-capacity performance for our system.

7.2.2 Asynchronous Transmission

A major challenge of MIMO systems is the inter-antenna synchronization (IAS) problem. The synchronization issue becomes acute in cooperative scenarios due to the asynchronous nature of relay nodes in the network. We have considered perfect synchronization in our proposed

schemes, although in practice it is difficult to acquire accurate system-level synchronization without imposing a high additional synchronization overhead and implementational complexity. The investigations of [194] revealed that the time-synchronization errors encountered in a cooperative scenario impose a significant performance degradation. Additionally, the propagation delays arising both from the different node locations in a cooperative scheme and from the multipath-induced delay-spread contribute to the sampling offset errors, which further aggravates the effect of synchronization errors. For mitigating the performance degradation imposed by synchronization errors in a cooperative regime, a number of space-time codes were proposed in [195, 196], which invoke space-time equalization under the assumption that the perfect knowledge of the CSI and/or of the relative delays is available at the receiver. In [197, 198], multi-carrier aided STCs were proposed specifically for dispersive links. However, all these schemes suffer from a high computational complexity.

In order to dispense with system-level synchronization between the RF chains associated with the transmit AEs, asynchronous STSK (ASTSK) was proposed in [49, 57]. This scheme operates in a way similar to the SM/SSK systems, because a single AE is activated at each symbol duration, whilst maintaining the benefits of the STSK system. However, the ASTSK scheme imposes a further constraint on the design of DMs. More specifically, the ASTSK DMs must not contain more than a single non-zero element in each column. Indeed, obtaining suitable DMs which are capable of meeting the required capacity and/or BER performance targets, while satisfying the power constraint mentioned in (2.29), is a challenging task. The design of a beneficial asynchronous MC STSK arrangement in the context of large-scale MIMOs [199, 200] constitutes a set of major open challenges for our future research. More specifically, similarly to the SM/SSK schemes, ASTSK has the potential of low-cost hardware design in the context of large-scale MIMO systems [201, 202].

7.2.3 Multiuser Multicell Scenario

Our MC STSK scheme relying on both co-located as well as on distributed AEs may be further investigated for employment in multiuser, multicell systems. The proposed scheme may be employed in a coordinated multipoint (CoMP) communications scenario, where the different base stations (BSs) operate in a coordinated manner in order to mitigate the intercell interference and to increase the cell edge throughput. The scheme may also be considered for employment in heterogenous networks including femto/pico BSs, fixed/mobile relays and cognitive radios as well as inappropriate interference mitigation arrangements. The concept of *area spectral efficiency* (ASE) was coined in [203] for quantifying the spectral efficiency per unit area of a cellular mobile radio system. In [204], the ASE of soft-decision space-time-frequency-shift keying (STFSK) aided slow-frequency-hopping multiple access (SFHMA) was investigated. A

holistically optimized system incorporating our MC STSK scheme may be considered for providing a high ASE.

7.2.4 Coded Modulation Aided MC STSK Scheme

The MC STSK scheme may be amalgamated with the family of classic coded modulation schemes, such as trellis-coded modulation (TCM) [125, 205, 206], turbo trellis-coded modulation (TTCM) [207], the bit-interleaved coded modulation (BICM) and bit-interleaved coded modulation relying on iterative decoding (BICM-ID). The bandwidth-efficient BICM scheme has been widely studied, for example in [208–210]. We have employed a near-capacity three-stage coding similar to the BICM technique for our MC STSK schemes. However, a comprehensive study of the coded modulation aided multi-carrier STSK scheme and its performance constitutes a major element of our future study.

7.2.5 Network Coding for Cooperative MC STSK Scheme

Network coding is a recent concept conceived in the seminal paper by Ahlswede *et al.* [211] and it is especially beneficial for the sake of increasing the attainable network throughput, the scalability and robustness. Rather than simply replicating and relaying the SN's transmissions at the RNs, signals are recombined at the intermediate nodes for example by their 'Ex-OR' operation or by other linear combination techniques, which are then retransmitted. This was shown to be particularly beneficial in terms of approaching the maximum achievable information flow of the network. Network coding may be employed in our cooperative MC STSK scheme for further enhancing the ASE. Network coding has the potential of improving the robustness, while simultaneously increasing the attainable throughput and reducing the delay of our system.

7.2.6 Subcarrier Allocation and Scheduling of MC STSK Schemes

We have also the further motivation to design joint power- and sub-carrier allocation scheme for our OFDMA/SC-FDMA based STSK DL/UL scenarios. There are numerous popular allocation algorithms, such as the Greedy algorithm [212], the Hungarian algorithm [213] and the Worst Subcarrier Avoidance (WSA) technique [214] etc. Hence the performance of efficient power and sub-carrier allocation techniques has to be investigated in the context of our multi-carrier STSK scheme, such as the one proposed by Liu and Yang for low-complexity subcarrier-power allocation in [215]. When considering the multiuser, multicell scenarios, appropriate upper layer concepts may be conceived for providing multiuser diversity. Specifically, channel-quality dependent multi-carrier as well as multiuser scheduling has to be invoked for allocating both the spectral and the power resources to different users for the sake of maximizing an objective

function such as for example the total throughput [216]. The performance of different scheduling algorithms also has to be compared. In [217, 218], the authors designed oppotunistic relay selection schemes for the SC-FDMA uplink. The performance of sophisticated relay selection schemes has to be studied in the context of cooperative multi-carrier STSK.

7.2.7 Energy-efficient MC STSK Design

Against the backdrop of rising energy cost and carbon footprint of cellular networks, 'green' wireless systems designed for a high throughput, whilst maintaining a high Quality-of-Service (QoS) and flexible scalability represent a few of the compelling needs of future communication systems. This necessitates the development of power-efficient, low-complexity solutions, whilst satisfying the target QoS as well as the throughput requirements. An appropriate design metric to be invoked may be the normalized energy-efficiency (EE) [219] expressed as the throughput per unit energy. Our scheme has the potential of considerably reducing the power consumption of wireless systems as a benefit of its inherent diversity-multiplexing gain tradeoff. The scheme activates a single DM at any symbol instant and the DMs may be designed for minimizing the overall energy consumption/dissipation. Furthermore, cross-layer-aware upper layer schemes may be designed for supporting energy-efficient operation of our scheme.

Appendix A

Dispersion Matrices for MC CSTSK/DSTSK Schemes

A.1 Dispersion Matrices for the MC CSTSK Schemes

The dispersion matrices of our MC CSTSK schemes were generated by employing an exhaustive search for minimizing the PEP under the power constraint of (2.29) [32, 49]. Specifically:

- Dispersion matrix for the BPSK-modulated CSTSK $(2, 2, 2, 1)$ scheme:

$$\boldsymbol{A}_1 = \boldsymbol{I}_2$$

- Dispersion matrices for the BPSK-modulated CSTSK $(2, 2, 2, 2)$ scheme:

$$\boldsymbol{A}_1 = \begin{bmatrix} -0.68261 - j0.108604 & 0.521750 + j0.507026 \\ 0.728032 + j0.221643 & 0.326144 + j0.554461 \end{bmatrix}$$

$$\boldsymbol{A}_2 = \begin{bmatrix} 0.159683 + j0.598742 & -0.59185 + j0.521820 \\ 0.745319 + j0.204706 & -0.07058 - j0.625333 \end{bmatrix}$$

- Dispersion matrices for the BPSK-modulated CSTSK $(2, 2, 2, 4)$ scheme:

$$\boldsymbol{A}_1 = \begin{bmatrix} -0.62798 - j0.591703 & -0.21073 + j0.487383 \\ -0.18250 - j0.380009 & 0.578338 - j0.679255 \end{bmatrix}$$

$$\boldsymbol{A}_2 = \begin{bmatrix} 0.384918 + j0.318313 & -0.44844 + j0.719217 \\ 0.460011 - j0.745615 & -0.50207 - j0.111899 \end{bmatrix}$$

$$\boldsymbol{A}_3 = \begin{bmatrix} 0.764867 - j0.088718 & -0.36210 - j0.462671 \\ -0.68682 - j0.080819 & -0.15158 - j0.748802 \end{bmatrix}$$

$$\boldsymbol{A}_4 = \begin{bmatrix} -0.087918 + j0.636725 & -0.68354 + j0.432746 \\ -0.706649 + j0.277730 & 0.410307 + j0.433029 \end{bmatrix}$$

- Dispersion matrices for the QPSK-modulated CSTSK $(2, 2, 2, 4)$ scheme:

$$\boldsymbol{A}_1 = \begin{bmatrix} 0.0706286 - j0.724047 & -0.34919 + j0.172634 \\ 0.0590843 - j0.378128 & -0.75165 - j0.779475 \end{bmatrix}$$

$$\boldsymbol{A}_2 = \begin{bmatrix} 0.009874 + j0.781335 & -0.39559 - j0.898581 \\ -0.01537 - j0.283969 & -0.58525 - j0.0457301 \end{bmatrix}$$

$$\boldsymbol{A}_3 = \begin{bmatrix} -0.44174 - j0.553705 & -0.58142 - j0.557075 \\ 0.202951 + j0.885996 & 0.055187 + j0.143760 \end{bmatrix}$$

$$\boldsymbol{A}_4 = \begin{bmatrix} 0.417664 - j0.428972 & 0.357802 - j0.328512 \\ 0.914539 - j0.331804 & -0.21631 + j0.642132 \end{bmatrix}$$

- Dispersion matrices for the BPSK-modulated CSTSK $(2, 2, 2, 8)$ scheme:

$$\boldsymbol{A}_1 = \begin{bmatrix} 0.490615 + j0.285835 & -0.05457 + j0.537095 \\ 0.664871 - j0.722890 & -0.22712 - j0.496953 \end{bmatrix}$$

$$\boldsymbol{A}_2 = \begin{bmatrix} -0.13912 - j0.804336 & 0.640451 + j0.696194 \\ 0.344340 + j0.404008 & -0.39372 + j0.078824 \end{bmatrix}$$

$$\boldsymbol{A}_3 = \begin{bmatrix} -0.22089 - j0.764160 & 0.740787 - j0.331307 \\ -1.01609 - j0.585726 & 0.091152 - j0.885433 \end{bmatrix}$$

$$\boldsymbol{A}_4 = \begin{bmatrix} -0.66174 - j0.159235 & -0.53109 - j0.63638 \\ 0.709018 - j0.909580 & -1.12723 + j0.309776 \end{bmatrix}$$

$$\boldsymbol{A}_5 = \begin{bmatrix} 0.136287 - j0.950395 & -0.69784 - j0.766231 \\ -0.03667 - j0.391224 & 0.722999 - j0.278409 \end{bmatrix}$$

$$\boldsymbol{A}_6 = \begin{bmatrix} -0.06576 - j0.880872 & 0.030519 - j0.096179 \\ -0.40567 + j0.190354 & 0.155844 + j1.291880 \end{bmatrix}$$

$$\boldsymbol{A}_7 = \begin{bmatrix} 0.356444 - j0.952773 & -0.37021 + j0.262445 \\ 0.573447 + j0.720187 & -0.20058 + j0.442297 \end{bmatrix}$$

$$\boldsymbol{A}_8 = \begin{bmatrix} -0.00844 - j0.644137 & -1.04764 + j0.563001 \\ -0.14116 - j0.248972 & -0.06942 - j0.289428 \end{bmatrix}$$

- Dispersion matrices for the BPSK-modulated CSTSK $(3, 2, 2, 2)$ scheme:

$$\boldsymbol{A}_1 = \begin{bmatrix} -0.60261 - j0.974351 & -0.17069 + j0.050189 \\ -0.17273 + j0.094880 & -1.04201 + j0.263649 \\ 0.032973 - j0.191071 & -0.14009 + j0.150957 \end{bmatrix}$$

$$\boldsymbol{A}_2 = \begin{bmatrix} 0.178581 + j0.237927 & 1.149810 + j0.317412 \\ -0.07755 + j0.948592 & -0.39879 - j0.100663 \\ 0.057166 + j0.0266048 & -0.15761 + j0.056209 \end{bmatrix}$$

A.2 Dispersion Matrices for the MC DSTSK Schemes

The DMs of our MC DSTSK schemes were directly generated unitary matrices by employing random search for minimizing the PEP under the power constraint of (2.29) [49, 171].

- Dispersion matrix for the BPSK-modulated DSTSK $(2, 2, 2, 1)$ scheme:

$$\boldsymbol{A}_1 = \boldsymbol{I}_2$$

- Dispersion matrices for the BPSK-modulated DSTSK $(2, 2, 2, 2)$ scheme:

$$\boldsymbol{A}_1 = \begin{bmatrix} 0.028179 + j0.048991 & 0.735407 - j0.675265 \\ -0.42205 - j0.904811 & 0.044743 - j0.034529 \end{bmatrix}$$

$$\boldsymbol{A}_2 = \begin{bmatrix} -0.02114 + j0.298813 & 0.632639 + j0.714166 \\ -0.85975 + j0.413629 & 0.096163 - j0.283706 \end{bmatrix}$$

- Dispersion matrices for the QPSK-modulated DSTSK $(2, 2, 2, 4)$ scheme:

$$\boldsymbol{A}_1 = \begin{bmatrix} 0.511388 + j0.028406 & 0.857951 + j0.039947 \\ -0.12163 - j0.850225 & 0.077072 + j0.506344 \end{bmatrix}$$

$$\boldsymbol{A}_2 = \begin{bmatrix} -0.05908 - j0.891632 & -0.04651 + j0.446474 \\ 0.110036 + j0.435195 & 0.069359 + j0.890891 \end{bmatrix}$$

$$\boldsymbol{A}_3 = \begin{bmatrix} 0.070268 + j0.291534 & -0.75307 - j0.58562 \\ 0.536267 - j0.788979 & -0.02287 - j0.299009 \end{bmatrix}$$

$$\boldsymbol{A}_4 = \begin{bmatrix} 0.511300 - j0.250363 & 0.313400 + j0.760047 \\ 0.806445 + j0.159805 & 0.146283 - j0.550192 \end{bmatrix}$$

A.3 Dispersion Matrices for the GA-optimized MC CSTSK Schemes

The DMs of our MC CSTSK schemes were also generated by employing GA-based optimization illustrated in Section 2.3.2 for minimizing the PEP under the power constraint of (2.29) [131, 134].

- Dispersion matrix for the BPSK-modulated CSTSK $(2, 2, 2, 1)$ scheme:

$$\boldsymbol{A}_1 = \boldsymbol{I}_2$$

- Dispersion matrices for the BPSK-modulated CSTSK $(2, 2, 2, 2)$ scheme:

$$\boldsymbol{A}_1 = \begin{bmatrix} -0.34800 + j0.536949 & 0.638518 + j0.414693 \\ -0.68694 + j0.344526 & -0.29261 - j0.578536 \end{bmatrix}$$

$$\boldsymbol{A}_2 = \begin{bmatrix} 0.382709 + j0.646123 & -0.55772 + j0.348868 \\ 0.524060 + j0.401772 & 0.448477 - j0.605068 \end{bmatrix}$$

- Dispersion matrices for the QPSK-modulated CSTSK $(2, 2, 2, 4)$ scheme:

$$\boldsymbol{A}_1 = \begin{bmatrix} -0.85921 + j0.504184 & 0.413484 + j0.100935 \\ -0.08643 + j0.009546 & -0.79022 + j0.440901 \end{bmatrix}$$

$$\boldsymbol{A}_2 = \begin{bmatrix} -0.20129 + j0.424267 & 0.118137 - j0.608894 \\ -0.84983 - j0.239303 & -0.74817 - j0.235646 \end{bmatrix}$$

$$\boldsymbol{A}_3 = \begin{bmatrix} -0.81709 - j0.380897 & -0.01538 - j0.737604 \\ -0.17934 + j0.393842 & 0.658412 + j0.148989 \end{bmatrix}$$

$$\boldsymbol{A}_4 = \begin{bmatrix} 0.083231 - j0.150406 & 0.583613 + j0.691723 \\ -0.96236 + j0.210492 & 0.400807 + j0.142369 \end{bmatrix}$$

Glossary

3GPP	3rd Generation Partnership Project
AE	Antenna Element
AF	Amplify-and-Forward
Approx-log-MAP	Approximate-Logarithmic-Maximum *a posteriori*
AWGN	Additive White Gaussian Noise
BER	Bit Error Ratio
BICM	Bit-interleaved Coded Modulation
BICM-ID	Bit-interleaved Coded Modulation with Iterative Decoding
BLAST	Bell Laboratories Layered Space-Time
BS	Base Station
CCDF	Complimentary Cumulative Distribution Function
CCI	Co-Channel Interference
CCMC	Continuous input Continuous output Memoryless Channel
CDD	Conventional Differential Detection
CDMA	Code Division Multiple Access
CE	Channel Estimation
CIR	Channel Impulse Response
Coherence bandwidth	The maximum bandwidth or frequency interval over which two frequencies of a signal are likely to experience correlated fading

COST207-TU12	A 12-tap dispersive typical urban channel model proposed by the European Cooperation in Science and Technology (COST)
CP	Cyclic Prefix
CRC	Cyclic Redundancy Check
Crossover	A Genetic Algorithm operator which takes more than one parent solutions and produces a child solution from there
CSI	Channel State Information
CSTSK	Coherent Space-Time Shift Keying
DAB	Digital Audio Broadcasting
DCM	Dispersion Characterizing Matrix. A matrix constructed by the column-wise vectorial stacking of the DMs set used in LDC or STSK
DCMC	Discrete input Continuous output Memoryless Channel
Delay spread	The square root of the second central moment of delay power spectral density
DF	Decode-and-Forward
DFT	Discrete Fourier Transform
DL	Downlink
DL/UL	Downlink/Uplink
DLDC	Differential Linear Dispersion Code
DM	Dispersion Matrix
DMT	Diversity-Multiplexing Tradeoff
DN	Destination Node
DOA	Direction-of-Arrival
DOD	Direction-of-Departure
DPSK	Differential Phase-Shift Keying
DSFM	Differential Space-Frequency Modulation
DSTSK	Differential Space-Time Shift Keying
DVB	Digital Video Broadcasting
EGC	Equal Gain Combining

Elitism	A Genetic Algorithm process of selecting the high-fitness individual
EVD	Eigen-Value Decomposition
EXIT	EXtrinsic Information Transfer
FD	Frequency Domain
FDCHTF	Frequency Domain Channel Transfer Function
FDCHTM	Frequency Domain Channel Transfer Matrix
FDE	Frequency Domain Equalizer
FIR	Infinite Impulse Response
GA	Genetic Algorithm
HSDPA	High-Speed Downlink Packet Access
IDFT	Inverse Discrete Fourier Transform
IEI	Inter-Element Interference
IFDMA	Inteleaved Frequency Division Multiple Access
IRI	Inter-relay Interference
ISI	Inter-Symbol Interference
LDC	Linear Dispersion Code
LFDMA	Localized Frequency Division Multiple Access
LLR	Logarithmic Likelihood Ratio
LTE	Long Term Evolution
MC	Multicarrier
MC DS-CDMA	Multicarrier Direct Sequence Code Division Multiple Access
MC-CDMA	Multicarrier Code Division Multiple Access
MI	Mutual Information
MIMO	Multiple-Input Multiple-Output
ML	Maximum Likelihood
ML-MUD	Maximum Likelihood - Multiuser Detector

MMSE	Minimum Mean Squared Error
MMSEC	Minimum Mean Squared Error Combining
MRC	Maximal Ratio Combining
MSDD	Multiple-Symbol Differential Decoding
MSDSD	Multiple-Symbol Differential Sphere Decoding
MT-CDMA	Multitone Code Division Multiple Access
MUD	Multiuser Detector
MUI	Multiuser Interference
Mutation	A Genetic Algorithm operator which produces the child solution by flipping a single or more bit of the parent
OF	Objective Function
OFDM	Orthogonal Frequency-Division Multiplexing
OFDMA	Orthogonal Frequency Division Multiple Access
ORC	Orthogonality Restoring Combining
OVSF	Orthogonal Variable Spreading Factor
PAM	Pulse Amplitude Modulation
PAPR	Peak-to-Average Power Ratio
PED	Partial Euclidean Distance
PEP	Pairwise Error Probability. The probability of a codeword being wrongly decoded as another codeword
QAM	Quadrature Amplitude Modulation
QPSK	Quadrature Phase Shift Keying
RMO	Real-valued Multiplication Operation
RN	Relay Node
RSC	Recursive Systematic Convolutional
SC	Selection Combining
SC-FDE	Single-Carrier Frequency Domain Equalizer
SC-FDMA	Single-Carrier Frequency Division Multiple Access
SCM	Single-Carrier Modulation

SD	Spatial Domain
SDM	Spatial Division Multiplexing
SDMA	Space-Division Multiple Access
Selection	A Genetic Algorithm process of choosing a population for future population
SI	Self-Interference
SISO	Single-Input Single-Output
SM	Spatial Modulation
SN	Source Node
SNR	Signal-to-Noise Ratio
SR	Successive Relaying
SSK	Space Shift Keying
ST	Space-Time
STS	Space-Time Spreading
STSK	Space-Time Shift Keying
SUD	Single-User Detection
SUS	Stochastic Universal Sampling. A method of weighted random sampling extensively used in Genetic Algorithms for selecting potentially useful solutions for recombination, which exhibits less bias and spread than the classic Roulette Wheel Sampling (RWS)
SVD	Singular-value Decomposition
TCM	Trellis-Coded Modulation
TD	Time Domain
TTCM	Turbo Trellis-Coded Modulation
TU	Typical Urban
UL	Uplink
URC	Unity Rate Code
V-BLAST	Vertical Bell Laboratories Layered Space-Time
VAA	Virtual Antenna Array

WCDMA Wideband Code Division Multiple Access
WINNER Wireless INitiative NEw Radio project
WLAN Wireless Local Area Network

ZF Zero Forcing

Bibliography

[1] A. Goldsmith, S. A. Jafar, N. Jindal, and S. Vishwanath, "Capacity limits of MIMO channels," *IEEE Journal on Selected Areas in Communications*, vol. 21, no. 5, pp. 684–702, June 2003.

[2] H. Sampath, S. Talwar, J. Tellado, V. Erceg, and A. J. Paulraj, "A fourth-generation MIMO-OFDM broadband wireless system: Design, performance, and field trial results," *IEEE Communications Magazine*, vol. 40, no. 9, pp. 143–149, September 2002.

[3] H. Bolcskei, D. Gesbert, and A. J. Paulraj, "On the capacity of OFDM-based spatial multiplexing systems," *IEEE Transactions on Communications*, vol. 50, no. 2, pp. 225–234, February 2002.

[4] A. J. Paulraj, D. A. Gore, R. U. Nabar, and H. Bolcskei, "An overview of MIMO communications - a key to gigabit wireless," *Proceedings of the IEEE*, vol. 92, no. 2, pp. 198–218, February 2004.

[5] L. Hanzo, O. Alamri, M. El-Hajjar, and N. Wu, *Near-Capacity Multi-Functional MIMO Systems (Sphere-Packing, Iterative Detection and Cooperation)*. John Wiley & Sons, May 2009.

[6] D. G. Brennan, "Linear diversity combining techniques," *Proceedings of the IRE*, vol. 47, no. 6, pp. 1075–1102, June 1959.

[7] M. S. Alouini and A. J. Goldsmith, "Capacity of Rayleigh fading channels under different adaptive transmission and diversity-combining techniques," *IEEE Transactions on Vehicular Technology*, vol. 48, no. 4, pp. 1165–1181, July 1999.

[8] S. M. Alamouti, "A simple transmit diversity technique for wireless communications," *IEEE Journal on Selected Areas in Communications*, vol. 16, no. 8, pp. 1451–1458, October 1998.

[9] V. Tarokh, H. Jafarkhani, and A. R. Calderbank, "Space-time block codes from orthogonal designs," *IEEE Transactions on Information Theory*, vol. 45, no. 5, pp. 1456–1467, July 1999.

[10] V. Tarokh, N. Seshadri, and A. R. Calderbank, "Space-time codes for high data rate wireless communication: Performance criterion and code construction," *IEEE Transactions on Information Theory*, vol. 44, no. 2, pp. 744–765, March 1998.

[11] B. Hassibi and B. M. Hochwald, "High-rate codes that are linear in space and time," *IEEE Transactions on Information Theory*, vol. 48, no. 7, pp. 1804–1824, July 2002.

[12] H. Jafarkhani, "A quasi-orthogonal space-time block code," *IEEE Transactions on Communications*, vol. 49, no. 1, pp. 1–4, January 2001.

[13] B. Hochwald, T. L. Marzetta, and C. B. Papadias, "A transmitter diversity scheme for wideband CDMA systems based on space-time spreading," *IEEE Journal on Selected Areas in Communications*, vol. 19, no. 1, pp. 48–60, January 2001.

[14] A. J. Paulraj and T. Kailath, "Increasing capacity in wireless broadcast systems using distributed transmission/directional reception (DTDR)," U. S. Patent 5,345,599, filed 1992, issued 1994.

[15] G. J. Foschini, "Layered space-time architecture for wireless communication in a fading environment when using multiple antennas," *Bell Laboratories Technical Journal*, vol. 1, no. 2, pp. 41–59, Autumn 1996.

[16] E. Telatar, "Capacity of multi-antenna Gaussian channels," *European Transactions on Telecommunications*, vol. 10, no. 6, pp. 585–595, November-December 1999.

[17] G. J. Foschini, G. D. Golden, R. A. Valenzuela, and P. W. Wolniansky, "Simplified processing for high spectral efficiency wireless communication employing multi-element arrays," *IEEE Journal on Selected Areas in Communications*, vol. 17, no. 11, pp. 1841–1852, November 1999.

[18] A. Goldsmith, *Wireless Communications*. Cambridge University Press, 2005.

[19] D. Tse and P. Viswanath, *Fundamentals of wireless communication*. New York, NY, USA: Cambridge University Press, 2005.

[20] M. Jiang and L. Hanzo, "Multiuser MIMO-OFDM for next-generation wireless systems," *Proceedings of the IEEE*, vol. 95, no. 7, pp. 1430–1469, July 2007.

[21] M. Cooper and M. Goldburg, "Intelligent antennas: Spatial division multiple access," *ArrayComm: Annual Review of Communications*, pp. 999–1002, 1996.

[22] L. Hanzo, J. Blogh, and S. Ni, *3G, HSPA and FDD versus TDD Networking: Smart Antennas and Adaptive Modulation*. New York, NY: John Wiley & Sons, 2008.

[23] L. C. Godara, "Application of antenna arrays to mobile communications. Part I: Performance improvement, feasibility, and system considerations," *Proceedings of the IEEE*, vol. 85, no. 7, pp. 1031–1060, July 1997.

[24] L. C. Godara, "Application of antenna arrays to mobile communications. Part II.: Beamforming and direction-of-arrival considerations," *Proceedings of the IEEE*, vol. 85, no. 8, pp. 1195–1245, August 1997.

[25] J. H. Winters, "Smart antennas for wireless systems," *IEEE Personal Communications*, vol. 5, no. 1, pp. 23–27, February 1998.

[26] A. Kaye and D. George, "Transmission of multiplexed PAM signals over multiple channel and diversity systems," *IEEE Transactions on Communication Technology*, vol. 18, no. 5, pp. 520–526, October 1970.

[27] S. Applebaum, "Adaptive arrays," *IEEE Transactions on Antennas and Propagation*, vol. 24, no. 5, pp. 585–598, September 1976.

[28] J. H. Winters, "Optimum combining in digital mobile radio with cochannel interference," *IEEE Journal on Selected Areas in Communications*, vol. 2, no. 4, pp. 528–539, July 1984.

[29] J. H. Winters, J. Salz, and R. D. Gitlin, "The impact of antenna diversity on the capacity of wireless communication systems," *IEEE Transactions on Communications*, vol. 42, no. 2/3/4, pp. 1740–1751, February/March/April 1994.

[30] H. Krim and M. Viberg, "Two decades of array signal processing research: the parametric approach," *IEEE Signal Processing Magazine*, vol. 13, no. 4, pp. 67–94, July 1996.

[31] A. Wittneben, "A new bandwidth efficient transmit antenna modulation diversity scheme for linear digital modulation," in *Proceedings of the IEEE International Conference on Communications (ICC'93)*, vol. 3, Geneva, Switzerland, May 1993, pp. 1630–1634 vol.3.

[32] R. W. Heath Jr. and A. J. Paulraj, "Linear dispersion codes for MIMO systems based on frame theory," *IEEE Transactions on Signal Processing*, vol. 50, no. 10, pp. 2429–2441, October 2002.

[33] N. Seshadri and J. H. Winters, "Two signaling schemes for improving the error performance of frequency division duplex (FDD) transmission systems using transmitter antenna diversity," *International Journal of Wireless Information Networks (IJWIN)*, vol. 1, no. 1, pp. 49–60, January 1994.

[34] B. L. Hughes, "Differential space-time modulation," *IEEE Transactions on Information Theory*, vol. 46, no. 7, pp. 2567 –2578, November 2000.

[35] V. Tarokh and H. Jafarkhani, "A differential detection scheme for transmit diversity," *IEEE Journal on Selected Areas in Communications*, vol. 18, no. 7, pp. 1169–1174, July 2000.

[36] B. L. Yeap and L. Hanzo, "Reduced complexity I/Q turbo detection for space-time trellis-coded systems," *IEEE Transactions on Vehicular Technology*, vol. 53, no. 4, pp. 1278–1286, July 2004.

[37] T. H. Liew and L. Hanzo, "Space-time trellis and space-time block coding versus adaptive modulation and coding aided OFDM for wideband channels," *IEEE Transactions on Vehicular Technology* , vol. 55, no. 1, pp. 173–187, January 2006.

[38] G. D. Golden, G. J. Foschini, R. Valenzuela, and P. W. Wolniansky, "Detection algorithm and initial laboratory results using V-BLAST space-time communication architecture," *Electronics Letters*, vol. 35, no. 1, pp. 14–16, January 1999.

[39] Y. Huang, J. Zhang, and P. M. Djuric, "Bayesian detection for BLAST," *IEEE Transactions on Signal Processing*, vol. 53, no. 3, pp. 1086–1096, March 2005.

[40] P. Vandenameele, L. V. D. Perre, M. G. E. Engels, B. Gyselinckx, and H. J. D. Man, "A combined OFDM/SDMA approach," *IEEE Journal on Selected Areas in Communications*, vol. 18, no. 11, pp. 2312–2321, November 2000.

[41] M. Munster and L. Hanzo, "Parallel-interference-cancellation-assisted decision-directed channel estimation for OFDM systems using multiple transmit antennas," *IEEE Transactions on Wireless Communications* , vol. 4, no. 5, pp. 2148–2162, September 2005.

[42] V. Tarokh, A. Naguib, N. Seshadri, and A. R. Calderbank, "Combined array processing and space-time coding," *IEEE Transactions on Information Theory*, vol. 45, no. 4, pp. 1121–1128, May 1999.

[43] J. Liu and E. Gunawan, "Combining ideal beamforming and Alamouti space-time block codes," *Electronics Letters*, vol. 39, no. 17, pp. 1258–1259, August 2003.

[44] H. Kim and J. Chun, "MIMO structure which combines the spatial multiplexing and beamforming," in *Proceedings of the IEEE 59th Vehicular Technology Conference, Spring (VTC-2004 Spring)*, Milan, Italy, May 2004, pp. 108–112.

[45] M. Tao and R. S. Cheng, "Generalized layered space-time codes for high data rate wireless communications," *IEEE Transactions on Wireless Communications*, vol. 3, no. 4, pp. 1067–1075, July 2004.

[46] Y. A. Chau and S.-H. Yu, "Space modulation on wireless fading channels," in *Proceedings of the IEEE Vehicular Technology Conference (VTC-2001 Fall)*, Atlantic City, NJ, USA, October 2001, pp. 1668–1671.

[47] R. Mesleh, H. Haas, S. Sinanovic, C. W. Ahn, and S. Yun, "Spatial modulation," *IEEE Transactions on Vehicular Technology*, vol. 57, no. 4, pp. 2228–2241, July 2008.

[48] J. Jeganathan, A. Ghrayeb, L. Szczecinski, and A. Ceron, "Space shift keying modulation for MIMO channels," *IEEE Transactions on Wireless Communications*, vol. 8, no. 7, pp. 3692–3703, July 2009.

[49] S. Sugiura, S. Chen, and L. Hanzo, "Coherent and differential space-time shift keying: A dispersion matrix approach," *IEEE Transactions on Communications*, vol. 58, no. 11, pp. 3219–3230, November 2010.

[50] R. Mesleh, H. Haas, C. W. Ahn, and S. Yun, "Spatial modulation - a new low complexity spectral efficiency enhancing technique," in *Proceedings of the First International Conference on Communications and Networking in China (CHINACOM'06).* Beijing, China: IEEE, October 2006, pp. 1–5.

[51] R. Mesleh, S. Engelken, S. Sinanovic, and H. Haas, "Analytical SER calculation of spatial modulation," in *Proceedings of the IEEE 10th International Symposium on Spread Spectrum Techniques and Applications (ISSSTA '08)*, Bologna, Italy, August 2008, pp. 272–276.

[52] J. Jeganathan, A. Ghrayeb, and L. Szczecinski, "Spatial modulation: Optimal detection and performance analysis," *IEEE Communications Letters*, vol. 12, no. 8, pp. 545–547, August 2008.

[53] S. Sugiura, S. Chen, and L. Hanzo, "A unified MIMO architecture subsuming space shift keying, OSTBC, BLAST and LDC," in *Proceedings of the IEEE 72nd Vehicular Technology Conference Fall (VTC 2010-Fall)*, Ottawa, Canada, September 2010, pp. 1–5.

[54] S. Sugiura, S. Chen, and L. Hanzo, "Cooperative differential space-time spreading for the asynchronous relay aided CDMA uplink using interference rejection spreading code," *IEEE Signal Processing Letters*, vol. 17, no. 2, pp. 117–120, February 2010.

[55] S. Sugiura, C. Xu, S. X. Ng, and L. Hanzo, "Reduced-complexity coherent versus non-coherent QAM-aided space-time shift keying," *IEEE Transactions on Communications*, vol. 59, no. 11, pp. 3090–3101, November 2011.

[56] S. Sugiura, S. Chen, and L. Hanzo, "Generalized space-time shift keying designed for flexible diversity-, multiplexing- and complexity-tradeoffs," *IEEE Transactions on Wireless Communications*, vol. 10, no. 4, pp. 1144–1153, April 2011.

[57] S. Sugiura, S. Chen, and L. Hanzo, "A universal space-time architecture for multiple-antenna aided systems," *IEEE Communications Surveys and Tutorials*, vol. 14, no. 2, pp. 401–420, Second Quart. 2012.

[58] ETSI, "Radio Broadcasting Systems: Digital Audio Broadcasting (DAB) to mobile, portable and fixed receivers," European Telecommunications Standards Institute (ETSI) EN 300 401, Tech. Rep., May 1997.

[59] ETSI, "Digital Video Broadcasting: Framing structure, channel coding, and modulation for digital terrestrial television," European Telecommunications Standards Institute EN 300 744, Tech. Rep., August 1997.

[60] H. Sari and G. Karam, "Orthogonal frequency-division multiple access and its application to CATV network," *European Transactions on Telecommunications*, vol. 9, no. 6, pp. 507–516, November-December 1998.

[61] IEEE 802.11, "IEEE standard for wireless LAN medium access control (MAC) and physical (PHY) layer specifications," IEEE LAN/MAN Standards Committee, Tech. Rep., November 1997.

[62] ETSI, "Radio equipment and systems, High PErformance Radio Local Area Network (HYPERLAN) Type 1," European Telecommunications Standards Institute (ETSI) ETS 300 652, Tech. Rep., October 1996.

[63] M. L. Doelz, E. T. Heald, and D. L. Martin, "Binary data transmission techniques for linear systems," *Proceedings of the IRE*, vol. 45, no. 5, pp. 656–661, May 1957.

[64] R. W. Chang, "Synthesis of band-limited orthogonal signals for multichannel data transmission," *Bell Systems Technical Journal*, vol. 45, pp. 1775–1796, December 1966.

[65] R. W. Chang, "Orthogonal frequency division multiplexing," U. S. Patent 3,488,445, filed 1966, issued 1970.

[66] S. Weinstein and P. Ebert, "Data transmission by frequency-division multiplexing using the discrete Fourier transform," *IEEE Transactions on Communication Technology*, vol. 19, no. 5, pp. 628–634, October 1971.

[67] B. Hirosaki, "An orthogonally multiplexed QAM system using the discrete Fourier transform," *IEEE Transactions on Communications*, vol. 29, no. 7, pp. 982–989, July 1981.

[68] L. Cimini Jr., "Analysis and simulation of a digital mobile channel using orthogonal frequency division multiplexing," *IEEE Transactions on Communications*, vol. 33, no. 7, pp. 665–675, July 1985.

[69] M. Alard and R. Lassalle, "Principles of modulation and channel coding for digital broadcasting for mobile receivers," *EBU Technical Review*, no. 224, pp. 168–190, August 1987.

[70] J. M. Cioffi, "A multicarrier primer," ANSI T1E1.4 Committee Contribution, no. 91-157. Amati Communications Corporation and Stanford University. 408-257-1717 or 415-723-2150., Tech. Rep., November 1991.

[71] R. V. Nee and R. Prasad, *OFDM for Wireless Multimedia Communications*, 1st ed. Norwood, MA, USA: Artech House, Inc., 2000.

[72] C. S. Lee, T. Keller, and L. Hanzo, "OFDM-based turbo-coded hierarchical and non-hierarchical terrestrial mobile digital video broadcasting," *IEEE Transactions on Broadcasting*, vol. 46, no. 1, pp. 1–22, March 2000.

[73] L. Hanzo, M. Munster, B. J. Choi, and T. Keller, *OFDM and MC-CDMA for Broadcasting Multi-User Communications, WLANs and Broadcasting*. John Wiley & Sons, July 2003.

[74] C. Williams, M. A. Beach, and S. Mclaughlin, "Robust OFDM timing synchronisation," *Electronics Letters*, vol. 41, no. 13, pp. 4–5, June 2005.

[75] H. Chen, W. Gao, and D. Daut, "Spectrum sensing for OFDM systems employing pilot tones," *IEEE Transactions on Wireless Communications*, vol. 8, no. 12, pp. 5862–5870, December 2009.

[76] R. M. Gray, "Toeplitz and circulant matrices: A review," *Foundations and Trends in Communications and Information Theory*, vol. 2, no. 3, August 2005.

[77] R. S. Blum, G. L. Ye, J. H. Winters, and Y. Qing, "Improved space-time coding for MIMO-OFDM wireless communications," *IEEE Transactions on Communications*, vol. 49, no. 11, pp. 1873–1878, November 2001.

[78] R. J. Piechocki, P. N. Fletcher, A. R. Nix, C. N. Canagarajah, and J. P. McGeehan, "Performance evaluation of BLAST-OFDM enhanced Hiperlan/2 using simulated and measured channel data," *Electronics Letters*, vol. 37, no. 18, pp. 1137–1139, May 2001.

[79] Y. Li, J. H. Winters, and N. R. Sollenberger, "MIMO-OFDM for wireless communications: Signal detection with enhanced channel estimation," *IEEE Transactions on Communications*, vol. 50, no. 9, pp. 1471–1477, September 2002.

[80] L. Giangaspero, L. Agarossi, G. Paltenghi, S. Okamura, M. Okada, and S. Komaki, "Co-channel interference cancellation based on MIMO OFDM systems," *IEEE Wireless Communications*, vol. 9, no. 6, pp. 8–17, December 2002.

[81] G. L. Stuber, J. R. Barry, S. W. McLaughlin, Y. Li, M. Ingram, and T. G. Pratt, "Broadband MIMO-OFDM wireless communications," *Proceedings of the IEEE*, vol. 92, no. 2, pp. 271–294, February 2004.

[82] L. Hanzo and B. J. Choi, "Near-instantaneously adaptive HSDPA-style OFDM versus MC-CDMA transceivers for WIFI, WIMAX, and next-generation cellular systems," *Proceedings of the IEEE*, vol. 95, no. 12, pp. 2368–2392, December 2007.

[83] A. Stamoulis, S. N. Diggavi, and N. Al-Dhahir, "Intercarrier interference in MIMO OFDM," *IEEE Transactions on Signal Processing*, vol. 50, no. 10, pp. 2451–2464, October 2002.

[84] H. El-Gamal, A. R. Hammons Jr., Y. Liu, M. P. Fitz, and O. Y. Takeshita, "On the design of space-time and space-frequency codes for MIMO frequency-selective fading channels," *IEEE Transactions on Information Theory*, vol. 49, no. 9, pp. 2277–2292, September 2003.

[85] J. H. Moon, Y. H. You, W. G. Jeon, K. W. Kwon, and H. K. Song, "Peak-to-average power control for multiple-antenna HIPERLAN/2 and IEEE802.11a systems," *IEEE Transactions on Consumer Electronics*, vol. 49, no. 4, pp. 1078–1083, November 2003.

[86] D. Huang and K. Letaief, "Symbol-based space diversity for coded OFDM systems," *IEEE Transactions on Wireless Communications*, vol. 3, no. 1, pp. 117–127, January 2004.

[87] W. Su, Z. Safar, and K. J. R. Liu, "Full-rate full-diversity space-frequency codes with optimum coding advantage," *IEEE Transactions on Information Theory*, vol. 51, no. 1, pp. 229–249, January 2005.

[88] M. Borgmann and H. Bolcskei, "Noncoherent space-frequency coded MIMO-OFDM," *IEEE Journal on Selected Areas in Communications*, vol. 23, no. 9, pp. 1799–1810, September 2005.

[89] L. Hanzo, L.-L. Yang, E. L. Kuan, and K. Yen, *Single and Multi-Carrier DS-CDMA: Multi-User Detection, Space-Time Spreading, Synchronisation, Networking and Standards*. New York, NY: John Wiley & Sons, 2003.

[90] G. Fettweis, J. P. Linnartz, and N. Yee, "Multi-carrier CDMA in indoor wireless radio networks," in *Proceedings of the IEEE International Symposium on Personal, Indoor and Mobile Radio Communications (PIMRC'93)*, Yokohama, Japan, September 1993, pp. 109–113.

[91] K. Fazel and L. Papke, "On the performance of convolutionally-coded CDMA/OFDM for mobile radio communication system," in *Proceedings of the IEEE International Symposium on Personal, Indoor and Mobile Radio Communications (PIMRC'93)*, Yokohama, Japan, September 1993, pp. 468–472.

[92] A. Chouly, A. Brajal, and S. Jourdan, "Orthogonal multicarrier techniques applied to direct sequence spread spectrum CDMA systems," in *Proceedings of the IEEE Global Telecommunications Conference (GLOBECOM'93)*, Houston, USA, November-December 1993, pp. 1723–1728.

[93] V. D. Silva and E. S. Sousa, "Performance of orthogonal CDMA codes for quasi-synchronous communication systems," in *Proceedings of the IEEE International Conference on Universal Personal Communications (ICUPC'93)*, Ottawa, Canada, October 1993, pp. 995–999.

[94] L. Vandendorpe, "Multitone direct sequence CDMA system in an indoor wireless environment," in *Proceedings of IEEE First Symposium of Communications and Vehicular Technology in the Benelux*, Delft, The Netherlands, October 1993, pp. 4.1.1–4.1.8.

[95] S. Hara and R. Prasad, "Overview of multi-carrier CDMA," *IEEE Communications Magazine*, vol. 35, no. 12, pp. 126–133, December 1997.

[96] H. G. Myung, J. Lim, and D. J. Goodman, "Single carrier FDMA for uplink wireless transmission," *IEEE Vehicular Technology Magazine*, vol. 1, no. 3, pp. 30–38, September 2006.

[97] N. Benvenuto and S. Tomasin, "On the comparison between OFDM and single carrier modulation with a DFE using a frequency-domain feedforward filter," *IEEE Transactions on Communications*, vol. 50, no. 6, pp. 947–955, June 2002.

[98] L.-L. Yang, *Multicarrier Communications*. John Wiley & Sons, 2009.

[99] T. Walzman and M. Schwartz, "Automatic equalization using the discrete frequency domain," *IEEE Transactions on Information Theory*, vol. 19, no. 1, pp. 59–68, January 1973.

[100] H. Sari, G. Karam, and I. Jeanclaude, "Transmission techniques for digital terrestrial TV broadcasting," *IEEE Communications Magazine*, vol. 33, no. 2, pp. 100–109, February 1995.

[101] D. Falconer, S. L. Ariyavisitakul, A. Benyamin-Seeyar, and B. Eidson, "Frequency domain equalization for single-carrier broadband wireless systems," *IEEE Communications Magazine*, vol. 40, no. 4, pp. 58–66, April 2002.

[102] D. Falconer and S. L. Ariyavisitakul, "Broadband wireless using single carrier and frequency domain equalization," in *Proceedings of the 5th International Symposium on Wireless Personal Multimedia Communications (WPMC)*, vol. 1, Honolulu, Hawaii, USA, October 2002, pp. 27–36.

[103] WINNER, "The WINNER II air interface: Refined multiple access concepts," IST-4-027756 WINNER II, D4.6.1, Tech. Rep., November 2006.

[104] N. Benvenuto, R. Dinis, D. Falconer, and S. Tomasin, "Single carrier modulation with nonlinear frequency domain equalization: An idea whose time has come - again," *Proceedings of the IEEE*, vol. 98, no. 1, pp. 69–96, January 2010.

[105] A. Wilzeck, Q. Cai, M. Schiewer, and T. Kaiser, "Effect of multiple cariier frequency offsets in MIMO SC-FDMA systems," in *Proceedings of the International ITG/IEEE Workshop on Smart Antennas*, Vienna, Austria, February 2007.

[106] U. Sorger, I. D. Broeck, and M. Schnell, "Interleaved FDMA - a new spread-spectrum multiple-access scheme," in *Proceedings of the IEEE International Conference on Communications (ICC'98)*, vol. 2, Atlanta, Georgia, USA, June 1998, pp. 1013–1017.

[107] G. Berardinelli, L. A. R. Temino, S. Frattasi, M. I. Rahman, and P. Mogensen, "OFDMA vs. SC-FDMA: Performance comparison in local area IMT-A scenarios," *IEEE Wireless Communications*, vol. 15, no. 5, pp. 64–72, October 2008.

[108] C. Ciochina and H. Sari, "A review of OFDMA and single-carrier FDMA," in *Proceedings of the European Wireless Conference (EW 2010)*, Lucca, Italy, April 2010, pp. 706–710.

[109] V. Dalakas, P. T. Mathiopoulos, F. D. Cecca, and G. Gallinaro, "A comparative study between SC-FDMA and OFDMA schemes for satellite uplinks," *IEEE Transactions on Broadcasting*, vol. 58, no. 3, pp. 370–378, September 2012.

[110] T. Cover and A. E. Gamal, "Capacity theorems for the relay channel," *IEEE Transactions on Information Theory*, vol. 25, no. 5, pp. 572–584, September 1979.

[111] A. Sendonaris, E. Erkip, and B. Aazhang, "User cooperation diversity Part I and II: System description," *IEEE Transactions on Communications*, vol. 51, no. 11, pp. 1927–1948, November 2003.

[112] E. C. van der Meulen, "Three-terminal communication channels," *Adv. Appl. Probab.*, vol. 3, pp. 120–154, 1971.

[113] J. N. Laneman, D. N. C. Tse, and G. W. Wornell, "Cooperative diversity in wireless networks: Efficient protocols and outage behavior," *IEEE Transactions on Information Theory*, vol. 50, no. 12, pp. 3062–3080, December 2004.

[114] Y. Fan, C. Wang, J. Thompson, and H. V. Poor, "Recovering multiplexing loss through successive relaying using repetition coding," *IEEE Transactions on Wireless Communications*, vol. 6, no. 12, pp. 4484–4493, December 2007.

[115] L. Kong, S. X. Ng, R. G. Maunder, and L. Hanzo, "Near-capacity cooperative space-time coding employing irregular design and successive relaying," *IEEE Transactions on Communications*, vol. 58, no. 8, pp. 2232–2241, August 2010.

[116] M. I. Kadir, L. Li, S. Chen, and L. Hanzo, "Successive-relaying-aided decode-and-forward coherent versus noncoherent cooperative multicarrier space-time shift keying," *IEEE Transactions on Vehicular Technology*, vol. 62, no. 6, pp. 2544–2557, July 2013.

[117] M. I. Kadir, S. Sugiura, J. Zhang, S. Chen, and L. Hanzo, "OFDMA/SC-FDMA aided space-time shift keying for dispersive multiuser scenarios," *IEEE Transactions on Vehicular Technology*, vol. 62, no. 1, pp. 408–414, January 2013.

[118] M. I. Kadir, S. Chen, and L. Hanzo, "A reduced-complexity detector for OFDMA/SC-FDMA-aided space-time shift keying," in *Proceedings of the 78th IEEE Vehicular Technology Conference, Fall (VTC2013-Fall)*, Las Vegas, USA, September 2013, pp. 1–5.

[119] M. Driusso, F. Babich, M. I. Kadir, and L. Hanzo, "OFDM aided space-time shift keying for dispersive downlink channels," in *Proceedings of the 76th IEEE Vehicular Technology Conference, Fall (VTC2013-Fall)*, Quebec City, Canada, September 2012, pp. 1–5.

[120] M. I. Kadir, S. Chen, K. V. S. Hari, K. Giridhar, and L. Hanzo, "Iterative soft multiple-symbol differential sphere decoding aided multicarrier space-time shift keying," *IEEE Transactions on Vehicular Technology*, (under review).

[121] M. I. Kadir, S. Sugiura, S. Chen, and L. Hanzo, "MC-CDMA aided multi-user space-time shift keying in wideband channels," in *Proceedings of the IEEE Wireless Communications and Networking Conference (WCNC-2013)*, Shanghai, China, 2013, pp. 2643–2648.

[122] P. W. Wolniansky, G. J. Foschini, G. D. Golden, and R. A. Valenzuela, "V-BLAST: An architecture for realizing very high data rates over the rich-scattering wireless channel," in *Proceedings of the International Symposium on Signals, Systems, and Electronics (ISSSE 1998)*, Pisa, Italy, September-October 1998, pp. 295–300.

[123] E. Viterbo and J. Boutros, "A universal lattice code decoder for fading channels," *IEEE Transactions on Information Theory*, vol. 45, no. 5, pp. 1639–1642, July 1999.

[124] M. Dorigo and T. Stützle, *Ant Colony Optimization*. Cambridge, Massachusetts: The MIT Press, 2004.

[125] G. Ungerboeck, "Channel coding with multilevel/phase signals," *IEEE Transactions on Information Theory*, vol. 28, no. 1, pp. 55–67, January 1982.

[126] L. Zheng and D. N. C. Tse, "Diversity and multiplexing: A fundamental tradeoff in multiple-antenna channels," *IEEE Transactions on Information Theory*, vol. 49, no. 5, pp. 1073–1096, May 2003.

[127] S. X. Ng and L. Hanzo, "On the MIMO channel capacity of multidimensional signal sets," *IEEE Transactions on Vehicular Technology*, vol. 55, no. 2, pp. 528–536, March 2006.

[128] G. J. Foschini and M. J. Gans, "On limits of wireless communications in a fading environment when using multiple antennas," *Wireless Personal Communications*, vol. 6, pp. 311–335, March 1998.

[129] B. Hassibi and B. M. Hochwald, "Cayley differential unitary space-time codes," *IEEE Transactions on Information Theory*, vol. 48, no. 6, pp. 1485–1503, June 2002.

[130] S. Sugiura, "Coherent versus non-coherent space-time shift keying for co-located and distributed MIMO systems," Ph.D. dissertation, University of Southampton, United Kingdom, 2010.

[131] F. Babich, A. Crismani, M. Driusso, and L. Hanzo, "Design criteria and genetic algorithm aided optimization of three-stage-concatenated space-time shift keying systems," *IEEE Signal Processing Letters*, vol. 19, no. 8, pp. 543–546, August 2012.

[132] R. Rajashekar, K. V. S. Hari, and L. Hanzo, "Field extension code based dispersion matrices for coherently detected space-time shift keying," in *Proceedings of the IEEE Global Telecommunications Conference (GLOBECOM'11)*, Houston, Texas, USA, December 2011, pp. 1–5.

[133] D. Torrieri and M. C. Valenti, "Efficiently decoded full-rate space-time block codes," *IEEE Transactions on Communications*, vol. 58, no. 2, pp. 480–488, February 2010.

[134] M. Jiang and L. Hanzo, "Unitary linear dispersion code design and optimization for MIMO communication systems," *IEEE Signal Processing Letters*, vol. 17, no. 5, pp. 497–500, May 2010.

[135] D. E. Goldberg, *Genetic Algorithms in Search, Optimization and Machine Learning*, 1st ed. Boston, MA, USA: Addison-Wesley Longman Publishing Co., Inc., 1989.

[136] K. A. D. Jong, *Evolutionary Computation - A Unified Approach.* MIT Press, 2006.

[137] J. E. Baker, "Reducing bias and inefficiency in the selection algorithm," in *Proceedings of the Second International Conference on Genetic Algorithms and their application.* Hillsdale, NJ, USA: L. Erlbaum Associates Inc., July 1987, pp. 14–21.

[138] L. Hanzo, P. J. Cherriman, and J. Streit, *Wireless video communications - second to third generation systems and beyond*. IEEE, 2001.

[139] M. Patzold, *Mobile Fading Channels*. New York, NY, USA: John Wiley & Sons, Inc., 2003.

[140] R. Steele and L. Hanzo, *Mobile Radio Communications*, 2nd ed. New York, NY, USA: John Wiley & Sons, Inc., 1999.

[141] COST 207, "Digital land mobile radio communications, final report," Office for Official Publications of the European Communities, Luxembourg, Tech. Rep., 1989.

[142] T. Keller and L. Hanzo, "Adaptive multicarrier modulation: a convenient framework for time-frequency processing in wireless communications," *Proceedings of the IEEE*, vol. 88, no. 5, pp. 611–640, May 2000.

[143] S. ten Brink, J. Speidel, and R. H. Yan, "Iterative demapping and decoding for multilevel modulation," in *Proceedings of the IEEE Global Telecommunications Conference (GLOBECOM'98)*, vol. 1, Sydney, Australia, November 1998, pp. 579–584.

[144] P. Robertson, E. Villebrun, and P. Hoeher, "A comparison of optimal and sub-optimal MAP decoding algorithms operating in the log domain," in *Proceedings of the IEEE International Conference on Communications (ICC'95)*, vol. 2, Seattle, USA, June 1995, pp. 1009–1013 vol.2.

[145] L. Hanzo, T. Liew, and B. Yeap, *Turbo Coding, Turbo Equalisation and Space-Time Coding for Transmission over Fading Channels*. John Wiley & Sons, 2002.

[146] M. Tüchler, "Design of serially concatenated systems depending on the block length," *IEEE Transactions on Communications*, vol. 52, no. 2, pp. 209–218, February 2004.

[147] S. ten Brink, "Convergence behavior of iteratively decoded parallel concatenated codes," *IEEE Transactions on Communications*, vol. 49, no. 10, pp. 1727–1737, October 2001.

[148] H. A. Ngo, C. Xu, S. Sugiura, and L. Hanzo, "Space-time-frequency shift keying for dispersive channels," *IEEE Signal Processing Letters*, vol. 18, no. 3, pp. 177–180, March 2011.

[149] L.-L. Yang and L. Hanzo, "Multicarrier DS-CDMA: A multiple access scheme for ubiquitous broadband wireless communications," *IEEE Communications Magazine*, vol. 41, no. 10, pp. 116–124, October 2003.

[150] L.-L. Yang, W. Hua, and L. Hanzo, "A multicarrier DS-CDMA system using both time-domain and frequency-domain spreading," in *Proceedings of the IEEE Vehicular Tech-*

nology Conference (VTC 2003-Fall), vol. 4, Orlando, Florida, USA, October 2003, pp. 2426–2430.

[151] L.-L. Yang, W. Hua, and L. Hanzo, "Multiuser detection in multicarrier CDMA systems employing both time-domain and frequency-domain spreading," in *Proceedings of the IEEE Personal, Indoor and Mobile Radio Communications (PIMRC 2003)*, vol. 2, Beijing, China, September 2003, pp. 1840–1844.

[152] L.-L. Yang and L. Hanzo, "Broadband MC DS-CDMA using space-time and frequency-domain spreading," in *Proceedings of the IEEE Vehicular Technology Conference (VTC 2002-Fall)*, vol. 3, Vancouver, Canada, September 2002, pp. 1632–1636 vol.3.

[153] C. W. You and D. S. Hong, "Multicarrier CDMA systems using time-domain and frequency-domain spreading codes," *IEEE Transactions on Communications*, vol. 51, no. 1, pp. 17–21, January 2003.

[154] C.-M. Yang, P.-H. Lin, G.-C. Yang, and W. C. Kwong, "2D orthogonal spreading codes for multicarrier DS-CDMA systems," in *Proceedings of the IEEE International Conference on Communications (ICC '03)*, vol. 5, Alaska, USA, May 2003, pp. 3277–3281.

[155] J. P. Woodard and L. Hanzo, "Comparative study of turbo decoding techniques: an overview," *IEEE Transactions on Vehicular Technology*, vol. 49, no. 6, pp. 2208–2233, November 2000.

[156] S. Sugiura, "Dispersion matrix optimization for space-time shift keying," *IEEE Communications Letters*, vol. 15, no. 11, pp. 1152–1155, November 2011.

[157] A. Ghosh, R. Ratasuk, B. Mondal, N. Mangalvedhe, and T. Thomas, "LTE-Advanced: Next-generation wireless broadband technology," *IEEE Wireless Communications*, vol. 17, no. 3, pp. 10–22, June 2010.

[158] H. G. Myung, J. Lim, and D. J. Goodman, "Peak-to-average power ratio of single carrier FDMA signals with pulse shaping," in *Proceedings of the IEEE 17th International Symposium on Personal, Indoor and Mobile Radio Communications (PIMRC'06)*, Helsinki, Finland, September 2006, pp. 1–5.

[159] H. G. Myung, K. Oh, J. Lim, and D. Goodman, "Channel-dependent scheduling of an uplink SC-FDMA system with imperfect channel information," in *Proceedings of the IEEE Wireless Communications and Networking Conference (WCNC 2008)*, Las Vegas, USA, March-April 2008, pp. 1860–1864.

[160] J. Lim, H. G. Myung, K. Oh, and D. Goodman, "Channel-dependent scheduling of uplink single carrier fdma systems," in *Proceedings of the IEEE Vehicular Technology Conference (VTC-2006 Fall)*, Montreal, Canada, September 2006, pp. 1–5.

[161] L. Hanzo, S. X. Ng, T. Keller, and W. T. Webb, *Quadrature Amplitude Modulation: From Basics to Adaptive Trellis-Coded, Turbo-Equalised and Space-Time Coded OFDM, CDMA and MC-CDMA Systems*. John Wiley & Sons, 2004.

[162] J. R. Barry, E. A. Lee, and D. G. Messerschmitt, *Digital communication (3rd ed.)*. Springer, 2003.

[163] G. Berardinelli, L. A. R. de Temino, S. Frattasi, M. Rahman, and P. Mogensen, "OFDMA vs. SC-FDMA: performance comparison in local area IMT-A scenarios," *IEEE Wireless Communications*, vol. 15, no. 5, pp. 64–72, October 2008.

[164] J. Hagenauer, "The EXIT chart - introduction to extrinsic information transfer in iterative processing," in *Proceedings of the European Signal Processing Conference*, Vienna, Austria, September 2004, pp. 1541–1548.

[165] W. C. Jakes and D. C. Cox, *Microwave Mobile Communications*. New York, NY, USA: John Wiley and IEEE Press., 1994.

[166] J. N. Laneman and G. W. Wornell, "Distributed space-time-coded protocols for exploiting cooperative diversity in wireless networks," *IEEE Transactions on Information Theory*, vol. 49, no. 10, pp. 2415–2425, October 2003.

[167] T. Wang, A. Cano, G. B. Giannakis, and J. N. Laneman, "High-performance cooperative demodulation with decode-and-forward relays," *IEEE Transactions on Communications*, vol. 55, no. 7, pp. 1427–1438, July 2007.

[168] L. Li and L. Hanzo, "Multiple-symbol differential sphere detection aided successive relaying in the cooperative DS-CDMA uplink," in *Proceedings of IEEE Wireless Communications and Networking Conference (WCNC'11)*, Cancun, Mexico, March 2011, pp. 1875–1880.

[169] L. Li, L. Wang, and L. Hanzo, "Successive AF/DF relaying in the cooperative DS-CDMA uplink: Capacity analysis and its system architecture," *IEEE Transactions on Vehicular Technology*, vol. 62, no. 2, pp. 655–666, February 2013.

[170] P. Zhang, S. Chen, and L. Hanzo, "Differential space-time shift keying-aided successive-relay-assisted decode-and-forward cooperative multiuser CDMA," *IEEE Transactions on Vehicular Technology*, vol. 62, no. 5, pp. 2156–2169, June 2013.

[171] C. Xu, S. Sugiura, S. X. Ng, and L. Hanzo, "Reduced-complexity noncoherently detected differential space-time shift keying," *IEEE Signal Processing Letters*, vol. 18, no. 3, pp. 153–156, March 2011.

[172] J. N. Laneman, D. N. C. Tse, and G. W. Wornell, "Cooperative diversity in wireless networks: Efficient protocols and outage behavior," *IEEE Transactions on Information Theory*, vol. 50, no. 12, pp. 3062–3080, December 2004.

[173] S. Verdú, *Multiuser Detection*. New York, NY, USA: Cambridge University Press, 1998.

[174] M. J. Gans, "A power-spectral theory of propagation in the mobile-radio environment," *IEEE Transactions on Vehicular Technology*, vol. 21, no. 1, pp. 27–38, February 1972.

[175] W. C. Jakes and D. C. Cox, *Microwave Mobile Communications*. New York, NY: Wiley-IEEE Press, 1994.

[176] A. Ashikhmin, G. Kramer, and S. ten Brink, "Extrinsic information transfer functions: Model and erasure channel properties," *IEEE Transactions on Information Theory*, vol. 50, no. 11, pp. 2657–2673, November 2004.

[177] L. Hanzo, Y. Akhtman, L. Wang, and M. Jiang, *MIMO-OFDM for LTE, WIFI and WIMAX: Coherent versus non-coherent and cooperative turbo-receivers*. John Wiley & Sons, 2001.

[178] D. Divsalar and M. K. Simon, "Multiple-symbol differential detection of MPSK," *IEEE Transactions on Communications*, vol. 38, no. 3, pp. 300–308, March 1990.

[179] L. Lampe, R. Schober, V. Pauli, and C. Windpassinger, "Multiple-symbol differential sphere decoding," *IEEE Transactions on Communications*, vol. 53, no. 12, pp. 1981–1985, December 2005.

[180] V. Pauli and L. Lampe, "On the complexity of sphere decoding for differential detection," *IEEE Transactions on Information Theory*, vol. 53, no. 4, pp. 1595–1603, April 2007.

[181] B. M. Hochwald and S. ten Brink, "Achieving near-capacity on a multiple-antenna channel," *IEEE Transactions on Communications*, vol. 51, no. 3, pp. 389–399, March 2003.

[182] V. Pauli, L. Lampe, and R. Schober, ""Turbo DPSK" using soft multiple-symbol differential sphere decoding," *IEEE Transactions on Information Theory*, vol. 52, no. 4, pp. 1385–1398, April 2006.

[183] V. Pauli, L. Lampe, and J. Huber, "Differential space-frequency modulation and fast 2-D multiple-symbol differential detection for MIMO-OFDM," *IEEE Transactions on Vehicular Technology*, vol. 57, no. 1, pp. 297–310, January 2008.

[184] R. H. Clarke, "A statistical theory of mobile radio reception," *Bell System Technical Journal*, vol. 47, pp. 957–1000, July 1968.

[185] V. Pauli and L. Lampe, "Tree-search multiple-symbol differential decoding for unitary space-time modulation," *IEEE Transactions on Communications*, vol. 55, no. 8, pp. 1567–1576, August 2007.

[186] R. Schober and L. Lampe, "Noncoherent receivers for differential space-time modulation," *IEEE Transactions on Communications*, vol. 50, no. 5, pp. 768–777, May 2002.

[187] E. Chiavaccini and G. M. Vitetta, "Further results on differential space-time modulations," *IEEE Transactions on Communications*, vol. 51, no. 7, pp. 1093–1101, July 2003.

[188] L. Wang, "Low-complexity near-optimum detection techniques for non-cooperative and cooperative MIMO systems," Ph.D. dissertation, University of Southampton, United Kingdom, 2010.

[189] N. Seshadri and P. Hoeher, "On post-decision symbol-reliability generation," in *Proceedings of the IEEE International Conference on Communications (ICC'93)*, vol. 2, Geneva, Switzerland, May 1993, pp. 741–745.

[190] M. El-Hajjar and L. Hanzo, "EXIT charts for system design and analysis," *IEEE Communications Surveys and Tutorials*, 2013, to be published.

[191] M. Tüchler and J. Hagenauer, "EXIT charts of irregular codes," in *Proceedings of the Conference on Information Science and Systems (CISS 2002)*, Princeton, NJ, March 2002, pp. 748–753.

[192] L. Hanzo, R. G. Maunder, J. Wang, and L.-L. Yang, *Near-Capacity Variable-Length Coding: Regular and EXIT-Chart-Aided Irregular Designs*. John Wiley & Sons, 2010.

[193] N. Wu and L. Hanzo, "Near-capacity irregular-convolutional-coding-aided irregular precoded linear dispersion codes," *IEEE Transactions on Vehicular Technology*, vol. 58, no. 6, pp. 2863–2871, July 2009.

[194] R. C. Palat, A. Annamalai, and J. H. Reed, "Accurate bit-error-rate analysis of bandlimited cooperative OSTBC networks under timing synchronization errors," *IEEE Transactions on Vehicular Technology*, vol. 58, no. 5, pp. 2191–2200, June 2009.

[195] X. Li, "Space-time coded multi-transmission among distributed transmitters without perfect synchronization," *IEEE Signal Processing Letters*, vol. 11, no. 12, pp. 948–951, December 2004.

[196] Y. Li and X.-G. Xia, "A family of distributed space-time trellis codes with asynchronous cooperative diversity," *IEEE Transactions on Communications*, vol. 55, no. 4, pp. 790–800, April 2007.

[197] Z. Li and X.-G. Xia, "An Alamouti coded OFDM transmission for cooperative systems robust to both timing errors and frequency offsets," *IEEE Transactions on Wireless Communications*, vol. 7, no. 5, pp. 1839–1844, May 2008.

[198] M. Sharp, A. Scaglione, and B. Sirkeci-Mergen, "Randomized cooperation in asynchronous dispersive links," *IEEE Transactions on Communications*, vol. 57, no. 1, pp. 64–68, January 2009.

[199] K. Wu, Y. J. Cheng, T. Djerafi, and W. Hong, "Substrate-integrated millimeter-wave and Terahertz antenna technology," *Proceedings of the IEEE*, vol. 100, no. 7, pp. 2219–2232, July 2012.

[200] L. Hanzo, M. El-Hajjar, and O. Alamri, "Near-capacity wireless transceivers and cooperative communications in the MIMO era: Evolution of standards, waveform design, and future perspectives," *Proceedings of the IEEE*, vol. 99, no. 8, pp. 1343–1385, August 2011.

[201] M. D. Renzo, H. Haas, A. Ghrayeb, S. Sugiura, and L. Hanzo, "Spatial modulation for generalized MIMO: Challenges, opportunities and implementation," *Proceedings of the IEEE*, submitted.

[202] E. G. Larsson, F. Tufvesson, O. Edfors, and T. L. Marzetta, "Massive MIMO for next generation wireless systems," *IEEE Communications Magazine*, submitted.

[203] M.-S. Alouini and A. J. Goldsmith, "Area spectral efficiency of cellular mobile radio systems," *IEEE Transactions on Vehicular Technology*, vol. 48, no. 4, pp. 1047–1066, July 1999.

[204] H. A. Ngo and L. Hanzo, "Area spectral efficiency of soft-decision space-time-frequency shift-keying-aided slow-frequency-hopping multiple access," *IEEE Transactions on Vehicular Technology*, vol. 61, no. 3, pp. 1433–1439, March 2012.

[205] G. Ungerboeck, "Trellis-coded modulation with redundant signal sets part I: Introduction," *IEEE Communications Magazine*, vol. 25, no. 2, pp. 5–11, February 1987.

[206] G. Ungerboeck, "Trellis-coded modulation with redundant signal sets part II: State of the art," *IEEE Communications Magazine*, vol. 25, no. 2, pp. 12–21, February 1987.

[207] P. Robertson and T. Worz, "Bandwidth-efficient turbo trellis-coded modulation using punctured component codes," *IEEE Journal on Selected Areas in Communications*, vol. 16, no. 2, pp. 206–218, February 1998.

[208] L. Lampe and R. Schober, "Bit-interleaved coded differential space-time modulation," *IEEE Transactions on Communications*, vol. 50, no. 9, pp. 1429–1439, September 2002.

[209] C. H. Choi and G. H. Im, "Bit-interleaved coded multilevel modulation for single-carrier frequency-domain equalization," *IEEE Communications Letters*, vol. 14, no. 3, pp. 193–195, March 2010.

[210] R. Tee, R. G. Maunder, and L. Hanzo, "EXIT-chart aided near-capacity irregular bit-interleaved coded modulation design," *IEEE Transactions on Wireless Communications*, vol. 8, no. 1, pp. 32 –37, January 2009.

[211] R. Ahlswede, N. Cai, S.-Y. Li, and R. W. Yeung, "Network information flow," *IEEE Transactions on Information Theory*, vol. 46, no. 4, pp. 1204–1216, July 2000.

[212] Y. Kim and J. Kim, "A 2-D subcarrier allocation scheme for capacity enhancement in a clustered OFDM system," *IEICE Transactions*, vol. 90-B, no. 7, pp. 1880–1883, July 2007.

[213] W. K. Harold, "The Hungarian method for the assignment problem," *Naval Research Logistics Quarterly*, vol. 2, pp. 83–97, March 1955.

[214] N. Y. Ermolova and B. Makarevitch, "Performance of practical subcarrier allocation schemes for OFDMA," in *Proceedings of the IEEE 18th International Symposium on Personal, Indoor and Mobile Radio Communications (PIMRC 2007)*, Athens, Greece, September 2007, pp. 1–4.

[215] T. Liu, C. Yang, and L.-L. Yang, "A low-complexity subcarrier-power allocation scheme for frequency-division multiple-access systems," *IEEE Transactions on Wireless Communications*, vol. 9, no. 5, pp. 1564–1570, May 2010.

[216] J. Lim, H. G. Myung, K. Oh, and D. J. Goodman, "Channel-dependent scheduling of uplink single carrier FDMA systems," in *Proceedings of the IEEE 64th Vehicular Technology Conference (VTC-2006 Fall)*, Montreal, Canada, September 2006, pp. 1–5.

[217] J. Zhang, L.-L. Yang, and L. Hanzo, "Power-efficient opportunistic amplify-and-forward single-relay aided multi-user SC-FDMA uplink," in *Proceedings of the IEEE 71st Vehicular Technology Conference (VTC-2010 Spring)*, Taipei, Taiwan, May 2010, pp. 1–5.

[218] J. Zhang, L.-L. Yang, and L. Hanzo, "Energy-efficient channel-dependent cooperative relaying for the multiuser SC-FDMA uplink," *IEEE Transactions on Vehicular Technology*, vol. 60, no. 3, pp. 992–1004, March 2011.

[219] G. Li, Z. Xu, C. Xiong, C. Yang, S. Zhang, Y. Chen, and S. Xu, "Energy-efficient wireless communications: Tutorial, survey, and open issues," *IEEE Transactions on Wireless Communications*, vol. 18, no. 6, pp. 28–35, December 2011.

Index

Author Index

D

E

M

N

O

P